Jb. Geol. B.-A.	ISSN 0016-7800	Band 133	Heft 1	S. 5–87	Wien, März 1990

The Altkristallin of the Kreuzeck Mountains, SE Tauern Window, Eastern Alps – Basement Crust in a Convergent Plate Boundary Zone

By LEONORE HOKE*)

With 48 Text-Figures, 9 Tables and 5 Plates

Österreichische Karte
Blatt 181

Kärnten
Kreuzeck Gruppe
Tauern-Gebiet
Austroalpin
Altkristallin
Kretazische Metamorphose
Variszische Metamorphose
Extensive Deformationszone
Geochronologische Altersdaten

Contents

*) Author's address: Dr. LEONORE HOKE, Department of Earth Sciences, Parks Road, Oxford, OX1 3PR, England.

Zusammenfassung

In dieser Arbeit werden detailierte Struktur-, Metamorphose und geochronologische Daten vom Altkristallin (Kreuzeck-Gruppe), SE Tauern Gebiet präsentiert. Die Untersuchungen zeigen, daß sich das Altkristallin während der Alpinen Orogenese nicht als einheitliche, steife Deckeneinheit verhalten hat, sondern eine Krustenverdickung erfahren hat, die zu einer Versenkungsmetamorphose in der mittleren Kreide führte, gefolgt von einer Krustenverdünnung, während der die kretazische Metamorphose-Abfolge stark ausgedünnt wurde.

Im Untersuchungsgebiet, in der nördlichen Kreuzeck-Gruppe, treten zwei Einheiten auf. Sie unterscheiden sich in Gesteinszusammensetzung, struktureller und metamorpher Entwicklung und unterschiedlichen geochronologischen Altersdaten. In der nördlichen Polinik-Einheit hat eine Phase der Krustenverdickung (D_2-Deformation) zu einer Versenkungsmetamorphose geführt, die maximale Temperaturen von 620±60°C bei 6,25±1,25 kb Druck um ca. 100 Ma, erfahren hat. In der südlich gelegenen Strieden-Einheit hat die kretazische Metamorphose die Bedingungen der Grünschieferfazies nicht überschritten und überprägt eine variszische Hochtemperatur-Metamorphose. Eine von hohen Strain-Raten und dem Vorkommen von Myloniten gekennzeichnete Deformationszone (D_p-Deformation) trennt die beiden Einheiten, und befindet sich an der Basis der Strieden-Einheit. Bewegungsanzeiger, Metamorphose-Sachverhalte und geochronologische Daten deuten darauf hin, daß die Strieden-Einheit die Polinik-Einheit in NW-Richtung überfahren hat, während die beiden Einheiten von der kretazischen Metamorphose abkühlten (90–60 Ma). Dabei wurden 2–8 km der kretazischen Metamorphoseabfolge herausgeschnitten.

Diese Ergebnisse werden präsentiert und im größeren Rahmen der alpinen geologischen Entwicklung in den Ostalpen diskutiert.

Abstract

This study presents detailed structural, metamorphic and geochronological data from the Altkristallin (Kreuzeck Mountains) in the SE Tauern area. Evidence is presented which shows that the Altkristallin did not behave as a rigid body during Alpine convergence in the Cretaceous, but has experienced crustal thickening resulting in mid Cretaceous burial metamorphism, followed by post-metamorphic crustal thinning, which substantially thinned the Cretaceous metamorphic sequence.

In the study area two units can be distinguished, which differ greatly in lithologies, structural and metamorphic history and geochronological age data. In the north the Polinik Unit was affected by crustal thickening (D_2 deformation) prior to the burial metamorphism which reached peak temperatures of 620±60°C at 6.25±1.25 kb pressure at ca. 100 Ma. In the south, in the Strieden Unit, the Cretaceous metamorphism did not exceed lower greenschist facies conditions, and overprints a Variscan high temperature metamorphism. A discrete zone of high strain deformation (D_p deformation), characterised by the wide-spread occurrence of mylonites, which formed under greenschist facies conditions (main mylonite zone – MMZ), separates the two units and forms the base of the Strieden Unit. Kinematic indicators, metamorphic evidence and geochronological data, suggest that the Strieden Unit moved over the Polinik Unit in a NW direction, cutting out 2–8 km of the Cretacous metamorphic sequence. This occurred at and following the time when the two units passed through the K/Ar mica blocking temperatures at 90–80 Ma, and continued until 60 Ma.

These results are presented and discussed within the wider context of the Alpine orogeny.

1. Introduction

This publication presents a detailed study of part of a large allochthonous crystalline basement thrust sheet, referred to as the Altkristallin, in the Eastern Alps of Austria. The structural and metamorphic history of this substantial tectonic unit has important implications for our understanding of the behaviour of deeper crustal levels in zones of continental collision.

The Eastern Alps form part of a belt of intense deformation between the European Plate and the Adriatic region (Adria). It is not clear whether Adria acted as an

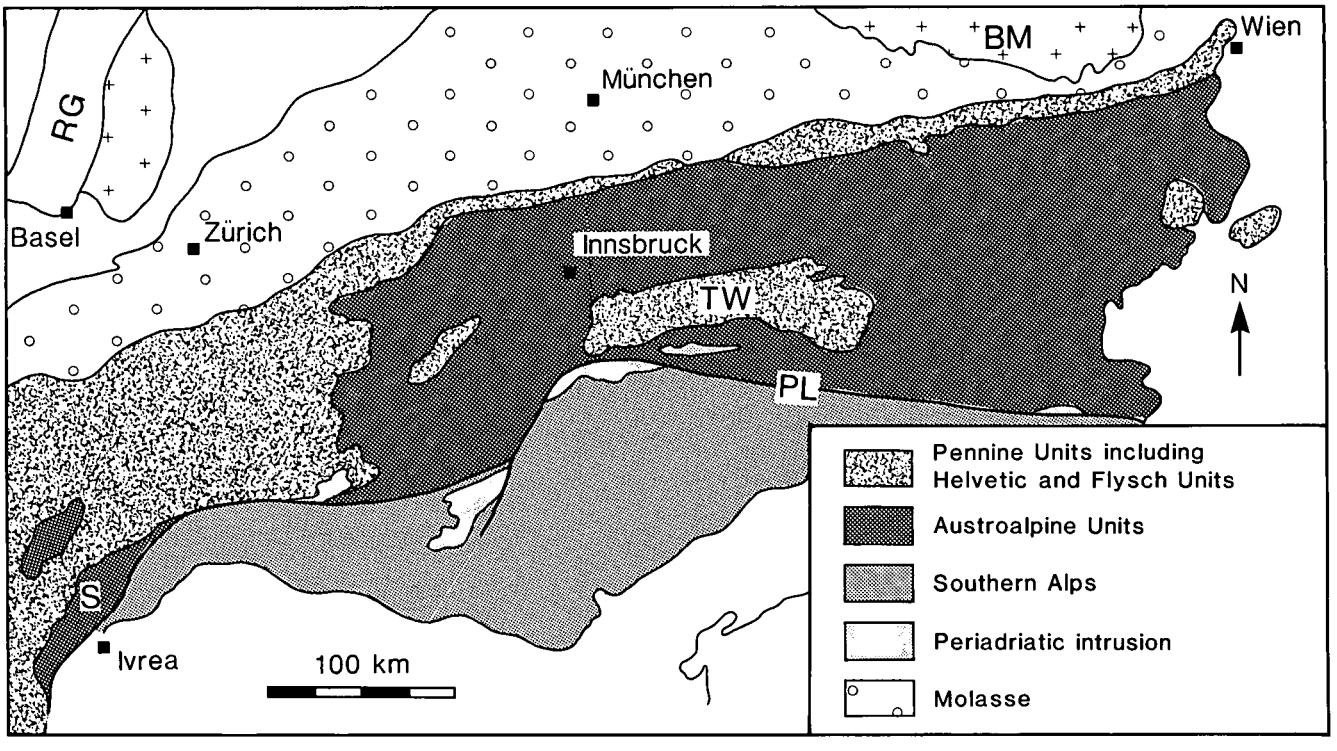

Text-Fig. 1.
Generalized geological map of the European Alps showing extent of the Austroalpine and Pennine units and major structural features.
TW = Tauern Window; PL = Periadriatic Lineament; S = Sesia Zone; RG = Rhine Graben; BM = Bohemian Massif.

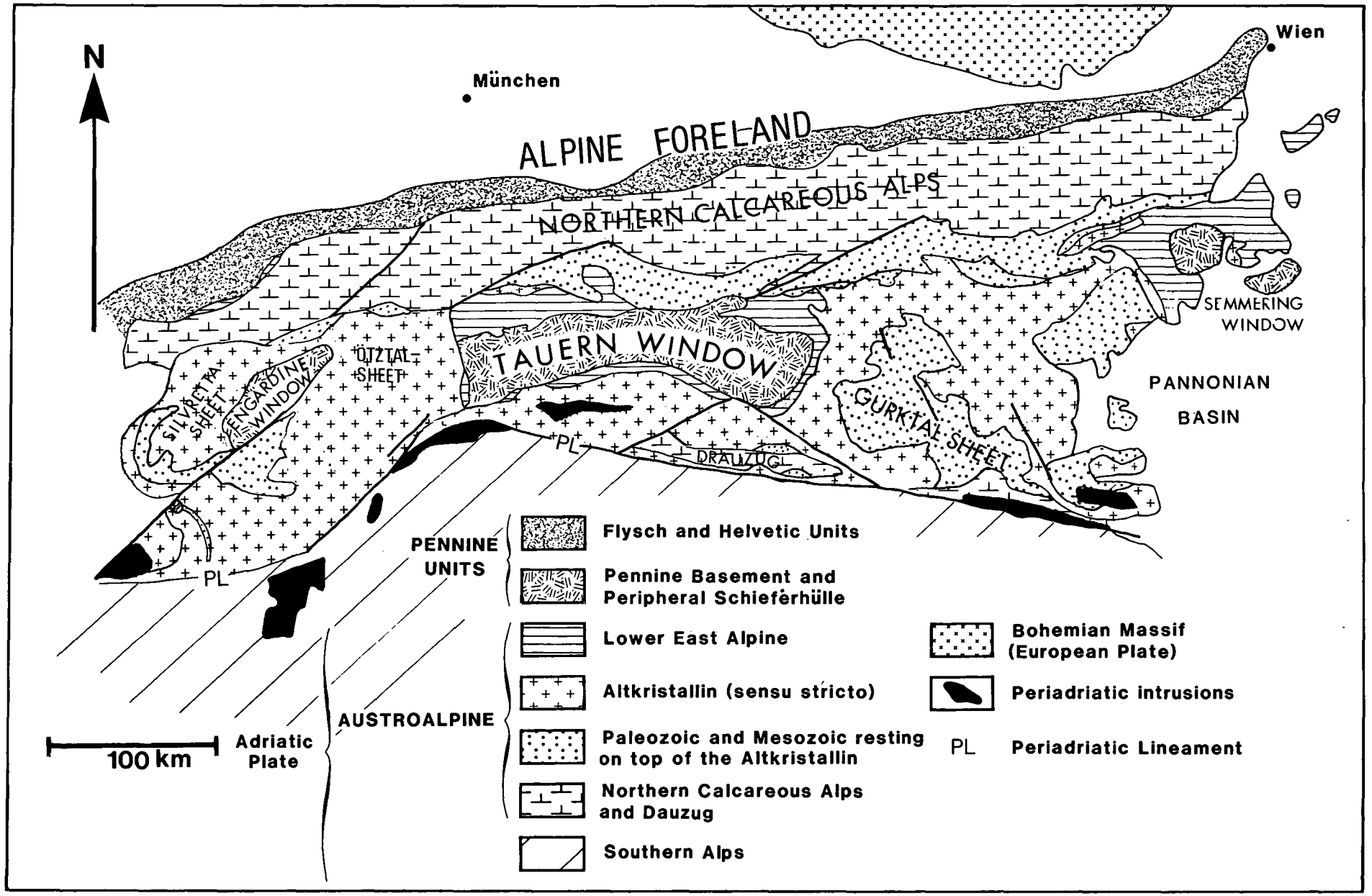

Text-Fig. 2.
Generalized geological map of the Eastern Alps, showing extent of the Altkristallin and its Palaeozoic and Mesozoic cover rock sequences.

independent microplate or as a promontary of the African plate (PLATT et al., 1989; DEWEY et al., 1973, 1989). From the Permian to early-mid Cretaceous, extension in the Tethyan region produced a broad zone of oceanic and thinned continental crust, referred to as the Pennine domain, between the two major plates (FRISCH, 1979). During subsequent convergence between Adria and Europe, the basement and its sedimentary cover were shortened, with the emplacement of the southern continental margin (Austroalpine nappes including the Altkristallin) onto the oceanic Pennine domain (Fig. 1). Continental collision between Adria and the European continental margin (Bohemian massif), marked by the onset of deformation in sediments on the stable European foreland, occurred in the Tertiary (OBERHAUSER, 1980; PLATT, 1987).

Allochthonous and para-allochthonous units can be studied best in tectonic windows, such as the Tauern Window, in the axial zone of the Eastern Alps. The largest of these allochthonous sheets is the Altkristallin, consisting of pre-Mesozoic crystalline rocks, and forming a more or less continuous E-W trending belt, ca. 500 km long and 50–130 km wide, extending the entire length of the Eastern Alps into Switzerland (Fig. 2). Mesozoic metasedimentary rocks extend beneath the Altkristallin for at least 120 km in a N–S direction.

2. The study area

The study area lies in the SE corner of the Tauern Window and is entirely within the Altkristallin rocks of the Kreuzeck mountains (Fig. 3). In the north, a major subvertical NW trending fault, which follows part of the Möll valley (Mölltal fault zone), separates the Altkristallin from the Pennine Units, exposed in the Tauern Window. South (15–20 km) of the edge of the Tauern Window, the Altkristallin is overlain by Palaeozoic phyllites, which in turn are unconformable overlain by the Permian and Mesozoic sediments of the Drauzug.

The previous work in the SE corner of the Tauern Window has been mainly geochronological studies, both within the Altkristallin and also across the margin of the Tauern Window (OXBURGH et. al., 1966; BREWER, 1969, 1970; LAMBERT, 1970; HAWKESWORTH, 1976; WATERS, 1976; DEUTSCH, 1984). The pattern of geochronological ages will be described in detail in Part 5.

Major structural subdivision of the Study area

Lithological layering, prominent schistosity, major fault and fold structures trend E to SE. The prominent foliation generally dips towards the south, so that on a km-scale the northern parts of the area are at structurally deeper levels, with respect to the foliation, than the southern parts.

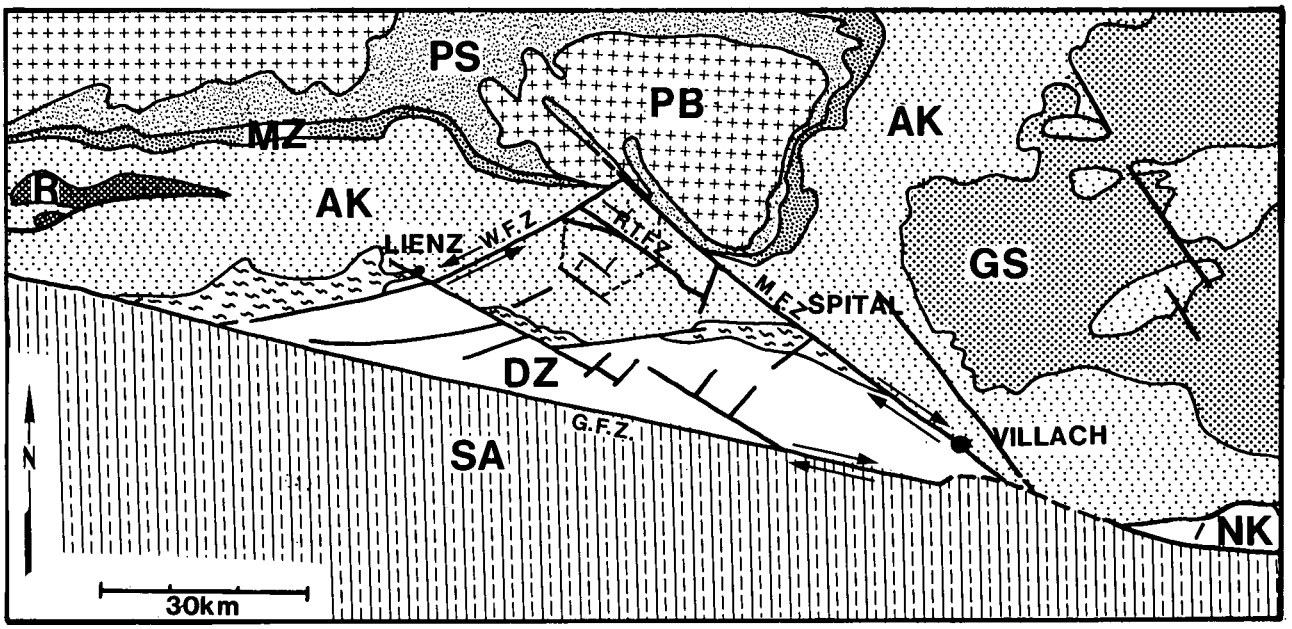

PB Pennine Basement
PS Peripheral Schieferhülle
MZ Matrei Zone
AK Altkristallin
GS Gurktal-sheet
DZ,NK Drauzug,Northern Karawanks
Phyllites
SA Southern Alps
R Rieserferner Intrusion
G.F.Z. Gailtal-fault zone
M.F.Z. Mölltal fault zone
W.F.Z. Wöllatratten faultzone
R.T.F.Z. Ragga Teuchl fault zone

Text-Fig. 3.
Generalized geological map of the south-east Tauern Window, showing location of the study area.

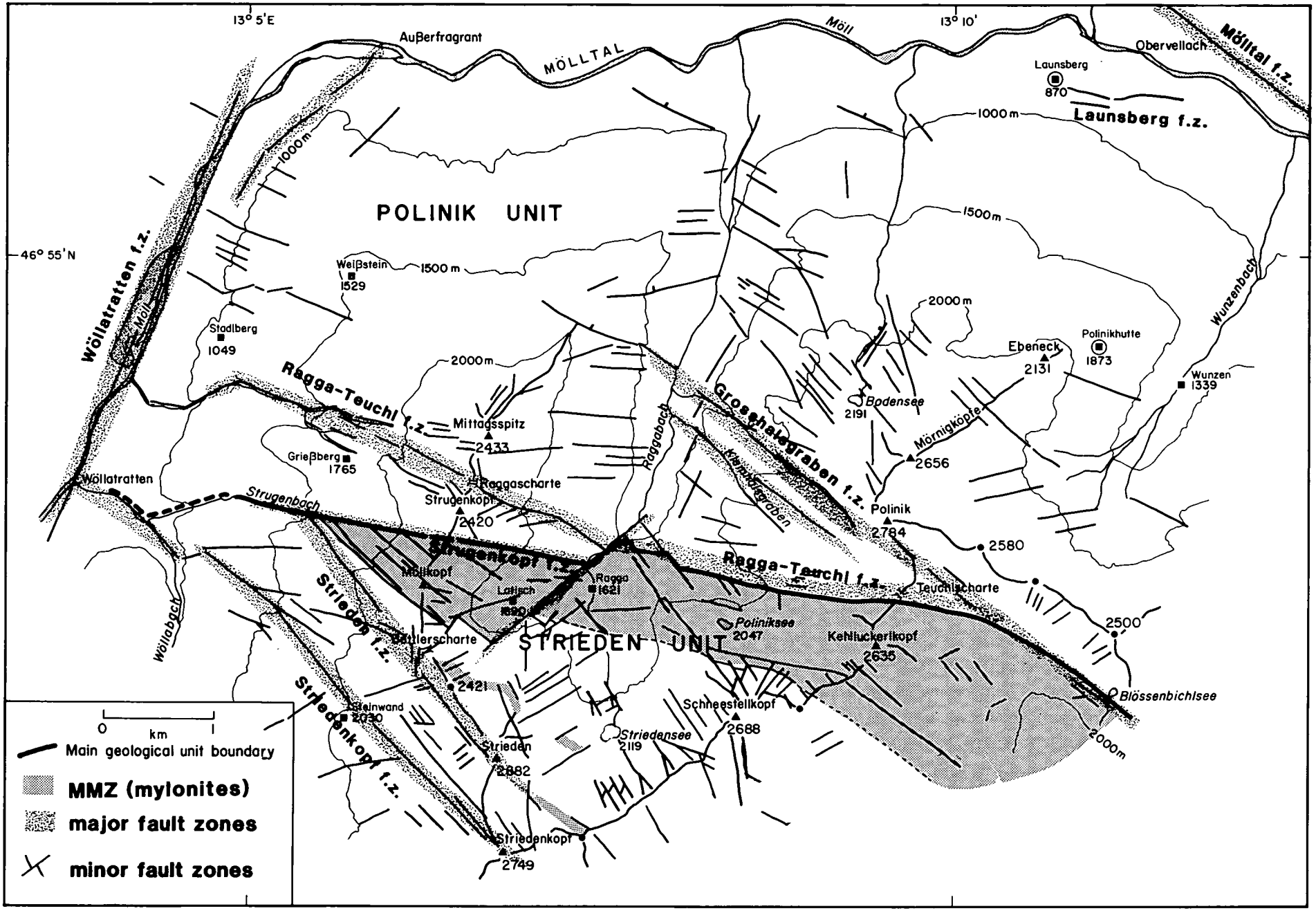

Text-Fig. 4.
Map of the study area, showing the locations of the Polinik and Strieden Units.
Also shown are major structural features, such as a zone of intense deformation at the boundary between the Polinik and Strieden Units, referred to as the main mylonite zone (MMZ), and other minor mylonite zones in the Strieden Unit and steeply dipping brittle fault zones.

An important zone of deformation within the Altkristallin, characterised by the widespread occurrence of mylonites (Fig. 4), trends WNW and marks the boundary between two distinct units which differ greatly in lithology, deformation and thermal history, with different K/Ar ages. Concordant K/Ar mica ages of c. 80 Ma are found north of the mylonites, whereas within them and further south, ages become progressively older towards the south, ranging between 100– 320 Ma (Fig. 41). The northern unit is called the Polinik Unit, named after the prominent mountain, Mt. Polinik (2784 m). The southern unit is called the Strieden Unit after Mt. Strieden (2682 m). The boundary between the two units is at the northern limit of the mylonites. This is marked in the study area by subvertical and east-trending, predominantly brittle, fault zones, which rework the mylonites along their length. These are referred to as the Ragga – Teuchl fault zone in the east and the Strugenkopf fault zone in the west (Fig. 4).

The organisation of this paper is based on the structural division described above. The geology of the Polinik and Strieden Units is described in sections 3 and 4 respectively. In a concluding section, this is discussed within the wider context of the geological history of the Eastern Alps.

3. The Polinik Unit, its Structural and Metamorphic History

3.1. Lithologies in the Polinik Unit

Medium grained (1–5 mm) quartzo-feldspathic schists and gneisses, referred to as the Polinik Schists, predominate. They contain discontinuous bodies of amphibolite, augengneiss and pegmatite. Garnet, staurolite and kyanite-bearing schists (aluminous metapelites) are rare, found only in the Mt.Polinik and Griessbergalm areas.

Augengneisses

Biotite augengneisses contain large (up to 5 cm long) and numerous K-feldspar augen, aligned within the foliation. They have been found in only one locality, about 500 m south of the Weissenstein Alm, forming tens of metres of exposure along a forest road, and apparently are concordant with the main schistosity.

Amphibolites

Amphibolites can be subdivided into two groups, depending on whether they contain clinopyroxene (cpx). Cpx-rich amphibolites contain abundant garnet, which are enclosed in pale green symplectites after clinopyroxene, with relict omphacite. These rocks have been derived from eclogites with the original mineral assemblage omph – gt – rut – qz (see appendix A for mineral abbreviations), preserved as relicts in the cores of amphibolite pods, where the rock is massive and contains randomly oriented pale green cm-sized columnar pseudomorphs of omphacite, surrounded by dark greeen amphibole, plagioclase and irregularly shaped garnet (0.2–1 cm in diametre). Margins of amphibolite pods are rich in biotite and oligoclase blasts which overgrow the contact with the surrounding schists and gneisses.

Unusual amphibolite pods are found along the Mörnigköpfe ridge, containing the texturally equilibrated mineral assemblage gt – cpx (di) – hb – qz ± plag.

Amphibolites, which do not contain clinopyroxene, contain garnet and have relict textures (plagioclase-hornblende symplectites after clinopyroxene and mineral zoning), suggesting a derivation from eclogite amphibolites.

Pegmatites

Pegmatites are rich in muscovite and plagioclase and occur sporadically throughout the Polinik Unit. They are intensely deformed, forming sheet-like bodies or irregular-shaped pods (up to 5 m wide), and may be locally concordant with the schistosity of the host rock, though cross-cutting on a large scale (Plate 1 – Fig. 6). In the core of metre thick pegmatite bodies, muscovite books, up to 5 cm across and 0.5 cm thick, are embedded in a coarse-grained plagioclase and quartz matrix which shows no shape fabric. Towards the margins, the grainsize progressively decreases and minerals have a strong planar fabric.

3.2. Deformation History of the Polinik Unit

Detailed studies in the Polinik Unit have made it possible to relate metamorphic and microstructural data to large scale structures and the tectonic evolution of the area.

Sets of structures have been correlated, using criteria such as orientation, style and position in the locally established deformation sequence.

Five major groups of regional structures can be distinguished (D_1 – D_5). F_1, F_3 and F_4 regional fold phases correspond with the sequence F_1, F_2, F_3, established

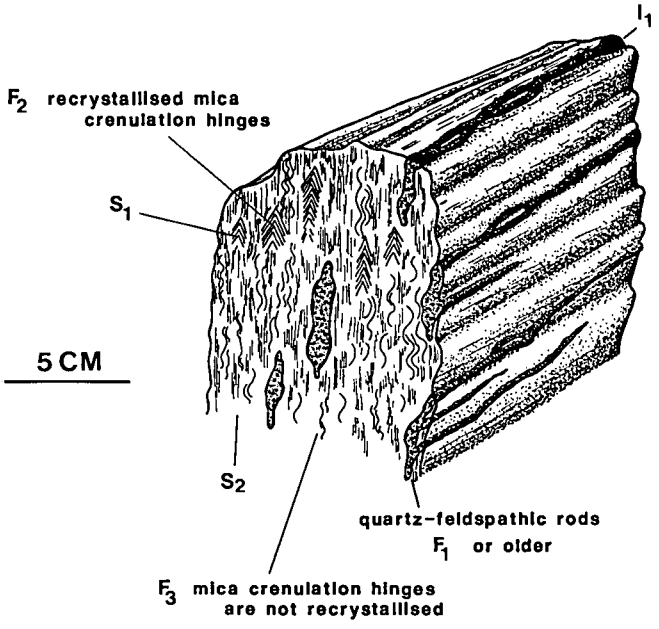

Text-Fig. 5.
Sketch of structural elements in quartzo-feldspathic schist, in the Raggaalm area (sample 7), showing refolding of D_1 fabrics during D_2 and D_3 deformation.
An early quartzo-feldspathic and mica-rich foliation (S_1) is crenulated by F_2 folds. F_1 quartz fold hinges define a lineation l_2 which is subparallel to the F_2 crenulation lineation. Subsequent crenulation occurred during D_3, and micas have not recrystallised in F_3 fold hinges.

by OXBURGH (1966) and WATERS (1976) in rock units equivalent to the Polinik Unit. The deformation history and major structures are summarised in Table 1 and in a cross-section (Fig. 9).

D_1 deformation resulted in the earliest regional structures, though evidence for earlier deformation has been recognised locally. Variscan pegmatites were intruded after D_1 deformation and are intensely deformed by D_2. D_2 deformation is post-dated by a Cretaceous amphibolite facies burial metamorphism, which was followed soon after by D_3. During D_3, the Polinik Unit was deformed into a km-scale recumbent fold, closing to the south. It was during or after the final stages of D_3 that the Polinik Unit was juxtaposed with the Pennine tectonic units. However, Tertiary movement along the Mölltal fault zone has obscured the original contact relationships. Younger deformation (D_4–D_5) resulted in regional warping and brittle faulting.

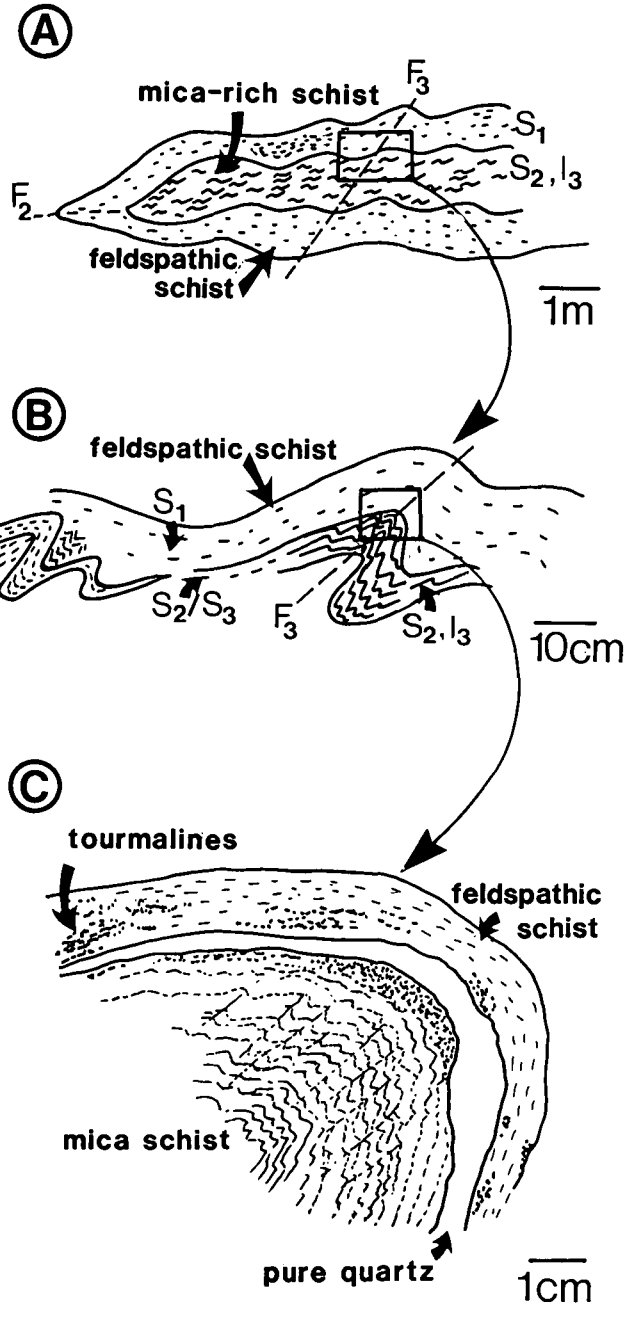

Text-Fig. 6.
Sketches of structural elements in Polinik Schists (ca. 1 km SW of Mt. Polinik), at a variety of scales.

a) Sketch of a tight, m-scale F_2 fold, defined by a deformed quartzo-feldspathic layer. Mica schists contain an axial planar cleavage (S_2), which is crenulated (F_3).

b) Sketch of crenulated mica schist in the cores of minor F_3 folds. Quartz layers on F_3 fold limbs are attenuated and are not crenulated.

c) Thin section of similar style F_3 fold, showing mm-scale F_3 crenulation of mica schist.

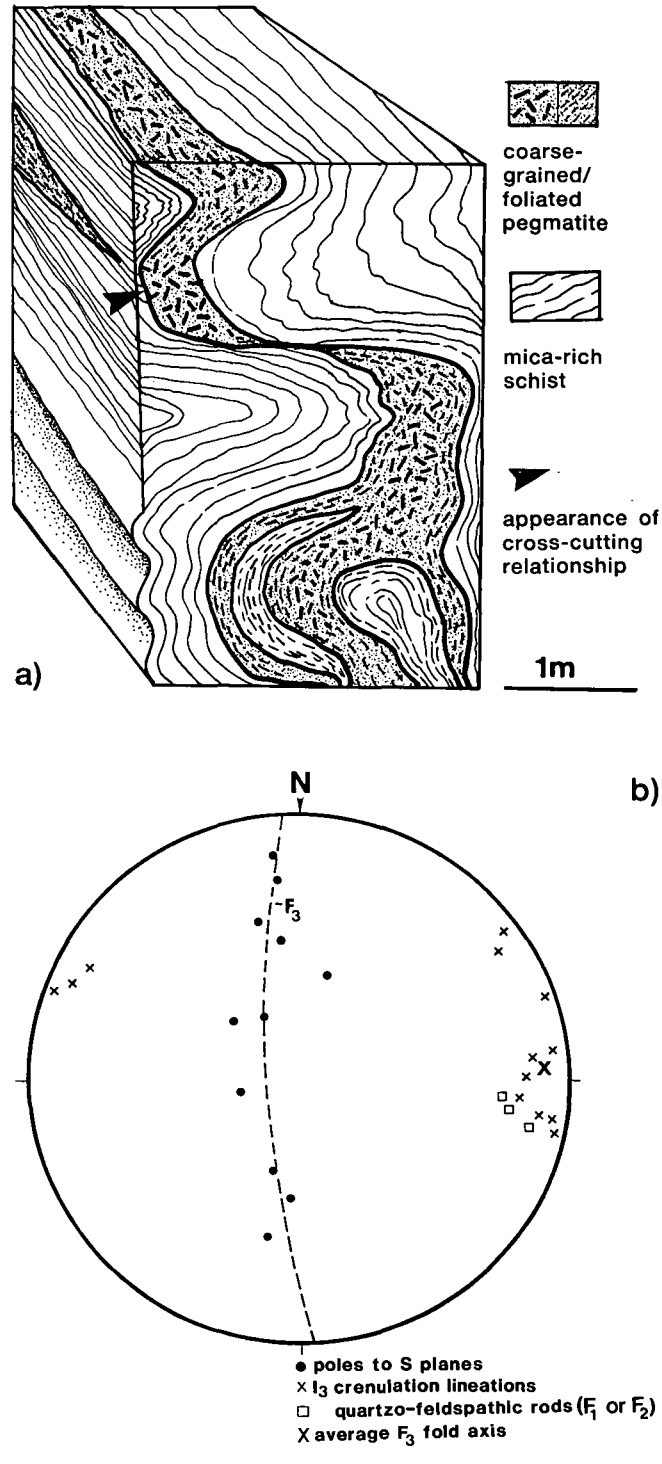

Text-Fig. 7.

a) Block diagram of a deformed pegmatite, intruding mica schist in the Polinik Unit, NNE of Bodensee. A pronounced foliation in the pegmatite (S_2), subparallel to the pegmatite margins, is folded by F_3 cascading subhorizontal folds. See Plate 1 – Fig. 6.

b) Equal area lower hemisphere stereographic plot of poles to S_2 foliation in the deformed pegmatite and the enclosing schists, and lineations. Poles to S_2 foliation lie on great circle with pole (X) consistent with F_3 fold axes.

D_1

D_1 fabrics are defined by a metamorphic segregation into mica and/or amphibole and quartzo-feldspathic layers (S_1), which are deformed by D_2 structures. A strong linear fabric (l_1), best developed in gneisses, is defined by the preferred orientation of stretched and broken garnets, quartzo-feldspathic rods and quartz-ribbons. Dismembered fold hinges (rods) also define a strong linear anisotropy (l_1 or older, Fig. 5).

D_2

D_2 caused a crenulation and substantial modification of S_1 (Figs. 5, 6). On a metre to 10's of metre-scale, S_1 is folded throughout the Polinik Unit into conspicuous 'M', 'Z' and 'S'-shaped tight folds (F_2), (Fig. 8, Plate 1 – Figs. 3–5), with subhorizontal fold axes which are nearly parallel to l_1 (within ±20°, Fig. 9B). However, no large scale D_2 folds have been found, though the change in minor fold asymmetry suggests a series of km-scale folds with subhorizontal E-trending fold axes. A variably developed crenulation cleavage, S_2, locally transposes the S_1 foliation and becomes the dominant foliation in less competent mica-rich lithologies. Eclogite amphibolite pods are aligned parallel to the S_2 foliation.

A pronounced lineation (l_2), which is either a crenulation lineation or the intersection of S_2 with S_1, parallels F_2 fold axes. The S_2 foliation is found in pegmatites, particularly at their margins (Fig. 7A, Plate 1 - Fig. 6). This is the earliest deformation fabric in the pegmatites, and therefore the pegmatites must have been emplaced after D_1, but prior to D_2. Rb/Sr two-mineral isochron ages from the coarse-grained centre of these pegmatites give ages of ca. 254 Ma (CLIFF, pers. com.). These are assumed to be emplacement ages and therefore post-date D_1 deformation, but pre-date D_2 deformation.

Inter D_2 – D_3 amphibolite facies metamorphism

Extensive growth of staurolite, kyanite, plagioclase and locally garnet in metapelites post-dates D_2 and pre-dates D_3. Staurolite, kyanite and individual mica laths cross-cut the S_2 foliation and plagioclase helicitically overgrows the earlier fabrics (Plate 2 – Figs. 1–3). K/Ar radiometric ages suggests that this mineral growth occurred in the Cretaceous (ca. 100 Ma). The P/T conditions during metamorphism are discussed in section 3.3.

D_3

Subhorizontal cascading asymmetrical folds (F_3) occur throughout the Polinik Unit (Fig. 9, Plate 1 – Figs. 1–5), trending E–NE, parallel to l_1 and l_2, and forming coaxial interference folds with F_2 (Fig. 7B, 9B). A distinct variation in fold asymmetry suggests the existence of a km- scale recumbent fold, closing to the south (Fig. 9). Crenulation of S_2 defines a crenulation lineation (l_3), which is parallel to F_3 axes. In crenulation hinges, staurolite, kyanite and micas are bent and broken (Plate 2 – Figs. 4–6) and have been mechanically rotated and transposed into the foliation.

In areas of intense D_3 deformation, kyanite and staurolite are partly altered to fine-grained aggregates of sericite, margarite and chlorite; garnets are partly replaced by chlorite. This alteration may have occurred during or after D_3 deformation.

D_4 and younger deformation

During D_4, the whole area was warped by upright, open, E-trending folds (Fig. 9), forming open antiforms and tightly pinched synforms, developed on a metre to a kilometre scale. Steep fault zones, which have accommodated several kilometres of both strike slip and dip slip displacement, cut D_4 and all earlier structures. These faults resulted in both N–S-shortening and E–W-extension. Pseudotachylite was generated along some fault surfaces (HOKE, in prep.).

3.3. Inter D_2–D_3 Cretaceous Amphibolite Facies Metamorphism

P/T conditions during the inter D_2–D_3 metamorphism have been estimated from microprobe chemical and textural analyses of staurolite, garnet and kyanite-bearing schists (aluminous metapelites). Samples were collected from a section between Mt. Polinik and the Polinik Alpine Hut (samples 68, 83, 81.3, 81.1, 81, 8, 77; Tables A,B).

3.3.1. Mineral phases

Garnets

Three generations of garnets have been recognised (Fig. 10, Plate 2 – Fig. 1) and all garnets may show some degree of chemical zoning.

- In some garnets, cores (garnet I) can be optically distinguished from their rims (garnet II), (Fig. 10). Garnet I tends to be full of quartz and tiny highly birefringent inclusions, but generally has a uniform chemical composition: almandine 73–75 mol.-%; spessartine 1.5 –3.6 mol.-%; pyrope 14–20 mol.-%; grossular 2–6 mol.-%. A chemical zonation is only developed near garnet I rims, where there is a slight decrease in Mg, and increase in Fe, while Ca and Mn show no significant variation.
- Garnet II is the most commonly found garnet generation, developed either as a clear rim around garnet I or as euhedral or spongy grains less than 1 mm in size. Garnet II often contains elongate rutile inclusions, and is found intergrown with staurolite, kyanite, biotite and muscovite.
  Garnet II is characterised by higher Mg (pyrope 18–25 mol.-%) and lower Fe contents than garnet I. The Mg/Mg+Fe ratio is higher and can show a marked variation, suggesting changing equilibrium conditions between ferromagnesian minerals as a result of increasing temperature and probably pressure during garnet growth.
- Garnet III does not contain inclusions and is difficult to distinguish optically from garnet II, though it forms chemically distinctive, narrow, 100–300 μ wide rims around garnet II, or more rarely occurs as swarms of tiny euhedral garnets in a quartz and mica-rich matrix. Garnet III is commonly characterised by a zonation showing a decrease in Mg and increase in Fe content (overall reduction in Mg/Mg+Fe ratio compared to garnet II), and an increase in both Mn and Ca, towards the rim. This suggests growth during the waning stages of metamorphism (HESS, 1971; TRACY, 1979; KERR, 1981). Garnet III

Text-Fig. 8.
Sketch of m-scale, gently plunging, fold interference patterns, observed in the Polinik Schists, in the Mt. Polinik area, produced by superposition of F_3 and F_2 folds.
Sketches are drawn as if viewed towards the west.
a) "S"-shaped F_3 folds on "M"-shaped F_2 folds.
b) "S"-shaped F_3 folds on "Z"-shaped F_2 folds.
Compare with Plate 1.

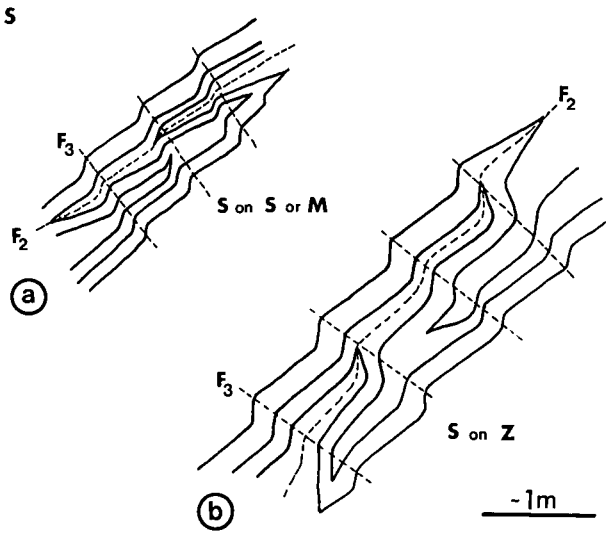

Text-Fig. 9.
Sketch of N–S cross-section through the Polinik Unit, showing an interpretation of the relation between structural elements.
A km-scale recumbent F_3 fold is folded into an F_4 antiformal structure. South of Mt. Polinik the structures are truncated by the Teuchl fault zone, with the formation of a subvertical shear fabric. Dismembered folds (possibly F_3) and a pronounced cleavage (S_3 or younger) occur near the base of the Altkristallin. The basal contact is not preserved in the study area, because it has been displaced by movement along the steeply dipping Mölltal fault zone. This cross-section suggests that the exposed structural thickness of the Polinik Unit, measured perpendicular to the prominent foliation, is not more than 2 km. Orientation data from Polinik Schists in the Mt. Polinik area are shown in an equal area lower hemisphere stereogram.

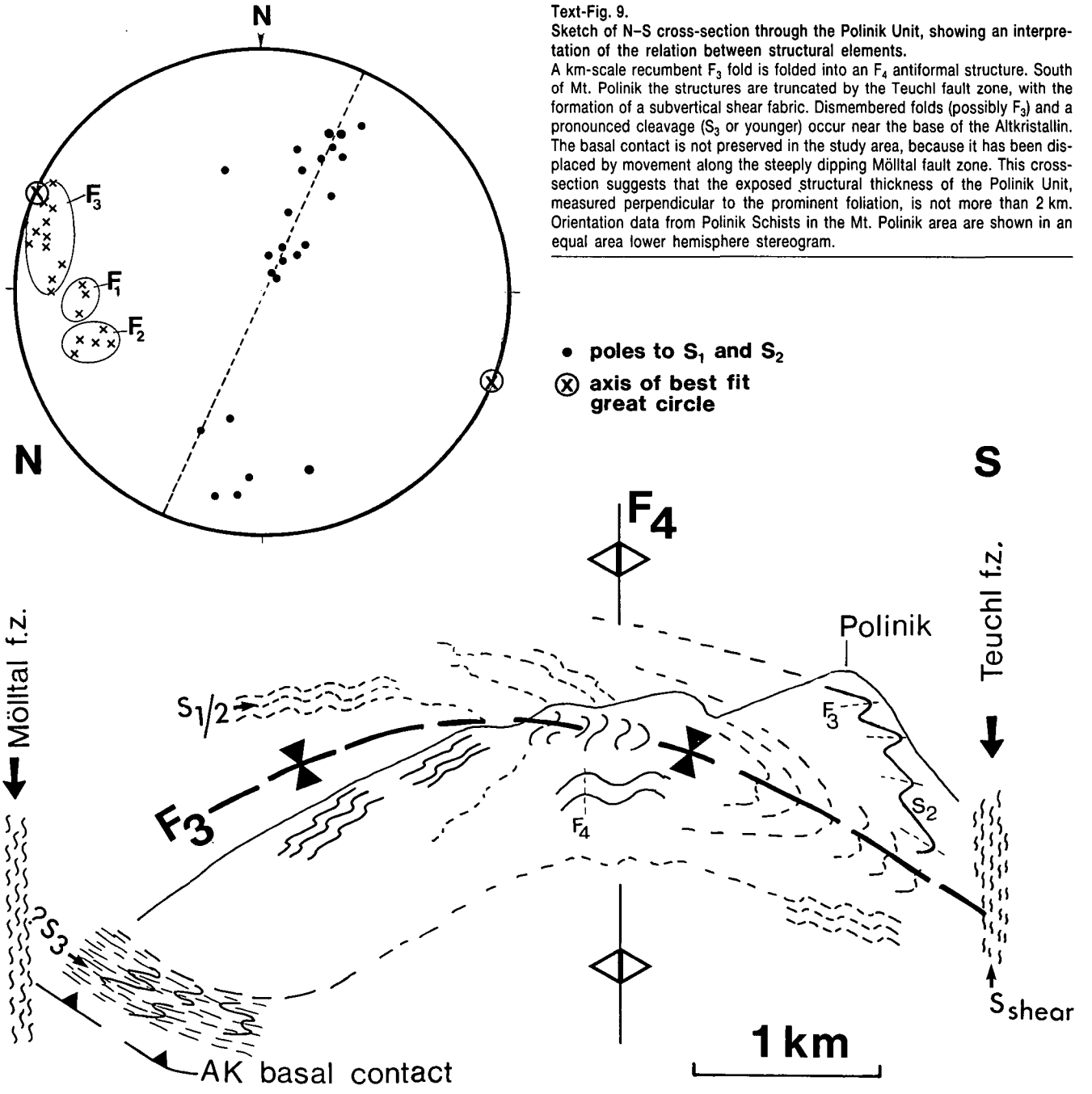

Table 1.
Summary diagram of the deformation history of the Polinik Unit, showing the correlation of fabric elements with large-scale structures.

DEFORMATION	AGE	METAMORPHISM	TECTONIC SIGNIFICANCE	POLINIK SCHISTS (METAPELITES, QUARTZOFELDSPATHIC SCHISTS) Large scale structures	Microstructures	MAFIC LITHOLOGIES Large scale structures	Microstructures	OTHER LITHOLOGIES
		?	? crystalline basement terrain					
Pre-D_1				pre-S_1: local occurrence in Mittagsspitz area		?		?
	Variscan	Upper greenschist facies to amphibolite facies	Ductile deformation. Major nappe displacement. Incorporation of mafic rocks/slivers into paragneiss-series of Polinik Unit.	S_1 Segregated quartzofeldspathic and mica-rich layers contain isoclinally folded and stretched quartzo-feldspathic rods (F_1 or earlier)				
D_1			Strong mineral lineation - possible transport direction during D_1	ℓ_1 mineral elongation lineation (? transport direction). Strong linear anisotropy.	Quartz-ribbon texture. Garnets: flattened and aligned in S_1. Quartzo-feldspathic rods	?		?
	post-Variscan	Upper greenschist facies to amphibolite facies	Crustal shortening: Regional folding ? Underplating of Polinik Unit	F_2 fold axes subparallel (±20°) to ℓ_1 rods. Folds have been modified to class 2 similar style tight to isoclinal folds during later deformation. Asymmetric minor folds.	Quartz ribbons folded.	Amphibolite-facies: amphibole and plagioclase inclusions in garnet cores		Emplacement of augengneisses post-dates ℓ_1. Emplacement of pegmatites: (>254 Ma) S_2 foliation in pegmatites (developed best along pegmatite margins) S_2 predominant foliation in augengneisses
D_2								
	?120 Ma	? P-metamorphism				Eclogite facies: garnet-omphacite-rutile-quartz. No shape or cryst. preferred orientation. Omphacite poikilitically overgrows euhedral garnets		
				? restricted occurrence of metre-size chevron folds (area 4)				

	~105 Ma	Thermal climax: amphibolite facies metamorphism	Prograde thermal event; thermal re-equilibration	S_2 axial planar cleavage in mica-rich lithologies Interpreted mineral assemblage: kyanite-staurolite-biotite-muscovite-quartz-plagioclase. Recrystallisation of quartz and mica-fabric. Crosscutting staurolite & kyanite.	Alteration of eclogite assemblage to amphibolite facies mineral assemblages Interpreted mineral assemblage: garnet-amphibole-plagioclase-biotite-sphene-quartz		
D_3	**80 Ma**	Cooling ~80-90 Ma Muscovite and biotite cooling ages Greenschist facies disequilibrium assemblages: Extensive hydrothermal alterations.	Recumbent folding. Possible emplacement of Polinik Unit onto Matrei Zone and Peripheral Schieferhulle Possible formation of a major shear zone between the Polinik and Strieden Units.	F_3 recumbent folding ~co-axial with ℓ_1 and F_2 Crystals bent and broken in crenulation hinges; Quartz subgrain formation can show preferred crystallographic orientation. ℓ_3 crenulation of S_2 Retrograde alterations of staurolite and kyanite to fine grained aggregates of sericite, chlorite and margarite Extensional vertical chlorite and quartz-filled veins oriented perpendicular to F_3 fold axes in fold cores. S_3 in intensely deformed areas (area 5, south of bend in river Möll). Axial planar cleavage. Predominant foliation in area 5: phyllonitic foliation. Breakdown of garnet to chlorite postdates S_3 formation; growth of epidote and zoisite in chlorite pseudomorphs. Intrusion of calcite veins	Alignment of minerals in foliation Hydrothermal alterations: new formation of chlorite, calcite, sphene, epidote, zoisite	F_3 folding of foliated pegmatites
		Tauernmetamorphism only affects					
D_4	~30 Ma	N-part lower greenschist facies	Monoclinal structure Culmination of the Polinik Unit N-S shortening	F_4 Upright folding with open antiforms and tightly pinched synforms effects the whole area and causes a regional reorientation of the earlier structures. With increasing D_4 increasing degree of retrograde alterations. ℓ_4 in area 5			
D_5		uplift and cooling	Predominant strike-slip faulting Predominant dip-slip displacement along faults and accompanying uplift.	Further N-S shortening is achieved by strike-slip movement along parallel sets of steep ~NW-SE and NE-SW trending conjugate faults Reactivation of faults as dip-slip faults	mesoscopic structures involve kink-folds, fracturing and flexural slip folding associated with faulting.		

has probably not achieved equilibrium with the other garnets, since it only forms narrow rims around garnet II.

Staurolite

Zoning patterns in staurolites are related to replacement of staurolite by white mica shimmer aggregates. Zn, released by the breakdown of staurolite in this retrograde reaction, was incorporated into the remaining staurolite to form a Zn-rich rim (up to 2.5 % ZnO), similar to the retrograde Mn-rich rims in garnets. Otherwise, staurolites appear to be unzoned.

Biotite

Individual biotite grains are always of uniform composition, however, biotites adjacent to garnets or

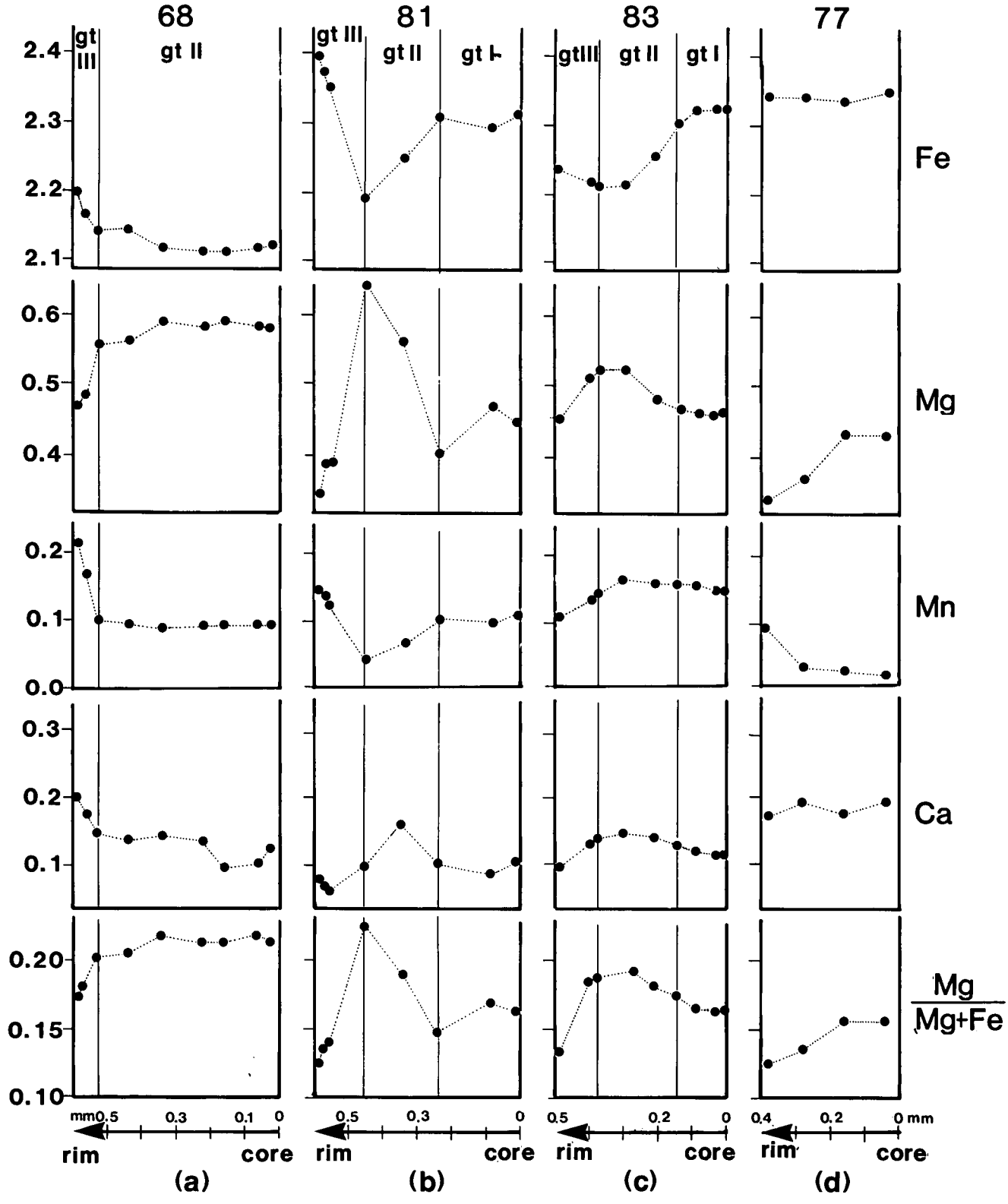

Text-Fig. 10.
Microprobe profiles of chemical composition across garnets in the Polinik schists (samples 61, 81, 83, 77; see Appendices B, C, D), showing zoning and compositional variations in different garnet generations (gt I, gt II, gt III).

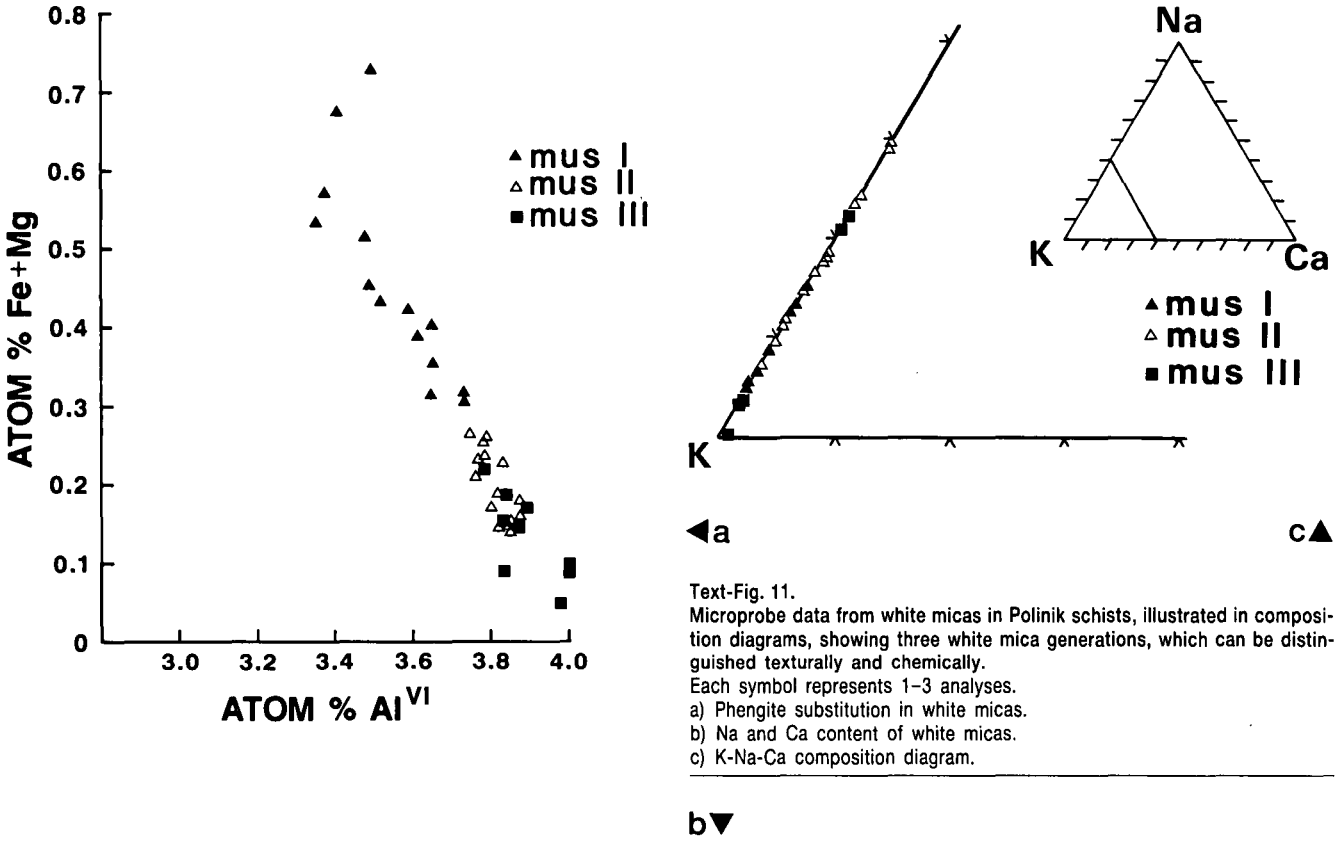

Text-Fig. 11.
Microprobe data from white micas in Polinik schists, illustrated in composition diagrams, showing three white mica generations, which can be distinguished texturally and chemically.
Each symbol represents 1–3 analyses.
a) Phengite substitution in white micas.
b) Na and Ca content of white micas.
c) K-Na-Ca composition diagram.

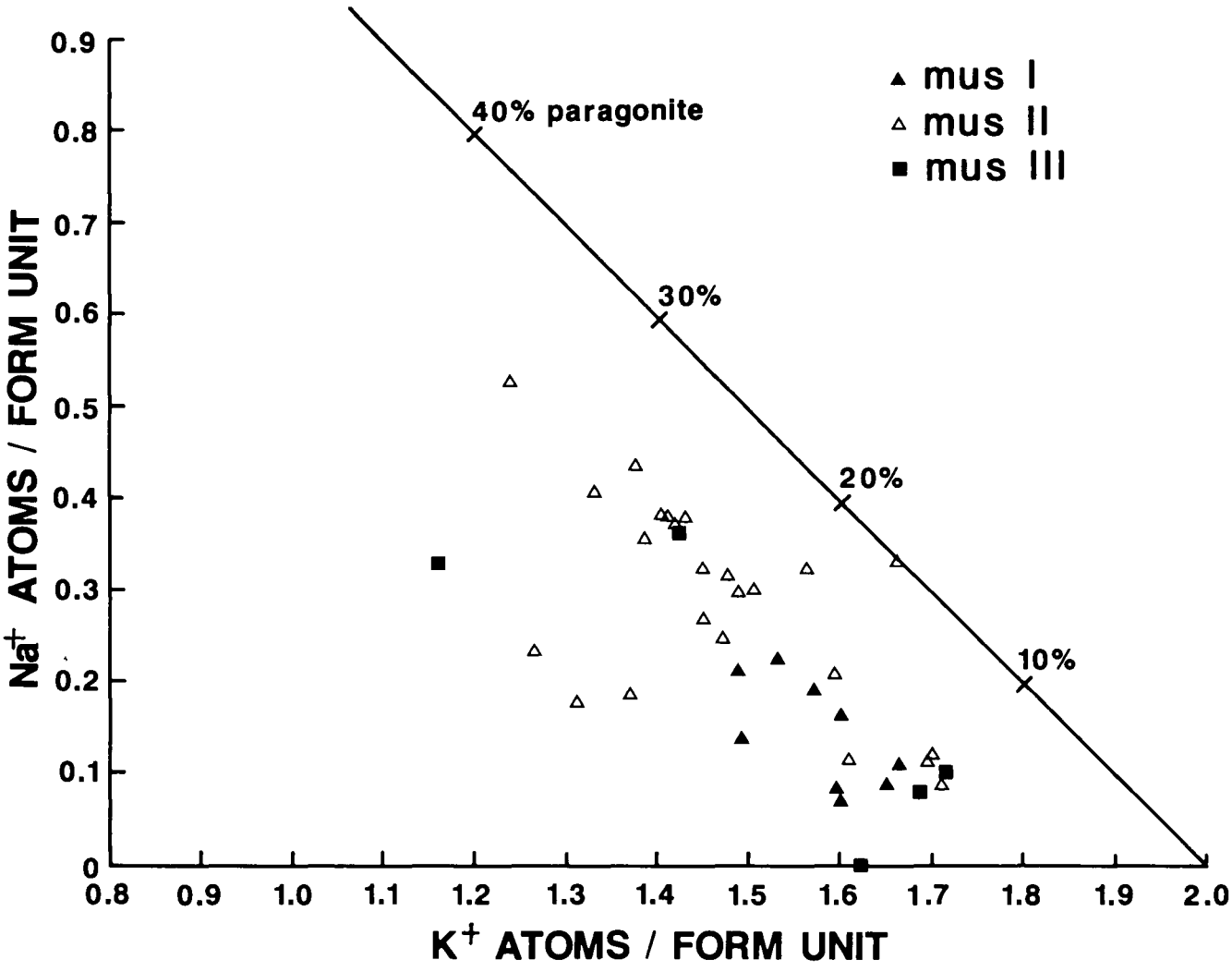

staurolites (with Mg-poor rims) can be richer in Mg than those away from other Fe-Mg bearing phases. The garnets have well defined rims, marked by a change in chemical composition, presumably as a consequence of ionic exchange with biotite. For instance, in sample 81, Mg/Mg+Fe ratios vary between 47–49 in biotites next to garnets, and are between 43.5–44 away from other Fe-Mg bearing phases.

All biotites contain significantly more Al than phlogopite and annite. This is largely due to the tschermak substitution $Al^{VI}Al^{IV}$ = (MgFe) $^{VI}Si^{IV}$ (DEER et al., 1966).

White mica

Three generations can be distinguished (Fig. 11):

- Coarse, aligned platy muscovite I, which defines the foliation S_2.
- Coarse, platy muscovite II which cuts across S_2 and, together with staurolite, kyanite, garnet II, biotite and quartz, forms a texturally equilibrated amphibolite facies mineral assemblage.
- White mica shimmer aggregates (muscovite III) which are retrograde and variably replace staurolite and kyanite and also occur in the kinked zones of coarse mica laths.

Fig. 11A illustrates the extent of phengite substitution in the different mica generations (phengite substitution:

$$Al^{3+[IV]} \cdot Al^{3+[VI]} = Si^{3+[IV]} \cdot (Fe,Mg)^{[VI]}).$$

There is a negative correlation between Fe+Mg and Al in the octahedral position, with a higher phengite content in muscovite I compared to muscovite II and III.

The paragonite content also systematically differs in the 3 muscovite generations (Fig. 11B,C). Muscovite I shows the smallest range in content of paragonite, varying between 4.8–15 mol.-%, which is generally lower than that of muscovite II (10–29.5 mol.-%), though partly overlapping with it. No free paragonite was detected in white mica. Muscovite III shows a bimodal distribution, occurring with 0–4 mol-% (almost pure muscovite) and 21–23 mol-% paragonite.

Most muscovites are deficient in alkalies, with Na+K+Ca totalling between 1.4–1.7 atoms per 22 oxygens. This phenomenon is generally attributed to H_3O^+ ions substituting for K^+ and Na^+ in the interlayer sites (BUTLER, 1967; CIPRIANI et al., 1971).

Chlorite

Chlorite variably replaces biotite and garnet. All analysed chlorites are of ripidolite composition (classification of HEY, 1954).

Plagioclase

Three generations of plagioclase have been distinguished:

- Plagioclase I is polysynthetically twinned and tends to be clouded with minute inclusions of probably white mica and/or zoisite. Its composition varies between 10–14 % anorthite with a slight decrease of anorthite towards the rim.
- Plagioclase II often forms clear rims around plagioclase I. It is rarely twinned, however it variably

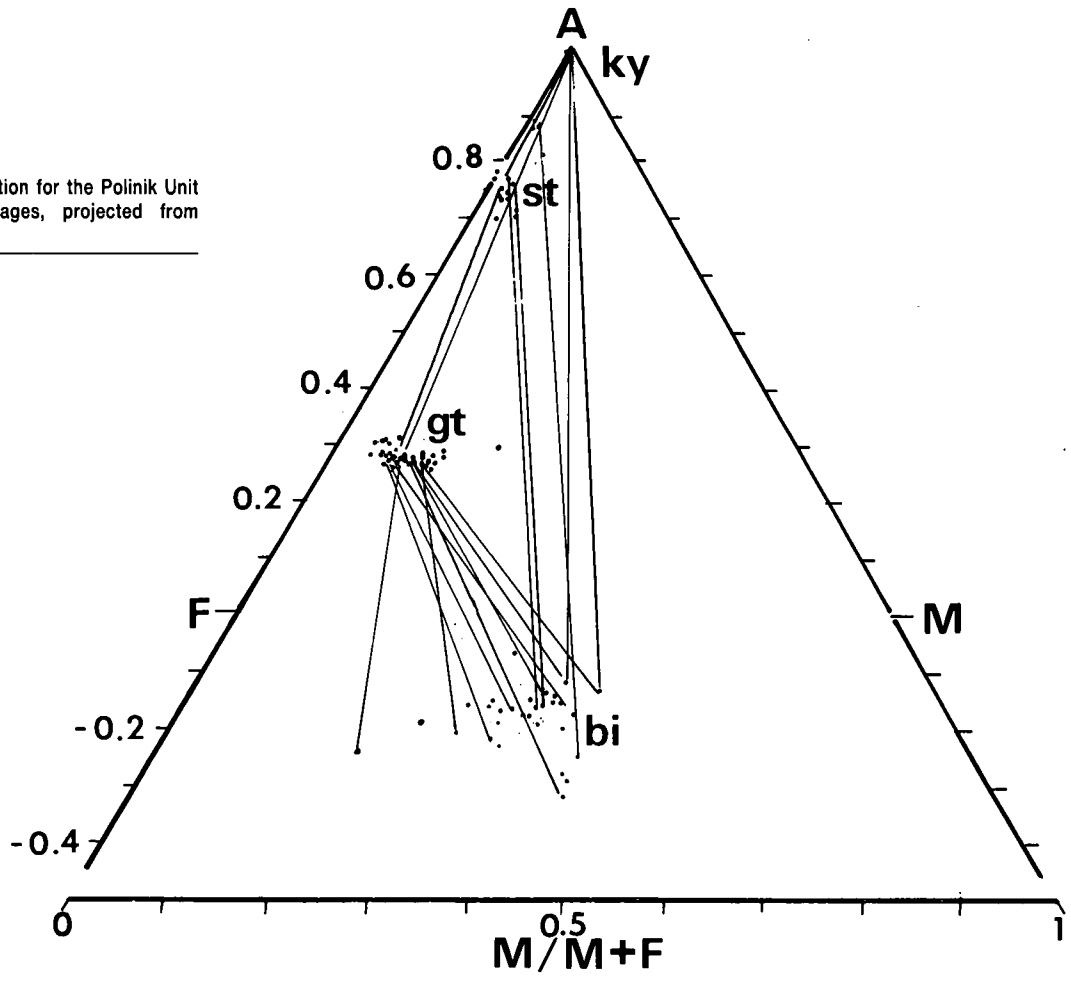

Text-Fig. 12.
AFM Thompson (1976) projection for the Polinik Unit metapelite mineral assemblages, projected from muscovite, quartz and water.

shows "gefüllte" textures, containing white mica microliths. It is the most commonly found plagioclase in metapelites and occurs closly associated with kyanite, staurolite, garnet II, muscovite II and biotite. It overgrows the S_2 foliation helicitically. It either shows a homogeneous composition or is inversely zoned with more albite rich cores and more anorthite rich rims. Compositions vary between 6.48–5.4 mol.-% anorthite and <1 mol.-% orthoclase, with a mean composition of 14 mol.-% anorthite.

Equilibria which might have controlled the composition of plagioclase II include:

$$\text{gros} + 2\,\text{ky} + \text{qz} = 3\,\text{an}$$
$$\text{pg} + \text{qz} = \text{ab} + \text{ky} + H_2O$$

Increasing temperature displaces both these equilibria in favour of the right hand side.

- Plagioclase III is almost of pure albite composition and is found in strongly altered samples associated with white mica shimmer aggregates.

3.3.2. P/T Sensitive Equilibria

The phases quartz – garnet II – biotite – muscovite II – kyanite – plagioclase II – staurolite – rutile – ilmenite form the most common mineral assemblage in Polinik Unit metapelites (Plate 2 – Fig. 2).

Mineral compatibility and phase relations in quartz and muscovite bearing metapelites can be represented in the AFM projection (Thompson 1975), projected from muscovite, provided that H_2O behaved as a perfectly mobile component during metamorphism (Fig. 12).

Internally consistant thermodynamic datasets (Powell & Holland, 1985; Holland & Powell, 1985) and published calibrations of appropriate geothermometers and geobarometers (see below) are used to evaluate the P-T conditions for the amphibolite facies equilibrium mineral assemblages.

The P/T conditions (Fig. 14) can be bracketed by the kyanite stability limits, and by the temperature sensitive breakdown of mica in the equilibrium:

$$\text{pg} + \text{qz} = \text{ky} + \text{ab} + H_2O$$

and by the pressure sensitve equilibrium

$$3\,\text{ilm} + Al_2SiO_5 + 2\,\text{qz} = \text{alm} + 3\,\text{rut}$$

Kyanite stability limits

Kyanite is the only Al_2SiO_5 polymorph observed in the Polinik Unit and is present in most aluminous metapelites. Therefore, peak metamorphic conditions throughout the Polinik Unit were within the kyanite field. Phase equilibria between the minerals kyanite, andalusite and sillimanite have been studied experimentally by Richardson et al. (1969) and Holdaway (1971) whose results are in good agreement. The position of the kyanite = sillimanite equilibrium puts a lower pressure limit for the peak metamorphism.

The equilibrium
paragonite + quartz = kyanite + albite + H_2O
in the system Na_2O – CaO – Al_2O_3 – SiO_2 – H_2O

This equilibrium was investigated, using the internally consistant data set of Powell & Holland (1985). This data set has been derived by optimising enthalpies over the whole data base simultaneously, with the result that there is very good agreement between most

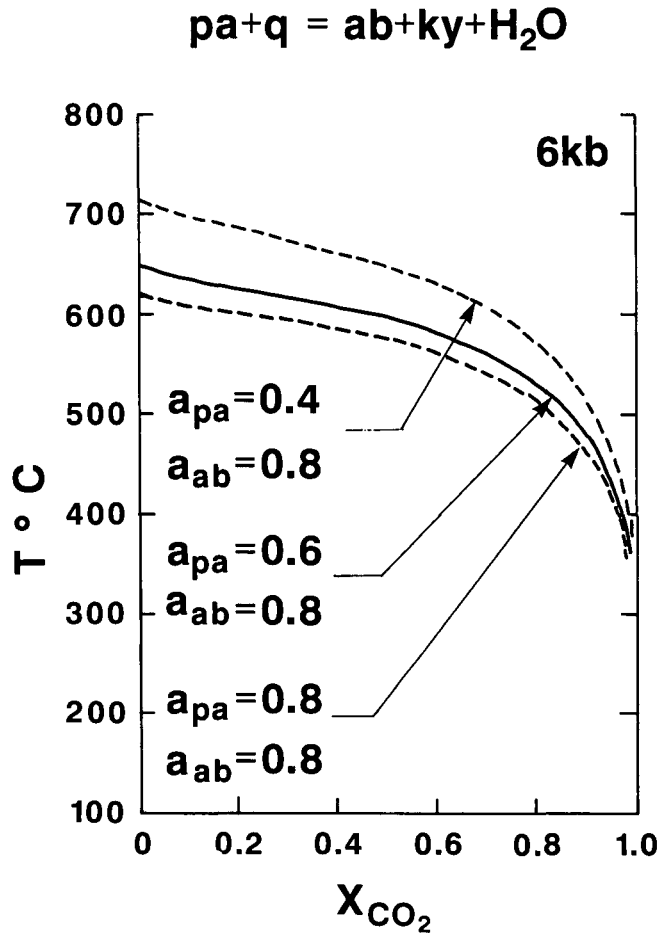

Text-Fig. 13.
Temperature – X_{CO_2} graphs for the reaction pa + qz = ab + ky + H_2O for different activities of albite and paragonite from Polinik Unit schists. Reaction lines were plotted using Holland's program Thermo (Holland et al., 1986).

calculated equilibrium curves and their corresponding experimental uncertainties. It also takes account of the compressibility and thermal expansion of minerals. The activity-composition relations used to calibrate the equilibrium constants are listed in Table 2.

Equilibrium curves were calculated for each sample using mean mineral compositions (representative probe analyses in Appendix D). Only minerals which are thought to still contain their peak metamorphic compositions (e.g. garnet II, white mica II, plagioclase II) have been used for the calibrations of equilibrium constants (Table 2).

The calculated equilibrium curves are subject to errors. A description of the common errors and how they propagate through the calculation has been outlined by Powell (1985).

The position of the mica dehydration equilibrium

$$\text{pg} + \text{qz} = \text{ky} + \text{ab} + H_2O$$

is relatively insensitive to errors in mineral composition. Temperatures calculated for this equilibrium are shown in Fig. 14. Fig. 13 shows the T – X_{CO_2} curves for a range of activities at 6 kbars. It can be seen that temperature is fairly insensitive to vapour compositions. Assuming that the diluent is CO_2, only low values of X_{H_2O} are required to reduce the temperature substantially. For example, X_{H_2O} of less than 0.2 is needed to bring the equilibrium temperature below 500°C.

Table 2.
Equilibrium constants used for thermodynamic calculations.

Component	Formula	Activity (a)	Activity coefficient (γ)	Reference
anorthite (an)	$CaAl_2Si_2O_8$	$0.25X_{an}(1+X_{an})^2\gamma$	$\exp\left\{\frac{(1-X_{an})^2(2050+9392\ X_{an})}{RT}\right\}$	Newton et al.(1980)
albite (ab)	$NaAlSi_3O_8$	$(X_{ab})^2(2-X_{ab})\gamma$	$\exp\left\{\frac{(1-X_{ab})^2(6746-9442\ X_{ab})}{RT}\right\}$	Newton et al.(1980)
grossular (gros)	$Ca_3Al_2Si_3O_{12}$	$(X_{ca}\gamma)^3(X_{Al})^2$	$\exp\left\{\frac{(3300-1.5T)(X_{py}^2+X_{py}X_{alm})}{RT}\right\}^*$	Newton and Haselton (1981)
almandine (alm)	$Fe_3Al_2Si_2O_{12}$	$(X_{Fe}\gamma)^3(X_{Al})^2$	$\exp\left\{\frac{(-3300+1.5T)(X_{py}X_{gr})}{RT}\right\}$	Ganguly and Kennedy (1974) Newton and Haselton (1981)
paragonite (pa)	$NaAl_2^{M1}Al^TSi^T{}_3O_{10}(OH)_2$	$9.48\left(X_{Na}\gamma\right)\left(X_{Al}^{M1}\right)^2\left(X_{\square}^{M2}\right)\left(X_{Al}^T\right)\left(X_{Si}^T\right)^3$	$\exp\left\{\frac{(1-N)^2(3250.5+0.167T)+(2342+0.454T)N^*)}{RT}\right\}$ $N^* = Na/(Na+K)$	Eugster et al.(1972) Powell (1978)
pyrope (py)	$Mg_3Al_2Si_2O_{12}$	$(X_{Mg}\gamma)^3(X_{Al})^2$	$\exp\ \frac{(3300-1.5T)(X_{gr}^2+X_{gr}X_{alm})}{RT}$	Newton (1986)

$R = 1.9872$ cal $deg^{-1}mol^{-1}$ * $X_{py} = X_{Mg} = Mg/Mg+Fe+Ca+Mn$, etc.

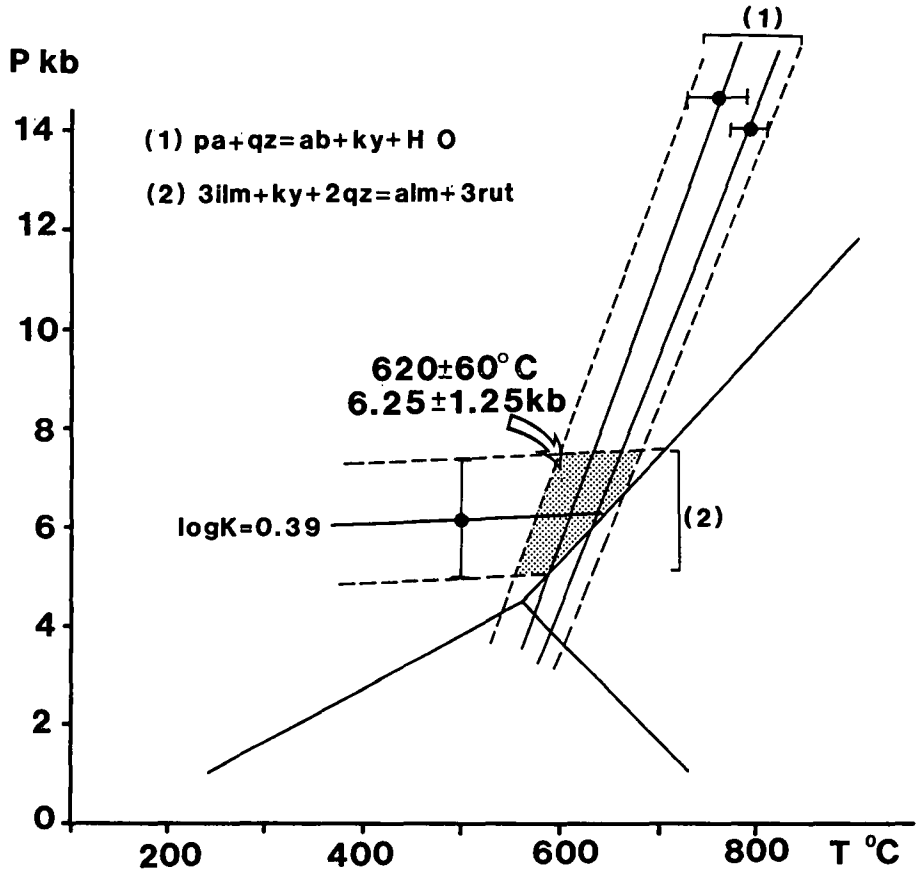

Text-Fig. 14.
Estimated metamorphic conditions (shaded region) for the Polinik Unit metapelites. Error bars (2 σ standard variations) are shown.

Table 3.
Pressure estimates based on the equilibrium 3 ilm + Al_2SiO_5 + 2 qz = alm + 3 rut (BOHLEN et.al., 1983). Pressures have been read off the P-T-logK plot presented in BOHLEN (op. cit.; Fig. 3).

SAMPLE	a_{alm}	K = $(1/a_{alm})$	log K	P(Kb) at 600°C
77	0.458897	2.179	0.3382	7.3
	0.5527	1.809	0.2575	8
81	0.473031	2.114	0.3251	7.4
	0.364785	2.741	0.4379	6
	0.344450	2.903	0.4629	5.8
	0.368711	2.712	0.4333	6
81.3	0.4910	2.037	0.3089	7.5
	0.5495	1.820	0.2600	7.8
	0.402404	2.485	0.3953	6.3
	0.485500	2.060	0.3138	7.4
	0.360269	2.776	0.4434	5.9
83	0.479314	2.086	0.3194	7.2
	0.399389	2.504	0.3986	6.2
	0.430532	2.323	0.3660	7.2
85.4	0.373715	2.966	0.4275	6.1
	0.358712	2.788	0.4452	5.7
	0.4385	2.281	0.3580	7.0
68	0.385067	2.593	0.4145	6.3
	0.3741	2.673	0.4270	6.1
9	0.5055	1.978	0.2963	7.6
	0.4602	2.173	0.3370	7.2

Pressure sensitive equilibrium in the system FeO – TiO_2 – Al_2O_3 – SiO_2

BOHLEN et al. (1983) calibrated the pressure sensitive equilibrium

3 ilmenite + Al_2SiO_3 + 2 quartz = almandine + 3 rutile.

Assemblages containing these reactants are common in the metapelites of the Polinik Unit. Ilmenite tends to be rimmed by rutile, suggesting that the reaction proceeded towards the right-hand side, and therefore estimates based on this geobarometer will give low pressure estimates. Retrogression textures have not been observed, such as rutile needles scattered in the titaniferous biotites. However rutile and ilmenite occur as inclusions in, or are intergrown with, garnet II. Therefore the assemblage garnet II, ilmenite, kyanite, rutile, and quartz can be confidently considered to be a peak metamorphic assemblage.

BOHLEN et al (1983) present a P-T-logK plot for this geobarometer. K is defined as:

$$K = \frac{(a_{ilm})^3 \cdot (a_{ky})}{a_{alm} \cdot (a_{rut})^3}$$

since kyanite and rutile occur as pure phases (a = 1), and analysed ilmenites closely approximate the ideal formula ($Fe^{2+}Ti^{4+}O_3$) and can be treated as a pure phase (no hematite solid solution), the equilibrium constant simplifies to: $K = 1/a_{alm}$ (Table 3).

The activity of almandine has been calculated using the expression given in Table 2, and varies between 0.344 and 0.485 at 600°C. Therefore logK varies between 0.4629 and 0.3138, with a mean of 0.3919 (Table 3). These values suggest pressures at 600°C of 6.2±1.2 kbars. As garnets are rich in almandine and are in the RAOULT's law region, activities are quite reliable and this barometer should be good.

Fig. 14 shows all the equilibria discussed above. The metamorphic conditions deduced from Polinik Unit metapelite are in the range of 620±60°C and 6.25±1.25 kbars.

4. The Strieden Unit

4.1. Introduction

Schists in the Strieden Unit show a varied mineralogy and a distinct metamorphic zonation, indicating increasing temperatures with increasing structural depth. They range from sillimanite-bearing metapelites, with evidence for partial melting in the most northerly outcrops, at the base of the Strieden Unit, to low-grade phyllites at structurally higher levels, further south, immediately underlying the Mesozoic Drauzug sequence. Marble and amphibolite occur throughout the Strieden Unit, forming concordant discontinuous bodies and bands of varying thickness. The amphibolites, in contrast to those in the Polinik Unit, show no textural evidence for a former eclogite assemblage.

Radiometric age data (BREWER, 1969, 1970, discussed in section 5) suggest that the high temperature mineral assemblages are Variscian in age. Alpine metamorphism did not exceed lowermost greenschist facies, which is in contrast to the mid Cretaceous amphibolite facies metamorphism in the Polinik Unit.

The Strieden Unit is separated from the Polinik Unit by subvertival fault zones. Immediately south of these faults, a 400–700 m wide zone of intense deformation forms the base of the Strieden Unit (Fig. 4). This is an important discrete tectonic contact within the Altkristallin sheet, referred to as the main mylonite zone (MMZ). Radiometric age data suggest it is late Cretaceous to early Tertiary in age (section 5). It generally dips towards the south (50–80°), trending WNW and can be traced across the entire width of the field area. It is comprised of mylonites, which formed during lower greenschist facies metamorphic conditions, derived from a variety of high grade rocks such as diopside-bearing marbles, cummingtonite-bearing amphibolites, augengneisses and pegmatites and sillimanite and andalusite-bearing metapelites.

Subvertical and undeformed N to NNW trending porphyritic, fine- grained, biotite and amphibole lamprophyre dykes (dated at 30–40 Ma, DEUTSCH, 1984) have been found throughout the Strieden Unit. They cut across the mylonites and suddenly terminate at the Ragge – Teuchl fault zone, and are not found in the Polinik Unit.

4.2. Deformation History of the Strieden Unit

The deformation history is complex and not easy to correlate with that in the Polinik Unit. Deformation events are labelled D_I–D_q, and at least four of these events (D_I–D_o) are probably Variscan or older (section 5). D_p deformation is the dominant deformation at the base of the Strieden Unit, in the MMZ, and occurred in the late Cretaceous–early Tertiary (section 5), postdated by D_q. Brittle faulting and the emplacement of dykes cut the D_q features and all earlier structures. The deformation history is summarised in Table 4.

4.2.1. D_I, D_m, D_n fabrics

In schists, D_I is defined by a segregation layering (S_I) consisting of alternating mm-thick quartzitic and micaceous (muscovite with graphite and illmenite) layers, and straight inclusion trails of ilmenite and graphite in garnet cores (garnet I, Fig. 15, Plate 3 – Figs. 2–4). In amphibolites, S_I is defined by layers rich in plagioclase, quartz, amphibole with rare epidote. In marbles, S_I consists of mm- thick, more weather-resistant, dolomite layers, or layers rich in quartz clasts or other impurities such as mica-laths, graphite trains, oxides and amphiboles.

D_m structures are the earliest to occur regionally. S_I is isoclinally folded (F_m), (Fig. 16). In schists, F_m is preserved as dismembered and isoclinal fold hinges, which form quartz rods (l_m) aligned within the foliation (S_m). Garnets (gtI) have rotated and have quartz pressure shadows parallel to S_m (Fig. 15). In amphibolites and marbles, S_I defines similar style, tight to isoclinal folds (F_m), with dm to m-scale wavelengths.

F_n folds form the most prominent folds above the MMZ, defined by the repetition of amphibolite, marble and metapelite zones on a 100–200 m scale, as well as the variation in the orientation of S_m on a 10–30 m scale.

On a regional scale, Fn forms upright to slightly N-verging open to tight folds with up to 100 m

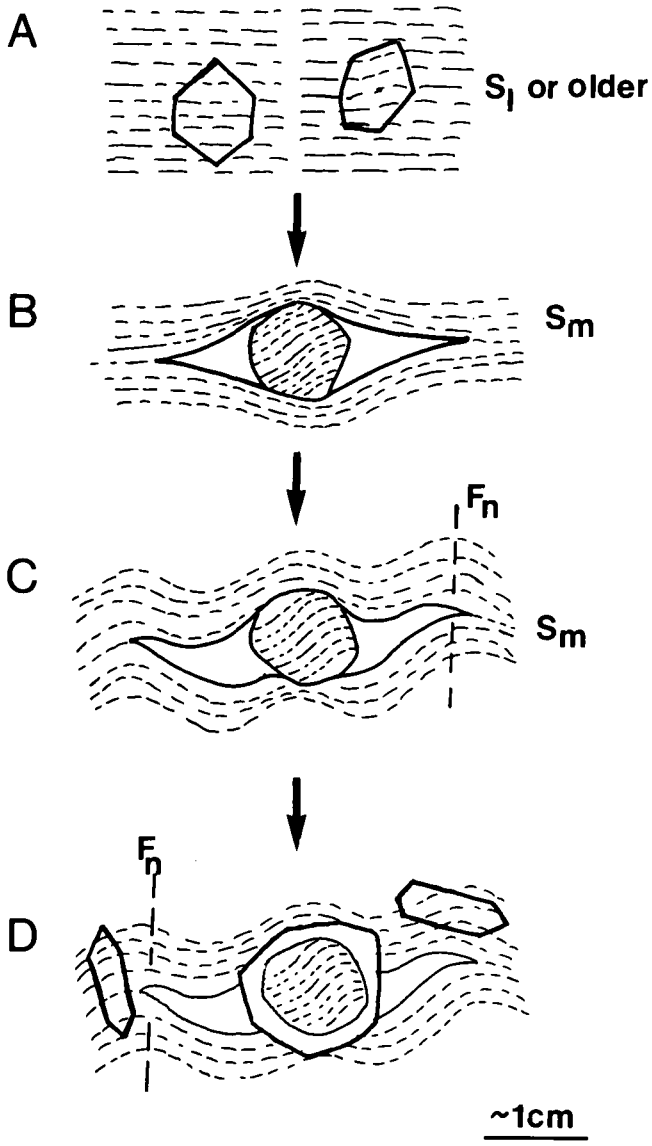

Text-Fig. 15.
Sketch of typical D_I, D_m and D_n fabrics in schists above the MMZ, in the Strieden Unit:
Superposition of fabrics shown in (d), suggests the following sequence of fabric development.
a) Garnet overgrows a foliation (S_I or older).
b) Garnets rotate during D_m deformation with the development of pressure shadow zones.
c) Pressure shadow zones are crenulated during D_n deformation.
d) Growth of garnet and staurolite occurs after D_n deformation.

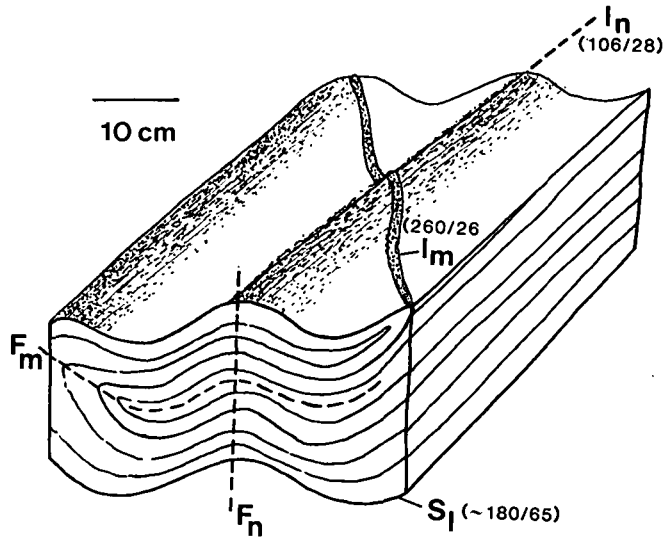

Text-Fig. 16.
Field sketch , showing D_m and D_n structural elements in Strieden Unit quartzo-feldspathic schists, 100 m north of Mt. Schneestellkopf.
An earlier quartzo-feldspathic foliation (S_I) is folded isoclinally (F_m). F_m axial planes are subsequently deformed by open F_n folds, with 10's cm wavelengths. D_n fold axes are markedly oblique to D_m fold axes.

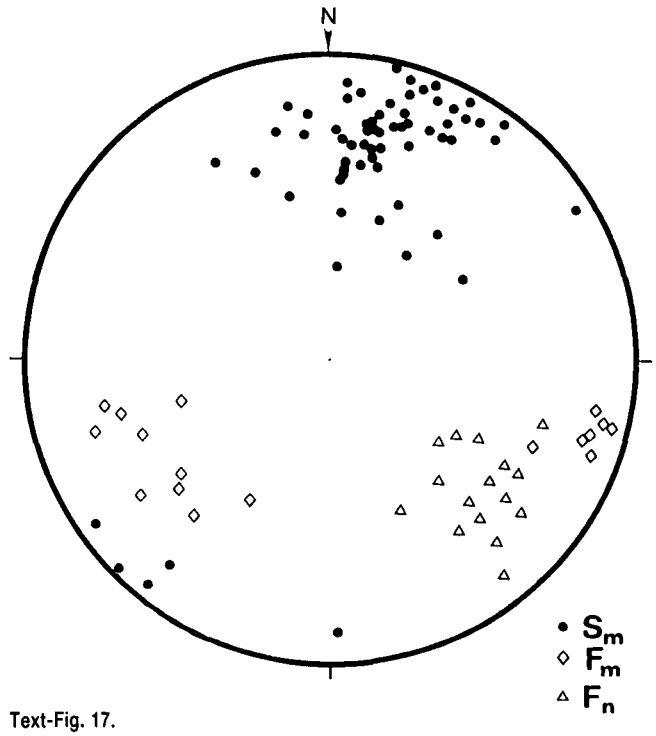

Text-Fig. 17.
Equal area stereogram showing relation between poles to the D_m foliation (S_m) and D_m and D_n fold axes (F_m, F_n) in the Mt. Schneestellkopf area.
F_n fold axes approximately lie on the pole to the great circle formed by poles to S_m.

wavelengths. Fold axes vary from subhorizontal to plunging gently E-SE (Fig. 17). Both Fm and Fn fold axes are nearly parallel, resulting in co-axial interference patterns on a dm- to 10's of metres-scale (Fig. 16). Minor dm- to m-scale parasitic folds, occurring in all lithologies, are associated with the large scale Fn structures, and show systematic changes in asymmetry. S_m is crenulated in the minor fold cores.

Further rotation of garnets (gtI) within the enclosing mica- and quartz-rich fabric occurred during D_n, and D_m pressure shadow zones were crenulated (Fig. 15). L_m quartz rods are deformed by D_n crenulations, and the angle between both crenulation lineations (F_n/I_n and F_m/I_m) is less than 30° (Figs. 16, 17).

4.2.2. Variscan High-Temperature Metamorphism and D_o

D_n deformation was followed by a static high-temperature metamorphism (section 4.3). In schists, the S_n foliation is overgrown by staurolite, garnet II (Fig. 15D), andalusite (Fig. 18) and sillimanite (Plate 3 – Fig. 1–6), and by diopside in marbles. The distinct metamorphic zonation in Strieden Unit schists indicates increasing

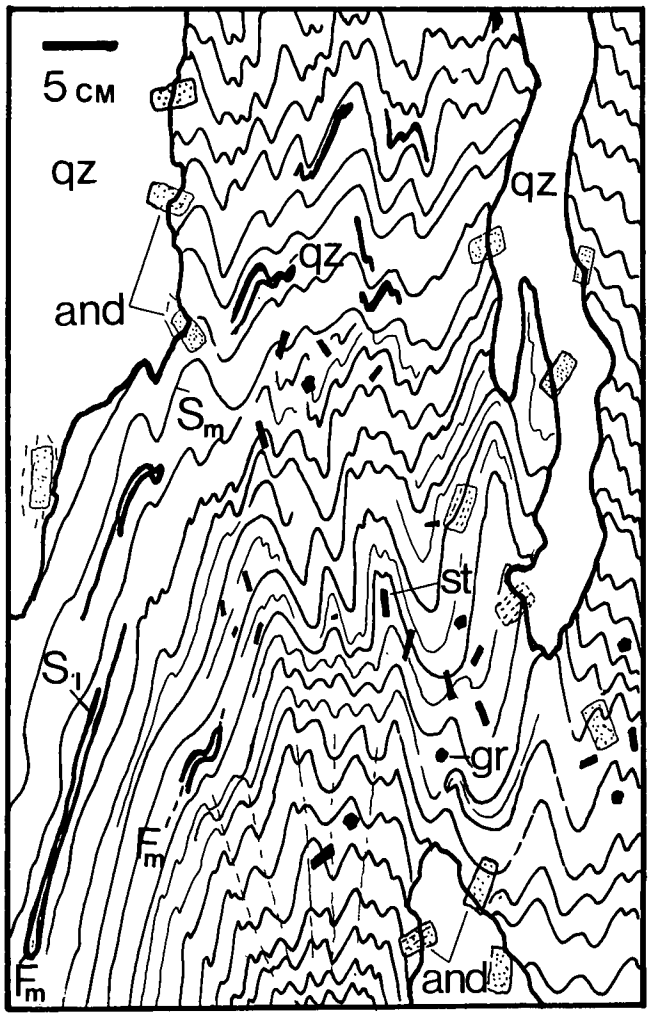

Text-Fig. 18.
Field sketch showing andalusite-bearing quartz veins which cut across F_n folds in aluminous metapelites in the Mt. Strieden area.
Andalusite, staurolite and garnet (garnet II) overgrow F_n crenulations and therefore post-date D_n deformation.

temperatures towards the base of the Strieden Unit during metamorphism (section 4.3.1.). Mineral assemblages, which overgrow the steeply dipping (60°SSE) S_m or S_n foliation, define S-SSE dipping isograd surfaces (dipping 0–20°S). Subsequent intense D_p deformation occurred at the base of the Strieden Unit under greenschist facies conditions.

There is evidence for localised deformation, referred to as D_0, in sillimanite bearing schists, with textural evidence for partial melting (Fig. 28, Plate 3 – Figs. 7,8). D_0 was either synchronous with or post-dates the formation of the high temperature minerals, such as sillimanite, but pre-dates the emplacement of pegmatites. Sillimanite- bearing gneisses, quartzitic biotite-rich schists, and rare dm-thick layers of cummingtonite amphibolite contain a well-developed foliation (D_{01}), defined by the alignment of the high-temperature minerals (sillimanite, biotite, quartz, feldspar, amphibole), which is folded (D_{02}) into ptygmatic folds. These structures are cross-cut by pegmatites which were emplaced at ca. 265 Ma (Cliff, pers. comm.). The localised occurrence of D_0 may be related to the thermal softening of rocks in and near a zone of partial melting (see Section 4.3).

4.2.3. D_p – D_q Fabrics

The MMZ is the product of high strain and plastic deformation under lower greenschist facies conditions. A suite of progressively formed structures (D_p–D_q) can be distinguished:

1) The main phase structures (D_n), consisting of the mylonitic foliation (S_p) and a stretching lineation (l_p) and associated folds (F_p).
2) Sets of microfaults and shear bands which formed at a late stage of D_p and caused extension parallel to the mylonitic foliation and lineation.
3) A set of open folds (F_q) and faults (with a thrust-sense displacement) which deform the mylonites, resulting in shortening approximately perpendicular to the mylonitic lineation.

Both boundaries of the MMZ are shown in Fig. 19, 20. The northern contact has been reworked cataclastically by movement along subvertical fault zones. The southern contact is either faulted, with an abrupt change in deformation style above the MMZ (e.g. in the Latisch area where undeformed and mylonitized pegmatites are juxtaposed with each other), or the mylonitic deformation decreases gradually with no sharp boundary to the MMZ (Poliniksee area, Fig. 20). In the latter case, the F_n fold geometry is progressively modified by D_p. Folds have been tightened and flattened and reorientated within the mylonitic foliation (S_p) (Fig. 21). Inter D_n–D_p mineral assemblages are aligned in the transposed foliation. F_n fold axes have been rotated towards parallelism with the mylonitic stretching lineation (l_p).

S_p and F_p in different lithologies

The substantial ductile strain during D_p has transposed the layering and schistosity into a new orientation, axial planar to F_p (S_p) (Fig. 23). However, the degree of transposition varies considerably in the wide range of lithologies found in the MMZ, such as augengneisses, pegmatites, marbles, amphibolites and quartz and mica-rich schists. In general, quartz is the only mineral which shows plastic deformation, deformed by slip along certain crystallographic planes, resulting in crystallographic preferred orientation patterns (Plate 4). Some dynamic recrystallisation occurred in micas. Feldspars behaved as resistant clasts, affected only by brittle deformation, which locally resulted in granulation of the clasts (Plate 5 – Figs. 3,7).

Quartzitic mylonites

A good mesoscopically visible foliation (S_p) is rarely developed in mylonites derived from quartzitic schists and quartzites . Instead, the mica fabric is a relict foliation (S_n) which is folded around F_p fold hinges (Fig. 23). S_p is only apparent on the microscopic scale, where it is defined by the preferred orientation of elongate quartz grains or quartz ribbons, which are aligned within F_p axial surfaces, with their elongation direction often perpendicular to or at a high angle to mica-rich layers (Fig. 23, Plate 4). Individual quartz ribbons have aspect ratios of 30 : 1 in large grains (up to 6 mm long) and 10 : 1 in smaller grains (0.2 mm long). Ribbon grains are variably recrystallised along grain margins or along subgrain boundaries to form grains less than 0.2 mm in diameter (matrix grains). Ribbon grains commonly have subgrain boundaries which make a constant angle with the grain elongation direction. In thin sections cut perpendicular to both S_p and l_p, quartz

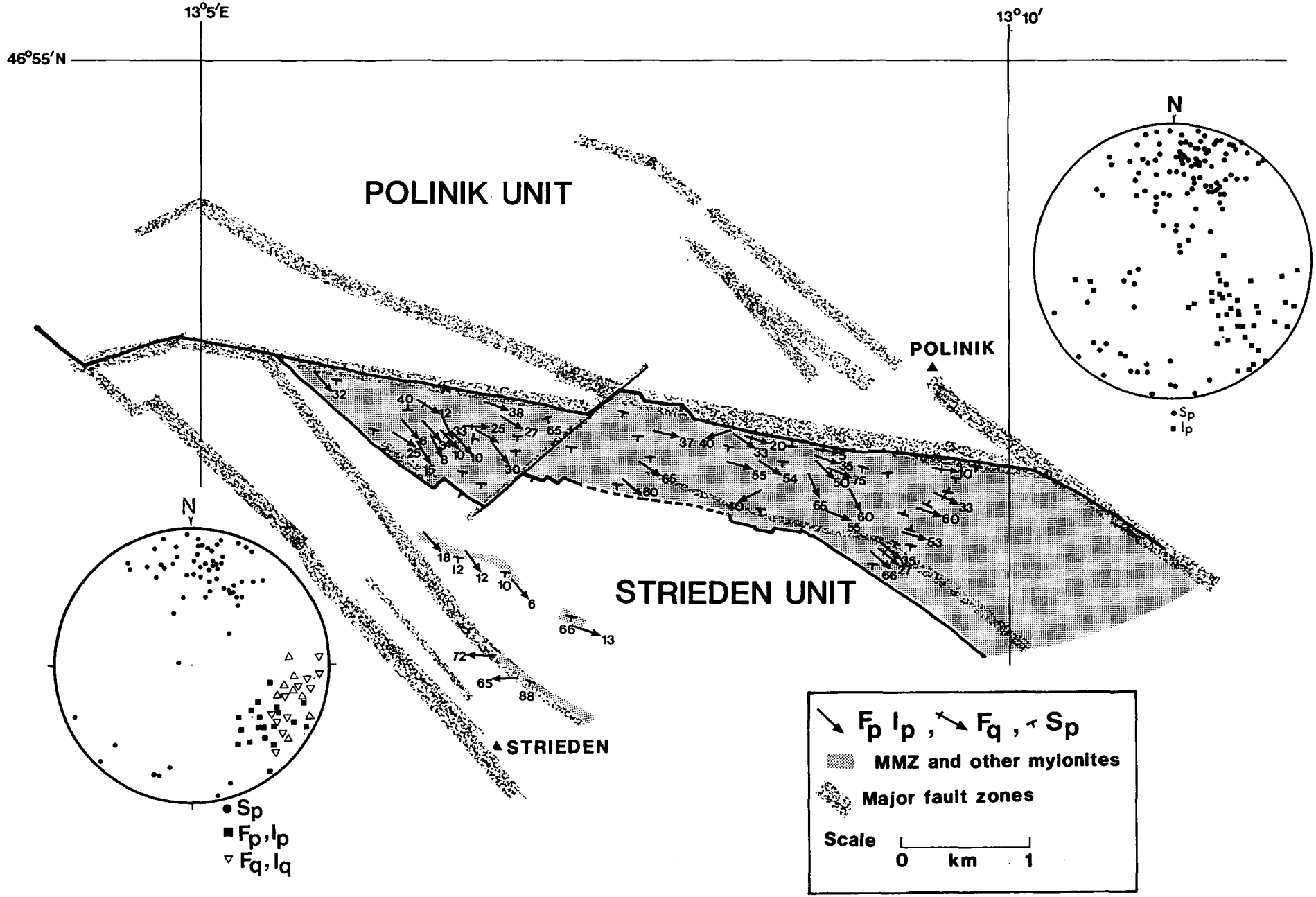

Text-Fig. 19.
Map showing the MMZ at the base of the Strieden Unit and D_p and D_q deformation orientation data (S_p, I_p, I_q).
D_p and D_q deformation is restricted to the MMZ and other minor mylonite zones. Equal area stereogram on the right-hand side contains all D_p orientation data collected in the study area. The equal area stereogram on the left- hand side, bottom corner, contains all D_p and D_q orientation data collected in the Latisch alm area.

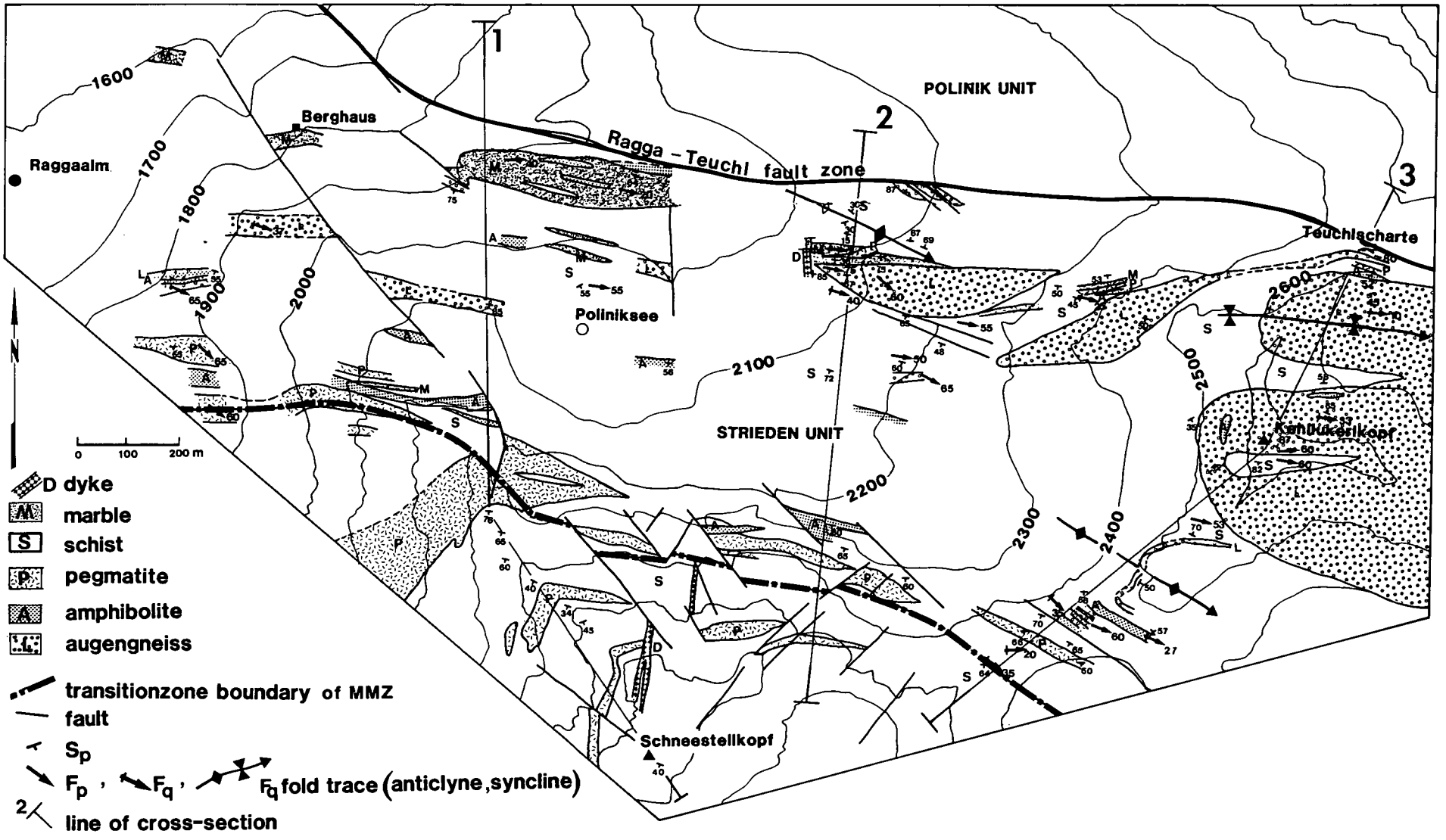

Text-Fig. 20.
Geological map of the area around Poliniksee (see Fig. 4 for location), showing the complex deformation and variety of lithologies in the MMZ. The position of the transitional top to the MMZ is also shown. Cross-sections are shown in Figs. 21, 22.

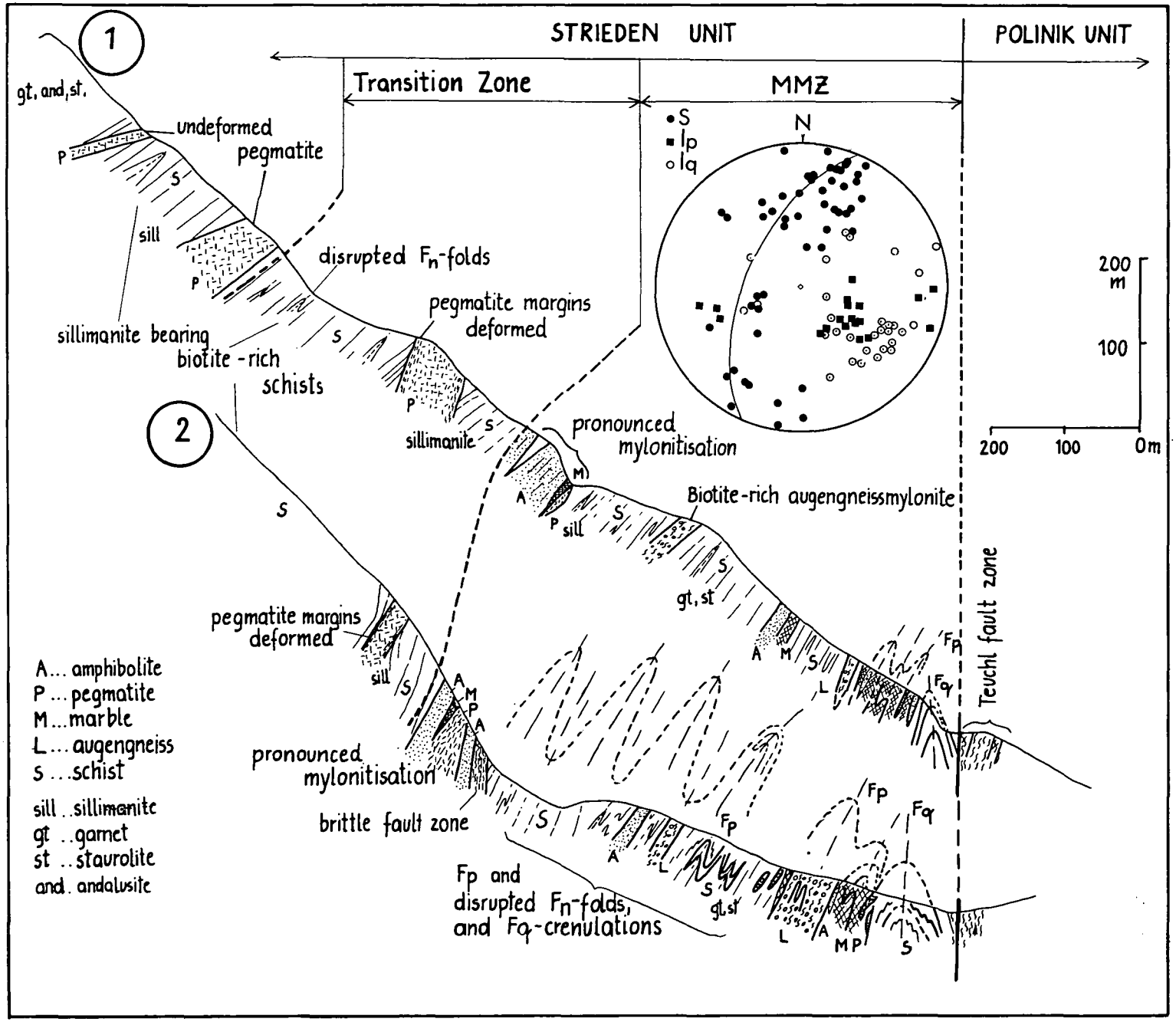

Text-Fig. 21.
Cross-sections through the base of the Strieden Unit (cross- sections 1 and 2 in Fig. 20).
Note the structural position of the MMZ (at the base of the Strieden Unit) and the increase in deformation, observed in pegmatites and from F_p fold structures, at progressively lower structural levels.

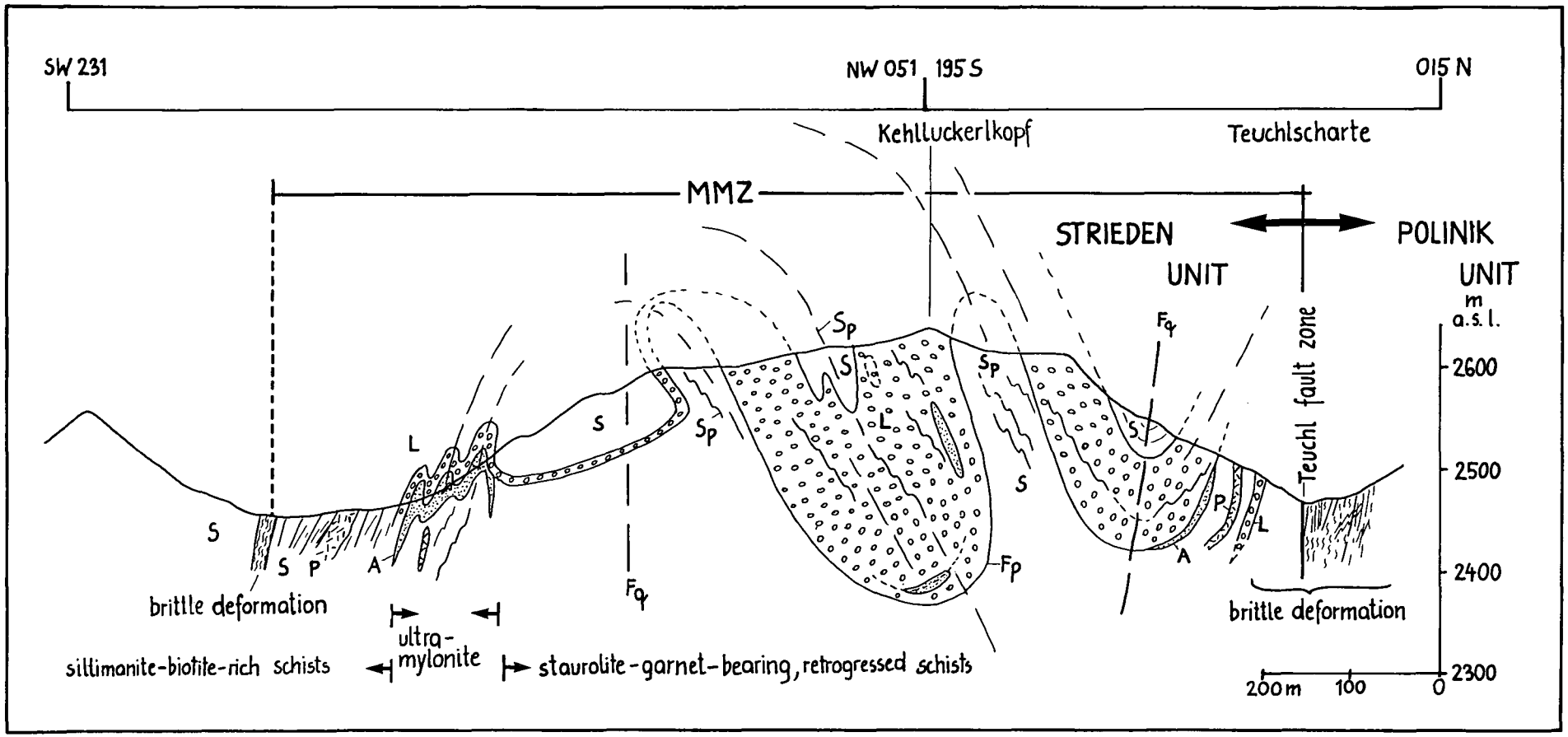

Text-Fig. 22.
Schematic cross-section across deformed Kehlluckerlkopf augengneiss (cross-section 3 in Fig. 20), looking up plunge of F_q folds, showing a major F_q synform and antiform.

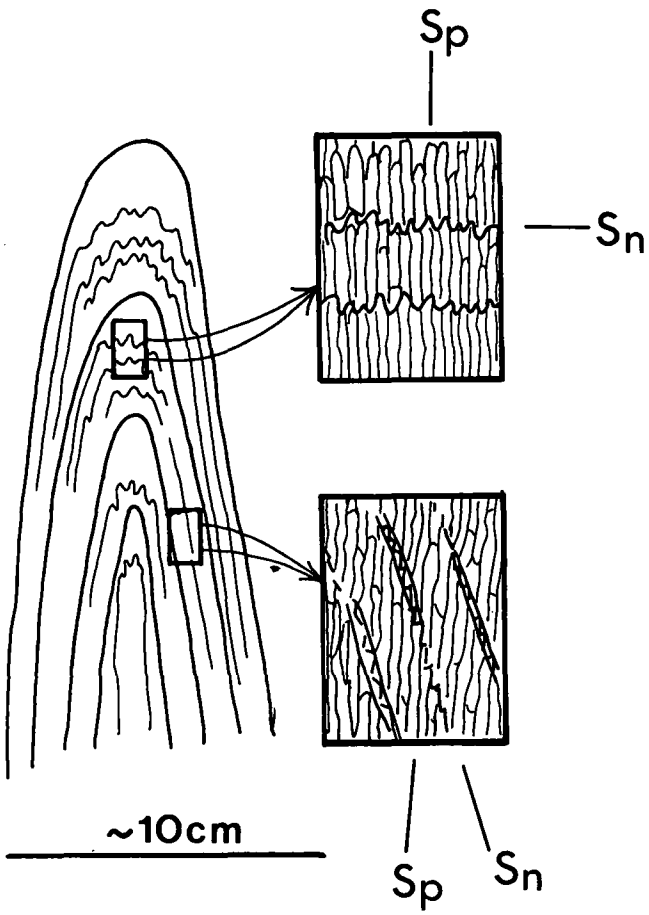

Text-Fig. 23.
Sketch showing the relation between D_p and pre-D_p fabrics in a sheared quartzitic schist.
A pre-D_p foliation (S_n) has been folded and crenulated in the core of a F_p fold, while a folded quartz band contains an axial planar fabric defining the D_p foliation (S_p). C-axes in quartz subgrains have a constant preferred orientation throughout the F_p fold structure.

bands are tightly folded on a mm-scale, with axial planes parallel to S_p and fold axes oriented subparallel to the stretching lineation l_p (Plate 4 – Figs. 3,4,5). The preferred crystallographic orientation of quartz subgrains is unaffected by these F_p folds.

Mylonitic amphibolites

S_p is parallel to a compositional layering and consists of 0.1–1 mm wide bands of pure quartz alternating with layers rich in porphyroclasts of green hornblende, plagioclase (20–30 % anorthite) and sphene aligned within a black, fine banded matrix of comminuted material (ultramylonite) derived from the parent rock (amph – plag – qz – sph – ore). With increasing deformation, the percentage of clasts and their grainsize decreases until, in extreme cases, cm-thick bands of ultramylonite, devoid of clasts, alternate with layers which are rich in aligned porphyroclasts. A mineral lineation (l_p) is defined by the preferred orientation of the porphyroclast grains which form rods in the well developed mylonitic foliation and define a stretching lineation (l_p).

Mylonitic marbles

S_p is apparent in thin section only, defined by the alignment of elongate calcite grains and occasional mica, chlorite and amphibole grains. S_p is either parallel to or cuts the compositional layering. The latter is defined by layers of impurities and concentrations of more weather resistant dolomite grains. Where marbles are intruded by pegmatites, D_p penetrative deformation appears to have been accommodated preferentially in the marbles. The pegmatites are boudinaged and contain the S_p foliation only near their margins. Thin amphibolite layers within marbles are also boudinaged and have been stretched, within S_p, parallel to l_p. The orientation of individual boudins is oblique to S_p, which is deflected around the boudins. The sense of shear, inferred from the sense of obliquity with respect to S_p, agrees with other shear sense indicators in the mylonites (see below).

Mylonitised pegmatites and augengneisses (Plate 5)

These have a well developed mesoscopic S_p which is defined by the preferred orientation of elongate and planar feldspar, tourmaline (restricted to pegmatites) and mica porphyroclasts, embedded in a rock matrix of fine-grained recrystallised quartz, granular feldspar and sericite. Rods of porphyroclasts of tourmaline and feldspar define an extensional lineation (l_p), (Plate 5 – Figs. 1,2,4).

Geometry of D_p fabric

S_p is axial planar to tight to isoclinal asymmetric folds, recognised on all scales, plunging E to ESE at 30–60° (Fig. 19). These refold F_n, forming complex interference patterns (co-axial refolding and doubly plunging geometries) ; F_p axes make angles of up to 85° with F_n, but are within 10° of l_p stretching lineation. On a cm-scale, S_p is itself locally deformed into asymmetric tight to isoclinal similar folds (Plate 4 – Figs. 3, 4, 5). These have variable vergences, with axial surfaces at a low angle or parallel to the mylonitic foliation. Fold axes are parallel to the mylonitic lineation. However, the quartz fabric shows a well developed crystallographic preferred orientation which is constant throughout the fold. These folds therefore probably nucleated after a strong foliation had already formed, possibly as a result of flow instability in a highly anisotropic material (PLATT et al., 1980) and were progressively amplified, flattened and rotated during continued flow in the mylonites. Fold axes may also have been rotated in opposite directions towards the long axis (x-direction) of the finite strain ellipsoid. This process leads to the formation of sheath folds. Sheath folds have been observed in the Kelluckerlkopf augengneiss, where m-scale elliptical traces of S_p are found in sections perpendicular to l_p, and in marbles south of Poliniksee.

Late phase D_p structures in mylonites

S_p is cut by microfaults (cm- to mm-scale). If the sense of movement along these faults is described relative to S_p, normal faults and thrust faults can be distinguished. Sets of faults with a normal fault sense (Plate 5 – Fig. 5) are observed in sections perpendicular to S_p and parallel to l_p. They tend to have a listric geometry and cut S_p at angles less than 37°. They intersect S_p at a high angle to l_p. Movement on such faults has resulted in extension along l_p in the plane of S_p. PLATT and BEHRMANN (1986) describe similar features, which they call extensional crenulation cleavage. Extensional crenulation is very common in mica-rich mylonites, where it forms single or conjugate sets with opposite senses of displacement. The cleavage zones contain fine aggregates of white mica (50–200μ) de-

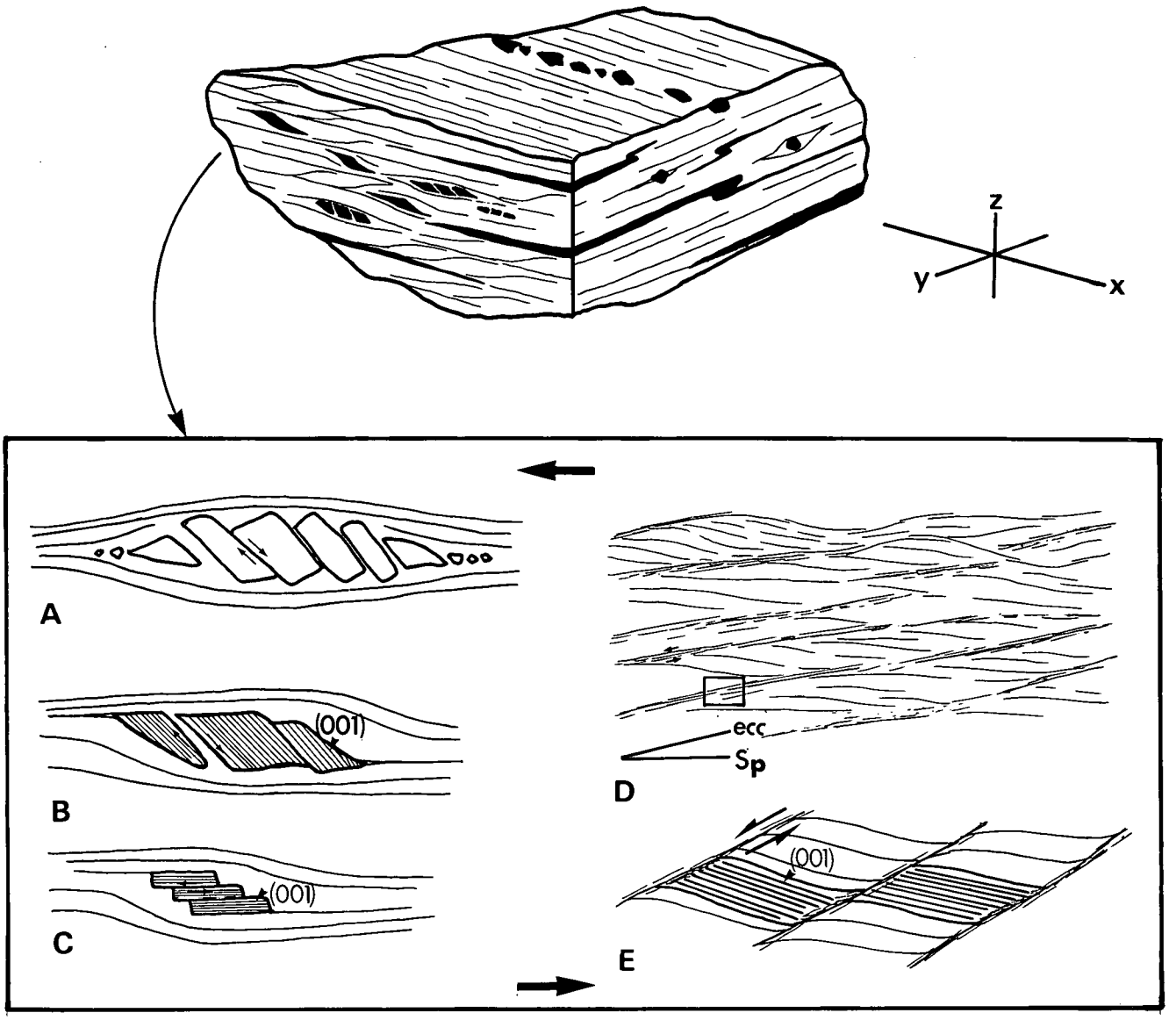

Text-Fig. 24.
Block diagram showing the mylonitic fabric observed in three orthogonal sections of a Strieden Unit quartzitic schist.
The sections are described relative to three orthogonal axes x, y and z. The x-axis is parallel to the mylonitic lineation and the z axis is perpendicular to the mylonitic foliation. Typical shear sense indicators (sinistral) are illustrated: A,B and C show various styles of microfaulting in porphyroclasts; D, E show extensional crenulation cleavages in a micaceous fabrica.

rived, but differing chemically, from coarser older grains. New grains are richer in iron, which suggests that they have formed during a phase of non-isochemical recrystallisation, which probably occurred during the progressive D_p deformation, when the fluid composition changed and the temperature decreased.

Both extensional faults and extensional crenulations probably formed in the last phases of D_p. Conjugate sets of faults, symmetrically oriented with respect to the mylonitic foliation, suggest that the deformation during at least the late phases of D_p may have deviated from non coaxial deformation (shear deformation) and may in places have resulted in coaxial flattening of S_p.

Faults with a thrust movement sense are commonly observed in thin sections perpendicular to both S_p and l_p. They too have a listric geometry and have accommodated shortening in a direction normal to l_p. Asymmetric mm- to cm-scale crenulations of S_p, with axes approximately parallel to l_p, appear to have been caused by drag on these faults.

Kinematic indicators

D_p occurs in a distinct zone of intense deformation within the Altkristallin, which is likely to have accommodated a large amount of relative motion of its boundaries. However, no displaced marker horizons have been found, and its boundaries cannot be precisely defined. Therefore, features of the internal deformation must be used to determine the sense of shear, defined as the sense of rotation of the vorticity (spin) of the strain field which acted during deformation in the MMZ. Knowledge of this provides considerable constraints on tectonic models for the development of the Altkristallin.

Microstructures and crystallographic fabrics in naturally deformed rocks have proved particularly useful in assessing the kinematics of deformation events (LISTER & WILLIAMS, 1979; SCHMID et al., 1986; BOUCHEZ et al., 1983; SIMPSON & SCHMID, 1983; BEHRMANN et al., 1982). A variety of fabrics, such as the orientation of minor shear bands, the preferred orientation of quartz c-axes

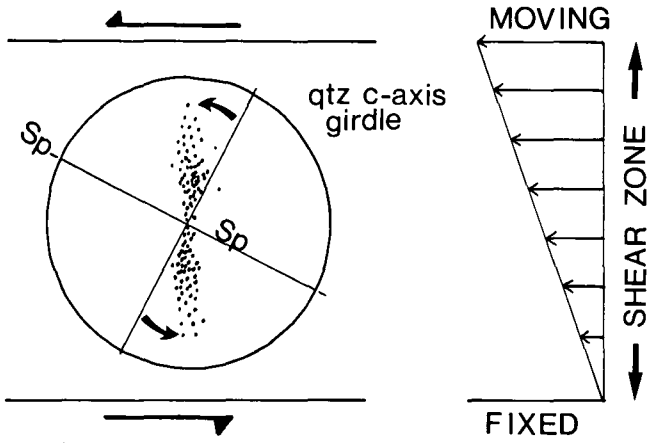

Text-Fig. 25.
Diagram showing the assumed relation between a single quartz c-axis girdle distribution and the mylonitic foliation (S_p), for the case of sinistral simple shear.
The c-axis girdle tends to be perpendicular to the shear zone walls (flow direction) and hence is rotated anticlockwise of the mylonitic foliation (S_p).

(CPO), and the asymmetry of pressure shadows and sigmoidal micas, have been used to deduce a sense of shear (Fig. 24, 25).

Quartz crystallographic preferred orientation

Various models (LISTER & WILLIAMS, 1979) suggest that the greatest concentration of quartz c-axes lie in a plane normal to the flow or shear direction and that the foliation marks the xy plane of the finite strain ellipsoid (BOUCHEZ, 1978). Therefore, the relative orientation of the flow direction, which is parallel to the shear zone walls in simple shear, and the mylonitic foliation can be used to deduce the sense of shear. If the former is anticlockwise of the latter, then the shear is sinistral (Fig. 25).

Using a Universal Stage microscope, C-axis orientations have been measured from dynamically recrystallised quartz ribbons in several orientated mylonite samples. The preferred orientation pattern of the crystallographic c-axes can show:

1) A distinct 'single girdle' topology with two maxima oriented at an angle of 60–80° to the S_p trace. The sense of shear is given by the asymmetry of the c-axes topology (Fig. 26B).

2) A single c-axes maximum, which forms angles of 35–45° with the y-axis, inclined 12–15° with respect to the yz plane (Fig. 26A).
The sense of shear deduced from this data agrees with that derived from other indicators: the orientation of muscovite fish, which, in pegmatite and augengneiss mylonites, form displaced and broken grains, displaced along (0001) planes and orientated oblique to S_p (Plate 5) ; shear bands, which consistantly make an angle of 30–40° with the mylonitic foliation (Plate 5 – Figs. 1,2,6) and have accommodated shear with associated drag of adjacent quartz layers; and the asymmetry of granulated tails of feldspar clasts, which can be traced for several centimetres along the mylonitic foliation before they taper out (Plate 5 – Fig. 7).

D_q deformation

On a regional scale, the orientation of S_p varies from gently to steeply dipping. The orientations of D_p fold axes and lineations are shown in Fig. 19 and in Plate 4 – Fig. 2. In the Kelluckerlkopf area, asymmetric folds (F_q), which deform the mylonitic foliation on a cm- to m-scale, can be correlated with large scale variations in the oientation of the mylonitic foliation (Fig. 22). Areas where S_p is steeply dipping or flat lying correspond to F_q fold limbs or hinges respectively.

The poles of the mylonitic foliation crudely lie on a great circle in the stereographic plot, and the pole to this great circle has a similar orientation to that of small scale F_q asymmetric folds. This suggests that the mylonitic foliation (S_p) has been folded on a large scale by a series of moderately plunging folds. The outcrop pattern of the Kehlluckerlkopf augengneiss, with the repetition of lenses of augengneiss and schists, marbles and amphibolites, may be the product of D_q.

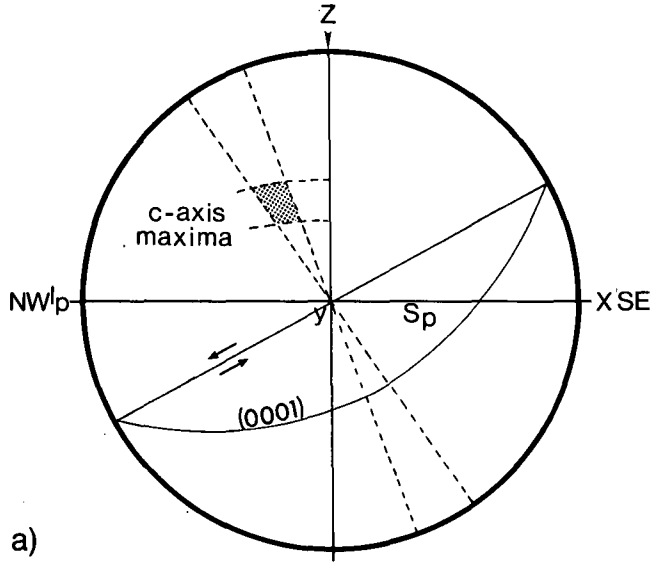

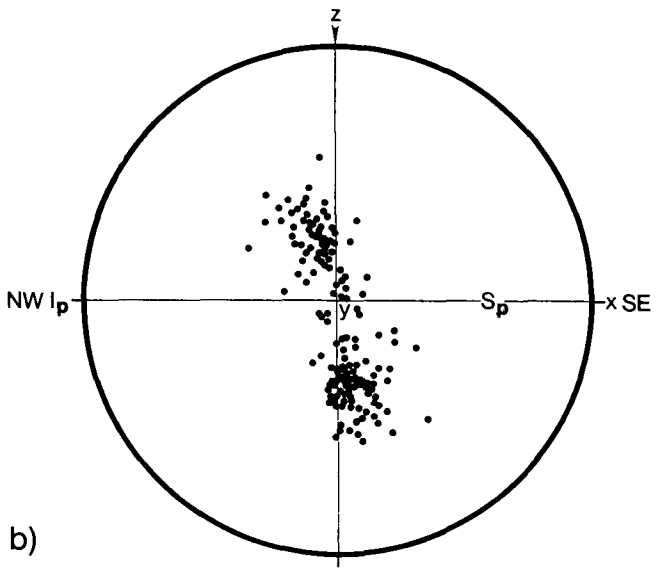

Text-Fig. 26.
Equal area lower hemisphere stereograms showing quartz c-axis distribution for quartz tectonites.
a) C-axis orientations in sample 329, measured with an optical microscope and sensitive tint plate, in two orthogonal sections parallel to the xz and yz sections (see Text. Fig. 24).
b) C-axis orientations in sample 382, measured on an universal stage..

D_q deformation is restricted to the MMZ. This may be explained in a number of ways:

- D_q occurred in a zone of weakness controlled by lithology, rock fabric or temperature.
- D_q occurs in the core of a large km-scale upright, ESE to SE trending, antiformal structure, which has been subsequently truncated by the Ragga – Teuchl fault zone.

In the latter case, D_q may correlate with the D_4 antiformal structures within the Polinik Unit. The correlation of D_q with deformation in the Polinik Unit is discussed in section 5.

D_q structures have been modified by movement along the Ragga-Teuchl fault zone. Away from the fault, the trend of F_q fold axes is markedly oblique to that of the fault, whereas, close to the fault, they trend more nearly parallel to the fault, as well as plunging more gently (Fig. 19). This suggests that F_q fold axes have been rotated about horizontal and vertical axes as a consequence of movement along the fault, and that movement along the fault zone contained a component of strike slip.

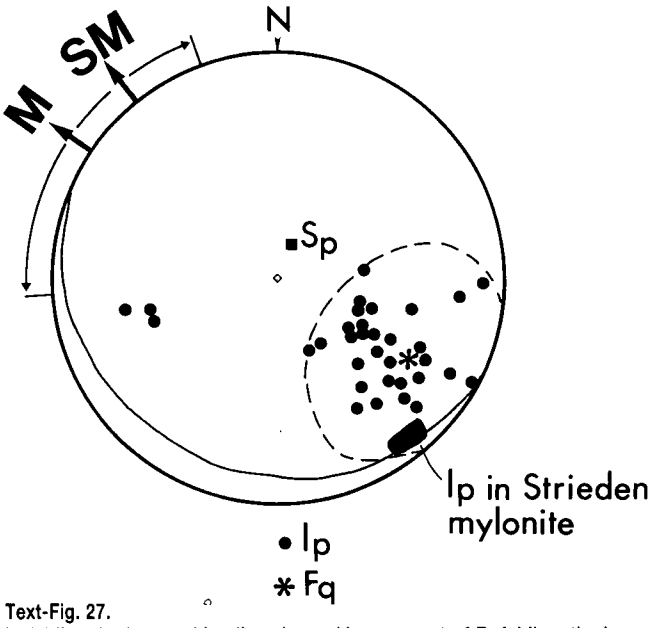

Text-Fig. 27.
Unfolding the l_p stretching lineation, taking account of F_q folding: the lower hemisphere equal area stereogram shows the l_p stretching lineations in the MMZ.
Lineations are scattered and do not lie on a single small circle about an average F_q axis. Dashed curve is the largest small circle about the average F_q axis wich encompasses most of the data. If the F_q axis is rotated to the horizontal (about a horizontal axis), the intersection of the circle with the edge of the stereogram gives an estimate of the range in unfolded lineation trends, assuming that the mylonitic foliation was horizontal initially. The median trend (and scatter, (M)), as well as that for the unfolded Strieden quartz mylonite (SM), are marked by arrows.

4.2.4. Original Orientation of S_p and l_p

The following evidence suggests that the mylonitic foliation originally formed as a sub-horizontal planar fabric:

1) In the structurally higher parts of the Strieden Unit, above the MMZ, thin mylonite zones (for instance the quartz mylonite near Mt. Strieden, Fig. 19), show no evidence for D_q, and hence may be near their original orientation, dipping at 15° or less.
2) After removing the effects of D_q on the mylonitic foliation (without correction of the fold plunge) in the MMZ, S_p dips gently (less than 30°) though in variable directions. This apparent variation in the orientation of S_p orientation, manifested in the variation (trend and plunge) of F_q fold axes, may be the result of subsequent warping and twisting of the deformed mylonite zone as a consequence of movement on the Ragga – Teuchl fault zone.

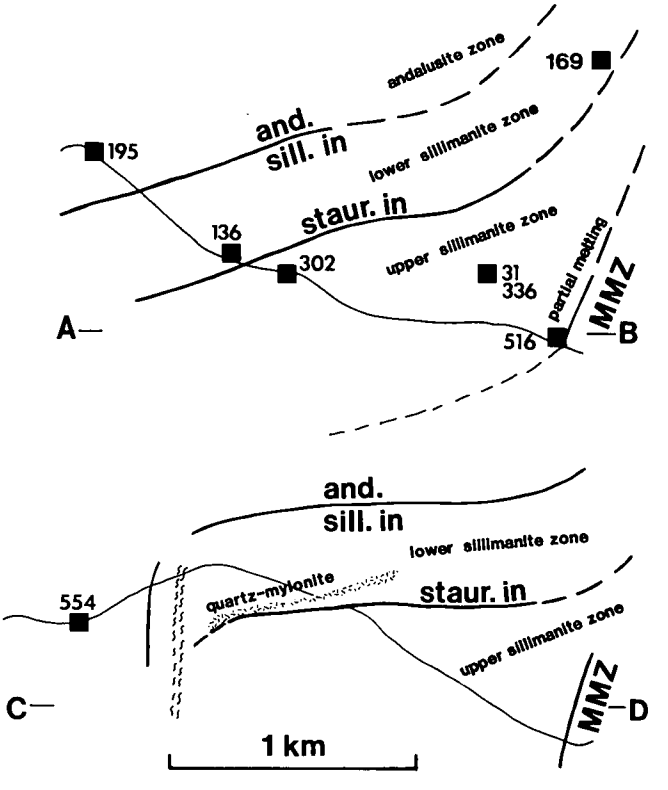

Text-Fig. 28.
a) Opposite page.
Topographic map of part of the Strieden Unit in the Latischalm and Striedenalm area, showing localities of samples (mineral assemblages of samples listed in Table 5) and isograds (cross-sections are shown in Fig. 28b).
b) This page.
Two cross-sections (see Fig. 28a), showing the geometry of the andalusite/sillimanite and staurolite-in isograd surfaces.

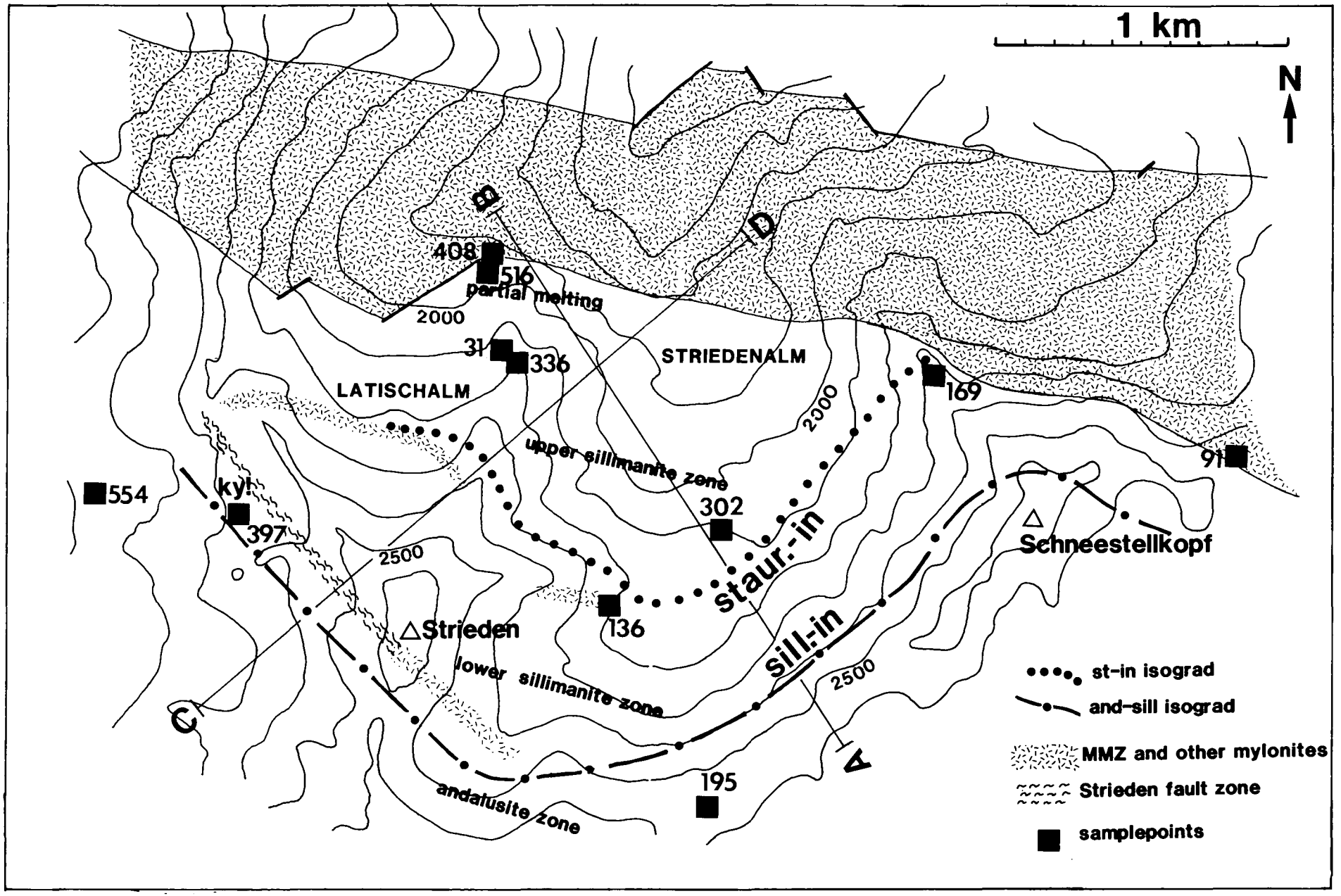
1 km
N
B
D
C
A
408
516
partial melting
2000
31
336
STRIEDENALM
LATISCHALM
169
91
upper sillimanite zone
554
ky!
397
2500
302
staur.-in
Schneestellkopf
Strieden
136
lower sillimanite zone
sill-in
2500
195
andalusite zone
st-in isograd
and-sill isograd
MMZ and other mylonites
Strieden fault zone
samplepoints

Table 4.
Summary of the deformation history of the Strieden Unit, showing correlation of fabric elements in different lithologies, with large-scale structures.

DEFOR-MATION	AGE	METAMORPHISM TECTONIC SIGNIFICANCE	SCHISTS & GNEISSES METAPELITES, QUARTZITIC SCHISTS Large scale- Micro-struct.	AMPHIBOLITES Large scale- Micro-struct.	OTHER LITHOLOGIES MARBLES, PEGMATITES, AUGENGNEISSES Large scale- Micro-struct.
		Deposition of sediments			
D_ℓ		Regional burial metamorphism	S_ℓ segregation layering, quartz segregations. S_ℓ preserved as graphite-trails and aligned ilmenite cryst. as inclusions in mus and gt.	Fsp and amph-rich segregation layering.	Compositional layering (dol, cc) in marbels. ? Intrusion of granite bodies ? Form part of the basement onto which the Palaeozoic sediments were deposited.
		Growth of gtI across S	growth of gtI and possibly stIacross S_ℓ		
D_m		Large-scale folding and imprication, seen along lithological contacts.	F_m isoclinal folds, l_m quartz-rods aligned in S_m gtI rotated in S_m, pressure shadows filled with qz & chl aligned parallel to l_m.	Tight folds in amph (F_m).	Isoclinal folding in marbles. ? Emplacement of granite-augengneiss-bodies as sheets ?
D_n		Large-scale folding.	S_m crenulated F_m large-scale E-W trending, N-verging open to tight folds. At base of Strieden Unit S_n axial planar to F_n. Pressure shadows crenulated, further rotation of gtI.	Refolded isoclinal F_m-folds in amphibolites.	Complex interference folds between F_m and F_n in marbles. ? Interfolding of augengneisses with marbles, schists and amphibolites.
M_v	? 320 Ma	Amphibolite facies metamor-phism, occurs in two stages:	Amph.facies stage 1: Qz-veins, containing euhedral and-crystals cut across F_n folds. St, biII, gtII, plagII cut across the S_m or S_n foliation. Amph.facies stage 2: sill replacing and stI → stII, gt → bi+sill, gt atoll struct. Direct evidence for partial melting in structural deepest position in the Strieden Unit.	Cross-cutting amphibole laths, plag porphyroblasts.	Diopside-bearing marble

$D_{o(1+2)}$	300 Ma	Restricted to lower sill-zone Cooling ages (K/Ar). Greenschist facies metamorphism	Tight F_{o2} folds, deforming sill-bearing schists (? plastic deformation of hot rocks). S_{o1} defined by the alignment of sill-bi-rich domains.	L_o amph. mineral lineatin.	
	265 Ma	Emplacement of pegmatites - in structural lower part of the Strieden Unit.			Emplacement of pegmatites as sheets and irregular-shaped bodies, cutting across D_n and D_o structures.
D_p	90-60Ma	Lowermost greenschist facies met. MMZ : subhorizontal main mylonite zone and minor thin mylonites, transport direction towards the NW D_p brings the Polinik Unit and the Strieden Unit together	D_p restricted to MMZ and thin mylonites. F^p isoclinal folding L^p stretching lineation S^p mylonitic foliation Earlier fabric elements rotated into parallelism with the mylonitic foliation S_p and the lineation l_p. Amphibolite mylonites. Amphibolite-boudins in marble-tectonite. l_p defined by quartz ribbons, which contain recryst. grains and sub-grains which show a cryst. preferred orientation. S_p deforms amph.facies mineral assemblages which are retrogressed to greenschist facies mineral assemblages. (sericite, chl, marg, ab). Grain-size reduction processes dominate over recrystallisation (seen only in qz and the new-formation of sericite). Extensional crenulation cleavage & extensional microfaulting of clasts at a late stage of D_p, causing further stretching within S_p and parallel to l_p.	F_p sheath-folds in Kehlluckerlkopf augengneiss. S_p in augengneisses defined by plastically deformed quartz grains, asymetrically aligned mica-fish, granulated feldspars. In pegmatites tourmaline rods often define L_p (pegmatite mylonites), boudinage of pegmatite bodies. Marble-tectonites (brittle def. processes dominate, cc and dol porphyroclasts are aligned in S_p. S_p in marble tectonites cuts across S^p_m
D_q	less than 60 Ma ago	Greenschist facies Restricted to MMZ NE directed shortening. Steepening of S_p towards the Ragga-Teuchl fault zone.	F_q folds(cm-100m) Smal-scale thrust faults cause l^q_p crenulations shortening of the mylonitic foliation perpendicular to l_p. Quartz preferred cryst. orientation deformed by crenulations and microthrusts.		
	30-40 Ma	Emplacement of subvertical dykes (N-S trending) contemporaneously with development of a conjugate set of sub vertical faults, N-S shortening and W-E extension.	Dykes cut across F_q		
	less than 30 Ma ago	Movement (strike-slip and dip-slip) along the Ragga-Teuchl fault zone. No dykes found north of this fault zone.			

Post-D_q deformation may also explain the scatter in l_p lineations, which might otherwise be expected to fall, on a stereogram, on a small circle about the F_q axis (assuming a mainly flexural flow mechanism of folding, accommodated along the mylonitic foliation), (Fig. 27). Lineations, which fall on the largest small circle about the average F_q axis, have been unfolded by

- rotating F_q to the horizontal (about a horizontal axis);
  then
- rotating (in both directions) the lineation along the rotated small circle to the horizontal.

The resultant two possible trends of the unfolded lineation give some estimate of the uncertainty in the original orientation of l_p, assuming that S_p was horizontal.

In general, microstructures suggest that the mylonites have developed in the following way:

1) Simple shear and plastic deformation in quartz bands.
2) Fracturing and extension of porphyroclasts (e.g. feldspar, tourmaline) parallel to the mylonitic foliation.
3) Shortening of the mylonitic foliation in a direction within the foliation and perpendicular to the lineation, accommodated along mesoscopic low-angle thrust faults and asymmetric folds.
4) Extension of the mylonitic foliation in a direction within the mylonitic foliation and perpendicular to that in (3), accommodated by meso- and microscopic normal faults with a listric fault geometry.

Evidence discussed earlier suggests that the mylonitic foliation (S_p) was originally subhorizontal. Assuming both this and that movement was parallel to the mylonitic lineation, microstructures suggest that, after removing the effect of D_q (discussed earlier), the original upper plate to the mylonitic shear zone moved NW (transport direction 300±40°), (Fig. 27), with a preferred direction of ca. 315°, relative to the lower plate.

4.3. Metamorphism of the Strieden Unit

4.3.1. Distribution of Minerals

(Figs. 28,29)

Schists in the Strieden Unit show a distinct high temperature metamorphic zonation. A high temperature (upper) sillimanite zone, with local evidence for partial melting, can be distinguished from a lower sillimanite zone, where sillimanite coexists with staurolite. A zone of andalusite-bearing schists can also be distinguished. The boundary between the sillimanite and andalusite zones defines a surface where sillimanite is in equilibrium with andalusite. Another surface, which marks the limit of staurolite occurrence, is subparallel to the sillimanite-andalusite transition zone. The intersections of these surfaces with the topography suggest that they dip gently (0–20° S–SE), but steepen up both near the MMZ (ca. 50° S) and the Strieden shear zone (ca. 90°) (Fig. 28B). The steepening near the MMZ may be due to D_q deformation, which folds the mylonitic foliation (S_p) (section 4). Furthermore, these surfaces are oblique to the MMZ. The MMZ cuts across the isograd surfaces at a shallow angle, and appears to cut down into higher grade rocks in the transport direction, towards NW. Sillimanite and andalusite-bearing schists are juxtaposed and deformed within the MMZ. In the following sections, the sillimanite-andalusite and staurolite surfaces are used as reference surfaces for determining the structural position of the metamorphic assemblages (Table 5). Therefore, the present maximum structural separation of samples discussed in this section is estimated to be about 1.5 km (ca. 0.5 kbar pressure difference).

4.3.2. Mineral Chemistry

Garnets

Garnets in andalusite-bearing metapelites (sample 554, Fig. 30A), show characteristic zoning patterns, and cores (gt I) can be texturally and chemically distinguished from rims (gt II). Garnets are generally euhedral and typically contain inclusions of quartz, ilmenite and graphite, in some cases showing evidence of rotation during growth (garnet I, Fig. 15; Plate 3 – Fig. 3). 'Normal' chemical zoning (HOLLISTER, 1966), characterised by bell-shaped patterns (Fig. 30A) for Mn and Ca, are typical, whereas Fe and Mg increase from the core towards the rim. The Mg zoning profile shows symmetrical maxima near the garnet rim, caused by a drop in the Mg/Fe ratio at the edges. At these Mg maxima, the mean garnet composition is: pyrope 8.8 mol-%; grossular 1 mol.-%; spessartine 3 mol.-%; almandine 87.2 mol.-%. In the cores of garnets, the composition is: pyrope 4.6 mol-%; grossular 5.6 mol.-%; spessartine 7.3 mol.-%; almandine 82.5 mol.-%.

The garnet rims (garnet II) are texturally different from the rest of the garnet (garnet I) ; they form clear, narrow, 100–500 μ wide, often discontinuous bands, often intergrown with small euhedral staurolite and biotite which crosscut the foliation S_n (Figs. 15, 18). It is therefore likely that the change in the garnet zoning pattern towards the garnet rim marks the crystallisation of new Fe- and Mg-bearing phases, such as staurolite and biotite; the resulting equilibria requiring the garnet to become less Mg-rich.

Within the sillimanite zone, garnets are variably replaced by biotite (e.g. samples 516.2, 136, Fig. 30B,C). In general, a modal rise of sillimanite and biotite is observed with increasing structural depth, and is accompanied by a decrease in staurolite, muscovite and garnet.

Corroded garnets form atolls, where garnet cores are replaced by coarse, randomly oriented biotite laths which contain bundles of fibrolitic sillimanite (Plate 3 – Fig. 1). The end-product of garnet breakdown is a matted knot of fibrolite intergrown with biotite, and still preserving the shape of the original garnet.

All analysed garnets within sillimanite-bearing rocks are characterised by an unusually high Mn or Ca content. In sample 516.2, which contains sillimanite-biotite pseudomorphs after garnet and rare garnet, the mean garnet core composition is: pyrope 8.2 mol.-%; grossular 3.2 mol.-%; spessartine 18.9 mol.-%; almandine 69.3 mol.-%; andradite 0.4 mol.-%. In this case, the high spessartine content (18.9 mol%), or in sample 136 the high grossular content (18.7 mol.-%), may have prevented garnet from further break down (Appendix D).

The Mn enrichment of garnet can be explained by either the result of:

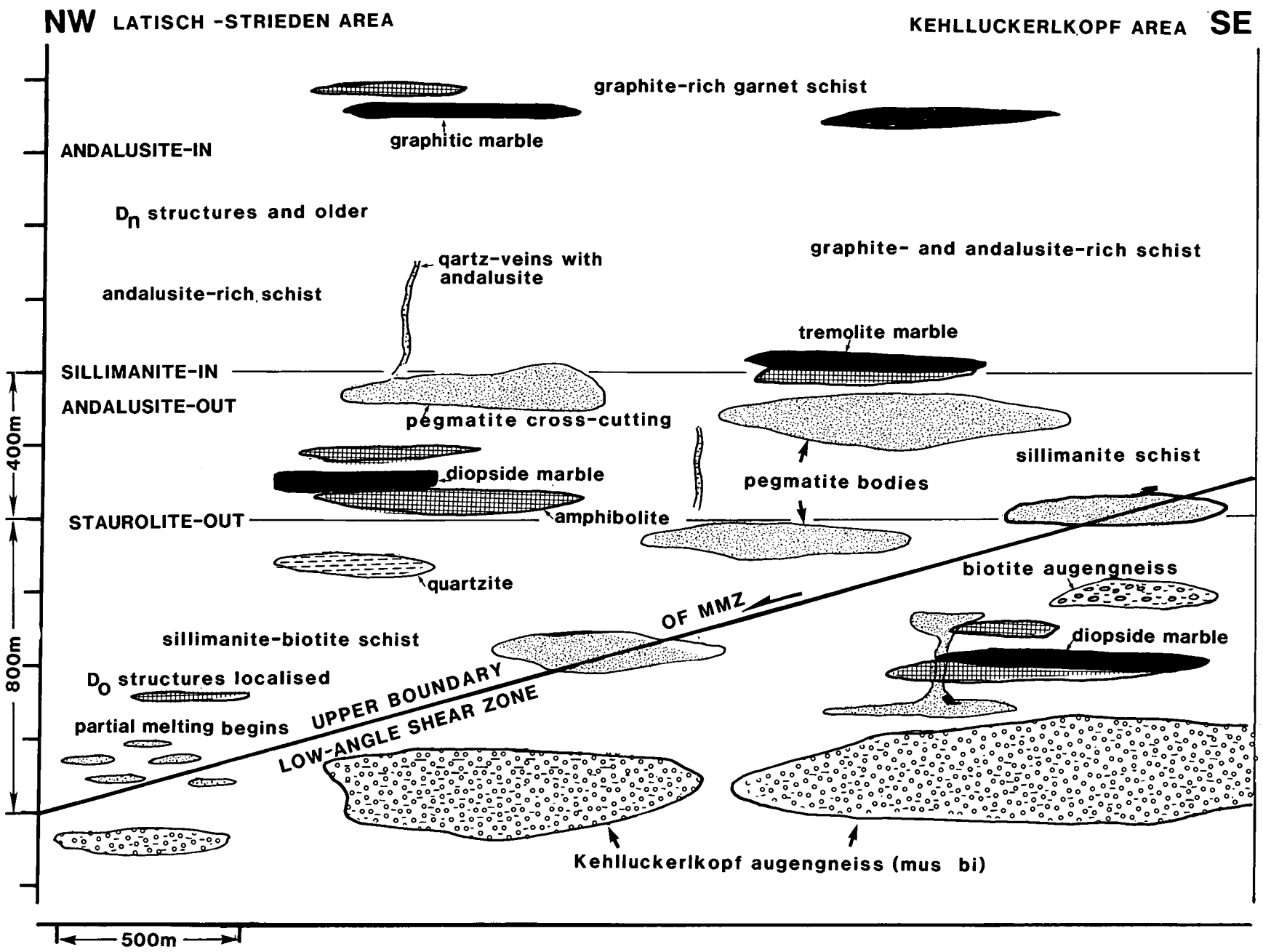

Text-Fig. 29.
Schematic summary cross-section through the basal part of the Strieden Unit, prior to the D_p and D_q deformation, parallel to the D_p stretching lineation (NW/SE), showing the metamorphic zonation in the different lithologies, and the postulated distribution of structural elements (D_n and D_0) prior to D_p and D_q deformation.

- replacement phenomena, with Mn concentrating in the remaining garnet as it breaks down;
  or
- the breakdown of ilmenite, releasing Mn, which was incorporated into garnet, while biotite accomodated the Ti.

Textural evidence suggests that ilmenite, which occurs as inclusions in garnets and also in the surrounding micas, recrystallised into coarse clots during garnet breakdown. Recrystallised ilmenite is typically more Mn-rich than primary ilmenite in the matrix (e.g. 0.9–1.2 % TiO_2 in the original ilmenite, 4–5 % TiO_2 in

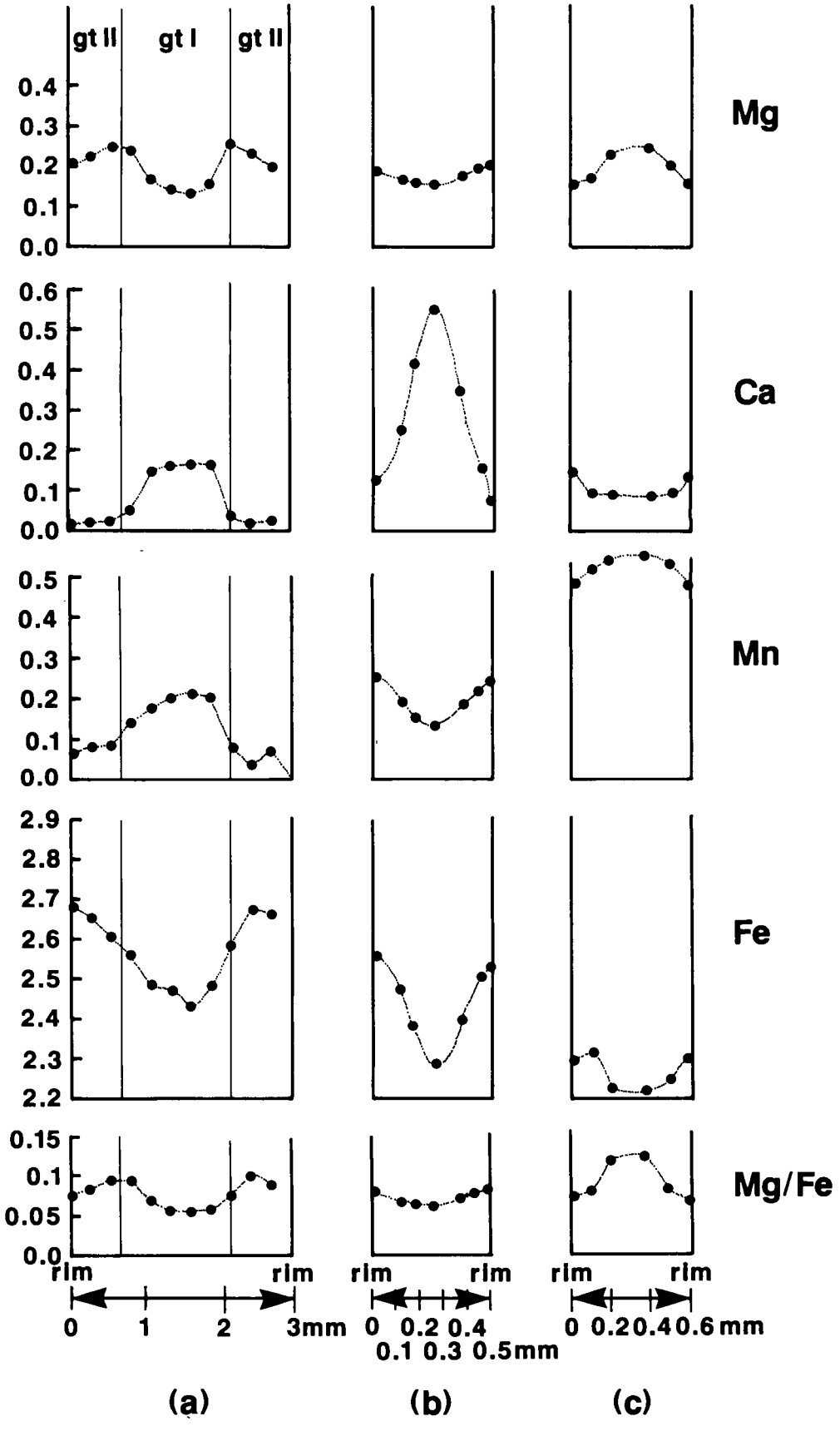

Text-Fig. 30.
Microprobe profiles of chemical compositions across garnets in the Strieden Unit schists, showing changes in chemical composition in different garnet generations (gtI, gtII).
a) From the andalusite zone, see Plate 3 – Fig. 3.
b) and c) Garnet profiles in schists in the sillimanite zone.

recrystallised ilmenite clots). Presumably, Mn in this ilmenite was derived from the breakdown of garnet, while the Ti and Fe came from the garnet and its original ilmenite inclusions.

Biotite

Sillimanite-free schists contain two biotite generations (samples 195,554):

- The older biotite generation (biotite I), which is aligned within the S_m foliation and also occurs as inclusions in garnet I, usually has a higher TiO_2 and $Fe_{tot}O$ content than
- a second generation (biotite II), which occurs as individual blades which cross-cut the S_m foliation. Biotite II is unzoned, with a homogeneous chemical composition throughout the thin section.

Biotites in sillimanite-bearing schists: In general, with increasing structural depth, a rise in the modal amount of biotite and sillimanite is accompanied by a decrease in the amounts of staurolite, muscovite and garnet. Biotites which occur as pseudomorphs after garnet, intergrown with sillimanite and also in the matrix, have a homogeneous composition on a thin section scale. However, on a regional scale, there is a trend towards more Fe-rich compositions at higher structural levels (Mg/Mg+Fe = 35–43), compared with those at deeper structural levels (Mg/Mg+Fe = 43–60). This trend reflects the relation between temperature of crystallisation and the composition of biotite end-members ($T_{Mg} > T_{Fe} > T_{Mn}$).

In the upper sillimanite zone, biotite, with inclusions of rutile needles, occurs intergrown with sillimanite fibrolite and shows ilmenite exsolution, particularly in kinked zones. This suggests that the original Ti content of biotites, during peak metamorphic conditions, may have been higher than their present content (1.9–2.6 TiO_2) and was exsolved during cooling.

White mica

(Fig. 31)

Two white mica generations can be distinguished:

- Coarse platy muscovite laths (mus I) aligned parallel to the S_m or S_n foliation;
  and
- fine-grained white mica aggregates (mus II) or shimmer aggregates which variably replace andalusite, sillimanite and staurolite.

All white micas are deficient in alkalis (Fig. 32C). The ratio of Na/Na+K in coarse grained muscovites (musc I) systematically varies and decreases with increasing structural depth: the mean value is 0.085 in sillimanite free schists, whereas it is 0.057 in sillimanite-bearing rocks. This K-enrichment in mus I is associated with a modal decrease of muscovite and a modal rise in sillimanite, which can be described by the continuous reaction:

Na-rich mus + qz = sill + ab + K-rich mus + H_2O

The occurrence of more sodic rims around plagioclase in sillimanite-bearing rocks also suggests this reaction, though these rims could also be related to exsolution of albite in plagioclase during cooling.

In any one sample, coarse grained platy muscovites (mus I) tend to be more sodic than the retrogressive muscovite (II). The latter co- exists with Na and Ca-rich muscovite (up to 7 % margarit), chlorite and albite, in shimmer aggregates replacing andalusite, sillimanite and staurolite.

Plagioclase

Three feldspar generations can be distinguished:

- The oldest plagioclase generation (plag I) occurs as inclusions in garnet I, where it is rarely observed. Here, the anorthite content varies between 20–41 mol.-%. The extreme anorthite content of 40 mol.-% is probably due to local Ca exchange between garnet and plagioclase.
- The second generation (plag II) predominates and occurs as coarse and often twinned grains, which overgrow S_n and typically contain trails of graphite and muscovite as inclusions, forming remnants of an older foliation. Plagioclase II is interpreted as one of the phases of the peak metamorphic mineral assemblage. Its composition is homogeneous or shows a slight inverse zoning in any one grain. On a regional scale, there is a progressive increase in the anorthite content with structural depth. The mean anorthite content in metapelites from andalusite-bearing schists and in the lower sillimanite zone is 13.7 mol-%, varying between 9.8–20 mol.-%, whereas in the upper sillimanite zone it is 26.9 mol.-% (varying between 22.4 and 30.42 mol.-%) respectively. The orthoclase content does not exceed 2 mol.-%.
  In the lower sillimanite zone, oligoclase is ri mmed by more sodic plagioclase which possibly formed in the reaction
  Na-rich mus + qz = sill + ab + K-rich mus + H_2O
  during peak metamorphic conditions.
  Another reaction which possibly has controlled the plagoclase composition is:
  gros + 2 Al_2SiO_5 + qz = 3 an.
- Pure albite compositions (plag III) are rare (< 2 mol.-% anorthite) and have only been found in shimmer aggregates, together with fine grained white mica and chlorite, which replace andalusite and staurolite. They are attributed to late stage alteration.

The sillimanite and andalusite Al_2SiO_5 polymorphs

The formation of both sillimanite and andalusite post-dates the D_n deformation.

Andalusite occurs as thin slender crystals in schists, largely replacing the mica-rich matrix and overgrowing garnet II, plagioclase II and staurolite (Plate 3 – Figs. 3,6; samples 554,195). It also occurs as euhedral, intergrown cm-sized crystals in quartz veins. Sillimanite predominantly occurs as fibrolite, nucleating and replacing biotite (Plate 3 – Fig. 1) and often intimately associated with ilmenite. It rarely forms prismatic crystals.

The chemical composition of both sillimanite and andalusite is fairly constant and approximates Al_2SiO_5. The only other ion detected during microprobe analyses is Fe_{tot}, which varies between 0–0.032 formula units, with a mean value of 0.006. It probably occurs as Fe^{3+}, replacing Al in the structure (Appendix D).

Staurolite

Two generations of staurolite can be distinguished (Plate 3 – Fig. 7), both of which seem to post-date D_n. They cross-cut each other and only differ chemically in their Zn content, with the second generation characterised by a higher ZnO content (up to 2.2 % ZnO) than

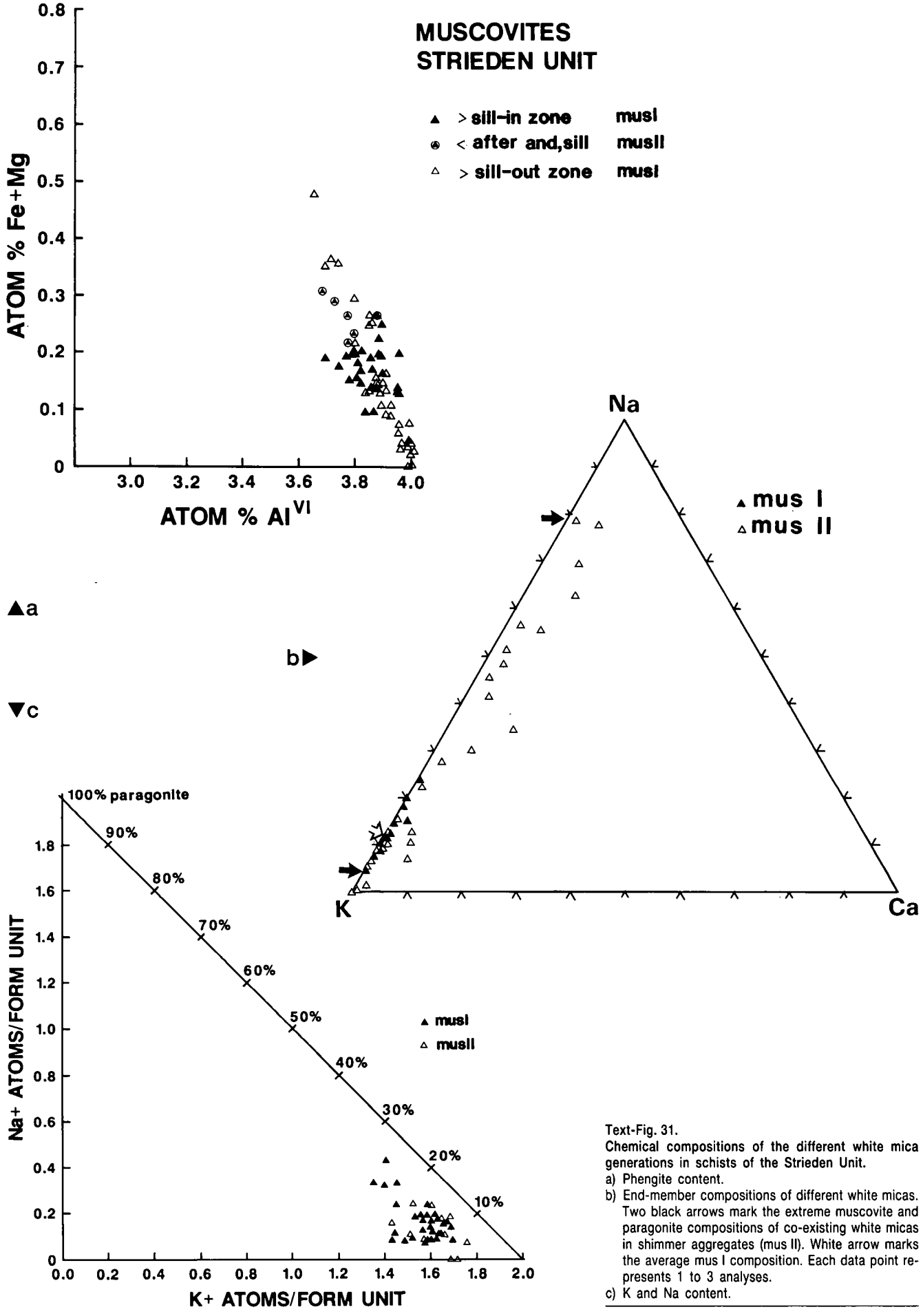

Text-Fig. 31.
Chemical compositions of the different white mica generations in schists of the Strieden Unit.
a) Phengite content.
b) End-member compositions of different white micas. Two black arrows mark the extreme muscovite and paragonite compositions of co-existing white micas in shimmer aggregates (mus II). White arrow marks the average mus I composition. Each data point represents 1 to 3 analyses.
c) K and Na content.

the first generation (ca. 0.3 % ZnO). Overall, the modal proportion of staurolite decreases with structural depth and individual staurolite crystals show an increased Zn-content. This can be described by the following continuous reaction:

low-Zn st + mus + qz = sill + bi + Zn-rich st + H_2O

in which the modal rise of sillimanite is ascribed to the continuous breakdown of staurolite.

Chloritoid

Chloritoid has only been found in shimmer aggregates, replacing andalusite. It forms fine-grained laths which overgrow the white mica fabric and occur associated with albite and chlorite.

Mg/Mg+Fe ratios in chloritoid range from 13–17, and the Mn content does not exceed 2 mol.-%. A possible chloritoid-forming reaction, which accounts for the localised mineral assemblage in which chloritoid is found, is:

5 pg + chl + 3 qz = 7 ctd + 5 ab +4 H_2O.

Chlorite

It occurs as a retrograde phase associated with the breakdown of garnet, staurolite and biotite, and also in shimmer aggregates. In the latter it can form cross-cutting blades.

All analysed chlorites are of ripidolite composition.

4.3.3. Phase relations

The different mineral assemblages within quartz – rich metapelites can be described in the system K_2O – FeO – MgO – SiO_2 – H_2O. They are shown on an AFM diagram , projected from the main potassium-bearing phase (muscovite or K-feldspar in muscovite free metapelites, Fig. 32), assuming that H_2O behaved as a mobile component during metamorphism, and ignoring the minor components TiO_2, Fe_2O_3, MnO, CaO, Na_2O.

Andalusite-bearing metapelites

(Fig. 32A)

In andalusite-bearing metapelites, the presence of four texturally equilibrated phases (st – gt – bi – and) suggests an univariant equilibrium. However, this is unlikely, because of the widespread occurrence of this assemblage. It is likely that the equilibrium assemblage buffered water with staurolite-producing and water consuming reactions such as:

7 gt + 5 mus + 6 H_2O = 6 st + 5 bi + 9 qz.

Textural evidence supports this reaction, and the presence of graphite in all andalusite-bearing metapelites suggests that the activity of water was less than

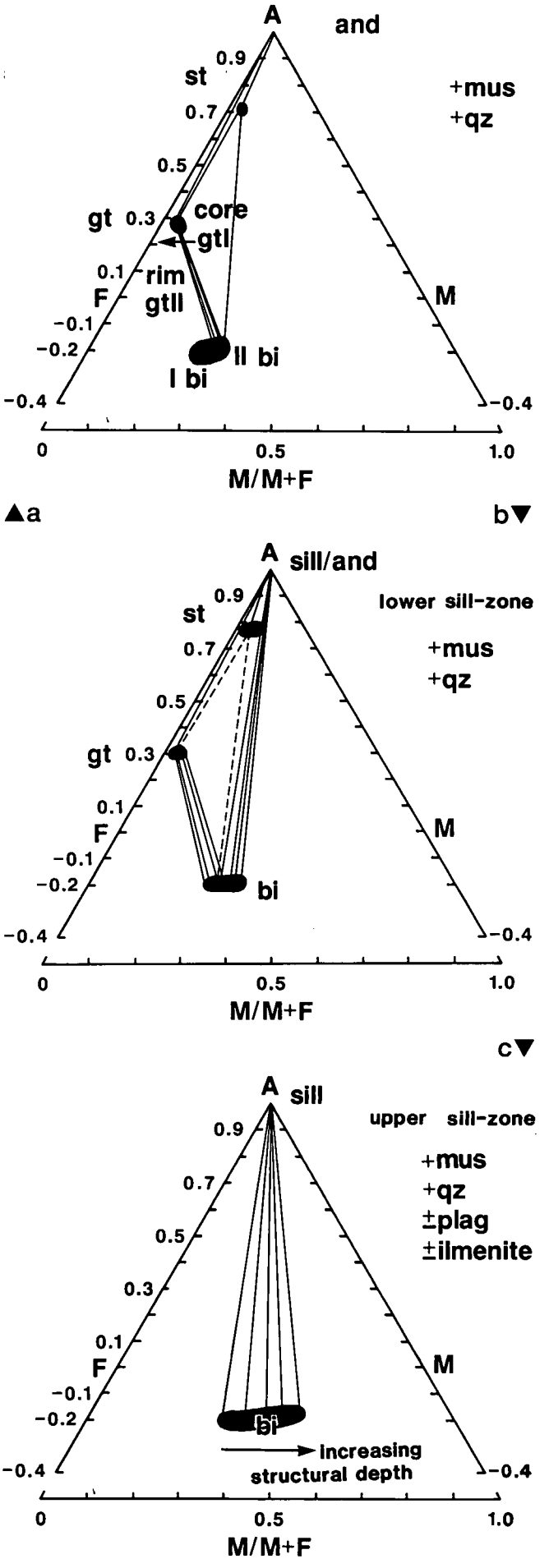

Text-Fig. 32.

Phase relations in quartz-rich metapelites of the Strieden Unit, described in the system K_2O – FeO – MgO – SiO_2 – H_2O on an AFM phase diagram. Phases are projected from the main potassium-bearing phase (muscovite or K-feldspar in muscovite-free metapelites), assuming that H_2O behaved as a mobile component during metamorphism, and ignoring the minor components, TiO_2, Fe_2O_3, MnO, CaO, Na_2O.

a) Andalusite-bearing schists; the phases staurolite, garnet, biotite and andalusite are shown.

b) Sillimanite-bearing schists from the lower sillimanite zone; the phases sillimanite, staurolite, garnet, biotite are shown.

c) Sillimanite-bearing schists from the upper sillimanite zone; the phases sillimanite and biotite are shown.

one, diluted by other components such as CH_4 or CO_2 during metamorphism. A low water activity is also suggested by the absence of fluid inclusions in the andalusite-bearing metapelites. The phase relations and mineral compatibilities explain also the breakdown of a more Mg-rich garnet (gt I) to staurolite, biotite II (more Mg-rich than biotite I), and almandine-rich garnet (gt II). The formation of staurolite appears to depend on

- the composition of garnet;
  and
- the availability of H_2O.

Lower sillimanite zone
(Fig. 32B)

The co-existance of staurolite and sillimanite on a thin section scale has been used to define the lower sillimanite zone (Fig. 28, Table 5). Within this zone, sillimanite replaces andalusite, and the modal proportion of staurolite decreases towards lower structural levels, accompanied by an increase in the staurolite Zn content. Locally two generations of staurolite occur, distinguished by their different Zn contents. The decrease in the modal proportion of staurolite can be explained by the staurolite consuming reaction:

st + Na-rich mus + qz =
sill + bi + K-rich mus + ab + H_2O + gt.

The disappearance of staurolite takes place within the stability field of muscovite and sillimanite.

The lower sillimanite zone is ca. 400 m thick (Fig. 28, Table 5) and is sandwiched between overlying andalusite-bearing metapelites and the underlying upper sillimanite zone (staurolite absent).

Upper sillimanite zone
(Fig. 32C)

It is defined by the presence of sillimanite without staurolite. The modal proportion of white mica decreases at structurally lower levels, accompanied by a progressive increase in the potassium content and decrease in the paragonite content of white micas. These changes can be explained by the reaction:

Na-rich mus + qz = sill + ab + K-rich mus + qz.

Garnet is progressively replaced, towards structurally lower levels, by biotite intergrown with sillimanite, described by the reactions:

gt + mus = bi + sill + qz
gt + Na-rich mus = bi + sill + ab + qz

Phase relations are shown in Fig. 32C which illustrates the increasing Mg/(Mg+Fe) ratio in biotite at structurally lower levels.

Partial melting
(Plate 5 – Fig. 28)

About 700 m below the top of the upper sillimanite zone, primary muscovite is absent in schists (e.g. sample 516). Muscovite only occurs as a retrograde phase, forming either small grains within or around feldspars, or large ragged crystals overgrowing biotite and sillimanite in cleavage zones. The disappearance of primary muscovite in the presence of quartz and plagioclase has been experimentally determined (STORRE & KARATKE, 1971, 1972) :

mus + qz + ab + H_2O = liquid + Al_2SiO_5.

This suggests that one might expect the products of anatectic melts in this part of the sillimanite zone, consisting of plagioclase, quartz, and Al_2SiO_5. The water content of such a melt would depend on that in the host rock. Biotite, which is ubiquitous, can be expected to behave as a refractory mineral (WICKHAM, 1987) . There is indeed some evidence for partial melting in the lowermost part of the sillimanite zone.

Within a small area, immediately above the upper boundary of the MMZ (200 m S of the Latischalm hut) , small leucogranitic pods (qz – ksp – plag – bi – sill) a few centimetres across, are found within sillimanite-biotite schists (Plate 3 – Figs. 9, 10). Within the pods, quartz, plagioclase and K-feldspar form a granular to polygonal texture with grains 0.5–2 mm across. The margins to the pods are cuspate in places, mantled by biotite (and sillimanite). The pods can be thought of as leucosomes, mantled by melanosomes or restites, which formed as a result of local melting of the surrounding schist (MEHNART, 1968) . Elsewhere, leucogranitic layers alternate with biotite-rich layers (Plate 3 – Fig. 9) . These have been deformed, containing a foliation, defined by the alignment of biotite laths, which is folded. These deformation structures are cut by pegmatites.

If the leucogranitic pods and layers do indeed represent partial melts, they place some constraints on the P/T conditions during metamorphism in the sillimanite zone (Fig. 38).

4.3.4. Metamorphic conditions

General considerations

❶ The experimentally determined stability field of staurolite, in the presence of muscovite and quartz

All examined metapelites, which contain staurolite, also contain quartz and muscovite. HOSCHEK (1969) has shown experimentally that in reactions which involve muscovite and quartz, staurolite with a MgO/(MgO+FeO) ratio between 0.2 and 0.4 breaks down at 575±15°C for a 2 kbar water pressure, and at 675±15°C for a 5.5 kbar water pressure. These temperatures may be too high because the reactions have not been experimentally reversed. The reaction line is plotted in Fig. 38.

❷ Stability of Al_2SiO_5 polymorphs

Andalusite and sillimanite are the main Al_2SiO_5 polymorphs in the Strieden Unit. Kyanite has only been found at one locality, about 200 m W of Saukopf (locality 397, Fig. 18A, Table 5) . However, the presence of all three polymorphs structurally close together suggests that metamorphic conditions in this part of the Strieden Unit were close to the triple point where the kyanite, sillimanite, and andalusite stability fields meet. This triple point has not been precisely determined, and the estimates of RICHARDSON et al. (1969), ALTHAUS (1967), and HOLDAWAY (1971) vary by several kilobars and up to a 100°C (see Fig. 38). SALJE (1986) shows that the thermodynamic equilibrium conditions depend very much on the structural state of the material, with the and =sill phase boundary becoming steeper in P/T space with increasing fibrolitization.

For the sake of argument, a triple point position, midway between that of RICHARDSON and HOLDAWAY, is used in this study (this is also used by HOLLAND & POWELL, 1985). However, as will be discussed later on, this may lead to important inconsistancies. The slopes of

Table 5.
List of mineral assembalges of analysed schists in the Strieden Unit, their structural position relative to the isograds, and thickness of mineral zones.

	SAMPLE	Mineral assemblage	- metres above (to isograds)			Total thickness in m
			and /sill isograd	st-in isograd	upper boundary of MMZ	
Andalusite zone	195	gt-st-bi-mi-qz-plag-zr-chl-ilm (and in adjacent rock)	200	650	1300	
	554	and-gt-st-bi-mi-qz-plag-zr-ap-chl-ilm	separated from all other samples by Streiden fault zone (Fig.8.1)			
Kyanite	397	sill-ky-qz-plag-tour-ap-mi-bi-ilm	just NE of Strieden fault zone			
LOWER sillimanite zone	136	sill-st-gt-bi-mi-qz-plag-tour-zr-chl-ilm-gph	-	100	850	400
	169	sill-bi-mi-qz-plag-ap-zr-ilm-gph	-	50	800	
UPPER sillimanite zone	302	sill-gt-mi-bi-qz-plag-ap-zr-ilm-gph	-	-	650	800
	336	sill-bi-mi-qz-plag-ap-tour-chl-or	-	-	350	
	31	sill-bi-mi-K.fsp-plag-gt-tour-zr-rut-ilm	-	-	350	
Zone of partial melting	408	sill-bi-mi-plag-qz-gt-ap-tour-ilm-rut	-	-	25	
	516.1	sill-bi-mus(secondary)-qz-plag-K.fsp-zr-ap-tour-ilm-rut	-	-	20	
	516.2	sill-bi-mus(secondary)-qz-gt-plag-ilm-rut	-	-	20	
Within the MMZ	514	and-sill-mi-bi-plag-qz-chl-rut-sph-or(hem)	-	-	-	
	70	sill-bi-gt-st-mi-bi-qz-plag-chl-ilm-ap-zr	-	-	-	
	91	sill-bi-gt-mi-qz-plag-tour-rut-ilm-hem-chl	-	-	-	

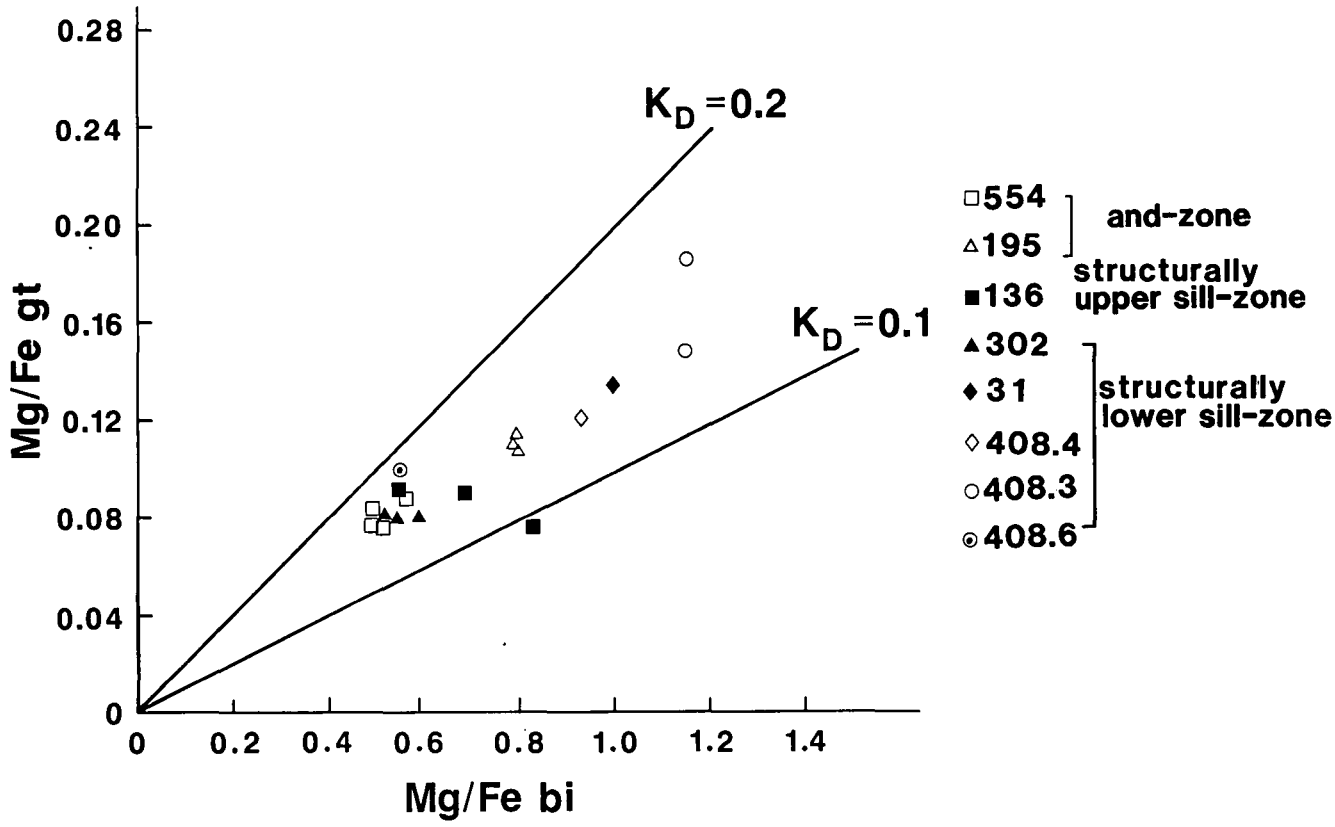

Text-Fig. 33.
Diagram illustrating Mg/Fe distribution in co-existing garnet and biotite pairs in different samples from the Strieden Unit, and their corresponding K_D values.

the boundaries to the stability fields, in a P/T diagram, are taken from HOLLAND and POWELL (1985), who essentially use a mean between HOLDAWAY's (1971) and RICHARDSON's et al. (1969) experimental determinations.

❸ Metamorphic conditions during the emplacement of pegmatites

The primary mineral assemblage observed in pegmatites, intruding sillimanite-bearing schists, is ksp – plag – qz – sill (±tour) with muscovite only occurring as a subsolidus phase.

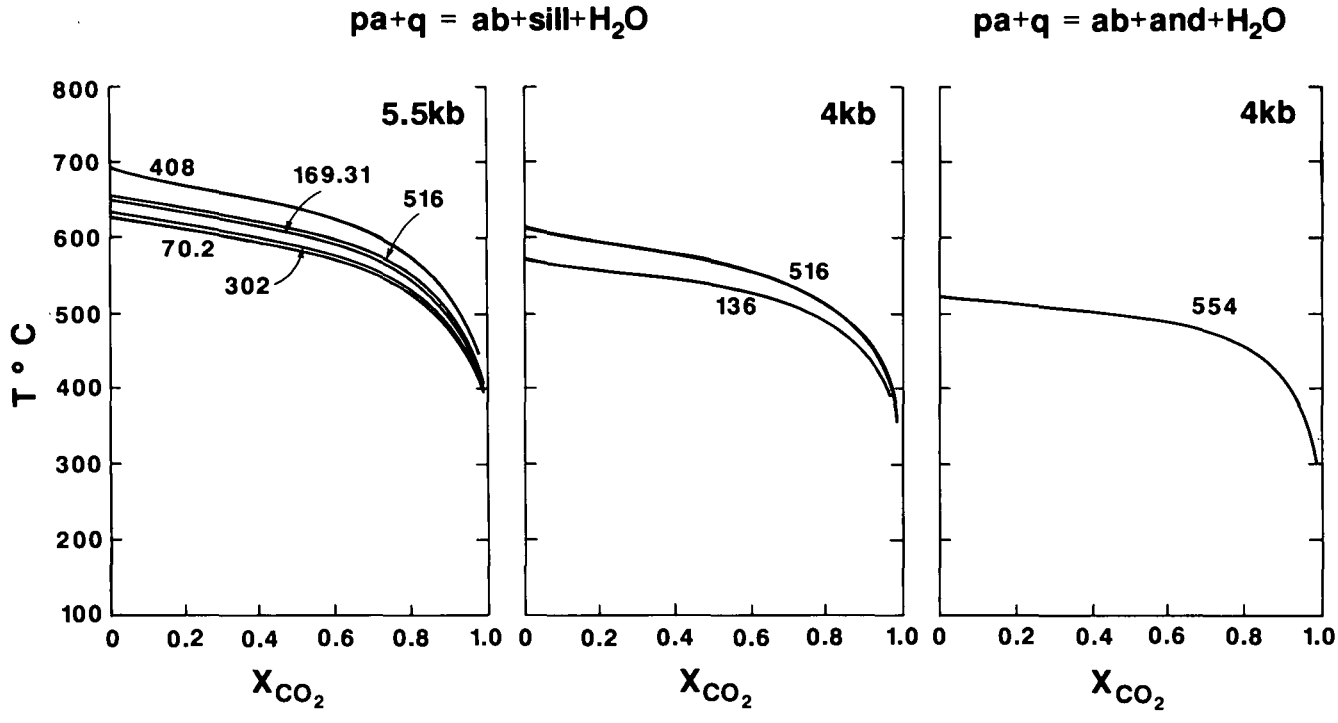

Text-Fig. 34.
Temperature – X_{CO_2} equilibrium curves at various pressures for the reaction pa + qz = ab + sill (and) + H_2O for different activities derived from the phases involved, in different schist samples of the Strieden Unit, using the program Thermo (HOLLAND et al., 1986).

The P/T field in which the pegmatites crystallised is constrained by the following:

- The absence of primary muscovite.
- The co- existence of ksp – plag – qz – sill.

The P/T conditions are therefore likely to fall in the triangular area in Fig. 37. The maximum pressure at which the primary assemblage ksp – plag – qz – sill has crystallised (muscovite absent), is ca. 3 kb (at 665°C) and therefore at approximately 10 km depth. The possible temperature range at which crystallisation has occurred is between 730–665°C (for a pressure range of 1–3 kb). After emplacement, the pegmatites must have cooled at a constant pressure towards the regional geothermal gradient present at the time, crossing the reaction line

$$ksp + Al_2SiO_5 + H_2O = mus + qz.$$

This led to the hydration reaction and breakdown of sillimanite and formation of subsolidus muscovite. This is supported by the observation that sillimanite in pegmatites is always mantled by muscovite. The abundance of muscovite, particularly at the pegmatite margins, suggests that there has been considerable interaction with water in these zones, resulting in the growth of muscovite and the obliteration of original igneous mineral textures.

The constraints on the metamorphic conditions of pegmatite emplacement suggest that the pegmatites have formed at lower pressures, and during a later separate event, than the abundent sillimanite found in the surrounding schists. Therefore the pegmatites cannot be regarded as the heat source required for the crystallisation of sillimanite in the metapelites. Geochronological date (section 5.3.2) also support this conclusion.

Pressure and temperature (P/T) calibrations

❶ Garnet-biotite geothermometer

Compositions from garnet II and adjacent biotites have been used, applying the method outlined by FERRY and SPEAR (1978). Garnets (except for sample 31) have suitably low Ca and Mn contents (Ca+Mn)/(Ca+Mn+Fe+Mg) ratios less than 0.2). However the Al^{IV} and Ti contents are high and the $(Al^{IV}+Ti)/(Al^{IV}+Ti+Mg+Fe)$ ratio is greater than the recommended 0.15 (varying between 0.1–0.27).

K_D values (Table 6, Fig. 33) vary between 0.094 and 0.171, corresponding to a temperature range at 6 kbars of 409–575°C (±50°C).

❷ Paragonite-albite geothermometer
(Figs. 34,35)

The same method is used as described in Section 3.3.2, using white mica II and plagioclase II. Paragonite activities vary between 0.36 and 0.78, and albite activities vary between 0.67 and 0.85. $T–X_{CO_2}$ curves for 5.5 and 4 kbars (Fig. 34) show that likely temperatures are fairly insensitive to vapour composition. X_{H_2O} of less than 0.3 is required to bring the equilibrium temperature below 550°C. Calibrated reaction lines are plotted in Fig. 35.

❸ Ilmenite-rutile geobarometer

The same method has been used as outlined in Section 3.3 and the results are shown in Fig. 36 and Table 7. This barometer could only be used in a few samples.

Results and discussion

The temperature and pressure constraints on samples from the Strieden Unit are summarised in Fig. 38, Table 8. This clearly shows a progessive decrease in both temperature and pressure towards structurally higher levels, as might be expected if the rocks have

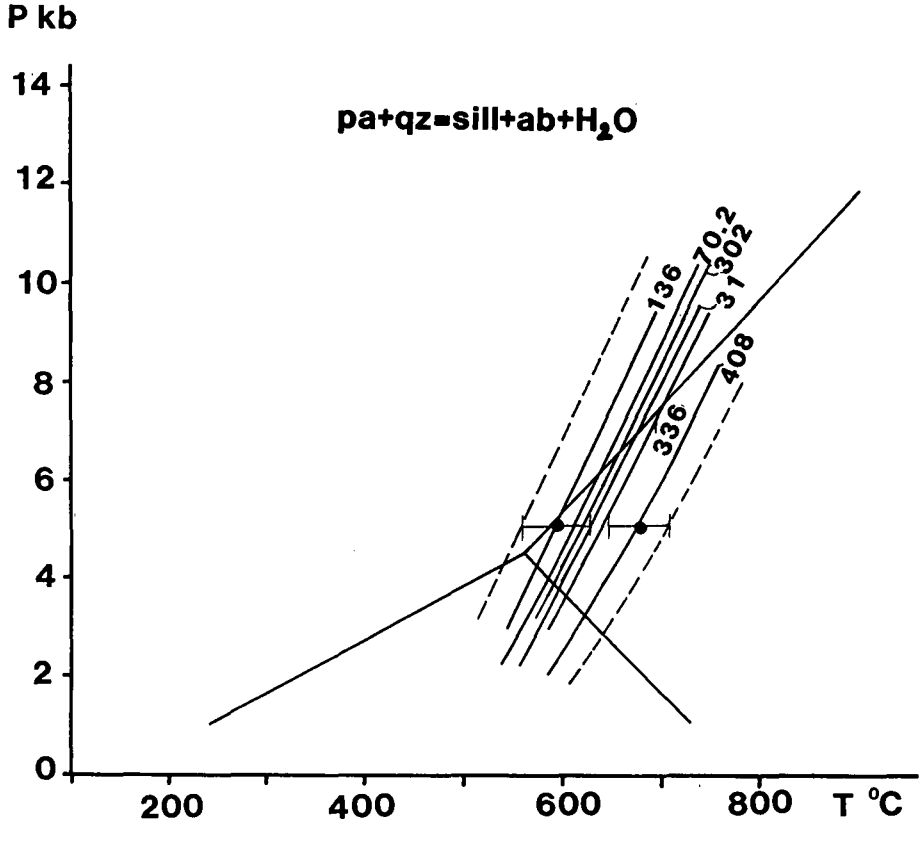

Text-Fig. 35.
Temperature–pressure plots for the equilibrium pa + qz = ab + sill (and) + H_2O for different samples of Strieden Unit schists.
Error bars show 2 sigma standard variation, using HOLLAND's et al. (1986) program Thermo.

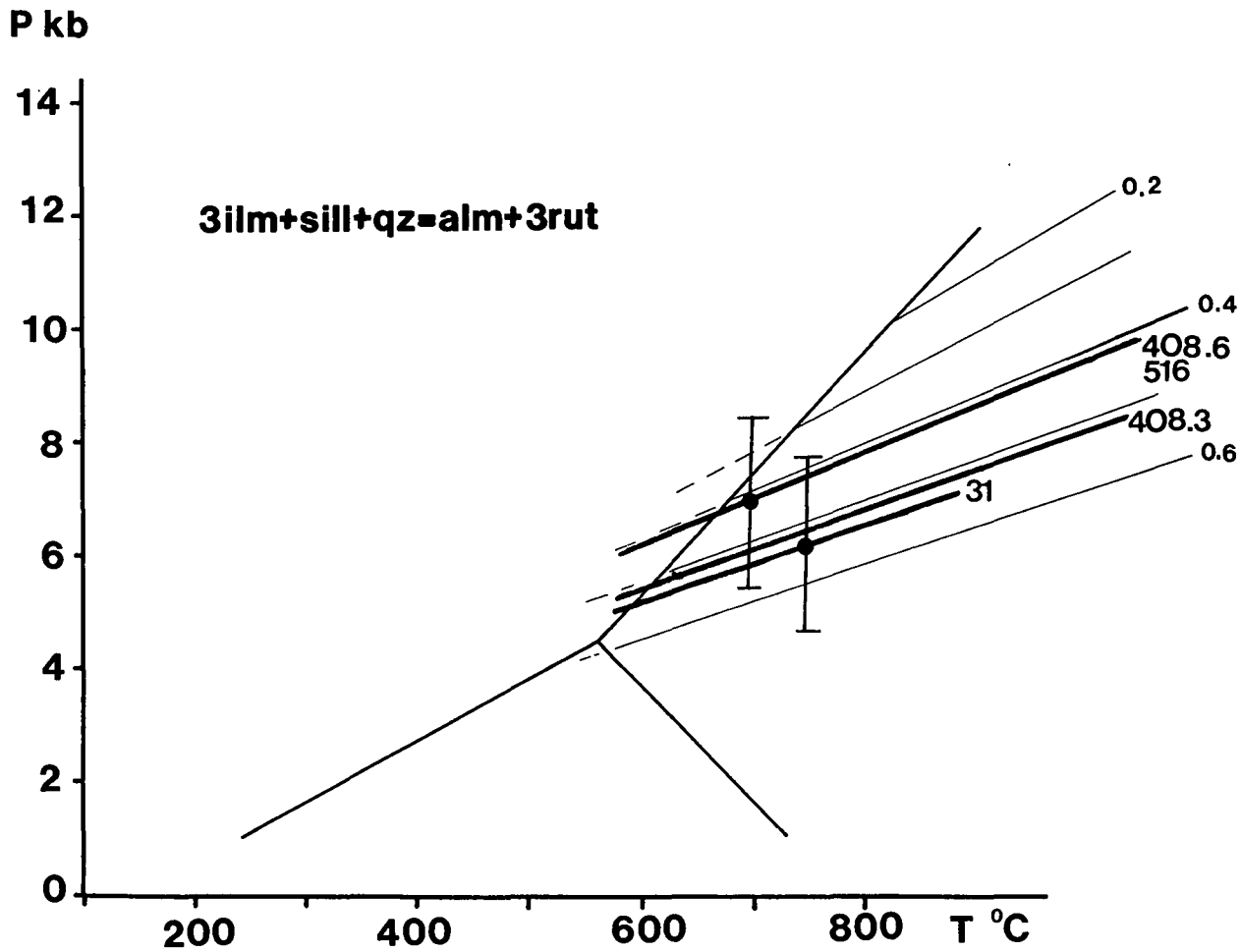

Text-Fig. 36.
P – T – $logK_D$ equilibrium reaction lines taken from BOHLEN et al. (1983) for different values of $logK_D$ (0.2–0.6) derived from the pressure sensitive reaction 3 ilm + sill + qz = alm + 3 rut.
$LogK_D$-values (Table 7) calculated for different samples of Strieden Unit schists and the corresponding pressures at 600°C, are shown.

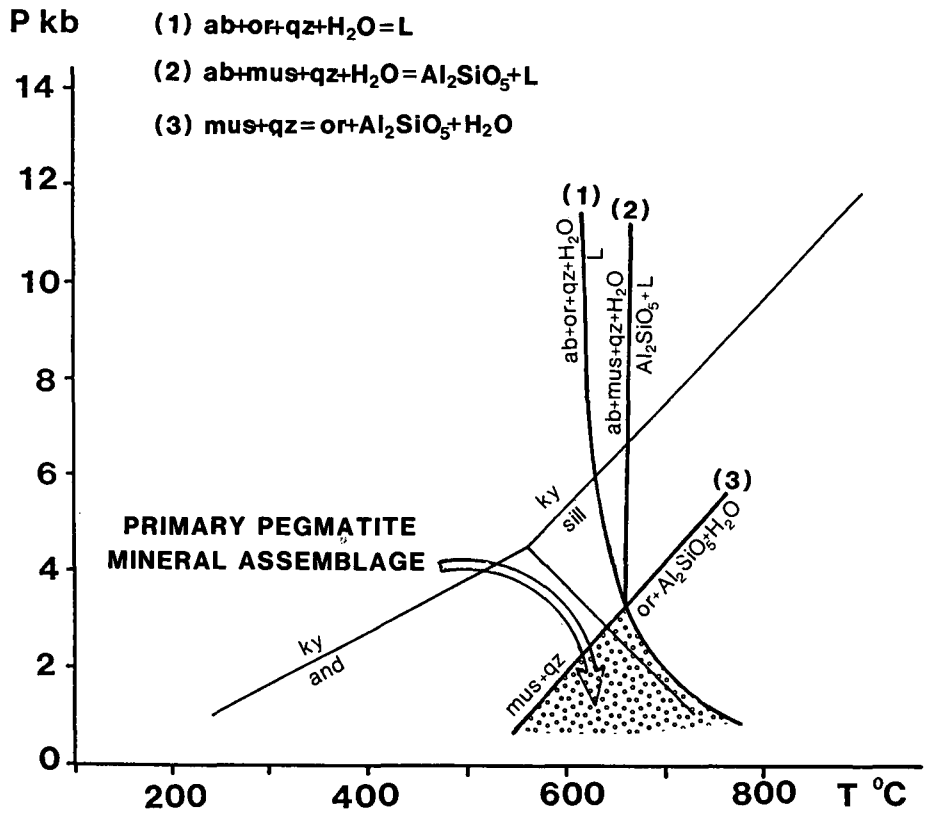

Text-Fig. 37.
Pressure–temperature diagram showing estimated conditions during emplacement of the ksp – plag – qz – sill ± tour pegmatites (no primary muscovite) at the base of the Strieden Unit.
The pegmatites crystallised at a maximum pressure of 3 kbars (at ca. 665°C). After emplacement, the pegmatites must have cooled, probably isobarically towards the regional geothermal gradient present at the time, crossing the reaction line (3) leading to the hydration reaction and breakdown of sillimanite and formation of subsolidus muscovite.

Table 6.
Mg/Fe ratios in co-existing garnet and biotite pairs from different samples of the Strieden Unit schists.
The distribution coefficients K_D = (Mg/Fe) gt / (Mg/Fe) bi for different garnet/biotite pairs are shown and the equilibrium temperatures T°(K) = (12454 + 0.057 × P) / (4.662–3R × lnK_D) (FERRY & SPEAR, 1978) are calculated.

SAMPLE	BIOTITE					GARNET				K_D	T°C 6kb ± 50°C	T°C 8kb ± 50°C
	Fe	Mg	Mn	Al^{IV}	Ti	Fe	Mg	Mn	Ca			
554	2.965	1.569	-	0.995	0.193	2.678	0.205	0.063	0.018	0.145	517	525
	3.070	1.528	-	0.985	0.192	2.661	0.205	0.077	0.027	0.155	538	545
	3.070	1.528	-	0.985	0.192	2.678	0.232	0.037	0.022	0.174	575	583
	2.569	1.444	-	0.289	0.142	2.689	0.237	0.038	0.016	0.157	542	549
195	2.571	2.028	-	1.000	0.159	2.488	0.277	0.153	0.04	0.141	510	517
	2.458	1.965	-	1.122	0.165	2.488	0.277	0.153	0.04	0.139	507	514
	2.458	1.965	-	1.122	0.165	2.485	0.284	0.143	0.038	0.143	514	521
136	2.370	1.964	-	1.135	0.180	2.373	0.185	0.259	0.12	0.094	409	415
	2.539	1.382	-	1.361	0.076	2.380	0.221	0.254	0.093	0.171	569	576
	2.602	1.798	-	1.000	0.256	2.352	0.215	0.246	0.101	0.132	492	499
31	2.263	2.299	0.016	0.979	0.197	1.911	0.258	0.673	0.104	0.133	494	500
302	2.782	1.445	-	1.097	0.266	2.347	0.190	0.275	0.089	0.156	540	547
	2.931	1.619	-	0.881	0.266	2.360	0.180	0.280	0.181	0.138	504	511
	2.784	1.637	-	1.003	0.270	2.392	0.194	0.292	0.103	0.138	504	511
408.6	2.963	1.617	0.022	0.883	0.261	2.15	0.219	0.532	0.032	0.187	599	607
408.3	2.243	2.579	-	0.705	0.211	2.014	0.375	0279	0.306	0.162	552	559
	2.243	2.579	-	0.705	0.211	2.023	0.300	0.343	0.280	0.129	485	492
408.4	2.502	2.322	0.16	0.674	0.182	2.192	0.266	0.272	0.253	0.131	489	496

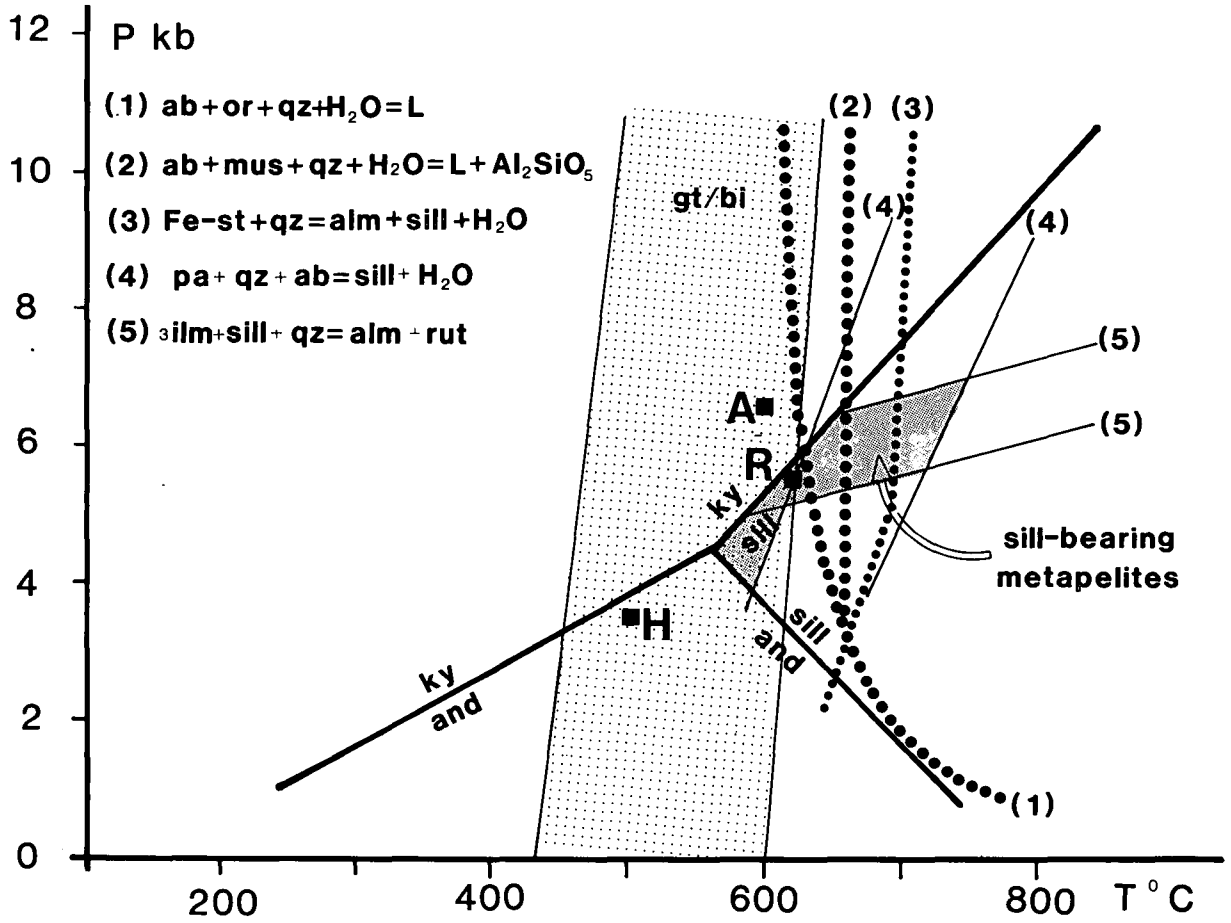

Text-Fig. 38.
Pressure-temperature estimates for peak Variscan metamorphic conditions in sillimanite-bearing schists of the Strieden Unit.
The position of the Al_2SiO_5 triple point has been determined experimentaly by various authors: A = ALTHAUS (1967) ; H = HOLDAWAY (1971) ; and R = RICHARDSON et.al. (1969). And - sill, and - ky and ky - sill equilibria have been plotted using HOLLAND & POWELL's (1986) data set, which predicts a position midway between R and H.

Table 7.
List of samples and pressures calculated for a fixed temperature of 600°C, using the reaction 3 ilm + sill + qz = alm + 3 rut (BOHLEN et al., 1983).
Pressures for various logK values have been taken from Fig. 3 in BOHLEN et al. (op. cit.).

SAMPLE	a_{alm}	K = $(1/a_{alm})$	log K	~P(Kb) at 600°C	P(Kb) at 800°C
516	0.392828	2.55	0.41	6.0	7.5
408.3	0.311118	3.21	0.51	5.0	6.5
408.6	0.392640	2.55	0.41	6.0	7.5
31	0.266581	3.75	0.57	4.5	6
8	0.269761	3.71	0.57	4.5	6

undergone a burial metamorphism. However, the uncertainties are large. The samples have experienced pressures of 5.5±1.5 kbars, and temperatures of 650±100°C, roughly falling on a line in P/T space with a gradient of 25–30°C/km. This is a reasonable 'normal' geothermal gradient, however the pressure differences between the structurally highest and lowest samples appears to be about 2.5 kbars, which is equivalent to about a 9 km structural height difference (Fig. 38). This is clearly incompatible with the presently observed maximum structural separation of about 1.5 km. There may be several explanations for this inconsistency:

1) It is an artifact of a combination of the large uncertainties in the P/T estimates, especially those based on the position of the Al_2SiO_5 triple point, and unconstrained systematic errors. If the Al_2SiO_5 triple point is in reality closer to that of RICHARDSON et al. (1969), at a higher pressure, the apparent pressure separation between the structurally lowest and highest samples is largely removed. However, even in this case P/T estimates of some samples will be out of the brackets given in Fig. 38, if they are to fall in the narrow pressure range suggested by the present structure.
2) Important structural deletion has occurred subsequent to the metamorphic imprint. An important mylonite zone, which shows an extensional fabric (D_p) cuts off the base of the metamorphic sequence. Other minor extensional deformation zones occur within the metamorphic sequence (section 4.2.3). However, the amount of crustal thinning is not known, though it does not seem likely that the thin mylonite zones within the metamorphic sequence have been responsible for deleting more than 7.5 kilometres of structural thickness, though they could have removed a kilometre or so.

5. Geological Synthesis

The differences between the Polinik Unit and the Strieden Unit, such as their structural separation, contrasting lithologies, different structural and metamorphic histories, make it difficult to provide a relative, let alone absolute, combined chronology for the study area, without using geochronological data, which require interpretation.

5.1. Geochronological Data from the SE Tauern Area

A large number of samples from the south-eastern Tauern area have been dated, using the K/Ar method (OXBURGH et al., 1966; BREWER, 1969, 1970; LAMBERT, 1970; WATERS, 1976; HAWKESWORTH, 1976; CLIFF et al., 1971; CLIFF, pers. com.) (Fig. 39).

5.1.1. General Considerations on the Significance of K/Ar ages

The K/Ar age of a mineral will depend to a large extent on the thermal history of the rock (Fig. 40). In the simplest case, the K/Ar age of a system gives the time elapsed since the system cooled below some critical temperature (blocking temperature) at which the rate of radiogenic argon escape from the system becomes negligible (DODSON, 1973). A combination of K/Ar ages from different minerals with different known blocking temperatures, such as muscovite and biotite, in a suite of rock samples from different structural depths, can be used to estimate uplift rates and the geothermal gradient that prevailed during cooling.

K/Ar ages are also affected by other factors:

1) The grain size of the potassium-bearing mineral: Large minerals are completely outgassed at higher temperatures or over a longer period than small grains, and therefore can give different ages from those obtained from small grains.
2) K-bearing minerals can form diagenetically at temperatures below their blocking temperatures. In this case, the mineral will either give an age dating mineral growth, or a mixed age if the host environment contains argon.
3) If, even at temperatures far above the blocking temperature, the mineral is in an environment with a high argon pressure, the mineral will record a mixed age after it has cooled, as the initial argon concentration immediately after cooling will not be zero (excess argon). The effects of excess argon have been described by BREWER (1969, 1970) and WATERS (1976) from the Altkristallin, within, and in areas adjacent to the study area.

Table 8.
Summary table listing all analysed schist samples in the Strieden Unit, and the various reactions and methods used to calculate P-T estimates. Constraints on the P-T conditions are given by the intersecton of the individual reaction lines.

SAMPLE	gt/bi (Ferry & Spear 1978) T(±50°C)	pg/ab (Holland & Powell 1985)	Al_2SiO_5	ilm/rut (Bohlen et al. 1983)	P/T field defined by intersection of reaction lines	Mineral zones
195	6kb:507-514°C 8kb:514-521°C	-	and	-	≤ 5.5kb 450-675°C	andalusite zone
554	6kb:517-575°C 8kb:525-583°C	4kb:615±5°C 6kb:674±6°C	and	-	≤ 5.5kb 500-650°C	
136	6kb:409-569°C 8kb:415-576°C	4kb:571±3°C 6kb:617±3°C	sill	-	4.2-5.5kb 550-625°C	LOWER sillimanite zone
169	-	4kb:607±6°C 6kb:657±7°C	sill	-		
302	6kb:504-540°C 8kb:511-547°C	4kb:598±3°C 6kb:647±3°C	sill	-	4.4-7.3kb 620-690°C	UPPER sillimanite zone
31	6kb:494°C 8kb:500°C	4kb:610±8°C 6kb:660±9°C	sill	600°C : 45kb	5.4kb 650±20°C	
408	6kb:485-599°C 8kb:492-607°C	4kb:648±10°C 6kb:703±11°C	sill	600°C : 5-6kb	5.5-7kb 675-750°C	
516	-	4kb:617±8 6kb:668±9	sill	600°C : 6kb	5-6.6kb 615-700°C	
70.2	-	4kb:590±7 6kb:638±7	sill	-		Within MMZ

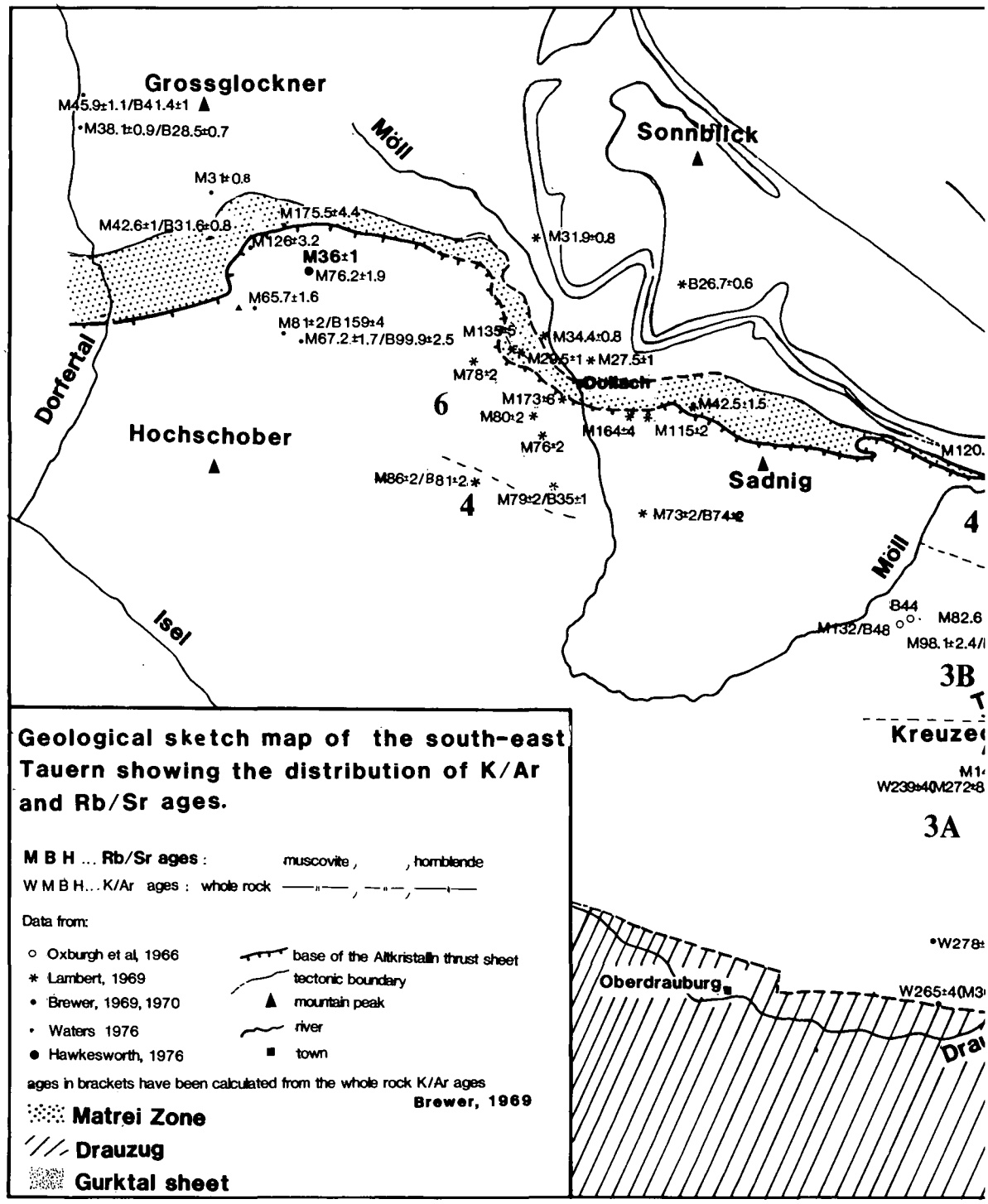

Text-Fig. 39.
Compilation of K/Ar and Rb/Sr whole rock and mineral geochronological age data in the SE Tauern area. Ages can be used to define age provinces (1, 2, 3a, 3b, 4, 5, 6; see text), characterised by a particular pattern of ages. Major geological units are also shown.

5.1.2. K/Ar age Distribution in Altkristallin Rocks of the Study Area and Adjacent Areas

In the light of the considerations discussed above, the Altkristallin in the study area and adjacent regions can be divided into six age provinces, trending W–E, which each show a particular pattern of ages (summarised in Figs. 39, 41). They demonstrate consistant age profiles (Fig. 42). Below the Permo-Mesozoic unconformity, in the Drauzug area, ages are Palaeozoic, becoming progressively younger, towards the N, with concordant K/Ar mica ages of ca. 80 Ma in the Polinik Unit. The latter are interpreted as cooling ages from a Cretaceous burial metamorphism (section 3.3.2) in which peak temperatures were reached at ca. 105 Ma (see age section on province 2).

Province 1

In the structurally highest parts of the Altkristallin, immediately below the Permo-Mesozoic unconformity surface in the Goldeck area, BREWER (1969, 1970) has measured uniform K/Ar whole rock and mica ages of 300–320 Ma (Fig. 39). The muscovite, biotite and whole rock ages are all similar and are considered to be true cooling ages from a Variscan regional metamorphism, and have not been disturbed subsequently.

Further west of this area, in the southernmost part of the Kreuzeck area, age province 1 is not apparent.

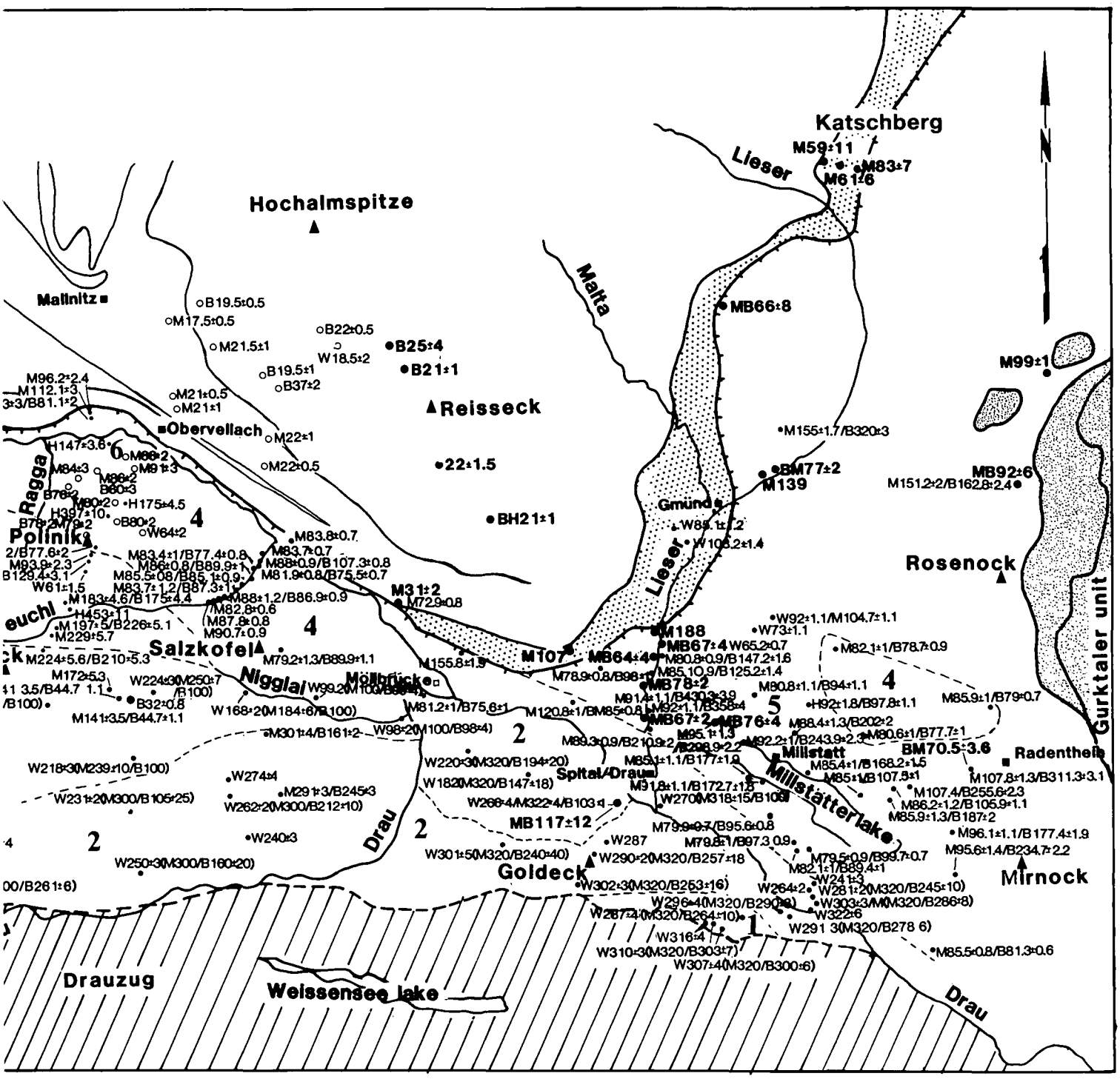

Here, the Drauzug sedimentary sequences rest unconformably on phyllites (possibly Palaeozoic in age) which in turn rest on higher grade schists of age province 2. The precise age of these phyllites and their structural relationship with the underlying Altkristallin schist is not clear. A structural break along the Drau valley is possible.

Province 2

Immediately north of age province 1, in the northern Goldeck and southern Kreuzeck areas, BREWER (op. cit.) has determined ages which are consistantly ca. 300 Ma for muscovite, and between 100 and 300 Ma for biotite, becoming younger towards the north (Figs. 39, 41). Many of these mineral ages were calculated from whole rock ages, and a knowledge of the volume proportions of biotite and muscovite in the rock. This assumes that muscovite and biotite are the only minerals which contribute to the whole rock age. BREWER (1970) constrained these calculated mineral ages with measured mineral ages from a few samples. He interpreted the ages of province 2 to be a consequence of a brief reheating of rocks at ca. 105 Ma (see below), which last cooled at ca. 300 Ma (as in province 1), at temperatures between the blocking temperatures of biotite (ca. 300°C) and muscovite (350–380°C). The biotites only partially outgassed, while the muscovites were unaffected and retained their Variscan cooling ages (Fig. 42).

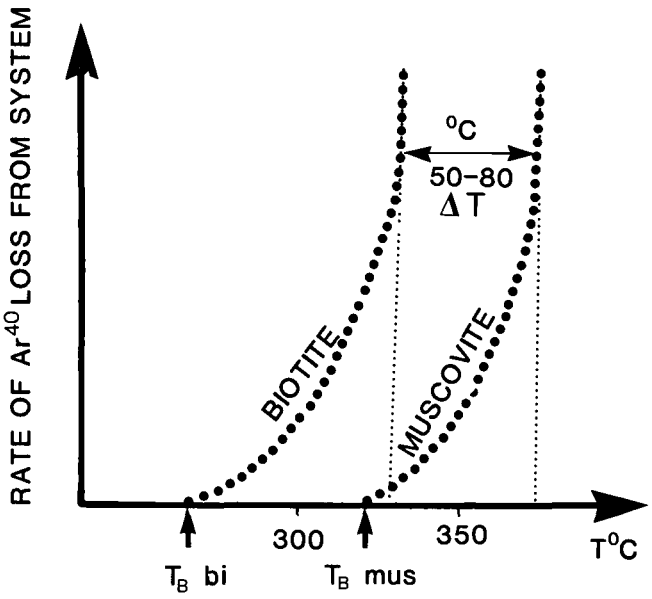

Text-Fig. 40.
Sketch diagram illustrating the likely relationship between temperature and the rate of Ar40 loss from muscovite and biotite.
The blocking temperature is defined here as the temperature at which the rate of argon loss is negligible. Above ca. 400°C, the K/Ar mica systems are considered to be fully open to argon diffusion.

An estimate of the age of the peak temperature reached during the Cretaceous metamorphism is given by one sample (G18), from which BREWER (1970) measured an unaffected Palaeozoic age in white mica of 322 Ma, but found that the biotite age has been reset during the Cretaceous, giving an age of 103±2 Ma. This sample must have experienced a critical temperature between the blocking temperatures of muscovite and that of biotite which could not have been maintained over a long period of time and therefore probably records the age of the peak temperature experienced by this sample during the Cretaceous metamorphism.

BREWER (1969) defined surfaces on which the rocks show identical biotite ages and also muscovite ages. He called these surfaces synchrons, which dip at about 10 degrees to the south and are assumed to have been parallel to the earth's surface ca. 100 Ma ago. The dip of these surfaces indicates that towards the north progressively deeper structural levels of the Altkristallin, with respect to these synchrons, are exposed.

Province 3A

Immediately north of province 2, within a ca. 1.8 km thick zone (measured perpendicular to the synchron surfaces), BREWER found rocks with biotite ages of ca. 100 Ma, and muscovite ages between ca. 300 Ma and 100 Ma, becoming progessively younger at deeper structural levels (Figs. 39,41,42). This zone is bound by subvertical fault zones (Fig. 41), which converge towards the east. Synchrons dip more steeply (20 degrees and steeper) near these fault zones. The age pattern in province 3A can be interpreted as a consequence of a brief reheating between the blocking temperature of muscovite, which approximately coincides with the temperature at which biotite became fully outgassed, and the temperature at which muscovite became fully outgassed (Fig. 42). If one assumes that this temperature difference is roughly the same as the temperature difference between the blocking temperatures of biotite and muscovite (50–80°C, Fig. 40) and that the synchrons reflect the instantaneous temperature distribution, one can calculate a geothermal gradient between 28 and 44°C/km (50–80°C/1.8 k m) across this zone.

Province 3B

North of province (3A), separated by a fault, ages measured by WATERS (1976) define a zone where both muscovite and biotite have ages between 150 and 250 Ma, intermediate between the 300 Ma and 100 Ma cooling ages (Fig. 41). This zone also includes the Strieden Unit. These mixed ages can be interpreted as a consequence of reheating, as in province 3A, somewhere between the blocking temperature of muscovite and the temperature at which muscovite became completely open to argon diffusion. However, the similarity of the biotite and muscovite ages needs to be explained. Rocks in province 3B are distinctly coarser grained (medium- to coarse-grained schists and gneisses with large muscovite and biotite crystals) than the fine-grained schists in provinces 3A and 2. BREWER (1969) also remarks on the grain-size difference, which he suggests might have affected the age pattern. It is suggested in this study, that because of the larger grain-size in province 3B, both muscovite and biotite were only partially outgassed, yielding intermediate cooling ages (Fig. 43).

Province 4

This province lies to the north of province 3B, separated from it by the Ragga-Teuchl and Strugenkopf fault zones (Fig. 41). Province 4 is characterised by muscovite and biotite ages of 80–90 Ma, which are interpreted as true cooling ages, and are discussed in more detail in the section dealing with the age of deformation and metamorphism in the Polinik Unit (section 5.2.1).

Province 5

Altkristallin rocks to the NE of the Drau valley, in the Millstätter lake area, yield anomalous K/Ar mica ages (BREWER, 1969, 1970) (Fig. 39). They are anomalous because the biotite ages are much older (by up to a factor of five times) than the co-existing muscovite ages, which is not a normal blocking temperature relation. BREWER (1969) discusses this problem and suggests that the age pattern is a result of excess argon (Fig. 42). The high argon pressure was due to argon outgassing at lower structural levels, as a consequence of reheating, with Ar migrating upwards and being trapped in the micas as the rocks cooled through the mica blocking temperatures.

Province 6

At the margins to the Tauern Window, within the Altkristallin near the basal contact, K/Ar ages (whole rock and mica ages) of less than 70 Ma years are found (OXBURGH et al., 1966; LAMBERT, 1970; WATERS, 1976; HAWKESWORTH, 1976), (Fig. 39). These were then believed to be a consequence of a Tertiary reheating (Tauern crystallisation), which has partly reset the Cretaceous cooling ages. This heating resulted in metamorphism within the Tauern Window, where rocks give K/Ar mica cooling ages ranging between 18 and

22.5 Ma (OXBURGH et al., 1966) (Figs. 39, 41). However, recent Rb/Sr dating along the base of the Altkristallin, of rocks characterised by an extensional deformation fabric which post-dates the Cretaceous metamorphism, has yielded 40– 50 Ma ages (WALLIS, 1988). WALLIS (1988) interpretes these ages to date the final stages of an extensional deformation which resulted in the contact relationships of the Altkristallin and the Matrei Zone. He also argues that these ages cannot be due to the Tauern metamorphism, which is too low in this area to reset the Rb/Sr systematics in white micas.

The sharp break in the pattern of ages across the margin of the Tauern Window which is seen north of the study area (Fig. 41) is interpreted as a consequence of movements along the Mölltal fault zone in the Tertiary.

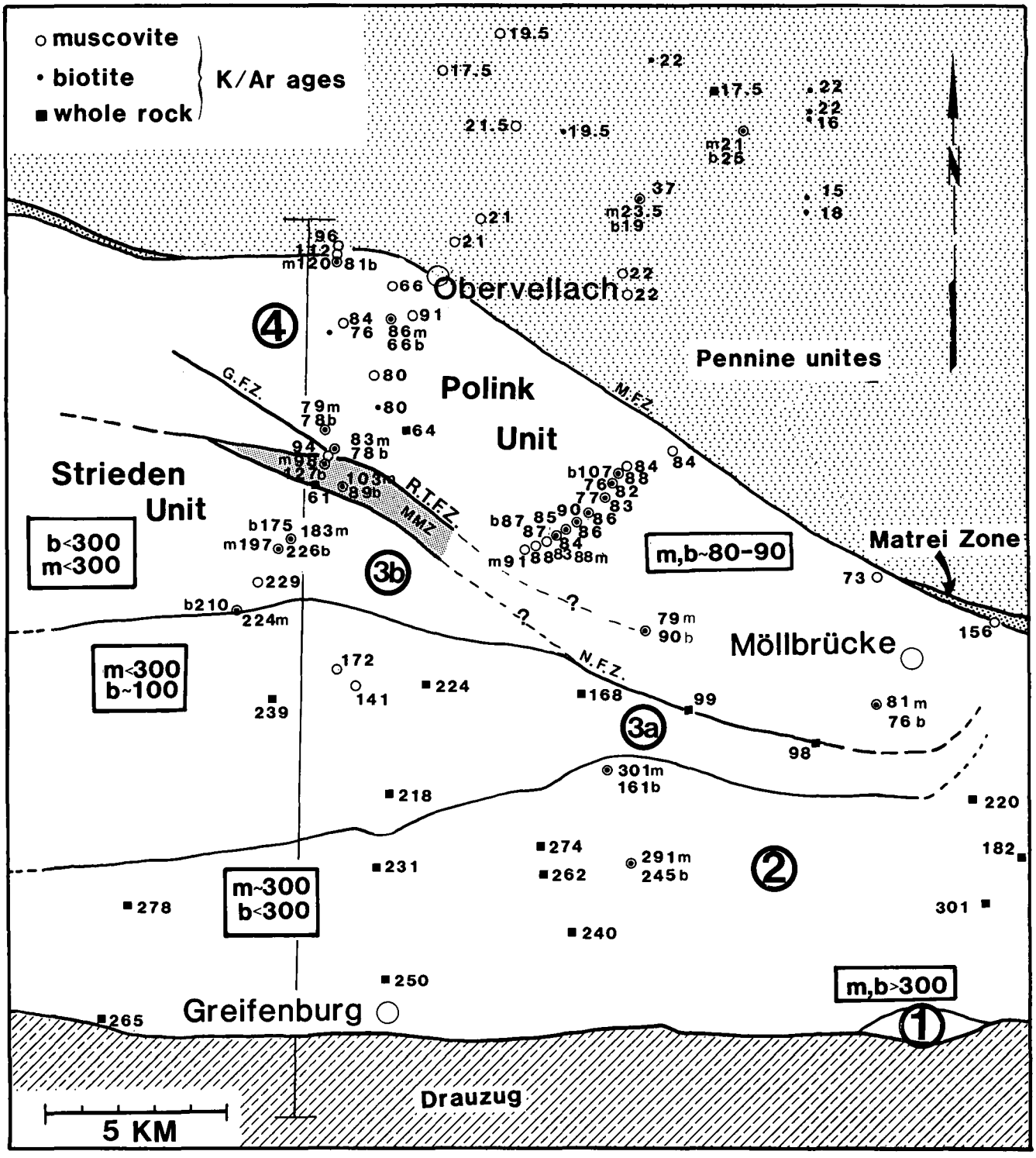

Text-Fig. 41.
K/Ar ages in the study area and in adjacent areas, labelled 1, 2, 3a, 3b, 4.
They define various age provinces, discussed in the text. A summary N-S cross-section is illustrated in Fig. 42. Major structural features are: M.T.Z. = Mölltal fault zone; R.T.F.Z. = Ragga Teuchl fault zone; G.F.Z. = Grießenegscharte fault zone; N.F.Z. = Nigglaibach fault zone; MMZ = Main Mylonite Zone.

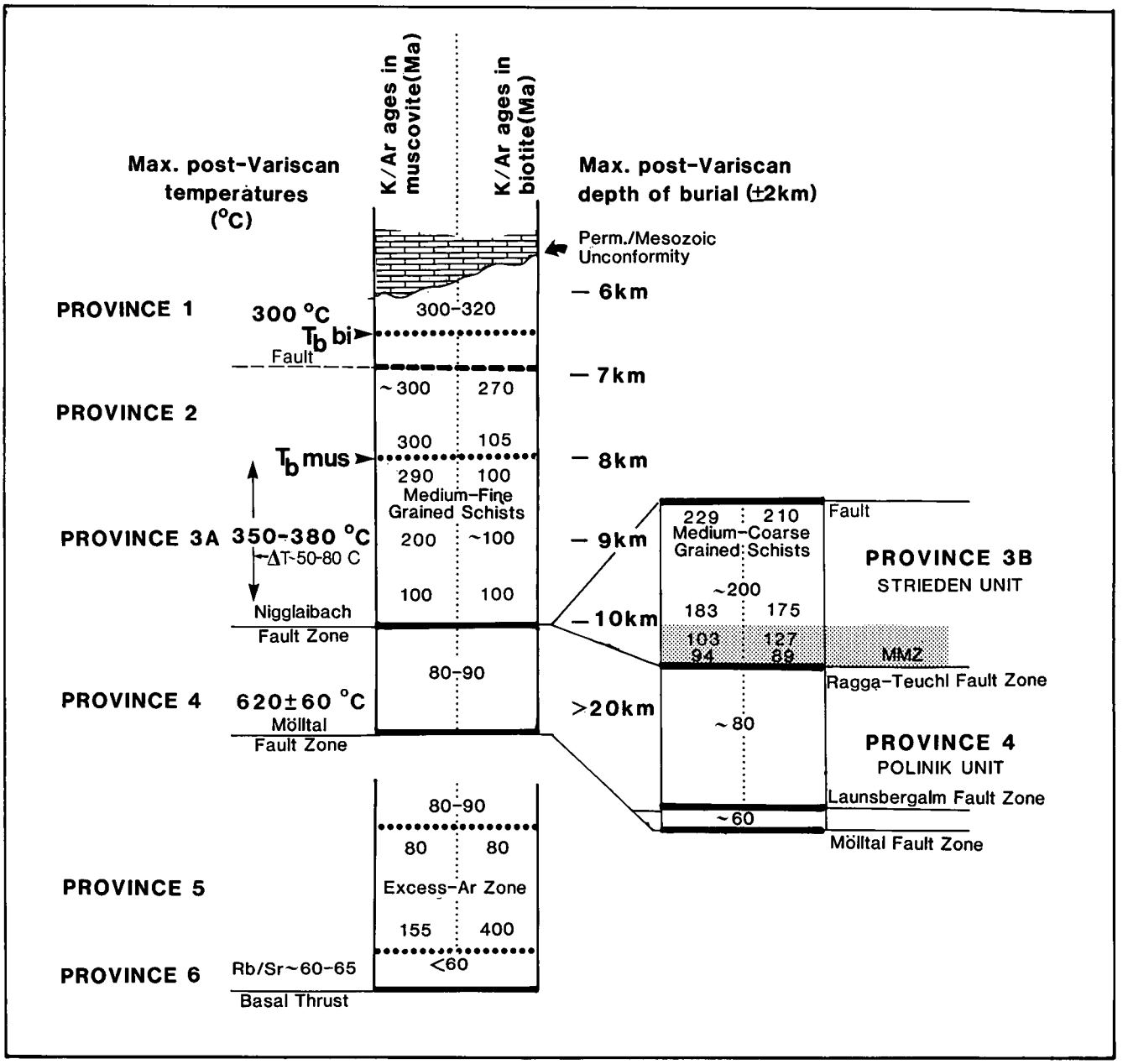

Text-Fig. 42.
Schematic section through the Altkristallin (see Fig. 41), illustrating the vertical distribution of age provinces and their suggested relation to maximum post-Variscan temperatures and maximum post-Variscan depth of burial.

5.1.3. Summary of the Regional Age Pattern

The age pattern depends on the precise temperature that any particular part of the rock pile reached during the Cretaceous metamorphism, how long it remained at that temperature, the grain size, and the argon pressure.

The age pattern can be used to define surfaces of identical ages (synchrons), which are assumed to be parallel to the earth's surface during the Cretaceous. These synchrons suggest that the Altkristallin, away from its northern margins (e.g. outside the Polinik Unit) has not been tilted regionally more than 20 degrees S since the Cretaceous, and that the presently exposed structural thickness (excluding the Polinik Unit), with respect to the synchrons, is probably not more than 6 km. The progressive change in ages with increasing structural depth, with respect to the synchrons, is assumed to reflect the thermal structure of the crust during cooling from the Cretaceous thermal event, and suggests a geothermal gradient during Cretaceous cooling between 28 and 44°C/km.

5.2. Age of Metamorphism and Deformation in the Polinik Unit

(Table 9)

5.2.1. Age of Amphibolite Facies Metamorphism in the Polinik Unit

In the Polinik Unit, K/Ar ages of muscovites and biotites are uniform and range between 76–83 Ma (OXBURGH et al, 1966), (Fig. 41). The dated muscovites and biotites form part of the equilibrium amphibolite facies mineral assemblage (st – gtII – bi – musII – ky – plag – qz). However, an older generation of muscovite (mus

l) can be distinguished using chemical and textural criteria, and biotites can show considerable variation in composition (ionic exchange with other Fe-Mg phases). Never-the-less, K/Ar mica ages are uniform, suggesting that all micas have been completely open to argon diffusion during peak metamorphism at ca. 105 Ma (see section 5.1.2, age province (2), and cooled through their blocking temperatures at ca. 80 Ma.

5.2.2. Age of D_3

The D_2 mica fabric and the inter D_2-D_3 amphibolite facies mineral assemblages are deformed by D_3 structures. It is suggested, that D_3 occurred shortly after the Cretaceous thermal peak and continued until after the rocks had cooled below their mica blocking temperatures:

1) D_3 mica crenulation hinges are often broken and fractured, suggesting low temperatures for deformation.
2) Quartz grains in F_3 fold hinges are elongate and aligned parallel to the F_3 fold axial surfaces, showing undulose extinction and no signs of annealing. VOLL (1960, 1976) estimates that temperatures of at least 275°C are needed before quartz recrystallises. Therefore D_3 deformation must have still been active at temperatures well below the blocking temperature of micas.
3) The similarity between co-existing muscovite and biotite ages suggests that cooling rates were fast, and hence one would not expect large age differences from samples at different structural depths. The expected uplift rates are estimated at 2–10 mm/a for geothermal gradients varying bet-

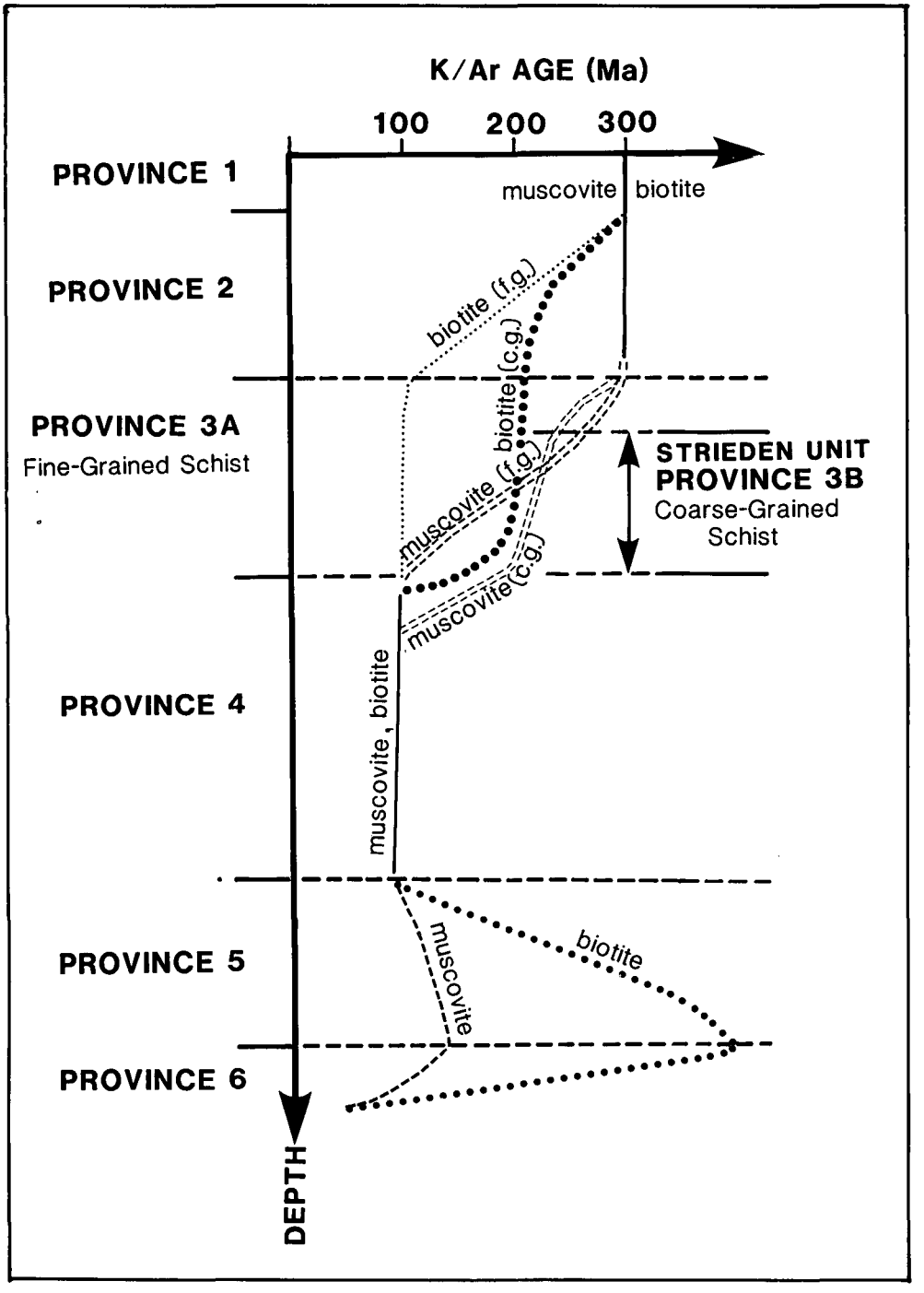

Text-Fig. 43.
Graph illustrating the variation of muscovite and biotite K/Ar ages with depth in the Altkristallin in the SE part of the Tauern area.
The pattern of ages in province (3A) and (3B) seem to be dependent on grain-size.

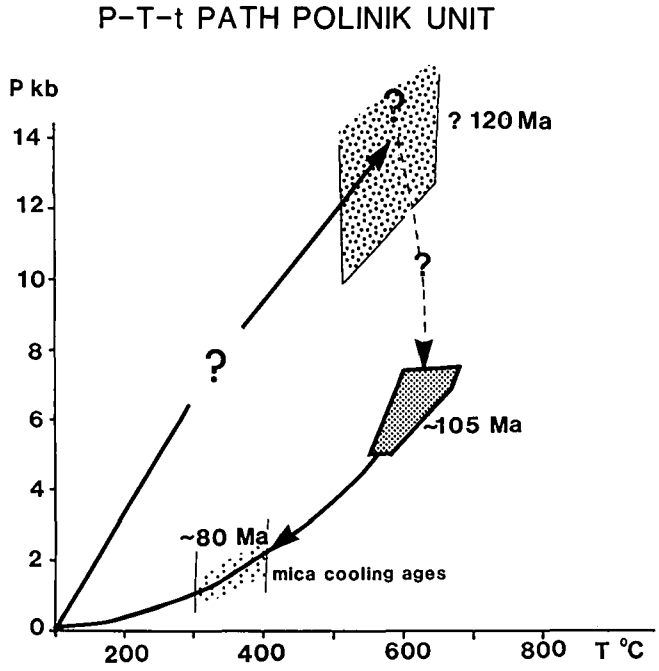

Text-Fig. 44.
P-T-time trajectory for the Polinik Unit, using available P-T estimates from the Polinik Unit schists and garnet amphibolites.
Ages are constrained by available geochronological data. However, a Cretaceous age the high pressure assemblages, found in the Polinik Unit, is speculative (see text for discussion).

ween 25–45°C/km, and assuming that ΔT of the mica blocking temperatures is between 50–80°C. The observed maximum structural thickness presently exposed in the Polinik Unit is less than 2 km, regardless of whether this is calculated for the Polinik Unit before or after D_3.

5.2.3. Age of Pegmatites

Pegmatites in the Polinik Unit are folded by D_3 and contain an internal D_2 fabric. However, no evidence for D_1 is seen in the pegmatites, and it is therefore concluded that they pre-date D_2 and post-date D_1. Rb/Sr two-mineral-isochron ages from the coarse-grained centre of the deformed pegmatite are ca. 254 Ma (CLIFF, pers. com.). It is assumed that this age is close to that of pegmatite emplacement, and has not been significantly reset during the Cretaceous metamorphism. Therefore D_2 is younger than 254 Ma.

5.3. Ages of Metamorphism and Deformation in the Strieden Unit

5.3.1. Age Data

Geochronological data for the Strieden Unit consist of K/Ar whole rock and mineral ages for schists and mylonites (WATERS, 1976), and Rb/Sr and K/Ar ages for pegmatites (CLIFF, pers. com.).

The Strieden Unit (excluding the MMZ) lies within age province (3B), (Figs. 41–43). It is characterised by similar K/Ar muscovite and biotite ages which are intermediate between the Variscan and Cretaceous cooling ages (ca. 200 Ma). One sample is anomalous, with a biotite age which is older than the co-existing muscovite age (mus197/bi226, possibly due to excess argon). In general, muscovite and biotite ages become progressively older towards structurally higher levels in the south (muscovite ages increasing from 183 to 229 Ma, biotite ages increasing from 175 to 210 Ma).

At the base of the Strieden Unit, within the MMZ, mica ages also show a pattern of increasing ages towards the south, with muscovite ages between 94 and 103 Ma, and biotite ages between 89 and 127 Ma. One sample shows evidence of excess argon, with the biotite age exceeding the muscovite age (mus98/bi127).

The northern margin of the MMZ is marked by subvertical brittle fault zones, which separates the MMZ from the Polinik Unit. However, though there is a change in the age pattern across the Polinik Unit–Strieden Unit boundary, it is not dramatic.

5.3.2. Age of Metamorphism in the Strieden Unit

The high temperature mineral assemblages in the Strieden Unit (formation of andalusite, staurolite, sillimanite) are interpreted as having a Variscan age. The pattern of K/Ar mica ages suggests that rocks in the Strieden Unit have only been partially outgassed during a Cretaceous thermal event (see description of age province 3 in section 5.1.2). It seems likely then that Cretaceous temperatures never exceeded that at which muscovite is completely outgassed (i.e <400°C) (Fig. 42). P/T estimates for the peak metamorphic mineral assemblages, suggest that temperatures exceeded 650°C (section 4). This metamorphism must therefore be older than the Cretaceous and is probably related to the mica cooling ages of province 1. In this case, the oldest muscovite age, which is 320 Ma, yields a minimum age for the Variscan peak metamorphism.

Pegmatites, which occur abundantly within sillimanite-bearing schists, post-date the formation of sillimanite and andalusite and pre-date the D_n deformation. A Rb/Sr whole rock age of 266±6 Ma has been obtained by CLIFF (pers. com., sample PTA2 from the Trögersee area) from a pegmatite showing these structural relations. The Cretaceous metamorphism did not reach high enough temperatures to reset significantly the Rb/Sr system in a coarse-grained pegmatite, and therefore this age must be close to, or at least is a minimum age for the emplacement of the pegmatite. Therefore sillimanite and andalusite growth occurred prior to 266 Ma, most likely during the Variscan metamorphism.

5.3.3. Age of Mylonites (D_p)

D_p deformation affected the high temperature mineral assemblages in the Strieden Unit, and pegmatites with a minimum age of emplacement of 266 Ma, therefore putting an upper age constraint of 266 Ma on the age of D_p deformation. D_p structures are cut by undeformed dacitic dykes which yield ages between 30 and 40 Ma (DEUTSCH, 1980), placing a minimum age constraint on D_p.

The following evidence suggests that the D_p deformation occurred at some time between 90 and 60 Ma:

1) Quartz microfabrics in the mylonites formed at low temperatures. Quartz forms ribbons with aligned subgrains which have a pronounced crystallographic preferred orientation and show undulose extinction. These textures suggest that quartz has not annealed into polygonal grains, but continued to de-

Table 9.
Constraints on the age of metamorphism and deformation in the Polinik and Strieden Units, showing possible correlations.

POLINIK UNIT	STRIEDEN UNIT
D_1 >250 Ma : stretching lineation	D_m, D_n >> 320 Ma : pre-date Variscan metamorphism
> 250 Ma : emplacement of leucocratic rocks (they cut across ℓ_1)	M_v > 320 Ma : peak of Variscan metamorphism: andalusite overprinted by sillimanite; partial melting
	D_o between 320 and 266 Ma: restricted to lower sillimanite zone
∿ 250 Ma : emplacement of pegmatites	∿ 266 Ma: emplacement of pegmatites
D_2 <250 Ma, possibly between 135 - 105 Ma : folding; foliation in pegmatites; possibly associated with underplating of the Polinik Unit resulting in high pressure mineral assemblages of the eclogite amphibolites.	
M_c ∿ 105 Ma : peak metamorphic temperatures during the Cretaceous metamorphic event, recorded in metapelites (600°C ± 25°C, 6 - 7 kb) and in the hydrous amphibolite facies alterations of the eclogite amphibolites.	M_c ∿ 105 Ma : lower greenschist facies metamorphic conditions
D_3 80 - 90 Ma : cooling of Polinik Unit through the K/Ar mica blocking temperatures; D_3 folding	D_p 90 - 60 Ma : cooling below the mica K/Ar blocking temperatures; formation of the main mylonite zone (MMZ)
∿ 65 Ma : final stage of emplacement of Polinik Unit onto the Lower East Alpine and the Peripheral Schieferhülle Units.	D_q between 60 and 40 Ma : folding of the MMZ
M_T 22 - 35 Ma Tauerncrystallisation: reheating of the base of the Polinik Unit in sub-area 5	30 - 40 Ma : emplacement of dykes
D_4 < 29±6 Ma arching (folding) of the Polinik Unit and the base of the Altkristallin (contact surface with the underlying units); flexural slip faults	< 30 Ma : faulting; movement along the Ragge Teuchl fault zone
≤ 22Ma faulting; movement along the Mölltal fault zone and other subvertical faults	

form, by slip along preferred crystallographic planes, well under its recrystallisation temperature (ca. 275°C, VOLL 1960, 1976). It therefore seems that D_p continued after the Strieden Unit had cooled through the mica blocking temperatures (ca. 350°C), i.e. is younger than ca. 90 Ma.

2) WATERS (1976) obtained a whole rock K/Ar age of 61 Ma from a fine-grained sericite- and chlorite-rich mylonite. This can be interpreted as dating the end of D_p deformation, assuming that the system has not cooled significantly below the temperature of beginning of retention of argon and that the mechanical grain-size reduction that occurred during D_p was sufficient to outgass the micas and reset the argon system. The rock therefore became closed when intense deformation ceased.

5.3.4. Age of D_q and Later Deformation

D_q structures deform the D_p mylonites, but are cut by dykes. It therefore must have occurred before ca. 40 Ma. An older age limit is more difficult to determine and depends on the interpretation of the D_p deformation age and correlation with deformation in the Polinik Unit. Movement on the Teuchl fault zone post-date D_q and also the emplacement of dykes, and therefore are younger than 40 Ma.

5.4. Geological History

The ages of deformation and metamorphism (Table 9), in the Polinik and Strieden Units, place constraints on their burial and temperature histories (Fig. 45). Estimated depths of burial are average depths, and these are large compared to thicknesses of the individual units. They can be derived from average metamorphic pressures, assuming that tectonic stresses are not significant (<0.5 kbars) and that 1 kbar is equivalent to ca. 3.5 km of overburden. Also, simple models of cooling (outlined in Fig. 40), and assumptions about the geothermal gradient can be used in conjunction with K/Ar mineral ages to give estimates of depth at particular times. Finally, the sedimentary history of the cover rock sequences, which overlie the Altkristallin, provide valuable information about uplift or subsidence.

The depth of burial history, when combined with the structural and metamorphic history of the study area, forms a powerful method for understanding the tectonic evolution of this part of the Eastern Alps (Fig. 45).

5.4.1. Pre-Variscan and Variscan Events

Evidence for the earliest structural and metamorphic events is well preserved only in the Strieden Unit, where metamorphic conditions were close to the Al_2SiO_5 triple point (5.5±1.5 kbars, 650±100°C, Section 4.3.4). This metamorphism occurred around 320 Ma (oldest muscovite K/Ar Variscan cooling age) and is Variscan in age (M_v). It post-dates at least two deformation events, D_n and D_m. At the time of peak metamorphic conditions, the Strieden Unit was at a depth of ca. 19 km. Temperatures appear to have been locally sufficient for partial melting, though there is no evidence for an unusually high geothermal gradient (e.g. greater than 25–30°C/km). Little can be said about the earlier deformation except that it involved crustal shortening, and may be Variscan or much older. D_1 in the Polinik Unit is also probably of Variscan age

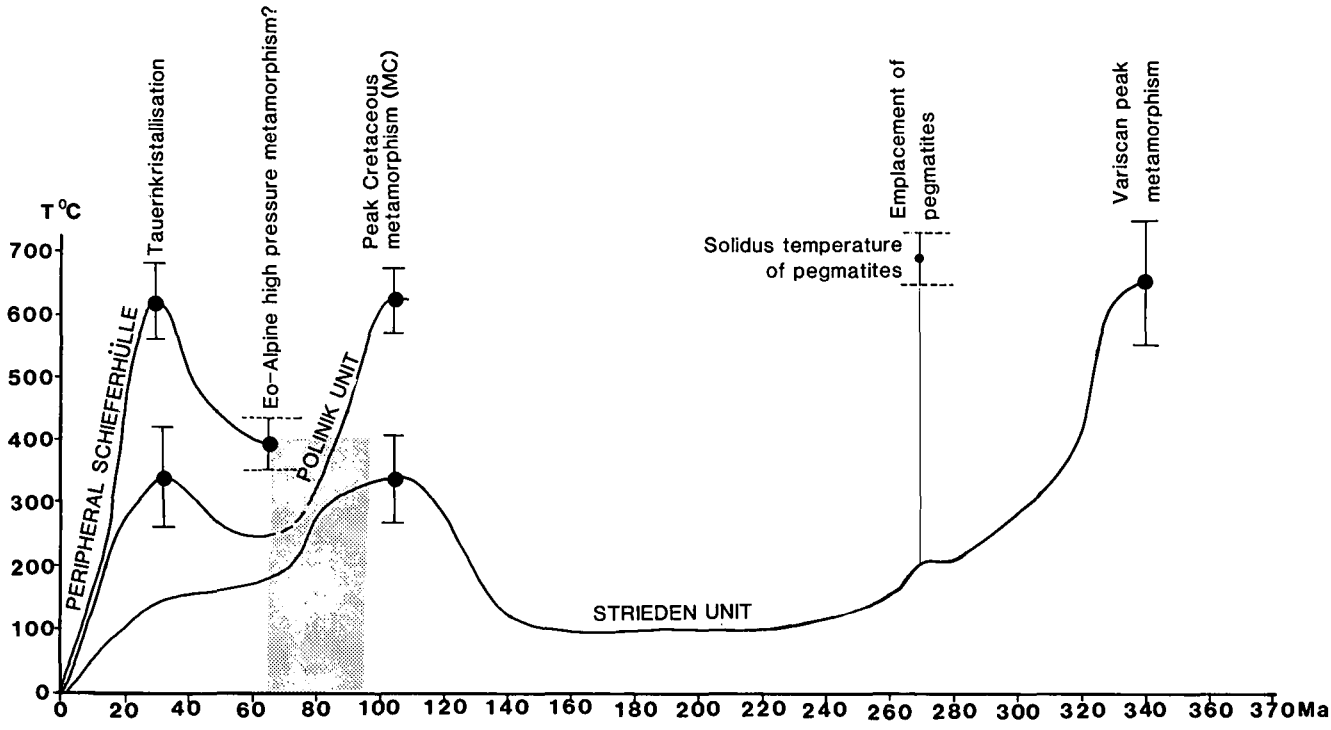

Text-Fig. 45.
a) Depth–Time (opposite page)
and
b) Temperature–Time graphs for the Strieden and Polinik Units and part of the Pennine Unit in the SE Tauern area, using all the available data (this page). Horizontal and vertical bars represent age and depth uncertainties respectively for a particular geological event. Where depth estimates are based on assumed geothermal gradients, derived from other evidence, the uncertainties are large.

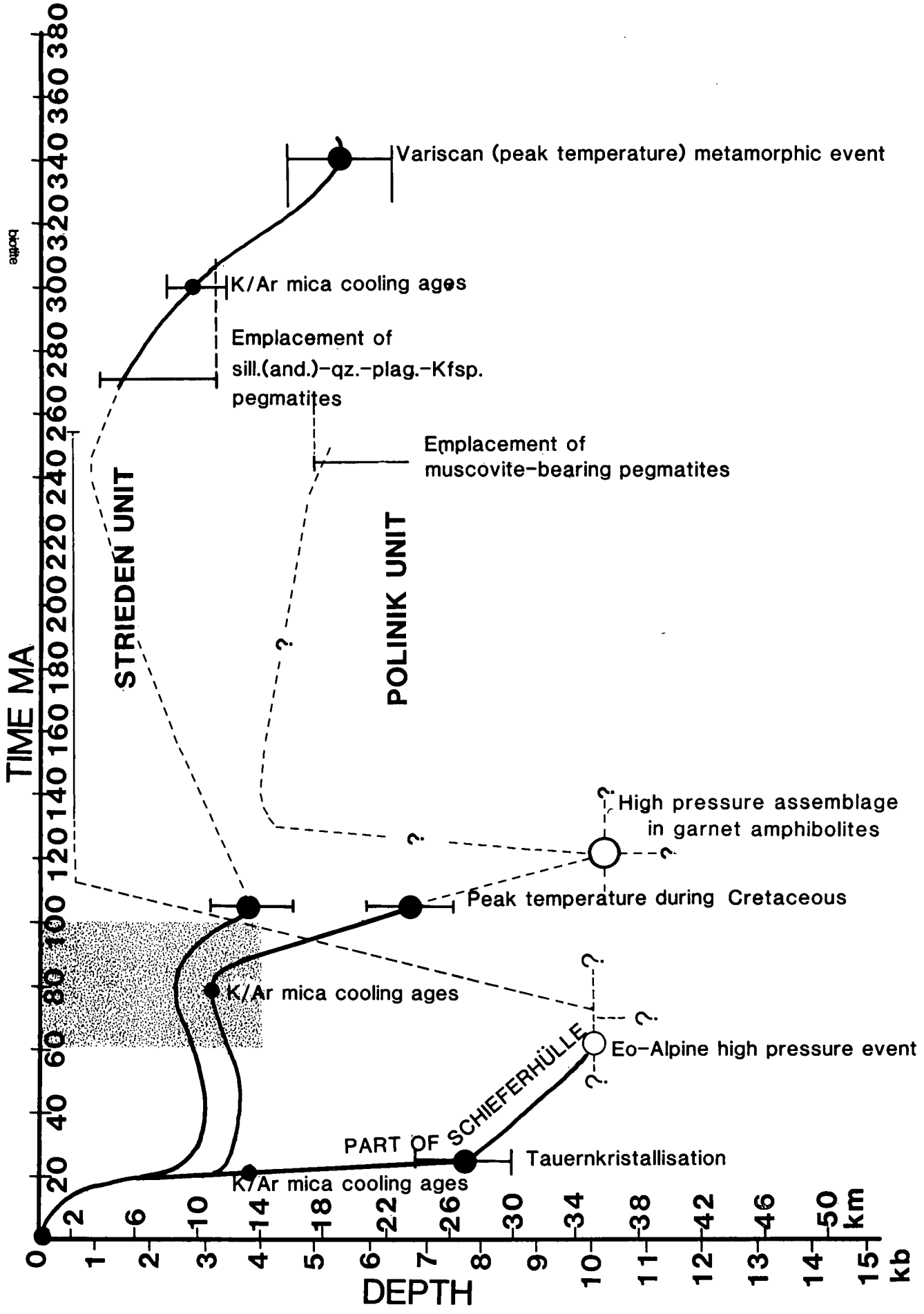
TIME MA
0 20 40 60 80 100 120 140 160 180 200 220 240 260 280 300 320 340 360 380
DEPTH
0 1 2 3 4 5 6 7 8 9 10 11 12 13 14 15 kb
2 6 10 14 18 22 26 30 34 38 42 46 50 km
Variscan (peak temperature) metamorphic event
K/Ar mica cooling ages
Emplacement of
sill.(and.)-qz.-plag.-Kfsp.
pegmatites
Emplacement of
muscovite-bearing pegmatites
STRIEDEN UNIT
POLINIK UNIT
High pressure assemblage
in garnet amphibolites
Peak temperature during Cretaceous
K/Ar mica cooling ages
Eo-Alpine high pressure event
PART OF SCHIEFERHÜLLE
Tauernkristallisation
K/Ar mica cooling ages

because it pre-dates pegmatite emplacement, which has a minimum age of 254 Ma.

The regional K/Ar mica age pattern suggests that the Strieden Unit cooled through the biotite blocking temperature of ca. 300°C at ca. 300 Ma. The mixed ages in age province (3B) can be interpreted as a consequence of localised partial resetting of Variscan cooling ages, either during a Cretaceous reheating event, or by pegmatite intrusion at ca. 266 Ma. Assuming that the geothermal gradient during cooling after M_V was at least as high as the average gradient during the peak metamorphic conditions during M_V (25–35°C/km), the Strieden Unit was probably not deeper than 12 km at ca. 300 Ma. Furthermore, the primary mineral assemblage in the pegmatites suggests maximum pressures of 3 kb (maximum depth of ca. 10 km) during their emplacement at 266 Ma. Thus, between the time of peak Variscan metamorphism (ca. 320 Ma) and pegmatite emplacement (ca. 266 Ma), the depth of the Strieden Unit progressively decreased by ca. 9 km. This suggests a history of tectonic or erosional unroofing in the period following peak Variscan metamorphism.

5.4.2. Permian to Jurassic History

From the Permian to the Late Jurassic, the Alpine region underwent crustal extension with the development of the Tethyan ocean between Adria and Europe.

In the Goldeck and southern Kreuzeck areas, the upper parts of the Altkristallin consist of low grade schists and phyllites. These are unconformably overlain by sediments (Drauzug sequences), with conglomerates (Gröden beds) at the base. The mid-Permian Gröden beds contain clasts of garnetiferous mica schists, tourmaline-rich schists, pegmatites, and phyllites. The unconformity surface dips at 30–40° SSW, and Variscan isograds in the Strieden Unit, and also the Cretaceous synchrons (discussed in section 5.1.2), generally dip at less than 20°S–SE. This implies that there has only been moderate tilting of the Strieden Unit and upper parts of the Altkristallin since the late Cretaceous. The structural thickness between the base of the Strieden Unit and the unconformity surface, normal to these tilted surfaces, is between 2.5 and 4.5 km. This estimate is based on the interpretation that the Strieden Unit (age province 3B) has had a similar burial history to that of age province 3A, and was overlain by rocks of age province 2 and 1 and the Mesozoic cover rock sequences. Assuming no subsequent thickening or thinning of this sequence, (see discussion in section 5.4.3), the Strieden Unit was at a depth of 2.5–4.5 km immediately prior to the deposition of the mid-Permian Gröden beds. Thus, there may have been several kilometres of further erosion since pegmatite emplacement at ca. 266 Ma, but prior to the mid Permian.

In the Drauzug sequences, the basal Gröden beds pass up into Triassic shallow marine carbonates, reaching a total thickness of ca. 5 km (TOLLMANN, 1977) suggesting slow subsidence. In the mid Jurassic, pelagic sediments, including radiolarites, Aptychus and red nodular limestones dominate (TOLLMANN, 1977). This change in the sedimentation pattern may be due to an increase in the rate at which the Tethyan ocean was opening, producing an increased water depth throughout the Tethyan region, estimated to be 2–3 km (JENKYNS, 1970). Such a water depth suggests that the Jurassic crust was thin and probably less than 12 km thick (Fig. 48). If so, the Strieden Unit must have been at a depth less than this, but deeper than the depth of the Mesozoic cover sequences, i.e. at a depth between 5–12 km.

5.4.3. Cretaceous Events

From the Early Cretaceous onwards, the tectonic development of the Eastern Alps can be described in terms of convergence between the two continental

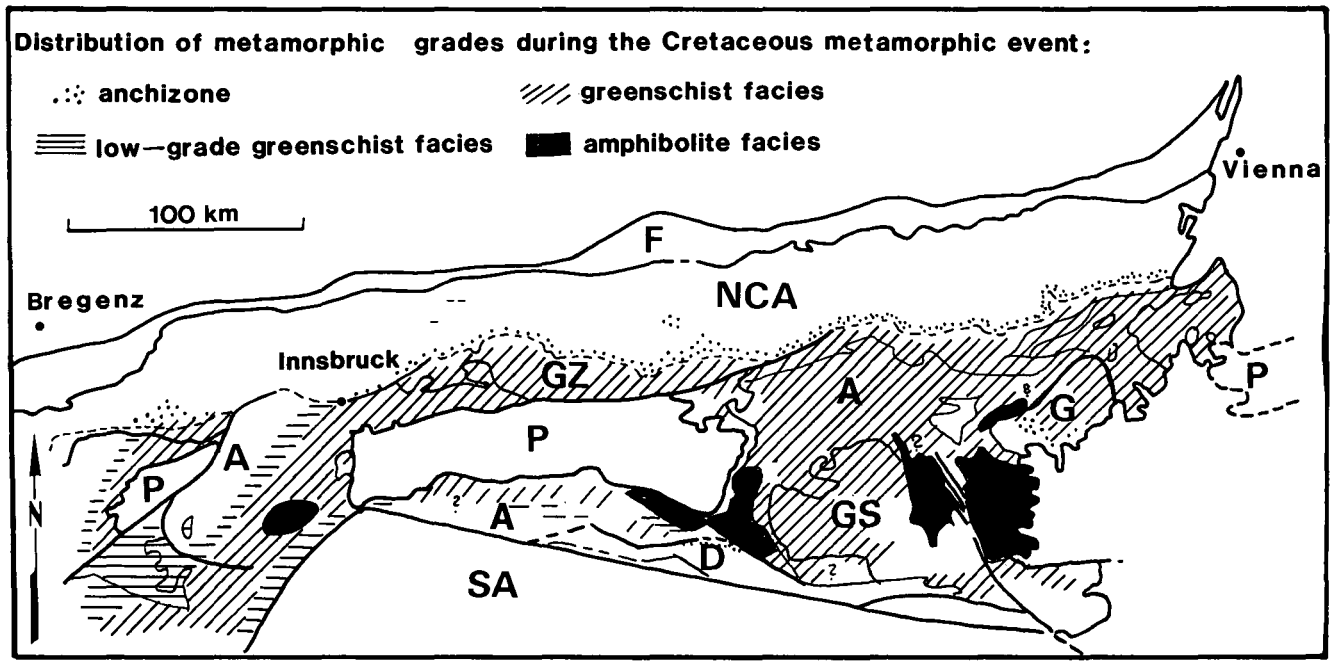

Text-Fig. 46.
Map showing the distribution of metamorphic grades during the Cretaceous metamorphism in the Eastern Alps.
Modified after FRANK (1987). A = Altkristallin, D = Drauzug, G = Graz Palaeozoic, Gs = Gurktal sheet, F = Flysch Zone, NCA = Northern Calcareous Alps, P = Pennine Units, SA = Southern Alps.

landmasses, Adria and Europe, with a subduction zone dipping underneath Adria (HAWKESWORTH et al., 1978; PLATT, 1986; FRISCH, 1976) (Fig. 48). Evidence of crustal shortening can be found at all crustal levels:

- Deformation in upper crustal levels, during the Neocomian to Cenomanian, pre-date the deposition of the Gosau beds. (SEDGWICK 1830). These were deposited on top of deformed, folded and thrusted Mesozoic cover rock sequences. Sedimentation in the Gosau beds starts with Cenomanian shallow water clastic sediments.
- Early Cretaceous crustal shortening can also be demonstrated at the base of the Gurktal Alps, where Palaeozoic quartz phyllites are thrust onto Mesozoic cover sequences (von GOSEN, 1982). Here, mineral growth , dated at ca. 100 Ma (HAWKESWORTH, 1976) and post-dating the formation of the thrust contact, suggests that movement was older than 100 Ma.

The Strieden and Polinik Units had a complicated geological history during the Cretaceous, and at some point they were brought together. There is no evidence for deformation in the Strieden Unit between ca. 266 Ma and the Late Cretaceous, in contrast to the Polinik Unit, which experienced D_2 deformation during this period. Therefore, the Polinik Unit may have been widely separated from the Strieden Unit, both vertically and horizontally, before they were juxtaposed.

Strieden Unit

K/Ar mica ages suggest that most of the Altkristallin, in the southern Kreuzeck area just below the Drauzug unconformity, was heated above the biotite blocking temperature in the Cretaceous and cooled again through the biotite blocking temperature at c. 100 Ma (Fig. 45B). Temperatures in the Strieden Unit (age province (3B)) did not exceed 400°C during the Cretaceous reheating event. Peak temperatures are assumed to have been reached just prior to the oldest Cretaceous biotite cooling age (103±2 Ma), which was measured in biotite co- existing with an undisturbed Variscan white mica (BREWER, 1970).

The amphibolite facies mineral assemblages in the Polinik Unit are considered to have crystallised during the peak of the Cretaceous thermal event (ca. 105 Ma). An average geothermal gradient of 22 to 34°C/km, at the Cretaceous thermal climax, can be calculated from the P/T conditions (Section 3.3.2). If this geothermal gradient is applicable to the Strieden Unit, then the Strieden Unit was at a temperature of 400°C and at a depth of 12 to 18 km at ca. 105 Ma (Fig. 47). It is interesting to note that the previous depth history of the Strieden Unit, outlined in section 5.4.2, places the Strieden Unit at the end of the Jurassic at a depth of 5–12 km, suggesting that an extra 0 to 13 km of overburden is required to account for the Cretaceous metamorphism. Thus, structural thinning in the Altkristallin, above the Strieden Unit, may have occurred since the Cretaceous. The Strieden Unit cooled through the biotite blocking temperature (ca. 300°C) between 90 and 100 Ma. Using the Cretaceous cooling geothermal gradient, calculated for age province (3A), this suggests that the Strieden Unit was at a depth between 6.5 and 12 km at 90–100 Ma. Typical P-T-time trajectories for a rock-pile undergoing uplift, suggest that the cooling geothermal gradient is usually higher than the peak metamorphic gradient, and this is compatible with the estimated gradients used here (22–34°C/km for peak metamorphism, and 25–45°C/km for cooling).

Polinik Unit

Amphibolite facies metamorphic pressures, deduced from metapelites, suggest that, the Polinik Unit during the temperature peak of the Cretaceous metamorphism (ca. 105 Ma), was at a depth of 20 to 26 km. If one considers that the crust during the Late Jurassic was probably only 12 km thick (see discussion, section 5.4.2), then a doubling of the crust (shortening by 50%) is necessary to account for the metamorphism in the Polinik Unit at ca. 105 Ma. D_2 deformation, which clearly pre-dates the Cretaceous peak metamorphic mineral assemblages in schists, might be an expression of the internal ductile shortening experienced by the deeper parts of the Altkristallin during crustal thickening. D_2 deformation is restricted to the Polinik Unit and no deformation of similar age has been observed in the Strieden Unit.

Eclogite amphibolite pods in the Polinik Unit record a history of progressive hydration and decompression from a high pressure metamorphism (in excess of 10 kbars) prior to the peak temperatures reached during the Cretaceous metamorphism. The hydration reactions suggest a history of warming, expulsion of water from the surrounding schists, and decompression, until P/T conditions were similar to those recorded by the surrounding schists. The ages of the primary eclogite assemblage and its alterations are not known, and it is possible that these are Cretaceous, suggesting that the Polinik Unit may have been at depths greater than 35 km in the Cretaceous, but prior to 105 Ma (Fig. 44). Burial of the Polinik Unit to these depths might have occurred by underthrusting in or near a subduction zone (Fig. 48). High pressure metamorphism in the Pennine units (estimated to have occurred at ca. 100 Ma in the Western Alps (HUNZIKER, 1974) is also attributed to burial in a subduction zone, beneath the structurally higher Pennine unites and the thickened Altkristallin with its stacked up cover rock sequences (Fig. 48).

The onset of subduction in the Eastern Alps is estimated at ca. 110–120 Ma. This is based on both the occurrence of detrital high- pressure minerals in Cenomanian–Turonian flysch (OBERHAUSER, 1968); and PLATT's (1987) estimate of the time required for high pressure rocks to reach the surface from a depth of 30 km (ca. 20 Ma).

Late Cretaceous Juxtaposition of the Polinik and Strieden Units

The history outlined for the Polinik Unit during the Creataceous is markedly different from that for the Strieden Unit, and both the vertical and horizontal separation between the two units must have been large. The vertical separation between the Polinik Unit and the Strieden Unit during the thermal peak of Cretaceous metamorphism (ca. 105 Ma) is difficult to assess. If one assumes that the geothermal gradient, estimated from the P/T conditions of the amphibolite facies assemblages in Polinik Unit metapelites, applies also for the Strieden Unit, then the base of the Strieden Unit lay 7–8 km above the top of the Polinik Unit (Fig. 47) at ca. 105 Ma.

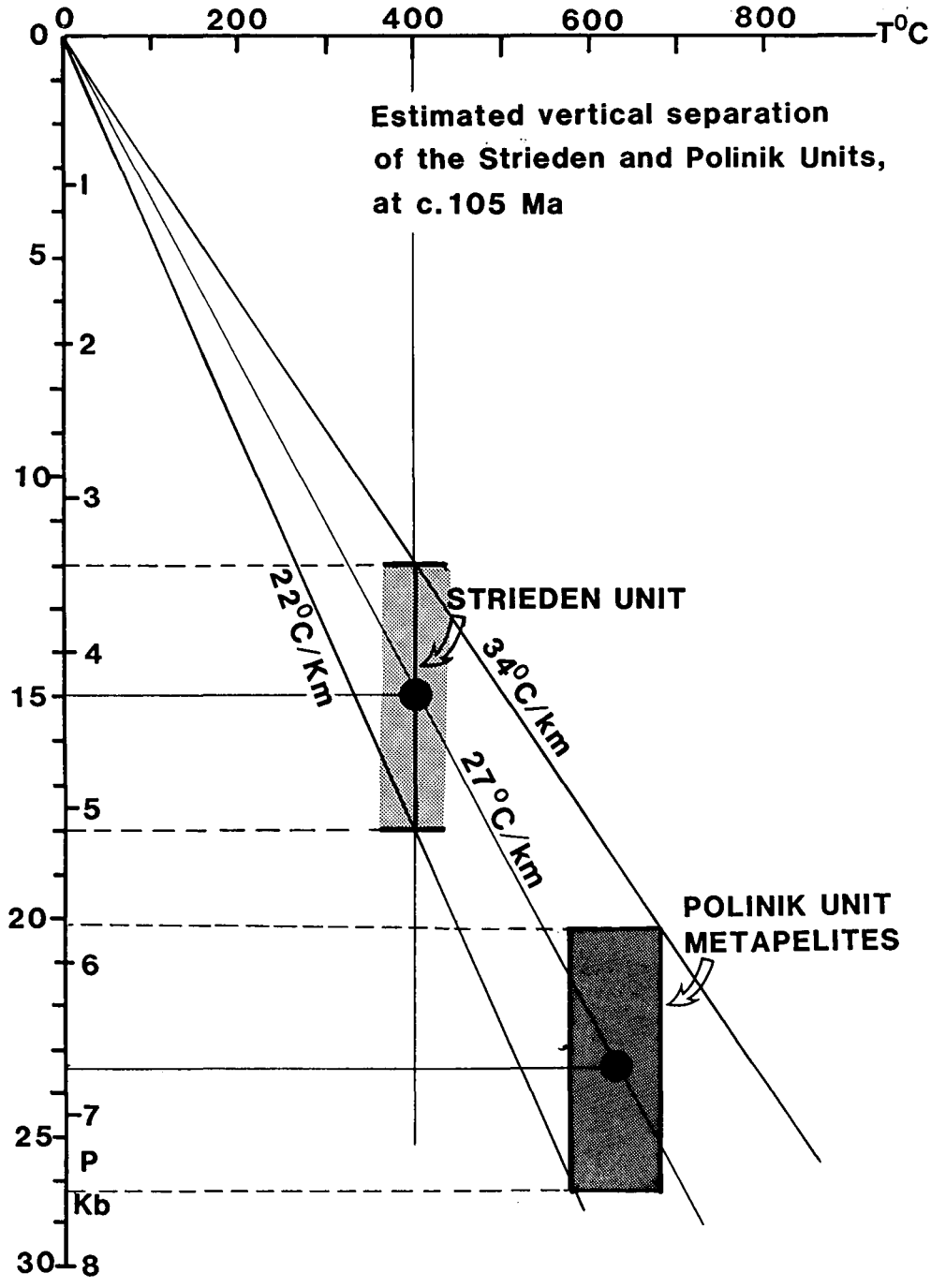

Text-Fig. 47.
Pressure-temperature graph, showing the possible vertical separation between the Polinik and Strieden Units at the climax of the Cretaceous metamorphism (ca. 105 Ma).
An average geothermal gradient between 22 and 34°C/km has been calculated, derived from Cretaceous peak temperaure mineral assemblages in metapelites in the Polinik Unit, at this time. Assuming that this geothermal gradient is also applicable to the Strieden Unit, then the Strieden Unit was at a temperature of 400°C and at a depth of 12 to 18 km at ca. 105 Ma.

The history following peak metamorphic conditions is constrained by the K/Ar mica ages. The continuity of the K/Ar ages, right across the Polinik Unit/Strieden Unit boundary, suggests that their juxtaposition must have ocurred during cooling, when both units passed through the 300–380°C temperature interval, recording similar mica K/Ar cooling ages. Since 105 Ma, there has been a change from a possible large vertical structural separation (up to 10 km) between the Polinik and Strieden Units, to an essentially small one.

Significance of D_p deformation

The MMZ is an important discrete high strain zone of deformation, which forms the base of the Strieden Unit and appears to have been originally flat lying. It was probably active between 60 to 90 Ma, shortly after the Cretaceous peak metamorphism. D_p kinematic indicators show that the upper plate (Strieden Unit) moved towards the NW relative to the lower plate (Polinik Unit). If the MMZ acted as a normal fault, along which the Strieden and Polinik Units were brought vertically closer together, it would account for the marked difference in peak Cretaceous temperatures and pressures (equivalent to 2–8 km structural thickness) between the two units. It would also account for the uplift and cooling of the Polinik Unit at ca. 80 Ma.

Other shear zones in the Altkristallin occur above the MMZ (e.g. Striedenkopf mylonite, Figs. 4, 19) and below, at the base of the Altkristallin, where it passes into the Matrei Zone and upper Pennine unit, (WALLIS, 1988)). Kinematic indicators in these shear zones are similar to D_p fabrics and also indicate NW movement of the upper plate relative to the lower plate.

Given a normal fault interpretation for the MMZ, it is suggested that D_3 in the Polinik Unit, which occurred

at high crustal levels during cooling of the Polinik Unit represents either,

- a widely distributed deformation in the footwall of the MMZ related to movement in the MMZ ($D_p = D_3$) or
- D_3 post-dates D_p and movement in the MMZ and is possibly related to D_q.

Late vertical movements

The Strieden and Polinik Units are presently juxtaposed along steep brittle fault zones, such as the Ragga – Teuchl and the Strugenkopf fault zones (Fig. 4), which truncate dykes dated at 30–40 Ma (DEUTSCH, 1984), (Fig. 20). The absence of the dykes in the Polinik Unit suggests a strike-slip component greater than 5 km (width of the study area) on the late brittle fault zones. This is because, if there were only vertical movements, one might expect to find deeper levels of the dykes exposed in the Polinik Unit.

The minimum estimate (2 km) for the vertical separation of the two units during Cretaceous peak metamorphism, could be explained by vertical movements on these brittle fault zones. However, this interpretation is not satisfactory, because it provides no role for the MMZ, which is a large zone of ductile shear. However, it is certain that the Polinik and Strieden Units were ultimately juxtaposed by movements on the Ragga-Teuchl and Strugenkopf fault zones, albeit relatively small ones (<2 km).

Regional metamorphic, structural and stratigraphic evidence or post-metamorphic crustal thinning

❶ Metamorphic evidence

The high pressure metamorphism experienced regionally in the Pennine Units, attributed to burial in a subduction zone (SELVERSTONE, 1985; HOLLAND & RAY, 1986), is estimated to have occurred at 78±12 Ma (RAITH et al., 1978). Pressures in excess of 8 kbars have been measured in the Upper Pennine Unit (HOLLAND & RAY, 1986) and pressures of at least 10 kbars in the lower Pennine Unit (SELVERSTONE, 1985). This suggests a depth of burial of 28 km and 35 km respectively. The total preserved overburden above the lower and upper Pennine Units, consisting of ca. 5 km of upper Pennine Unit (CLIFF et al., 1971) and a 10–15 km thick Austroalpine nappe pile (Altkristallin and the Mesozoic cover rocks), is far too thin in both cases to account for these pressures (15–20 km missing above the lower Pennine Unit, and 13– 18 km missing above the upper Pennine Unit).

In the Altkristallin, amphibolite facies Cretaceous metamorphism in the Polinik Unit requires an overburden of 20–26 km (ca. 6.5 kbars). However, the exposed overburden is at least 10 km too thin to account for the metamorphic pressures.

Cretaceous amphibolite facies metamorphism has been found elsewhere in the Altkristallin (Fig. 46), for instance in the Ötztal Alps, in the Schneeberg area (THÖNI, 1983; HOINKES, 1981; HOINKES et al., 1982). Here too, metamorphic conditions (6–7 kbars) require an overburden (ca. 23 km) which is greater than the presently observed overburden (ca. 13 km).

❷ Structural evidence

At the base of the Altkristallin, in the SE Tauern area, WALLIS (1988) has recognised a km-wide zone of distributed shear, which can be traced into the underlying Matrei Zone and the upper Pennine Unit. It post-dates the Cretaceous metamorphism. The extensional fabric in this shear zone formed under greenschist facies conditions, suggesting the same sense of shear as that in the MMZ (top to the NW sense of shear). Rb/Sr ages suggest that deformation was still active at 40–50 Ma. Kinematic and metamorphic studies suggest that at least 10 km of crustal thinning has been accomodated by this deformation zone. The extensional deformation described by WALLIS (1988), together with the D_p deformation in the MMZ at the base of the Strieden Unit, across which 2–8 km of structural thinning may have occurred, could account for 12–18 km of post-metamorphic crustal thinning. This is in good agreement with the estimated missing overburden required to explain the Cretaceous metamorphic conditions in the Pennine Units.

However, this does not explain the 'missing overburden problem' for the Tauern metamorphism at ca. 25 Ma, discussed by DROOP (1985). Pressures derived from mineral assemblages, dated at ca. 25 Ma in the Peripheral Schieferhülle, suggest an overburden between 22–30 km (DROOP, 1985), which appears to be incompatible with the thickness of the presently observed thrust pile. DROOP concludes that this missing overburden formed part of a thick thrust sheet (7±4 km thick), which overlay the Altkristallin (for instance, the Gurktal thrust sheet) and has been eroded away. DROOP suggests that the 'missing overburden' must be above the Altkistallin, as pressures estimated from the 30 Ma Rieserferner intrusion, which lies within the Altkristallin, suggest that it was emplaced at depths between 15 and 17 km (DROOP & CLIFF, unpubl. data).

However, the structural position of the Rieserferner intrusion within the Altkristallin is not clear, and it is possible that it is in fact right at the base of the Altkristallin. Present estimates of the thickness of the Altkristallin (12–15 km) and the overlying Drauzug (minimum thickness of 3 km) at 30 Ma may therefore be compatible with the depths of intrusion of the Rieserferner, without invoking missing overburden. But what about the peak metamorphic pressures in the Peripheral Schieferhülle during the Tauern Metamorphism at ca. 25 Ma? The K/Ar ages at the base of the Altkristallin have been only partially reset in the Tertiary, and hence the base of the Altkristallin was unlikely to have been much above 400°C at 25 Ma. Assuming that the geothermal gradient derived from DROOP's P/T estimates is applicable to the Altkristallin (20–27°C/km), then this suggests that the base of the Altkristallin was not deeper than 20 km at this time, and may have been shallower (say comparable to that of the Rieserferner, at 17 km). In this case, using DROOP's depth estimates for his assemblages, they are between 2 and 13 km below the base of the Altkristallin. This suggests that there may be missing crust at the base of the Altkristallin, though the lower depth estimates are compatible with the likely thickness of the Matrei Zone and Peripheral Schieferhülle (up to 8 km). An interesting possibility exists however, that crustal thinning occurred after the Tauern metamorphism (25 Ma), perhaps accommodated by the Mölltal fault zone, which acted as a normal fault zone. This deletion may be another manifestation of late-stage extension in an orogenic belt revealing the deeply buried metamorphic sequences (DEWEY, 1988).

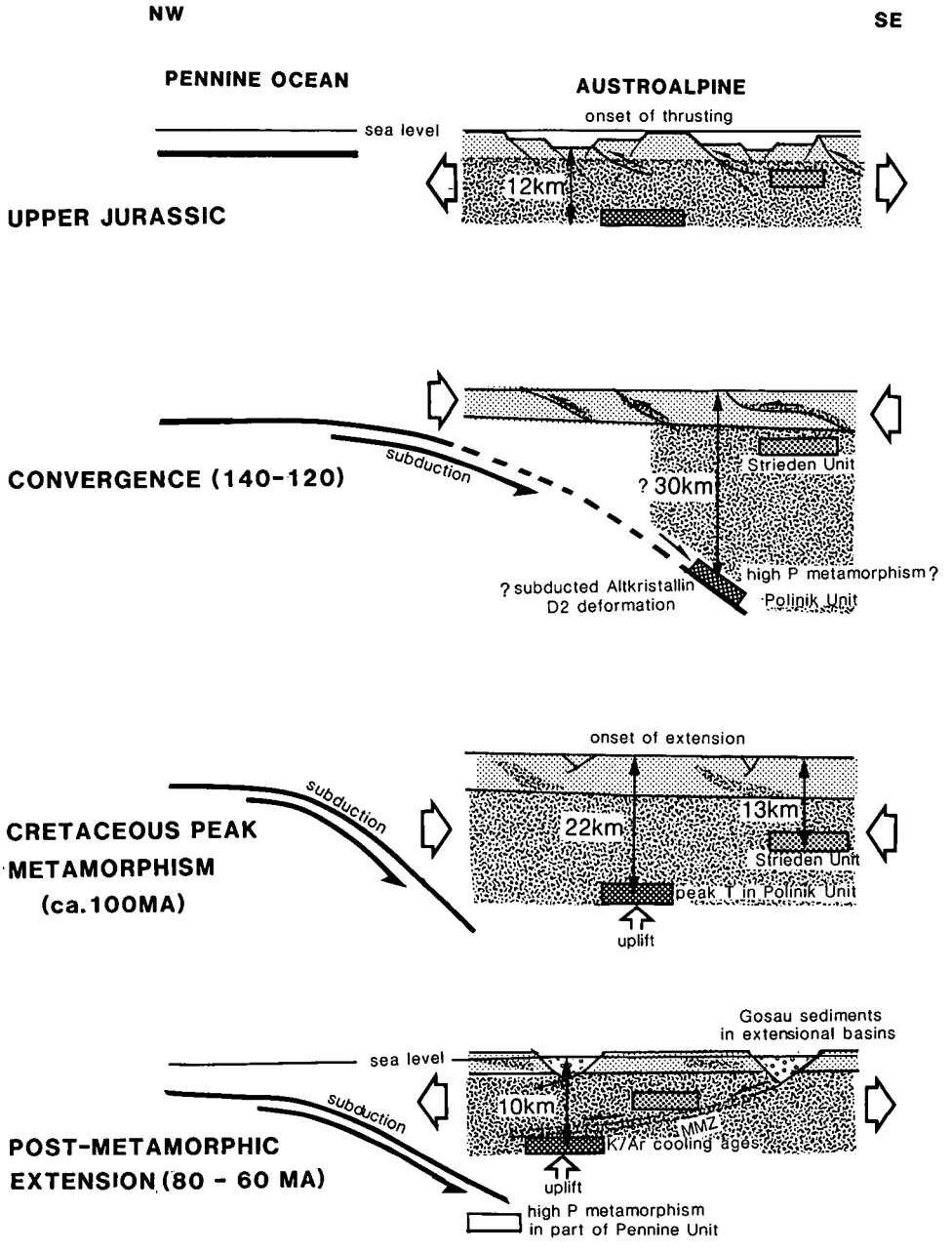

Text-Fig. 48.
Cartoon diagram illustrating the possible evolution of the Altkristallin as part of the Austroalpine sheet, since the Upper Jurassic.
Diagrams represent NW-SE cross-sections. In the Jurassic, the total crustal thickness probably did not exceed 12 km (see text for discussion). Convergence resulted in crustal shortening, expressed as D_2 deformation in the Polinik Unit. Subduction of the basal part of the Austroalpine sheet is based on the assumption, that the high pressure metamorphism, observed in amphibolites in the Polinik Unit, is Cretaceous. Crustal thickening ultimately lead to the mid-Cretaceous burial metamorphism with peak temperatures in the Polinik Unit of ca. 650°C. At that time, the Polinik Unit was at a depth of ca. 22 km (assumed to be the total thickness of the Austroalpine sheet) and was buried ca. 9 km below the Strieden Unit. Post-metamorphic extension in the Austroalpine sheet seems to coincide with the high pressure metamorphism (ca. 8 kb) observed in the Pennine Unit (HOLLAND & RAY, 1985). During this time, the Austroalpine experienced uplift and extension.

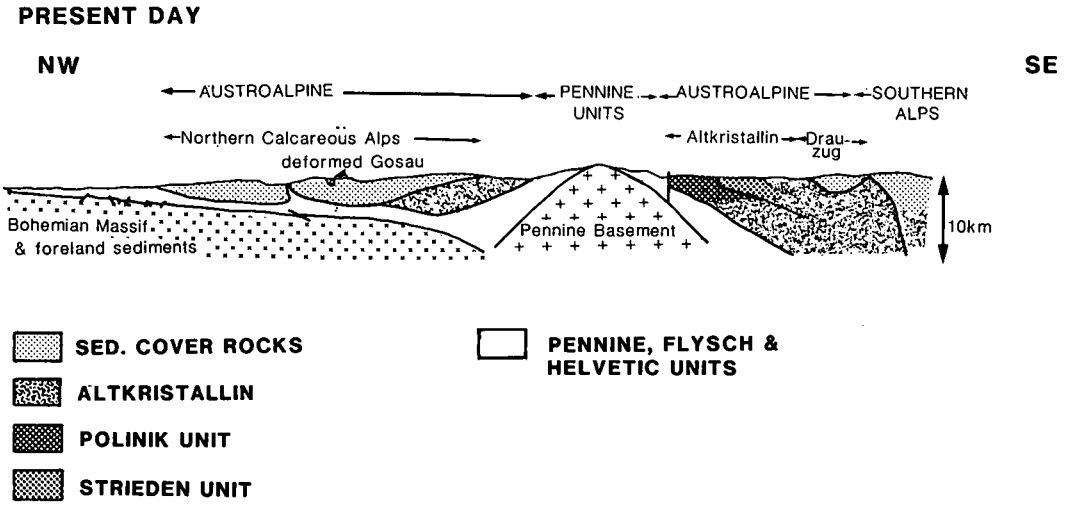

Post metamorphic extensional deformation is also a possible interpretation for the Grazer Palaeozoic area, in the eastern part of the Austrian Alps. Here the Grazer Palaeozoic, which has experienced a weak Variscan metamorphism, shows mixed K/Ar mica ages, which fall between the Variscan and Cretaceous mica cooling ages. These are interpreted as partially reset Variscan ages, during the Cretacous metamorphism. However, there is a sudden increase in metamorphic grade in the basal part of the Grazer Palaeozoic and also in the underlying Plattengneiss (a high strain, flat lying shear zone, which forms the top of the Altkristallin). This metamorphism yields Cretaceous K/Ar cooling ages of 80–90 Ma. This configuration suggests that the Plattengneiss shear zone acted as a low angle normal fault, which has substantially thinned the Cretaceous metamorphic sequence. Along this shear zone, hot (Cretaceous metamorphic event) Altkistallin basement rocks (yielding Cretaceous cooling ages) were juxtaposed with the 'cold' rocks (Grazer Palaeozoic sheet) on the down-thrown side of the low-angle normal fault, resulting in the resetting of Variscan mica ages.

❸ Sedimentary evidence

At the highest structural level, within the Austroalpine domain, sedimentation of the mid Cretaceous Gosau beds was taking place at the same time as the postulated crustal thinning observed in the Altkristallin and the Pennine Unit. The Gosau beds were deposited in fault bounded basins above the deformed and thickened Austroalpine nappes (Fig. 48). They also unconformably lie on rocks of the Grazer Palaeozoic, where they form 1–2 km thick sequences. Sedimentation started in the Cenomanian with shallow water brackish marine deposits. However, during the Campanian to early Maastrichtian, green claystones were deposited below the carbonate compensation depth (FAUPL & SAUER, 1978), suggesting a water depth of several kilometres. The thickness of sediments (several kilometres) and the water depth (also several kilometres) suggest a major phase of regional crustal extension affecting the Austroalpine. The timing of the syn-tectonic deposition of the Gosau beds in fault bound basins coincides with both, major crustal thinning at deeper structural levels, within the Altkristallin and in part of the Pennine Units (WALLIS, 1988) and with the Cretaceous mica cooling ages found in the Altkristallin (e.g. Polinik Unit).

Summary of the Cretaceous events
(Fig. 48)

The convergent tectonic history of the Eastern Alps is associated with crustal thickening, affecting both the Austroalpine and the Pennine units, and resulting in the Cretaceous burial metamorphism.

D_2 deformation might be the expression of ductile shortening experienced by the Polinik Unit during this stage of crustal thickening. It pre-dates the Cretaceous metamorphism and is restricted to the Polinik Unit. The Cretaceous metamorphism reached amphibolite facies metamorphic conditions at ca. 105 Ma in the Polinik Unit (620±60°C and 6.25±1.25 kbars), whereas in the Strieden Unit temperatures did not exceed the K/Ar blocking temperature of micas (300–380°C).

A major phase of crustal extension took place after crustal thickening and the Cretaceous metamorphism. This affected the Austroalpine and the Pennine Units and caused substantial thinning (12–18 km) of the Cretaceous metamorphic sequence.

It is suggested that post-metamorphic crustal thinning occurred during D_p deformation. During D_p deformation, the Strieden Unit moved over the Polinik Unit in a NW direction, cutting out 2–8 km of the Cretaceous metamorphic sequence.

PLATT (1986) and SELVERSTONE (1985, 1988) have both recognized the metamorphic evidence for post-metamorphic thinning in the Eastern Alps. Contemporaneous regional extension in an overall convergent tectonic setting is explained by PLATT (1986) as a consequence of gravitational collapse at high levels in a weak orogenic wedge, which is being continuously thickened at depth by underplating. This extension also provides a powerful mechanism, along with erosion, for bringing up deeply burried rocks (PLATT 1986; BEHRMANN et al., 1986).

Acknowledgment

This work forms part of a Ph.D. thesis, carried out in Cambridge, during tenure of a Churchill College studentship from 1982– 1986. Discussions with E.R. OXBURGH, D. WATERS, T. HOLLAND, N. RAY, N. WOODCOCK, J. PLATT, W. FRANK, M. THÖNI, I. FREY are greatfully acknowledged. L. SLOMAN, R. GOMO, S. LAMB provided assistance in the field. The manuscript benefitted from a careful review by S. LAMB .

Plate 1

Folding in the Polinik Unit.

Fig. 1: View of the southern slopes of Mt. Polinik (2784 m), showing hinge area (arrowed) of F_3 fold.

Fig. 2: Detail of fold shown in Plate 1 – Fig. 1.
Arrow points to the fold hinge of F_3 fold. Fold axis trends approximately E and plunges gently towards the W (lefthand side of the picture). Other F_3 hinges and limbs can be seen above the arrow. Rock surfaces which dip subparallel to the mountain slope form the longer limbs of asymmetric F_3 folds. Viewed towards the W (down plunge) the asymmetry of F_3 folds is anticlockwise ("S" folds) with fold axial planes dipping towards the north at 30–45° (Plate 1 – Figs. 3, 4).

Fig. 3: Close-up of an F_2 fold closure (also shown in Plate 1 – Figs. 1, 2, 4), showing the effect of minor F_3 folds (arrowed with subvertical axial planes) on an F_2 structure (arrowed with subhorizontal axial plane).
Hammer (30 cm long) for scale.

Fig. 4: Approximate profile section of F_3 folds (N–S section, viewed towards the E) from an outcrop above the one illustrated in Plate 1 – Figs. 1–3.
Arrow points to fold closure of F_2 fold. The interference pattern produced by superposition of minor F_2 and F_3 folds is a combination of "S" folds on "Z" folds when viewed down plunge of the F_3 folds (towards the west).
Hammer in centre of picture (30 cm long) for scale.

Fig. 5: Handspecimen of quartzo-feldspathic Polinik schist taken from the hinge area of a larger scale F_3 fold showing the preservation of small scale F_2 folds.
Locality is marked by an arrow on Plate 1 – Fig. 4. Quartzo-feldspathic layers are thickened in the hinge areas and attenuated on the limbs.

Fig. 6: Looking towards the east along a F_3 fold nose (down plunge) developed in a foliated pegmatite surrounded by metapelites of the Polinik Unit.
F_3 folds form cascading (subhorizontal) asymmetric folds striking approximately E with fold axes gently plunging towards the E (up to 6°). F_3 fold asymmetry is clockwise ("S" folds) when viewed down plunge (towards the E).
Locality: 300 m NE of the lake Bodensee.
Specimen 439; Harker collection number 147080.

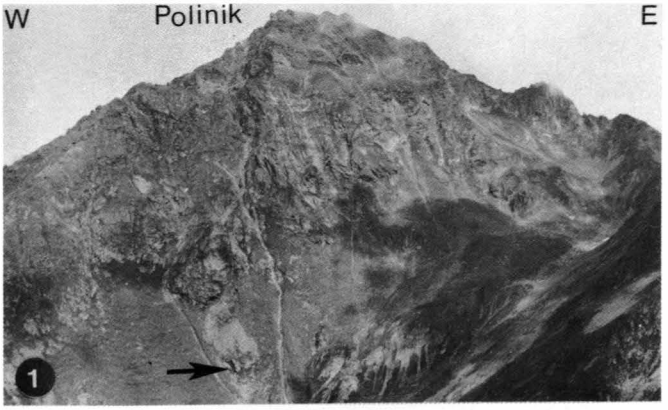
W
Polinik
E
1


W
E
2

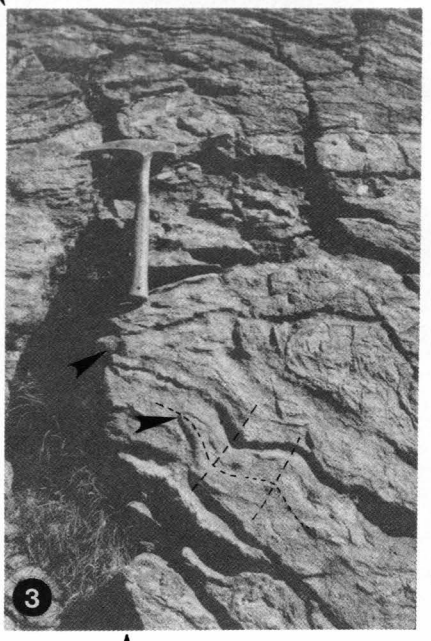
3

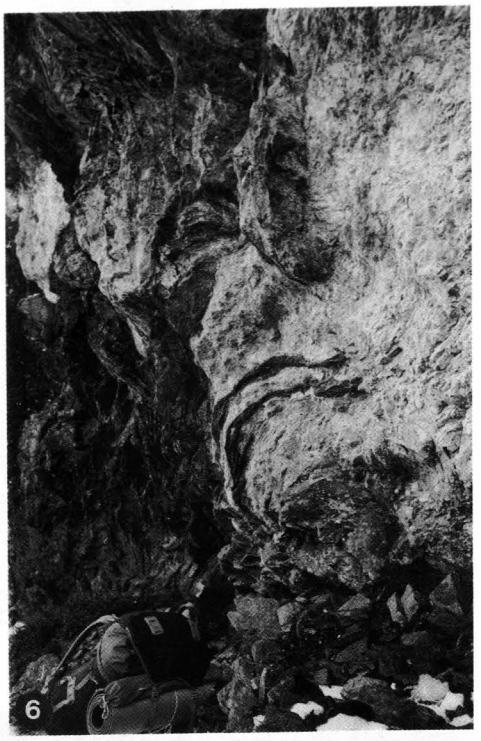
6

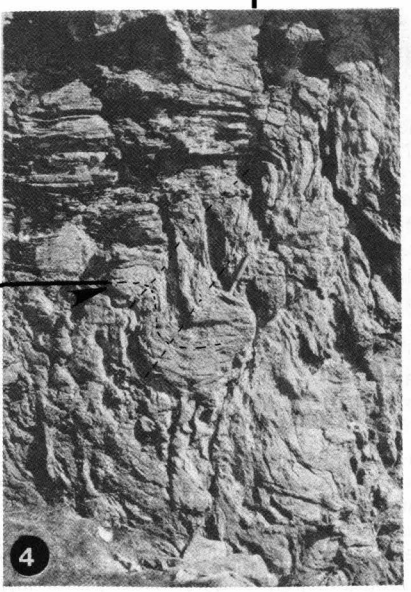
4


5
1cm

Plate 2

Mineral assemblages and textures in aluminous metapelites of the Polinik Unit.

Fig. 1: Photomicrograph (pp) of zoned garnet typically found in metapelites of the Polinik Unit.
Garnet 1 (gt 1) forms the inclusion-free core-region and garnet 2 (gt 2) forms the rim zone of the whole garnet. The solid line marks the electron microprobe traverse. The mineral zoning profile of this garnet is shown in Fig. 10.
Scale bar: 1 mm
Specimen 81.4; Harker collection number 147017.

Fig. 2: Photomicrograph (cp) of twinned staurolite (st) and kyanite (ky) surrounded by muscovite, biotite and quartz.
Scale bar: 1 mm
Specimen 81.4; Harker collection number 147017.

Fig. 3: Photomicrograph (pp) of mineral assemblage typically found in metapelites of the Polinik Unit.
It shows a lensoid domain within a mica-schist which contains the mineral assemblage ky – gt – st – qz – mi – bi – rut – ilm – plag.
Scale bar: 1 mm
Specimen 81.2; Harker collection number 147016.

Fig. 4: Photomicrographs (cp and pp) of S_2 mica cleavage folded by F_3.

Fig. 5: Kyanites (ky) are aligned within S_2 and have been deformed by F_3. Kyanites are slightly altered along their margins to a fine aggregate rich in sericite and margarite.
Scale bar: 1 mm
Specimen 85.1; Harker collection number 147021.

Fig. 6: Photomicrograph (cp) of deformed kyanite (ky).
Kyanite is kinked by F_3.
Scale bar: 1 mm
Specimen 77.16; Harker collection number 147019.

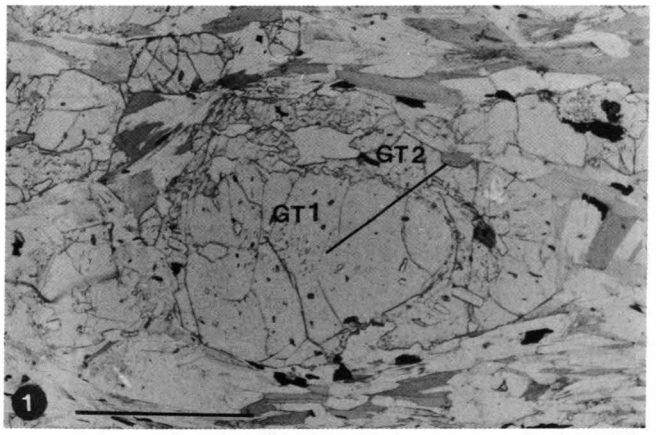
GT2
GT1
1

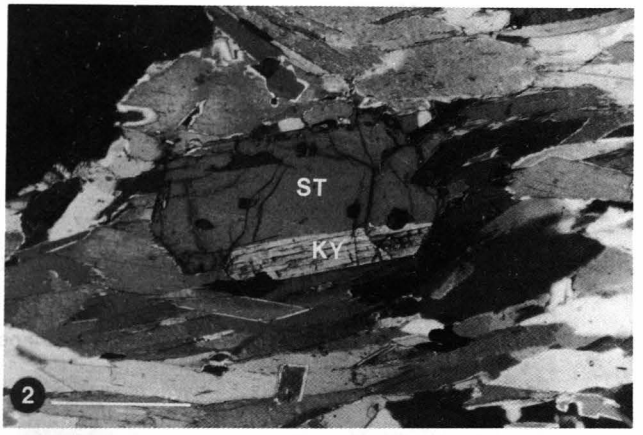
ST
KY
2

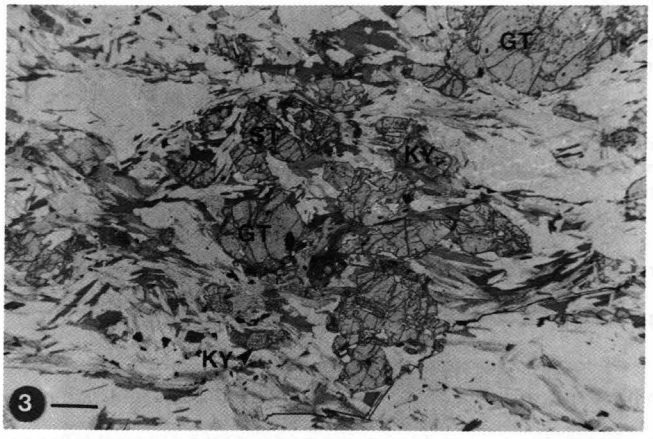
GT
ST
KY
GT
KY
3

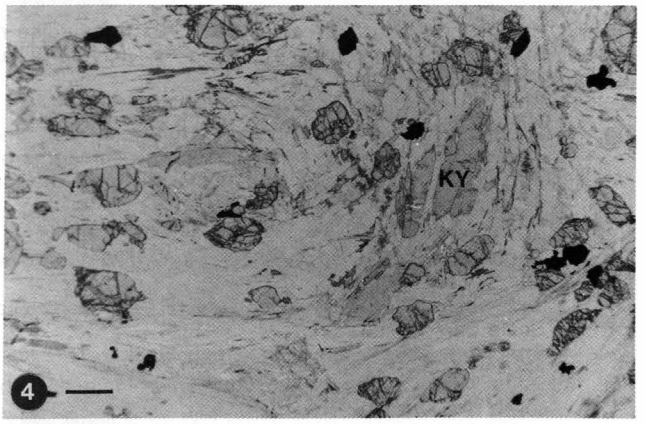
KY
4

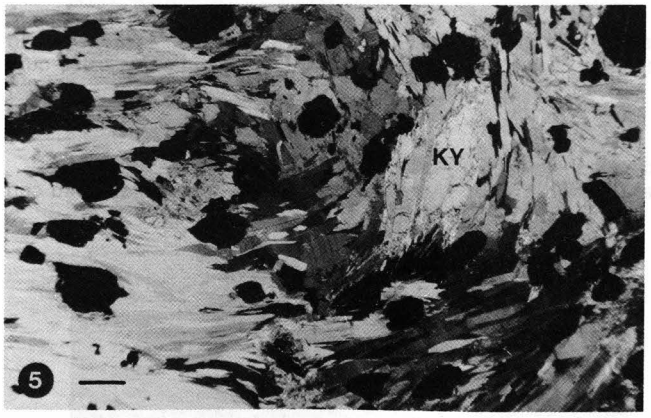
KY
5

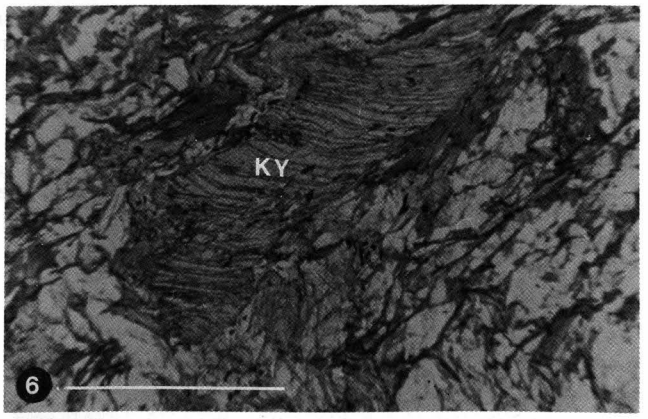
KY
6

Plate 3

Sillimanite-bearing quartzitic biotite-rich schists of the Strieden Unit.

Fig. 1: Photomicrograph (cp) of sillimanite fibrolite developed in biotite pseudomorphs after garnet.
Scale bar: 1 mm
Specimen 408.6; Harker collection number 147204.

Staurolite-garnet-andalusite-bearing aluminous metapelites of the Strieden Unit.

Fig. 2: Photomicrograph (pp, cp) of garnet- and staurolite rich graphitic mica-schist.
Fig. 4: Staurolite prisms grow across foliation (internal foliation marked by graphite trails and aligned ilmenite).
Scale bar: 1 mm
Specimen 157; Harker collection number 147247.

Fig. 3: Photomicrograph (pp) of garnet in graphite- and ilmenite-rich muscovite schists.
Garnet core shows internal foliation, the rim is free of inclusions. Locally the garnet rims are replaced by biotite. Also present are staurolite prisms which overgrow the foliation.
Scale bar: 1 mm
Specimen WÖ2; Harker collection number 147242.

Fig. 5: Photomicrograph (pp) of euhedral staurolite grain overgrowing a graphite- and imenite-rich crenulated muscovite foliation.
Other mineral phases present are biotite, quartz and garnet.
Scale bar: 1 mm
Specimen 520.1; Harker collection number 147248.

Fig. 6: Photomicrograph (cp) of euhedral staurolite grains which have overgrown a crenulated graphite- and ilmenite-rich muscovite foliation.
Internal foliation of staurolites (graphite trails, ilmenite) are not as intensely folded compared with the external foliation.
Scale bar: 1 mm
Specimen 520.2; Harker collection number 147248.

Fig. 7: Photomicrograph (pp) of staurolite- and garnet-bearing mica schist.
Garnets are partly altered to biotite. There are two generations of staurolite: Staurolite 1 is rich in quartz inclusions and in this case aligned within the foliation and staurolite 2 (higher Zn-content) is free of quartz inclusions and cross-cuts both the foliation and staurolite 1.
Scale bar: 1 mm
Specimen WÖ1; Harker collection number 147230.

Fig. 8: Photomicrograph (cp) of graphitic staurolite, garnet and andalusite-bearing schist.
Andalusite and staurolite porphyroblasts show an internal foliation marked by graphite and aligned ilmenite which can have an orientation different to the external foliation.
Scale bar: 1 mm
Specimen 520; Harker collection number 147248.

Textural evidence for partial melting.

Fig. 9: Small leucocratic pod (qz – ksp – plag – bi – sill) within aluminous metapelites (bi – sill – plag – ksp – qz).
Pod is mantled by biotite and sillimanite-rich layer, and may represent an early partial melt (leucosome) surrounded by a restite (melanosome).
Pod is a few cm across.
Locality: 150 m SSE of Latischalm hut.

Fig. 10: Leucocratic layers (plag – ksp – qz – sill – bi) interfolded with biotite- (and sillimanite)-rich layers.
This is interpreted as a melanosome and leucosome respectively which have undergone sunbstantial deformation. The foliation is defined by the alignement of biotite laths, and is labelled S_{01}. This foliation is folded by F_{02} folds.
Same locality as Plate 3 – Fig. 9.

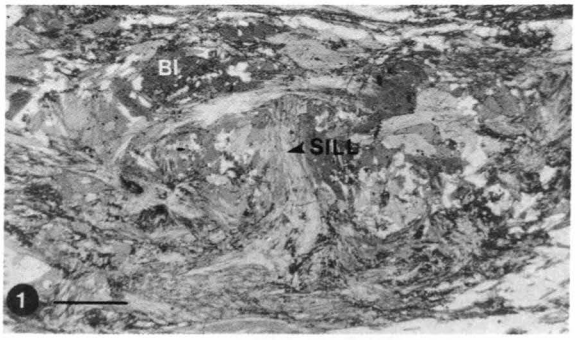
Bl
SILL
1


st
gt
2

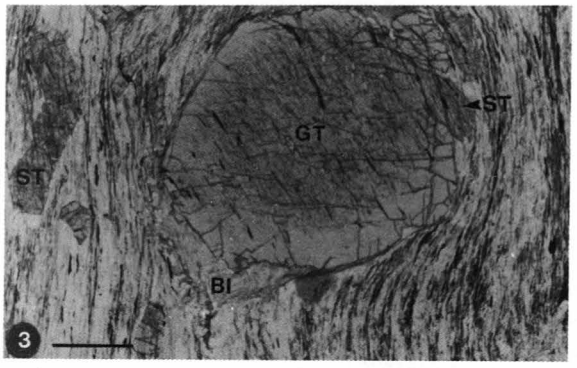
ST
GT
ST
Bl
3

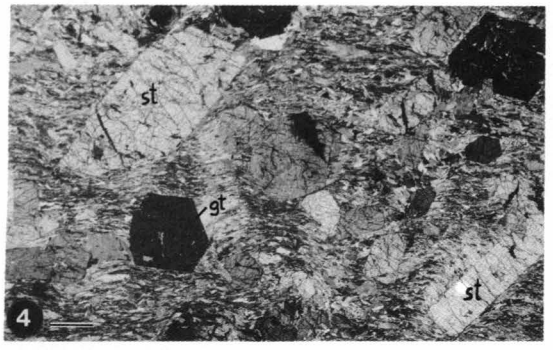
st
gt
st
4


st
5

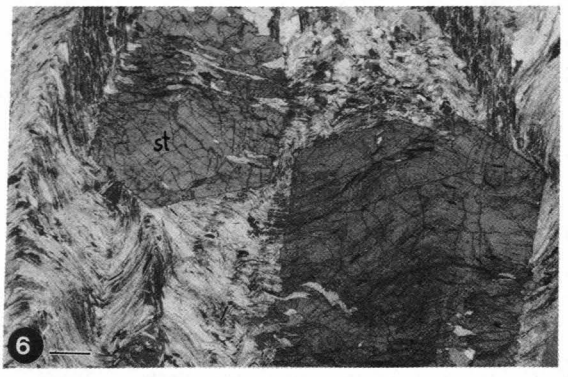
st
6

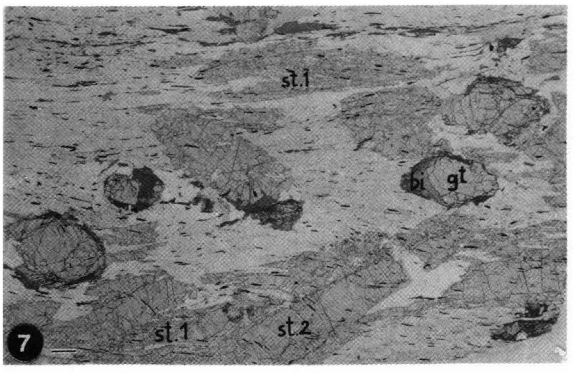
st.1
bi
gt
st.1
st.2
7

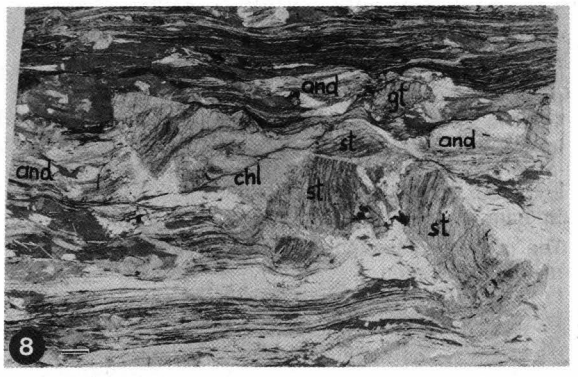
and
gt
st
and
and
chl
st
st
8

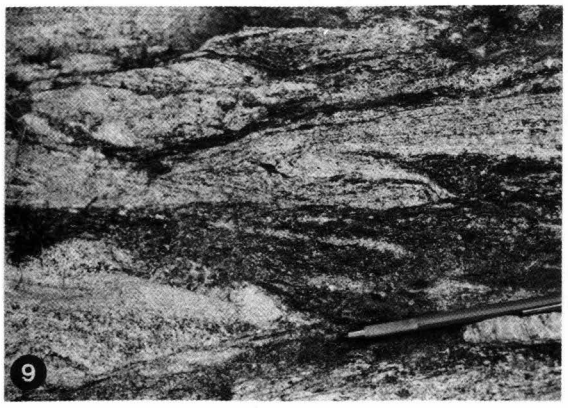
9

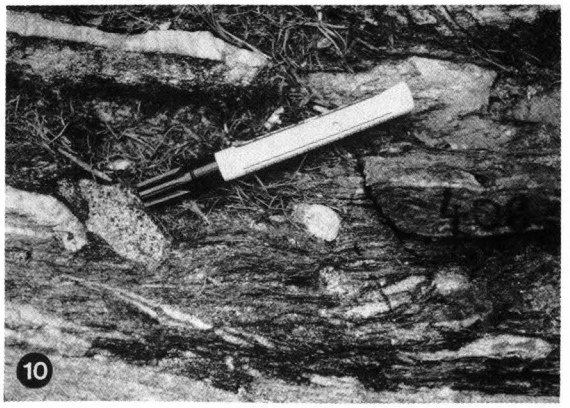
10

Plate 4

Quartz mylonites of the Strieden Unit.

Fig. 1: Polished section of a quartz mylonite which is orientated perpendicular to the mylonitic foliation and quartz elongation orientation (stretching lineation).
Tight to isoclinal mm-scale folding occurs in upper part of the hand specimen at the contact with fine-grained mica-rich layers. Fold axes are sub-parallel to the mylonitic foliation. The rock is a quartzitic biotite-rich fine-grained gneiss (in the lower part of the photograph).
Location: 550 NNE Strieden, ridge.
Specimen: 382.

Fig. 2: The mylonitc lineation (l_p) and foliation (S_p) are deformed by a tight fold (F_q) which has an axial plane oblique to the mylonitic foliation.
Locality: 700 m W of Latischalm hut.

Fig. 3: Photomicrographs (pp, cp) of part of the quartz mylonite hand specimen illustrated in Plate 4 – Fig. 1.

Fig. 4: Sections are perpendicular to the mylonitic lineation, which is defined by the shape fabric and preferred crystallographic

Fig. 5: orientation of quartz grains. Pure quartz bands are intensely interfolded with mica-rich layers. The fold axes are sub-parallel to the mylonitic lineation.
Scale bar: 1 mm.
Locality: 550 NNE Strieden, ridge; same as Plate 4 – Fig. 1.
Specimen: 382.

Fig. 6: Photomicrograph (cp) showing shape and preferred crystallographic orientation in elongate quartz grains (quartz ribbons).
Quartz ribbons show undulose extinction and can by dynamically recristallised to fine-grained elongate quartz grains.
Scale bar: 1 mm.
Locality: 400 m S of Strugenkopf.
Specimen: 327.

Fig. 7: Photomicrographs (cp) of deformed asymmetric kink folds in quartz ribbons.

Fig. 8: Section cut perpendicular to the foliation and mylonitc lineation. Mica-rich layers mark the fold axial planes of these kink folds.
Scale bar: 1 mm.
Locality: 500 m SSE of Strugenkopf.
Specimen: 329.

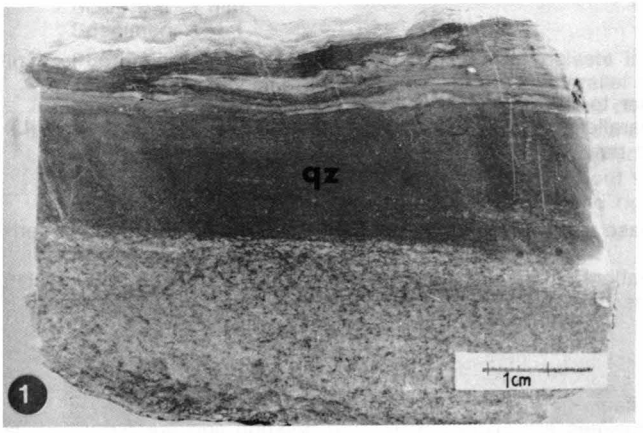
qz
1cm
1

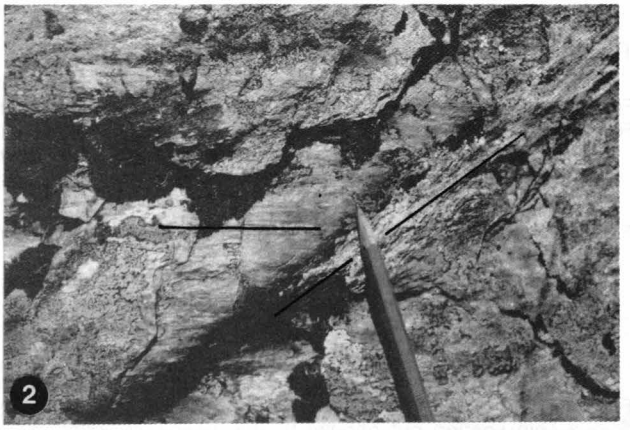
2

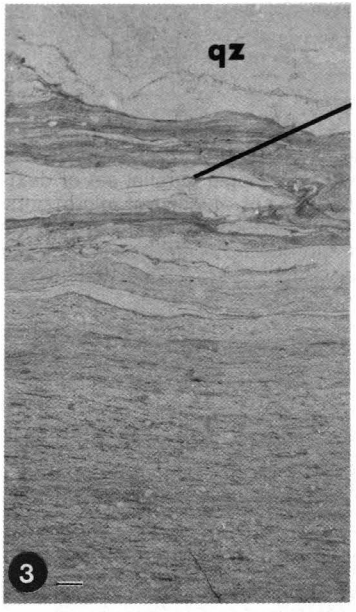
qz
3

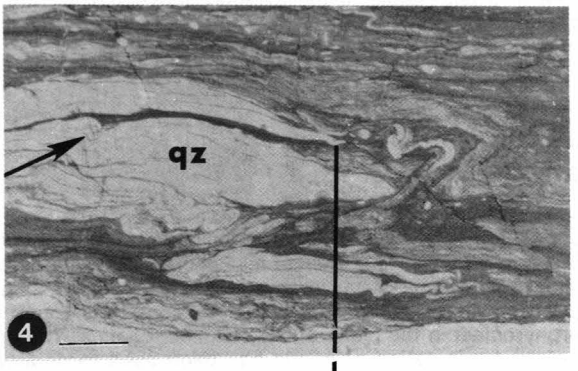
qz
4

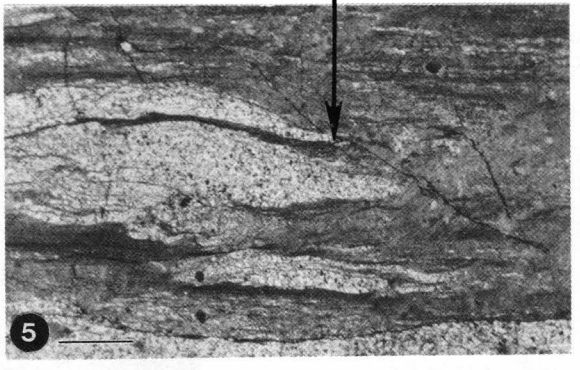
5

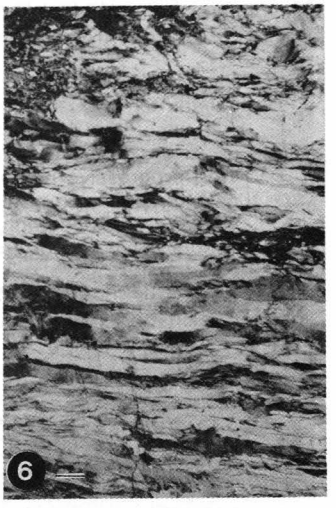
6


7

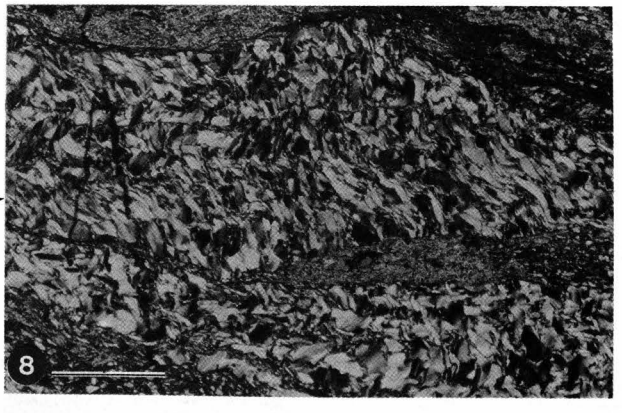
8

Plate 5

Pegmatite mylonites of the Strieden Unit.

Fig. 1: Hand specimen of a pegmatite mylonite, cut perpendicular to the foliation.
Fig. 2: H(A) shows a polished section of a hand specimen cut parallel and H(B) perpendicular to the lineation (marked as L). Cataclastically deformed tourmalines define rods oriented parallel to the lineation (stretching lineation).
Location: 500 m E of Möllkopf.
Specimen: 331.

Fig. 3: Photomicrographs (cp) of pegmatite mylonite with plagioclase and tourmaline porphyroclasts surrounded by quartz-sericite-rich matrix.
Thin section is cut parallel to the lineation (extensional lineation). There is a prominent quartz ribbon texture. Plagioclase clasts show narrowly spaced lamellar twinning (sometimes bent).
Scale: Shorter side of the photograph is 4 mm.
Locality: 450 m E of Möllkopf.
Specimen: 251.B.

Fig. 4: Photomicrograph (cp) of tourmaline-rich pegmatite mylonite.
Thin section cut parallel to the extension lineation. Tourmalines are aligned within the foliation and are deformed by parallel micro-faults which are at a high angle to the foliation. Movement on these micro-faults is dextral resulting in extension of the porphyroclast within the foliation.
Scale: Shorter side of the micrograph is 4 mm.
Specimen: 331.

Microstructures in mylonites.
Extensional crenulation cleavages.

Fig. 5: Photomicrograph (cp) of mm-scale banding defined by a compositional variation.
Layers rich in quartz, feldspar and white mica alternate with each other. Section cut parallel to the lineation. Phorphyroclasts include plagioclase and mica-fish. The fine-grained micaceous layers are deformed by a single parallel set of dextral extensional crenulation cleavages. Plagioclase porphyroclasts are cut by a single parallel set of sinistral microfaults. With progressive deformation the sinistral microfaults and the blocks they bound have undergone a clockwise rotation causing extension of the porphyroclast in the plane of the mylonitc foliation. The orientation of the shear bands together with the crystallographic preferred orientation of quartz has been used to deduce an overall dextral shear sense in a simple shear regime (chapter 7).
Scale bar: 1 mm.
Locality: 200 m E of Möllkopf.
Specimen: 256.A; Harker collection number 147178.

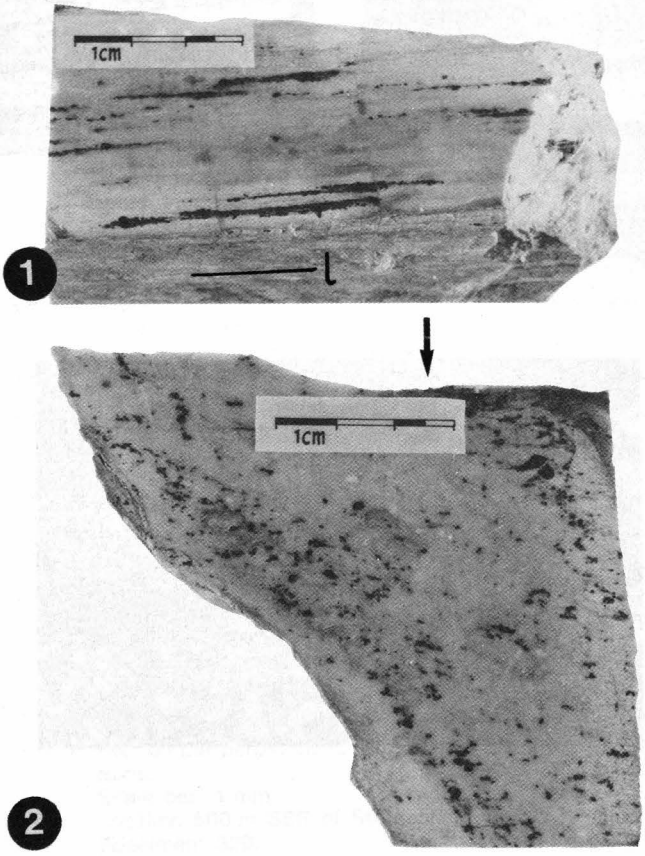

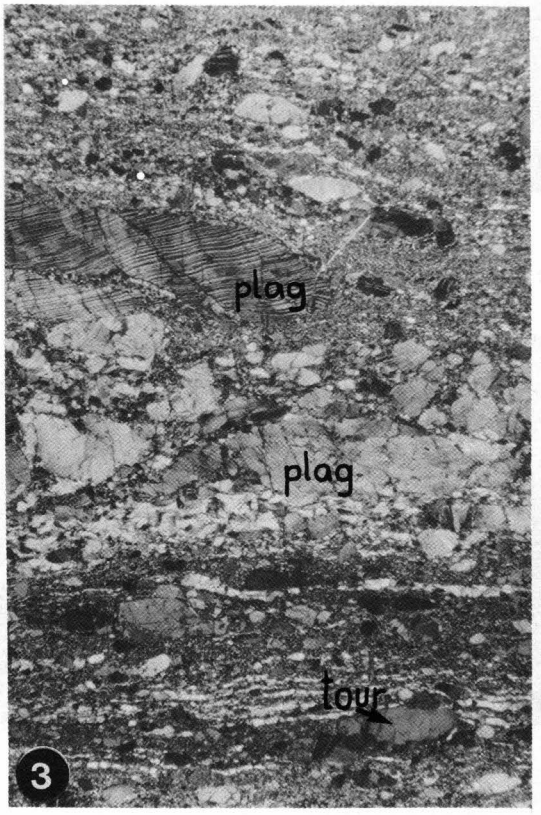

Fig. 6: Photomicrograph (cp) of an extensional crenulation cleavage developed in graphite- and mica-rich mylonite. The extensional crenulation cleavage postdates the mylonitic foliation. The mylonitic foliation between the extensional micro-faults is also folded and chemical alteration (chlorite-rich zones) occurs along micro-fractures oriented parallel to the extensional crenulation.
Scale bar: 1 mm.
Specimen: 171.1.

Fig. 7: Photomicrograph (cp) of plagioclase porphyroclasts in an augengneiss mylonite.
The large plagioclase porphyroclast is cut by parallel sinistral micro-faults. As movement occurred along these micro-faults, the faults and the blocks they bound rotated clockwise and the porphyroclast was progressively stretched within the mylonitic foliation. The porphyroclasts are surrounded by a matrix which has undergone extreme grainsize reduction with quartz grains showing a preferred crystallographic orientation. A predominant single set of dextral shear bands (extensional crenulation bands) is developed throughout the specimen. These shear bands have been used to deduce the overall shear sense in this rock (top moves to the right).
Scale bar: 1 mm.
Specimen: 502.2.

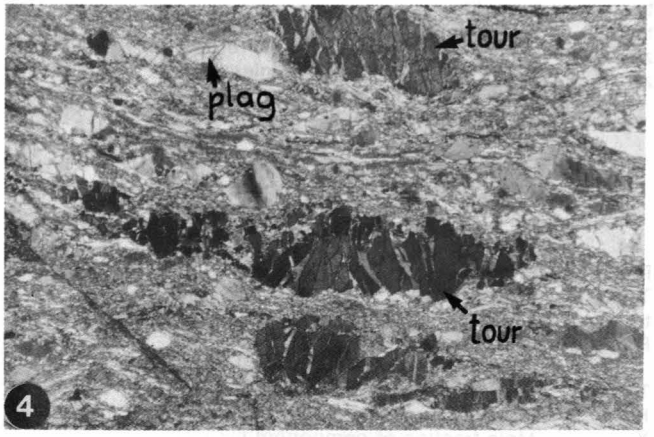

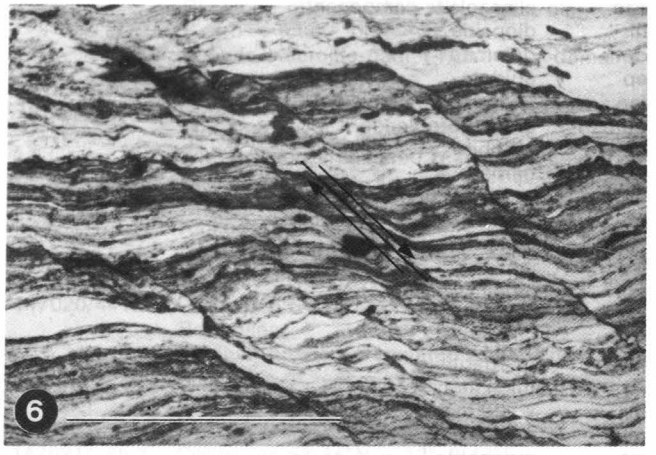

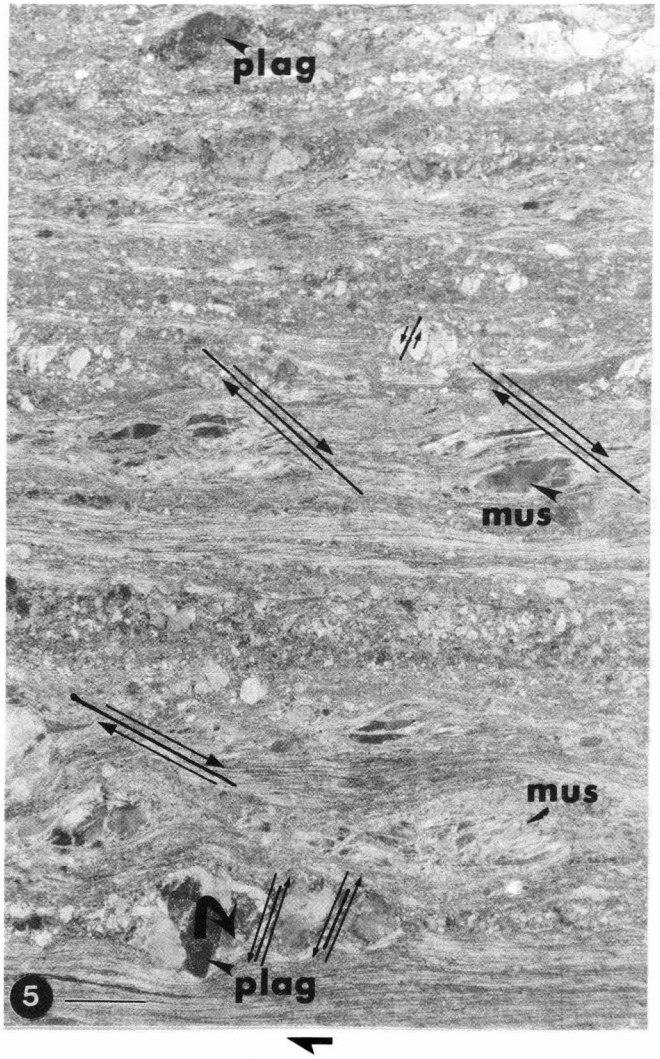

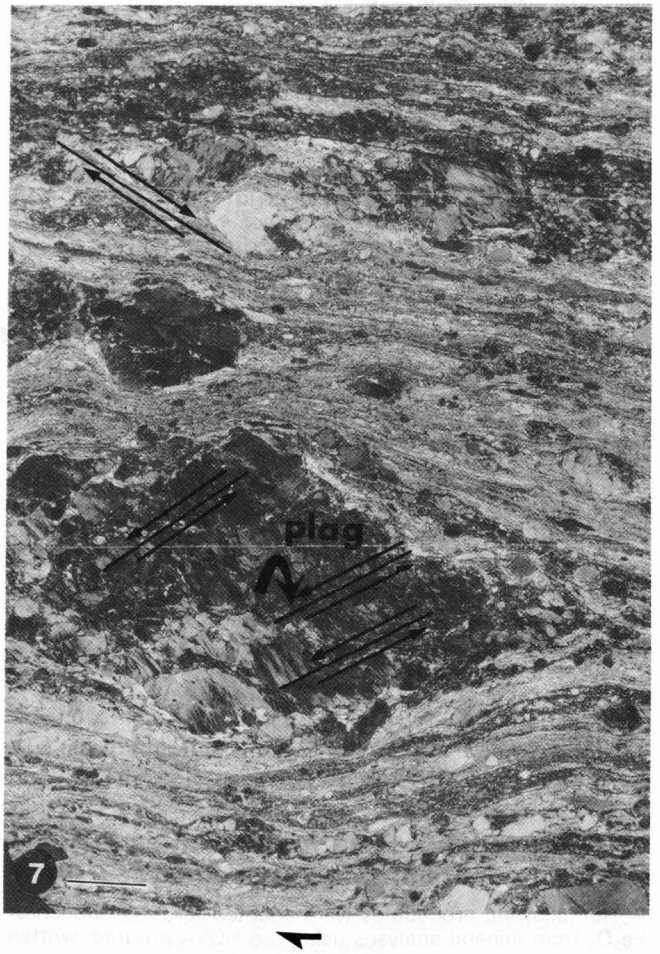

Appendix A

A.1. Mineral Abbreviations

ab	albite
alm	almandine component
amph	amphibolite (non specific)
an	anorthite component
and	andalusite
ap	apatite
bi	biotite
cc	calcite
chl	chlorite
cpx	clinopyroxene (non specific)
ctd	chloritoid
cum	cummingtonite
czo	clinozoisite component
di	diopside
dol	dolomite
ep	epidote
fsp	feldspar (non specific)
g.hb	green hornblende
gph	graphite
gt	garnet
gros	grossular component
hb	hornblende
hem	hematite
ilm	ilmenite
jd	jadeite
ksp	K-feldspar
ky	kyanite
marg	margarite
mc	mica (non specific)
mi	white mica
mus	muscovite
mt	magnetite
olig	oligoclase
omph	omphacite
ore	unidentified opaque
or	ortoclase
par	pargasite
pg	paragonite
pheng	phengite
phlog	phlogopite
plag	plagioclase
prp	pyrope component
py	pyrite
qz	quartz
rut	rutile
sill	sillimanite
spess	spessartine component
sph	sphene
st	staurolite
sym	symplectite
tour	tourmaline
tr	tremolite
tsch	tschermakite
zo	zoisite
zr	zircon

A.2. Other Abbreviations

P	Pressure
T	Temperature
t	Time
R	Gas constant (8.314 J $K^{-1}\cdot mol^{-1}$; 1.9872 cal $deg^{-1}\cdot mole^{-1}$
T (K)	= T (degree centigrade) + 273.15
K	Equilibrium constant
X_i	Mole fraction of component i
μ	Chemical potential
γ_i	Activity coefficient of component i
L	Liquid
a_i	Activity of component i
pp	Parallel polars
cp	Crossed polars
CPO	Crystallographic preferred orientation
MMZ	Main mylonite zone

Appendix B

B.1. Electron Microprobe Specification

Hardware

Probe designed and built in Cambridge. It uses a Si (Li) detector and pulse processor system interfaced to a Data General Nova 2 computer.

Software

Spectra processed by iterative peak stripping (STATHAM, 1976). Correction methods after SWEATMAN & LONG (1969).

Detection limits: Na ..... 0.25 %
Mg ..... 0.15 %
Al,Si ..... 0.10 %
K–Zn ..... 0.05 %

Relative accuracy: 2 % for major elements (with at least 5 % of element present.

B.2. Methods Used in Calculating Fe^{3+} in Minerals from Probe Analyses

The following procedures were adopted for recalculation of Fe_2O_3 from mineral analyses using the NOVA program written by Leslie KANAT (1985) available in the Department of Earth Sciences, in Cambridge.

Garnets X3 Y2 T3 O12

Formula proportions were calculated on the basis of 12 oxygens and the following site assignments were made:

1) Al^{3+} was allocated to fill the tetrahedal sites and the remainder allocated to octahedral sites.
2) Fe^{2+} was converted to Fe^{3+} until the sum of Al^{3+} + Fe^{3} + Cr^{3+} + Ti^{4+} = 2.0.

A new anion total was then calculated and the formula renormalised to 12 oxygens. The procedure is iterative, until the difference between the initial anion sum and final anion sum is less than 0.00001. The garnet composition can then be expressed in terms of the propotions of the six end members.

Other phases

All iron was assumed to be ferrous in carbonate phases, chlorite, chloritoid, feldspar, sphene, tourmaline, mica, etc.

Appendix C

List of Hand Specimens and Thin Sections Used in this Text

The first number gives the Cambridge University (Department of Earth Sciences) Harker collection number and the second refers to numbers used in the text.

POLINIK UNIT

Polinik Schists
Garnetiferous feldspathic paragneisses and schists

Fine-grained (average grain size <1 mm)

146977/ 8 Coord. 46°53'45"N – 13° 8' 2"E.
Raggaalm E.
Biotite-rich gneiss, deformed by kink-band.
Gt – mi – bi – chl – qz – plag – tour – zr – or (hem) – ap.
In the kinked zone micas are bent, and quartz shows undulose extinction.

Medium-grained (average grain size ~2 mm)

146988/ 77.5 Coord. 46°54'16"N – 13°10'20"E.
Mörnigköpfe E.
Tourmaline-rich, crenulated schist.
Gt – mi – bi – qz – plag – or – tour – zr – ap – or.

146989/ 77.6 Coord. 46°54'16"N – 13°10'20"E.
Mörnigköpfe E.
Tourmaline-rich gneiss.
Bi – mi – qz – plag – gt – chl – tour – or.

146990/ 77.7 Coord. 46°54'16"N – 13°10'20"E.
Mörnigköpfe E.
Crenulated feldspathic plagioclase-rich gneiss.
Bi – mi – qz – plag – gt – chl – or.
Lensoid domains of plagioclase and quartz within the foliation. Parallel sets of shear-bands are at a shallow angle to foliaton.

146991/ 77.9 Coord. 46°54'16"N – 13°10'20"E.
Mörnigköpfe E.
Blastomylonite.
Bi – mi – qz – plag – gt – chlor – tour – or – rut – ap.

146992/ 77.10 Coord. 46°54'16"N – 13°10'20"E.
Mörnigköpfe E.
F_2-fold core.
Bi – mi – qz – plag ('gefüllte' texture) – gt – chl – ap – zr – or.
Micas in fold-hinges recrystallised.
Folded quartz band: quartz grains show undulous extinction, serrated grain boundaries are partly recrystallised (mortar texture).

146993/ 77.11 Coord. 46°54'16"N – 13°10'20"E.
Mörnigköpfe E.
Crenulated schist, from F_3-fold core.
Bi – mi – qz – plag – gt – chl – tour – rut – sph – zr.
Micas are bent; quartz has recrystallised along grain boundaries (mortar texture).

Coarse-grained (average grain size >3 mm)

146999/ 81.5 Coord. 46°53'59"N – 13° 9'52"E.
Mörnigköpfe E.
Garnet-rich gneiss.
Gt – bi – mi – qz – plag – chl – rut – ap – zr – or – (hem).

Fresh aluminous metapelites

147016/ 81.2 Coord. 46°53'59"N – 13° 9'52"E.
Mörnigköpfe E.
Medium-grained metapelite.
Bi – mi – gt – ky – st – qz – plag –tour – zr – rut – or.
Kyanite-staurolite-tourmaline-rich lensoid domains. Staurolite-kyanite twins.

147017/ 81.4 Coord. 46°53'59"N – 13° 9'52"E.
Mörnigköpfe E.
Medium-grained metapelite.
Bi – mi – gt – st – ky – chl – qz – plag – rut – sph – tour – or.
Kyanite-staurolite-garnet-rich domains. Staurolite-kyanite-twins.

147019/ 77.16 Coord. 46°54'16"N – 13°10'20"E.
Mörnigköpfe E.
Fine-grained crenulated metapelite.
Bi – mi – gt – st – ky – chl – qz – plag – tour – or.
Kinked kyanite is aligned within the crenulated mica foliation. Conjugate kink-bands and associated box-fold.

147020/441.7 Coord. 46°54'16"N – 13° 9'25"E.
Bodensee.
Medium-grained crenulated metapelite.
Mi – bi – gt – st – ky (kinked) – qz – plag – tour – rut – ilm – chl – ap – zr.
Kyanite deformed by I_2-crenulation.

147021/ 85.1 Coord. 46°53'44"N – 13° 9'42"E.
Polinik.
Crenulated metapelite.
Mi – bi– gt – st – ky – marg – chl – qz – plag – tour – rut – sph – or (ilm).
Kyanites are altered and surrounmded by fine-grained aggregates of sericite and margarite.

147022/ 83.2 Coord. 46°53'44"N – 13° 9'30"E.
Polinik.
Coarse-grained metapelite.
Mi – bi – gt – st – ky – marg – qz – plag – chl – tour – rut – sph – or (ilm).
Fine-grained aggregates of margarite and sericite surround and partly replace kyanite.

147023/ 67 Coord. 46°53'42"N – 13° 9'44"E.
Polinik E.
Metapelite with domains rich in deformed plagioclase porphyroblasts (blastomylonite).
Bi – mi – qz – plag – gt – st – chl – rut – zr – or (ilm) – ap.
Quartz shows undulose extinction and has recrystallised grain boundaries (mortar textures); plagioclase porphyroclasts (augen texture).

147024/ 68 Coord. 46°53'43"N – 13° 9'44"E.
Polinik E.
Tourmaline-rich metapelite.
Mi – bi – gt – st – ky – qz – plag – chl – rut – or (ilm).

147025/ 77.3 Coord. 46°54'16"N – 13°10'20"E.
Mörnigköpfe E.
Medium-grained metapelite.
Bi – mi – gt – st – qz – plag – chl – zr – rut – ap – or (ilm).

Retrogressed metapelites – various stages.

147031/ 4 Coord. 46°53'43"N – 13° 7'55"E.
Raggaalm E.
Coarse-grained retrogressed metapelite containing feldspar eyes.

Gt – st (1.5 % ZnO) – mi – bi – chl – qz – plag (2 % An) – tour – rut –sph – zr – or (ilm).
Garnet forms elongate grains aligned within the foliation.

147034/ 83.4 Coord. 46°53'44"N – 13° 9'30"E.
Polinik.
Medium-grained retrogressed metapelite.
Bi – mi – qz – plag – gt – chl – st – tour – zr – rut – or.

147035/ 85.4 Coord. 46°53'44"N – 13° 9'42"E.
Polinik E.
Crenulated retrogressed metapelite (no hand specimen).
Bi – mi – qz – plag – gt – chl – tour – rut – zr – ilm.
Well-crystallised mica-fabric, two generations of garnets, fine-grained white mica pseudomorphs after staurolite and/or kyanite. Plagioclase porphyroblasts overgrowing crenulated mica fabric.

147032/ 7 Coord. 46°53'44"N – 13° 8'0"E.
Raggaalm E.
Blastomylonitic retrogressed metapelite:
Bi – mi – qz – plag – gt – chl – st – tour – zr – ap – sph – or.
Quartz shows strain textures and serrated quartz grain boundaries which can be recrystallised (mortar texture).

Pegmatites

147080/439 Coord. 46°54'28"N – 13° 9'32"E.
Bodensee S.
Foliated pegmatite. Contact pegmatite/metapelite:
Qz – plag – mus – chl – bi – gt – ap – or.
Sample taken from hinge-region of F_2 fold.
Additional sample of separated kinked muscovite books.

STRIEDEN UNIT

Metapelites

Staurolite-rich medium- to coarse-grained metapelites

147238/195.1 Coord. 46°52'15"N – 13° 7'35"E.
900 m S of Striedensee.
Kink-bands in staurolite-rich quartzitic mica schist.
St – bi – mus – or – chl – qz – plag.
Euhedral staurolites (0.3 cm) overgrow mica foliation. Ilmenite exsolution in biotite. Micas are kinked. Staurolite is altered along fractures to a fine-grained aggregate of sericite and chlorite.

147241/554 Coord. 46°52'50"N – 13° 5'54"E.
350 m ENE of Steinwandalm hut.
Andalusite-bearing, garnet-staurolite-mica schist.
And – st – gt – qz – plag – mus – bi – ilm – zr – chl – ap – ?sill.
Andalusite and staurolite porphyroblasts overgrow a crenulated (wavy) mica foliation. Alterations of garnet and staurolite to biotite and chlorite (randomly orientated). Kink-bands developed in all micas. Andalusite can contain fibrolitic mineral with a high relief (posiibly sillimanite). Quartz bands with polygonal texture.

Graphite-rich metapelites

147242/WÖ2 Coord. 46°53'46"N – 13° 4' 3"E.
400 m S of Wöllatratten.
Graphitic garnet-staurolite-bearing muscovite schist.
Gt – st – mus – bi – ilm – chl – gph – plag – ep – zr.
Garnets (0.5–1 cm) have graphite-rich cores and clear rims. They have pressure shadows filled with quartz, biotite and chlorite which are aligned within the foliation and parallel to the lineation. Staurolites cut across the graphite-rich muscovite foliation.

147247/157 Coord. 46°52'21"N – 13° 6'53"E.
450 m NNE of Striedenkopf.
Graphitic garnet-staurolite-rich mica schist:
Gt – st – mus – plag – bi – chl – qz – ilm – zr – tour – gph.
Graphitic, plagioclase-muscovite-rich foliation overgrown by kinked biotite and euhedral staurolite. Garnet altered to biotite and chlorite. Biotite altered to chlorite.

147248/520 Coord. 46°52'39"N – 13° 5' 3"E.
800 m W of Steinwandalm hut.
Graphitic staurolite-garnet-rich schist.
Gt – st – mus – bi – plag – qz – ilm – gph – zr – or (hem).
Graphitic muscovite-plagioclase-rich foliation cross-cut by biotite blades and euhedral staurolite grains. Garnets are altered to biotite and chlorite.

147249/520 Coord. 46°52'39"N – 13° 5' 3"E.
800 m W of Steinwandalm hut.
Graphitic garnet-staurolite-rich schist.
Gt – st – bi – mus – qz – plag – ilm – gph – zr – tour.
Graphite-rich plagioclase porphyroblasts are aligned within graphite-rich muscovite foliation. Complex folding defined by graphite trails. Biotite-rich zones surrounding garnets. Staurolite (cm-size) cross-cus folded graphitic foliation.

Prismatic andalusite and alterations in quartz-segregation-veins

147194/399 Coord. 46°52'51"N – 13° 6'18"E.
200 m SW of Saukopf.
Prismatic andalusite crystals with muscovite inclusions. Andalusite is altered along fractures to sillimanite, phengite, chlorite and rare margarite.
Sillimanite fibrolite with up to 3 mm long fibres form fan-shaped patterns with the apex of the fans aligned along fractures.
And – sill – pheng – chl – qz – sph – marg – ap.

147195/And Coord. 46°52'42"N – 13° 8'08"E.
200 m SW of –Schneestallkopf.
Prismatic andalusite crystals locally replaced by sillimanite, sericite, chlorite and chloritoid. Chloritoid seems to have grown prograd within the sericite aggregate.
And – sill – mus – ctd – qz – chl – ab.
Fan-shaped sillimanite fibrolite along fractures replaces andalusite.

Sillimanite-bearing quartzitic biotite schists

147202/516.1 Coord. 46°53'14"N – 13° 6'58"E.
150 m S of Latischalm hut.
Medium-grained sillimanite schist.
Sill – bi – mus – qz – plag – zr – ap – ilm – tour – rut.
Biotite intergrown with sillimanite fibrolite. Plagioclase contains ca. 25 % anorthite. Ilmenite exsolution in biotite. Sillimanite fibrolite concentrated together with biotite in lensoid cm-sized domains which are aligned within the foliation.

147203/516.2 Coord. 46°53'14"N – 13° 6'58"E.
150 m S of Latischalm hut.
Medium-grained mica schist.
Sill – bi – mus – qz – gt – plag – ilm – rut.
Banded rock with alternating layers rich in

muscovite, feldspar and biotite. Biotite intergrown with sillimanite fibrolite. Rare are coarse-grained prismatic sillimanite grains. Plagioclase contains up to 38 % anorthite.

147204/408.6 Coord. 46°53'16"N – 13° 7' 0"E.
100 m S of Latischalm hut.
Garnet relics in sillimanite-bearing quartzitic schist.
sill – bi – mus – plag – qz – gt – tour – ilm – rut.
Biotite with exsolved ilmenite and intergrown with sillimanite fibrolite. Garnet relicts surrounded by sillimanite fibrolite and biotite. Representative garnet composition: pyrope 7.44 %, almandine 1.2 %, spessartine 18.07 %, grossular 1.09 %, andratite 72.21 %. Sillimanite fibrolite partly altered to sericite. Crenulated quartz-sillimanite-rich layers.

147205/336 Coord. 46°53' 4"N – 13° 7' 0"E.
500 m SES of Latischalm hut, ridge.
Medium-grained quartzitic biotite-sillimanite schist containing shear band.
sill – bi – mus – plag – qz – chl – ap – or – tour.
Sillimanite partly replaced by sericite which mimics fibrolite growth. Sillimanite fibrolite intergrown with biotite. Biotite intergrown with sillimanite shows a higher TiO_2 contnet (up to 2.7 wt-% TiO_2) compared with sillimanite free biotite (up to 2.3 wt-% TiO_2).

147207/ 31.3 Coord. 46°53' 6"N – 13° 7' 2"E.
400 m S of Latischalm hut.
Medium-grained feldspathic biotite- rich sillimanite-bearing schist located within a metre of a pegmatite.
sill – bi – mus – ksp – plag – qz – gt – tour – ox – zr rut.
Plagioclase porphyroblasts locally show 'gefüllte' textures. Ilmenite exsolution in biotite; sillimanite fibrolite can cross quartz and feldspar grain boundaries; inclusion of garnet in plagioclase (ca. 30 % an). Fluid inclusions in plagioclase and quartz.

147211/302 Coord. 46°52'47"N – 13° 7'37"E.
50 m E of Striedensee.
Medium-grained sillimanite-bearing biotite schist.
sill – gt – bi – mus – qz – plag – ilm – ap – tour – gph – zr.
Ilmenite exsolution in biotite. Sillimanite fibrolite intergrown with biotite. Rare occurrence of prismatic sillimanite. Plagioclase contains approximately 16 % anorthite.

147214/136 Coord. 46°52'37"N – 13° 7'20"E.
400 m SW of Striedensee.
Sill – st – gt – qz – plag – bi – mus – chl – zr – tour – ox (ilm) – gph.
Web-textured garnets; graphite inclusions in plagioclase- and muscovite-rich layers; plagioclase contains 20 % anorthite.

147215/167 Coord. 46°52'59"N – 13° 7'59"E.
650 m NE of Striedensee.
Medium-grained sillimanite-bearing garnet-staurolite schist.
Sill – bi – mus – qz – plag – gt – st – ap – tour – zr – gph – ilm.
Web-textured garnets in quart-rich zones. Garnet can be partly replaced by biotite which can be intergrown with sillimanite fibrolite.

147216/397 Coord. 46°52'55"N – 13° 6'17"E.
200 m W of Saukopf.
Medium-grained sillimanite-rich kyanite-bearing metapelite.
Sill – ky – plag – qz – ilm – tour – ap – mi – bi.
Lensoid domains rich in biotite intergrown with sillimanite fibrolite. Kyanite (0.5 cm) in muscovite-rich domains. Specimen deformed by anastomosing shear foliation which is rich in opaques.

147217/169 Coord. 46°53' 3"N – 13° 8'13"E.
400 m SW of Poliniksee, ridge.
Medium-grained sillimanite-bearing quartzitic schist.
Sill – bi – mus – qz – plag – chl – or (ilm) – tour.
Sillimanite fibrolite locally replaced by sericite. Plagioclase contains 11 % anorthite.

147219/ 91 Coord. 46°52'54"N – 13° 9' 7"E.
700 m SW of Kehlluckerlkopf.
Medium-grained sillimanite-bearing biotite-rich feldspathic schist.
Sill – mus – bi – qz – plag – tour – hem – gt – chl – rut – ilm.
Sillimanite fibrolite is altered to a fine-grained aggregate of sericite. Rare are coarse-grained prismatic sillimanite grains. Plagioclase contains 21–28 % anorthite. Plagioclase porphyroblasts show 'gefüllte' textures.

Pegmatites

147142/251.1 Coord. 46°53'26"N – 13° 6'35"E.
450 m E of Möllkopf.
Blastomylonite.
Plag – ksp – qz – mus – or.
Porphyroblasts (eyes) consist of fractured K-feldspar, plagioclase and muscovite (cm-size). They are aligned within a foliation and surrounded by fine-grained quartz (quartz-ribbon texture) and sericite. Pull-apart fractures in feldspars are filled with quartz. A set of parallel micro-faults defines an extensional fracture cleavage.

Pegmatite mylonites

147151/251.A Coord. 46°53'26"N – 13° 6'35"E.
450 m E of Möllkopf.
Blastomylonite with plagioclase and tourmaline phenocrysts.
Thin section cut parallel to the lineation and perpendicular to the foliation.
Plag – tour – gt – mus – ksp – or –ap.
The mylonitic foliation consists of alternating layers rich in quartz (ribbon texture) and fractured plagioclase, fine-grained K-feldspar and tourmaline respectively. Fractured phenocrysts (cm-size) are all aligned with their long axes parallel to the lineation. Conjugate fracture-sets are developed in both plagioclase and tourmaline.

147157/331.A Coord. 46°53'26"N – 13° 6'38"E.
500 m E of Möllkopf.
Blastomylonite.
Thin section cut parallel to the lineation and perpendicular to the foliation.
Plag – qz – ksp – tour – gt – or – mi.
Tourmalines are aligned within the mylonitic foliation and show pull-apart fractures. Plagioclase porphyroblasts are stretched within the foliation. They are deformed by a single set of microfaults oriented at shallow angle to the foliation.

147168/331.B Coord. 46°53'26"N – 13° 6'38"E.
500 m E of Möllkopf.
Blastomylonite.
Thin section cut perpendicular to both foliation and lineation.
Plag – qz – ksp – tour – gt – or – mi.
In this section no clear foliation is developed. Rounded porphyroclasts of plagioclase, rare K-feldspar and tourmaline are surrounded by a fine-grained aggregate of quartz-sericite-feldspar.

Augengneisses

Biotite-rich augengneisses

147174/502.1 Coord. 46°53'16"N – 13° 8'14"E.
200 m W of Poliniksee.
Biotite-augengneiss mylonite.
Ksp – plag – bi – sph – or – qz – mus – chl – ap – tour – zo – ep – rut.
Eye-shaped composite porphyroclasts of granular plagioclase, K-feldspar and quartz. Groundmass is rich in sphen and apatite. Quartz shows crystallographic preferred orientation (ribbon-txture). Alternating zones rich in quartz and sphene-biotite-plagioclase. Biotite can be retrogressed to chlorite.

147179/256.A, 256.B Coord. 46°53'24"N – 13° 6'22"E.
200 m E of Möllkopf.
Mylonite with feldspar and muscovite porphyroclasts.
Thin section cut parallel to the lineation and perpendicular to the foliation.
Plag – ksp (microperthite) – mus –qz – or – tour – chl – gt – ep.
Alternating layers rich in sericite and quartz contain aligned porphyroclasts of muscovite (bent and kinked) and fractured plagioclase ('gefüllte' texture). Layers rich in granulated feldspar. In quartz layers grains are extemely fine-grained and show crystallographic preferred orientation (c-axes oriented at a shallow angle to mylonitic foliation). Granulated fine-grained garnets.

Quartzites

Quartz mylonites

147188/382.1 Coord. 46°52'52"N – 13° 6'54"E.
550 m NNE of Mt. Strieden, along ridge.
Preferred crystallographic orientation in pure quartz layer.
Section cut perpendicular to the mylonitic foliation and lineation. Pure quartz bands (1–1.5 cm wide) are interlayered with tourmaline- and mica-rich layers.
Qz – tour – ap – mus – or.
Tourmaline is fractured; mica is mainly sericite; rare are mica porphyroclasts. Large quartz grains show undulous extinction. Mica- and ore-rich layers define mylonitic foliation. All grain sizes less than 0,5 mm.

147186/382.2 Coord. 46°52'52"N – 13° 6'54"E.
550 m NNE of Strieden, ridge.
Pure quartz mylonite.
Section A cut perpendicular to the mylonitic foliation and lineation. Microtexture: quartz ribbons consist of single quartz grains with 0.05 mm-sized subgrains which show a common crystallographic preferred orientation and are orientated differently from the large ribbon-shaped grains (host grain). The contact of the quartz layer with the fine-grained schist is folded on a mm-scale with the fold axes oriented parallel to the mylonitic lineation.

147187/327 Coord. 46°53'32"N – 13° 6'29"E.
400 m S of Strugenkopf.
Pseudotachylite-beraring quartz-mylonite.
No hand specimen.
Qz – mus – or (hem) – chl – pseudotycylite.
Quartz ribbons show undulose extinction. Length of quartz ribbons vary from 6 mm to 0.03 mm.

147190/329 Coord. 46°53'30"N – 13° 6'33"E.
500 m SSE of Strugenkopf.
Interfolded pure quartz layers with mica-rich layers.
Quartz ribbons have been deformed into asymmetric kink bands with mica-rich layers aligned axial planar to these folds. This deformation texture is locally reworked into a microbreccia along single sets of parallel extensional faults.
Qz – gt – tour – mus – or (hem).

BRITTLE FAULT ZONE

147278/171.1 Coord. 46°53'01"N – 13° 8'14"E.
500 m NNE of Schneestallkopf, ridge.
Conjugate set of extensional faults deforming mica-quartz-graphite-rich ultramylonite. Movement on these faults caused offsets and folding of the mylonitic foliation. Quartz crystallographic preferred orientation is deformed (folded) by these faults.
Qz – plag – mi – chl – rut – or – grph – tour – py.

Appendix D

Selected Microprobe Analyses

GARNETS (METAPELITES) — POLINIK UNIT

ox\ID	83-16 core	83-17	83-18	83-19 →rim	83-26 rim	77-1 core	77-2	77-3	77-6 →rim	77-9 rim
SiO2	37.371	37.409	37.487	37.291	37.468	37.338	38.030	37.503	37.917	37.370
Al2O3	21.116	21.572	21.599	21.403	21.201	21.011	21.570	20.853	21.703	21.482
Fe2O3	0.009	-	-	-	-	0.121	-	0.201	-	-
FeO	33.930	33.033	33.468	34.432	34.212	34.663	35.200	34.999	35.643	35.792
TiO2	-	-	-	-	0.492	-	-	0.124	-	-
MgO	4.077	4.390	4.351	3.892	3.429	3.571	3.675	3.092	2.889	2.682
MnO	1.676	1.881	1.595	1.223	2.016	0.389	0.384	0.596	1.240	1.344
CaO	1.344	1.464	1.639	1.300	1.329	2.389	1.988	2.141	1.972	1.969
sums	99.523	99.749	100.139	99.541	100.147	99.482	100.847	99.509	101.324	100.639
formula cations on the basis of 12 oxygens										
Si	3.002	2.987	2.984	2.997	3.004	3.011	3.021	3.005	2.991	
Aliv	-	0.013	0.016	0.006	0.003	-	-	-	0.009	
Alvi	1.999	2.017	2.011	2.020	1.996	1.993	2.013	1.980	2.028	2.019
Fe3	0.001	-	-	-	-	0.007	-	0.012	-	-
Fe2	2.279	2.206	2.228	2.312	2.289	2.332	2.331	2.358	2.362	2.396
Ti	-	-	-	-	0.030	-	-	0.008	-	-
Mg	0.488	0.522	0.516	0.466	0.409	0.428	0.434	0.371	0.336	0.320
Mn2	0.114	0.127	0.108	0.083	0.137	0.027	0.026	0.041	0.083	0.091
Ca	0.116	0.125	0.140	0.112	0.114	0.206	0.169	0.185	0.167	0.169
sums	7.998	7.998	8.003	7.993	7.974	7.996	7.983	7.975	7.982	7.995
almSps	79.856	78.272	78.073	80.572	82.270	78.813	79.644	81.181	82.915	83.574
grsAnd	3.860	4.202	4.673	3.762	3.864	6.881	5.700	6.255	5.677	5.675
prp	16.284	17.526	17.254	15.666	13.866	14.306	14.656	12.564	11.408	10.751
Mg no.	17.636	19.148	18.809	16.766	15.154	15.511	15.686	13.602	12.468	11.780

Garnet — POLINIK UNIT

ox\ID	81.3-38 →rim	68-1 rim←	68-7	68-3 core	8-11	4-2 rim	4-5 rim	4-25 rim	85.4-1 core	85.4-2
SiO2	37.526	38.056	38.433	38.663	37.872	38.346	38.210	37.741	37.676	37.370
Al2O3	21.158	21.232	21.597	21.688	21.425	21.371	21.521	21.634	21.298	21.156
Fe2O3	-	0.123	-	-	-	0.269	-	-	-	0.095
FeO	34.832	32.444	32.556	32.360	29.452	33.641	33.253	34.600	32.267	32.331
TiO2	-	-	-	-	-	-	-	-	-	-
MgO	2.985	4.080	4.775	5.114	2.388	4.954	3.361	5.220	5.316	4.671
MnO	1.455	1.820	1.542	1.367	6.250	0.315	2.019	0.374	1.834	1.919
CaO	1.367	2.042	1.765	1.681	3.477	1.691	1.166	0.571	0.752	1.712
sums	99.283	99.797	100.668	100.873	100.824	100.587	99.530	100.140	99.143	99.255
formula cations on the basis of 12 oxygens										
Si	3.029	3.030	3.022	3.026	3.014	3.020	3.052	2.992	3.008	2.995
Aliv	-	-	-	-	-	-	-	0.008	-	0.005
Alvi	2.013	1.993	2.002	2.001	2.010	1.984	2.026	2.013	2.005	1.994
Fe3	-	0.007	-	-	-	0.016	-	-	-	0.006
Fe2	2.351	2.160	2.141	2.118	1.960	2.216	2.221	2.294	2.155	2.167
Ti	-	-	-	-	-	-	-	-	-	-
Mg	0.354	0.484	0.560	0.597	0.278	0.581	0.400	0.617	0.633	0.558
Mn2	0.099	0.123	0.103	0.091	0.421	0.021	0.137	0.025	0.124	0.130
Ca	0.118	0.174	0.149	0.141	0.297	0.143	0.100	0.048	0.064	0.147
sums	7.965	7.970	7.977	7.973	7.981	7.980	7.935	7.997	7.989	8.002
almSps	83.837	77.619	76.006	74.969	80.552	75.543	82.508	77.709	76.579	76.520
grsAnd	4.044	5.922	5.038	4.785	10.028	4.819	3.492	1.625	2.162	4.897
prp	12.119	16.459	18.956	20.246	9.419	19.638	14.000	20.665	21.259	18.583
Mg no.	13.094	18.307	20.721	21.974	12.439	20.787	15.262	21.188	22.695	20.474

Garnet

ox\ID	77-10 core	77-11	81.3-3	81.3-11	81.3-32 core	81.3-33	81.3-34	81.3-35	81.3-36	81.3-37
SiO2	37.398	37.998	37.982	37.701	38.317	38.207	38.149	38.118	38.027	38.075
Al2O3	21.369	21.646	21.464	21.360	21.419	21.461	21.273	21.590	21.430	21.450
Fe2O3	-	-	-	-	0.188	0.004	0.213	-	-	-
FeO	35.811	35.757	33.649	35.523	32.334	32.462	32.394	33.030	33.573	34.533
TiO2	-	-	-	-	-	-	-	-	-	-
MgO	3.199	2.477	4.018	2.666	4.993	4.982	4.981	4.625	4.612	4.139
MnO	0.575	1.451	0.439	1.403	1.950	1.809	1.634	1.356	1.086	1.088
CaO	1.815	1.350	2.227	1.696	1.401	1.257	1.289	1.334	1.250	1.104
sums	100.167	100.679	99.779	100.349	100.602	100.181	99.933	100.053	99.978	100.389
formula cations on the basis of 12 oxygens										
Si	2.997	3.029	3.022	3.019	3.018	3.020	3.023	3.019	3.019	3.021
Aliv	0.003	-	-	-	-	-	-	-	-	-
Alvi	2.016	2.034	2.014	2.016	1.989	2.000	1.987	2.016	2.006	2.007
Fe3	-	-	-	-	0.011	-	0.013	-	-	-
Cr	-	-	-	-	-	-	-	-	-	-
Fe2	2.400	2.384	2.239	2.379	2.130	2.146	2.147	2.188	2.229	2.292
Ti	-	-	-	-	-	-	-	-	-	-
Mg	0.382	0.294	0.476	0.318	0.586	0.587	0.588	0.546	0.546	0.489
Mn2	0.039	0.098	0.030	0.095	0.130	0.121	0.110	0.091	0.073	0.073
Ca	0.156	0.115	0.190	0.146	0.118	0.106	0.109	0.113	0.106	0.094
sums	7.993	7.954	7.971	7.973	7.982	7.980	7.977	7.973	7.978	7.976
almSps	81.931	85.834	77.298	84.217	76.240	76.579	76.383	77.565	77.929	80.214
grsAnd	5.235	3.988	6.469	4.953	3.989	3.596	3.705	3.853	3.599	3.184
prp	12.834	10.177	16.233	10.830	19.772	19.825	19.912	18.582	18.472	16.602
Mg no.	13.733	10.988	17.545	11.796	21.580	21.475	21.507	19.969	19.666	17.599

Garnet

ox\ID	85.4-3 →rim	85.4-7 rim	81.1-12 core	81.1-13	81.1-15	81.1-16	81.1-17 →rim	81-1 rim	81-5 rim	81-8 rim
SiO2	37.594	38.193	37.772	38.053	37.831	37.728	37.542	37.680	38.740	37.555
Al2O3	21.151	21.340	21.389	21.511	21.539	21.335	21.097	21.204	21.976	21.635
Fe2O3	-	-	-	-	-	-	-	-	-	-
FeO	32.596	32.668	32.188	32.237	33.498	34.811	33.853	35.639	31.958	35.185
TiO2	-	-	-	-	-	-	-	-	-	-
MgO	3.532	2.313	4.762	4.762	4.358	3.469	3.090	2.687	6.373	2.895
MnO	2.338	3.527	3.222	2.914	2.404	2.956	3.501	2.443	0.226	2.264
CaO	2.030	1.854	0.708	0.675	0.593	0.465	0.557	0.660	0.993	0.821
sums	99.241	99.895	100.041	100.152	100.223	100.764	99.640	100.313	100.266	100.355
formula cations on the basis of 12 oxygens										
Si	3.022	3.058	3.004	3.016	3.008	3.009	3.026	3.026	3.022	3.006
Aliv	-	-	-	-	-	-	-	-	-	-
Alvi	2.005	2.014	2.006	2.010	2.019	2.006	2.005	2.007	2.021	2.042
Fe3	-	-	-	-	-	-	-	-	-	-
Fe2	2.192	2.188	2.141	2.137	2.227	2.322	2.282	2.393	2.085	2.356
Ti	-	-	-	-	-	-	-	-	-	-
Mg	0.423	0.276	0.564	0.563	0.516	0.412	0.371	0.322	0.741	0.345
Mn2	0.159	0.239	0.217	0.196	0.162	0.200	0.239	0.166	0.015	0.154
Ca	0.175	0.159	0.060	0.057	0.051	0.040	0.048	0.057	0.083	0.070
sums	7.976	7.935	7.993	7.979	7.983	7.988	7.971	7.971	7.967	7.973
almSps	79.719	84.798	79.054	79.006	80.823	84.798	85.740	87.122	71.820	85.784
grsAnd	5.930	5.558	2.023	1.942	1.709	1.336	1.636	1.933	2.839	2.408
prp	14.351	9.644	18.923	19.053	17.468	13.866	12.624	10.945	25.341	11.808
Mg no.	16.184	11.204	20.863	20.838	18.820	15.080	13.990	11.844	26.219	12.787

MUSCOVITES (METAPELITES) — POLINIK UNIT

ox\ID	83-4	85-13	77-15	77-16	77-19	81.3-18	81.3-24	68-11	68-16	4-16
SiO2	44.781	45.336	46.335	45.616	48.349	53.296	45.493	46.440	46.638	46.248
Al2O3	35.628	35.253	33.550	34.902	30.487	32.831	37.033	35.179	36.174	34.836
FeO	1.120	0.880	1.470	1.130	1.711	0.483	0.435	0.784	0.699	1.238
TiO2	0.217	0.551	0.748	0.577	0.720	-	0.186	0.466	0.208	0.346
MgO	0.263	0.457	0.931	0.464	1.572	0.219	-	0.436	-	0.494
MnO	-	-	-	-	-	-	-	-	-	-
CaO	-	-	-	-	-	-	-	-	-	0.103
Na2O	0.513	1.447	0.830	1.123	0.316	1.332	1.426	1.104	1.248	0.311
K2O	9.526	7.989	8.838	8.588	9.164	7.054	8.279	8.932	8.537	9.783
Cl	-	-	-	-	-	-	-	-	-	-
sums	92.048	91.913	92.702	92.400	92.319	95.215	92.852	93.341	93.504	93.359
formula cations on the basis of 22 oxygens										
Si	6.127	6.166	6.285	6.194	6.581	6.850	6.111	6.235	6.226	6.240
Alvi	5.747	5.653	5.365	5.587	4.892	4.975	5.865	5.568	5.693	5.542
Fe2	0.128	0.100	0.167	0.128	0.195	0.052	0.049	0.088	0.078	0.140
Ti	0.022	0.056	0.076	0.059	0.074	-	0.019	0.047	0.021	0.035
Mg	0.054	0.093	0.188	0.094	0.319	0.042	-	0.087	-	0.099
Mn2	-	-	-	-	-	-	-	-	-	-
Ca	-	-	-	-	-	-	-	-	-	0.015
Na	0.136	0.382	0.218	0.296	0.083	0.332	0.371	0.287	0.323	0.081
K	1.663	1.386	1.530	1.488	1.591	1.157	1.419	1.530	1.454	1.684
Cl	-	-	-	-	-	-	-	-	-	-
sums	13.877	13.835	13.830	13.845	13.736	13.407	13.833	13.843	13.795	13.836
Mg no.	29.501	48.063	53.021	42.254	62.081	44.690	-	49.774	-	41.557
K	0.924	0.784	0.875	0.834	0.950	0.777	0.793	0.842	0.818	0.946
Na	0.076	0.216	0.125	0.166	0.050	0.223	0.207	0.158	0.182	0.046
Ca	-	-	-	-	-	-	-	-	-	0.008

Muscovites

ox\ID	4-20	4-29	85.4-9	85.4-16	85.4-18	85.4-26	81.1-10	81-29	81-11
SiO2	45.503	47.481	45.828	46.084	46.145	45.265	45.031	47.934	49.364
Al2O3	36.130	30.774	35.965	35.489	35.783	36.282	36.046	35.224	33.398
FeO	1.443	2.569	0.761	0.872	0.796	0.911	0.803	1.260	1.567
TiO2	0.635	0.765	0.584	0.531	0.499	0.393	0.392	0.663	0.647
MgO	0.407	1.861	0.282	0.263	0.306	0.234	-	0.726	1.294
MnO	-	-	-	-	-	-	-	-	-
CaO	0.101	-	-	-	-	0.105	-	-	-
Na2O	-	0.536	2.022	1.457	1.163	0.388	1.546	0.688	0.979
K2O	9.863	8.580	7.394	8.339	8.816	9.962	7.655	7.800	8.687
Cl	-	-	-	-	-	-	-	-	-
sums	94.082	92.566	92.836	93.035	93.508	93.540	91.473	94.295	95.936
formula cations on the basis of 22 oxygens									
Si	6.102	6.470	6.153	6.198	6.183	6.101	6.136	6.317	6.445
Alvi	5.712	4.944	5.692	5.627	5.652	5.765	5.791	5.473	5.141
Fe2	0.162	0.293	0.085	0.098	0.089	0.103	0.092	0.139	0.171
Ti	0.064	0.078	0.059	0.054	0.050	0.040	0.040	0.066	0.064
Mg	0.081	0.378	0.056	0.053	0.061	0.047	-	0.143	0.252
Mn2	-	-	-	-	-	-	-	-	-
Ca	0.015	-	-	-	-	0.015	-	-	-
Na	-	0.142	0.526	0.380	0.302	0.101	0.408	0.176	0.248
K	1.687	1.492	1.266	1.431	1.507	1.713	1.331	1.311	1.447
Cl	-	-	-	-	-	-	-	-	-
sums	13.822	13.796	13.839	13.840	13.845	13.884	13.798	13.624	13.768
Mg no.	33.449	56.349	39.772	34.958	40.654	31.400	-	50.660	59.539
K	0.991	0.913	0.706	0.790	0.833	0.936	0.765	0.882	0.854
Na	-	0.087	0.294	0.210	0.167	0.055	0.235	0.118	0.146
Ca	0.009	-	-	-	-	0.008	-	-	-

BIOTITES (METAPELITES) — POLINIK UNIT

ox\ID	83-27	77-5	77-13	81.3-8	81.3-13	68-10	68-18	68-9	8-12	4-9
SiO2	35.105	35.281	35.667	34.533	35.794	36.265	27.115	30.641	36.842	35.965
Al2O3	18.491	20.196	19.176	19.067	19.573	19.521	22.867	19.120	18.248	18.421
FeO	21.270	20.778	20.989	21.337	19.549	19.326	24.800	25.464	18.524	19.642
TiO2	2.015	0.855	1.871	0.888	1.383	1.372	0.473	-	2.146	2.025
MgO	7.869	8.518	8.071	9.571	9.645	9.757	11.998	11.877	9.962	9.342
MnO	0.106	-	-	-	-	-	0.230	0.257	0.136	-
CaO	-	-	-	0.094	-	-	-	-	-	0.110
Na2O	-	-	-	-	-	-	-	-	-	-
K2O	9.025	8.496	9.048	7.215	8.195	8.765	2.128	2.536	9.617	8.526
Cl	0.080	-	0.079	0.104	0.067	-	-	-	-	-
sums	93.943	94.124	94.883	92.786	94.191	95.006	89.611	89.895	95.475	94.031
formula cations on the basis of 22 oxygens										
Si	5.463	5.426	5.469	5.387	5.458	5.487	4.401	4.959	5.560	5.515
Al	3.392	3.662	3.466	3.507	3.518	3.482	4.375	3.648	3.247	3.330
Fe2	2.768	2.672	2.692	2.784	2.493	2.445	3.366	3.447	2.338	2.519
Ti	0.236	0.099	0.216	0.104	0.159	0.156	0.058	-	0.244	0.234
Mg	1.825	1.952	1.844	2.225	2.192	2.200	2.902	2.865	2.241	2.135
Mn2	0.014	-	-	-	-	-	0.032	0.035	0.017	-
Ca	-	-	-	0.016	-	-	-	-	-	0.018
Na	-	-	-	-	-	-	-	-	-	-
K	1.792	1.667	1.770	1.436	1.594	1.692	0.441	0.524	1.852	1.668
Cl	0.021	-	0.021	0.027	0.017	-	-	-	-	-
sums	15.511	15.478	15.477	15.487	15.430	15.462	15.574	15.478	15.499	15.420

Biotites

ox\ID	4-27	85.4-8	81.1-18	81-5	81-7	81-14	81-23
SiO2	35.741	34.911	36.219	35.441	36.394	36.690	36.554
Al2O3	18.903	18.515	19.419	19.168	19.758	19.607	19.647
FeO	22.493	21.637	18.004	20.564	18.895	16.923	18.939
TiO2	1.654	1.353	1.503	1.571	1.300	1.774	1.579
MgO	6.998	7.975	10.072	8.907	10.016	11.122	10.416
MnO	-	0.213	-	-	-	-	-
CaO	-	-	-	-	-	-	0.111
Na2O	-	-	-	-	0.420	-	-
K2O	8.777	8.958	8.621	8.442	8.560	8.299	8.043
Cl	-	0.063	-	-	-	-	-
sums	94.566	93.611	93.838	94.093	95.343	94.415	95.289
formula cations on the basis of 22 oxygens							
Si	5.528	5.465	5.510	5.452	5.474	5.501	5.477
Al	3.447	3.417	3.483	3.477	3.503	3.465	3.470
Fe2	2.910	2.833	2.291	2.646	2.377	2.122	2.373
Ti	0.192	0.159	0.172	0.182	0.147	0.200	0.178
Mg	1.613	1.861	2.284	2.042	2.245	2.485	2.326
Mn2	-	0.028	-	-	-	-	-
Ca	-	-	-	-	-	-	0.018
Na	-	-	-	-	0.122	-	-
K	1.732	1.789	1.673	1.657	1.642	1.587	1.537
Cl	-	0.017	-	-	-	-	-
sums	15.422	15.570	15.413	15.456	15.510	15.360	15.379

STAUROLITES (METAPELITES) POLINIK UNIT

ox\ID	83-2	83-23	81.3-28	68-20 rim	4-15 rim	4-17 core	4-18 rim	4-22 core	81.1-8 rim	81.1-9 core
SiO2	28.254	27.359	28.203	27.740	32.828	28.097	28.475	28.542	23.651	25.880
Al2O3	53.317	54.504	53.821	55.673	52.209	54.552	54.754	55.149	54.144	54:128
FeO	11:344	11.666	13.911	11.610	10:697	11.172	10:778	10:878	12:189	12:086
TiO2	0:578	0.519	0.605	0:487	0:575	0:520	0.564	0.540	0.433	0.589
MgO	0.748	0.582	1.404	0.741	0.449	0.756	0.596	0.550	-	-
MnO	0.254	0.262	-	0.286	-	0.210	0.212	0.193	-	0.202
CaO	-	-	-	-	-	-	-	-	-	-
Na2O	-	-	-	-	-	-	0.430	-	-	-
K2O	0.079	0.074	-	0.075	-	-	0:100	-	-	-
ZnO	0.980	0.778	0.295	0:807	1.265	1.212	1.320	1.342	0.629	0.456
sums	95.554	95.744	98.239	97:419	98:023	96:519	97:229	97.194	91.046	93:341
formula cations on the basis of 23 oxygens										
Si	3.981	3.852	3.897	3.835	4.457	3.917	3.941	3.943	3.524	3.744
Al	8.856	9.047	8.768	9.074	8:357	8.965	8:935	8.982	9.511	9.232
Fe2	1.337	1.374	1.608	1.342	1.215	1.303	1.248	1.257	1.519	1.462
Ti	0:061	0.055	0:063	0.051	0.059	0:055	0.059	0:056	0:049	0:064
Mg	0.157	0.122	0.289	0.153	0.091	0.157	0.123	0.113	-	-
Mn2	0:030	0.031	-	0.033	-	0.025	0.025	0.023	-	0.025
Ca	-	-	-	-	-	-	-	-	-	-
Na	-	-	-	-	-	-	0.115	-	-	-
K	0.014	0.013	-	0.013	-	-	0:018	-	-	-
Zn	0.102	0.081	0.030	0.082	0.127	0.125	0:135	0.137	0.069	0.049
sums	14:538	14.576	14.656	14.584	14:305	14:546	14:599	14:510	14.672	14.576
Mg no.	10.515	8.164	15.244	10.212	6.959	10.761	8.970	8.265	-	-

Staurolites

ox\ID	81-6	81-28	81-32
SiO2	28.163	28.176	27.895
Al2O3	54:585	54.469	54.030
FeO	12.527	12.819	13:690
TiO2	0.346	0.618	0.704
MgO	1:062	0.483	1:273
MnO	-	0.116	0:143
CaO	-	-	-
Na2O	-	-	-
K2O	0.085	-	-
ZnO	0.457	0.334	0.380
sums	97:225	97.015	98.115
formula cations on the basis of 23 oxygens			
Si	3.906	3.918	3.862
Al	8.926	8.930	8.818
Fe2	1.453	1.491	1.585
Ti	0.036	0.065	0.073
Mg	0:220	0.100	0.263
Mn2	-	0.014	0.017
Ca	-	-	-
Na	-	-	-
K	0.015	-	-
Zn	0.047	0.034	0.039
sums	14.602	14.552	14.656
Mg no.	13.124	6.292	14.215

Garnet

ox\ID	81-9 rim	81-22 rim
SiO2	37.922	37.881
Al2O3	21.415	21.585
Fe2O3	-	-
FeO	32.849	35.370
TiO2	-	-
MgO	3.998	3.280
MnO	2.415	1.875
CaO	1.639	0.706
sums	100.238	100.697
formula cations on the basis of 12 oxygens		
Si	3.015	3.015
Aliv	-	-
Alvi	2.007	2.026
Fe3	-	-
Fe2	2.184	2.355
Ti	-	-
Mg	0.474	0.389
Mn2	0.163	0.126
Ca	0.140	0.060
sums	7.982	7:972
almSps	79.280	84.667
grsAnd	4.717	2.055
prp	16.003	13.278
Mg no.	17.823	14.182

ILMENITE AND RUTILE (METAPELITES) POLINIK UNIT

ox\ID	77-12 ilmenite	68-19 ilmenite	85.4-19 ilmenite	85.4-21 rutile
SiO2	0.830	0.616	0.512	0.552
Al2O3	0.240	0.554	0.251	-
FeO	45.363	43.880	40.423	0.556
TiO2	52.330	51.853	52.148	95.133
MnO	0.863	2.932	4.790	-
sums	99.626	99.835	98.124	96.241
formula cations on the basis of 6 oxygens for ilmenite and 2 oxygenes for rutile				
Si	0.042	0.031	0.026	0.008
Al	0.014	0.033	0.015	-
Fe2	1.905	1.844	1.722	0.006
Ti	1.977	1.960	1:998	0.989
Mn2	0.037	0.125	0.207	-
sums	3.975	3.993	3.968	1.003

CHLORITES (METAPELITES) POLINIK UNIT

ox\ID	83-5	77-8	85.4-15
SiO2	24.105	24.513	23.957
Al2O3	21.975	22.266	22.984
FeO	27.777	27.622	28.331
TiO2	0.124	-	-
MgO	11:687	12.367	11.627
MnO	0:163	0.124	0:297
K2O	0:102	0:223	-
sums	85.933	87.115	87.196
formula cations on the basis of 28 oxygens			
Si	5.269	5.272	5.167
Al	5:662	5:646	5:844
Fe2	5:077	4:969	5.110
Ti	0.020	-	-
Mg	3.807	3.964	3.737
Mn2	0.030	0.023	0.054
K	0.028	0.061	-
sums	19.894	19.935	19.912

PLAGIOCLASES (METAPELITES) POLINIK UNIT

ox\ID	77-18	8-5	4-28	81-26
SiO2	65.349	61.716	66.350	64.184
Al2O3	21.647	24.230	20.745	22:534
FeO	-	-	-	0.155
CaO	2.309	5.301	1.502	3:126
Na2O	10.662	8:569	10.626	9:759
K2O	-	0.083	-	0.122
sums	99.967	99.899	99.223	99:880
formula cations on the basis of 8 oxygens				
Si	2.876	2.738	2.928	2.833
Alvi	1.123	1:267	1:079	1.173
Fe2	-	-	-	0:006
Ca	0.109	0.252	0.071	0.148
Na	0:910	0.737	0.909	0.835
K	-	0.005	-	0:007
sums	5.018	4.999	4.987	5.002
K	-	0.005	-	0.007
Na	0.893	0.742	0.928	0.844
Ca	0.107	0.254	0.072	0:149

TOURMALINES (METAPELITES) POLINIK UNIT

ox\ID	81.3-41	81.3-42	81-20
SiO2	36.064	36.154	36.446
Al2O3	32.170	31.630	32.276
FeO	5:506	4:242	4:312
TiO2	0.405	0.578	0:551
MgO	7.426	8.011	8.617
CaO	0.141	0.262	0.208
Na2O	2:377	2:104	2:421
sums	84:089	82:981	84:831
formula cations on the basis of 31 oxygens			
Si	7.567	7.629	7.541
Alvi	7.957	7.868	7.874
Fe2	0.966	0:749	0:746
Ti	0.064	0.092	0.086
Mg	2.322	2.519	2.657
Ca	0.032	0.059	0.046
Na	0.967	0.861	0.971
sums	19.874	19.776	19.922

GARNETS (METAPELITES)

ox/ID	136-1	136-7	136-4	302	31	408.3	408.16	516.2	STRIEDEN UNIT 554.5	554.7
	sillimanite-bearing								-- and-bearing --	
	rim	core	rim				incl.in plag		rim	core
SiO_2	37.589	38.431	37.309	37.414	37.781	38.196	37.988	37.696	37.274	37.239
Al_2O_3	20.923	20.889	20.883	20.989	21.837	21.013	20.874	20.892	21.047	20.929
Fe_2O_3	-	-	-	-	-	-	-	-	-	-
FeO	35.124	31.376	35.083	34.540	27.532	30.347	32.017	29.911	38.536	35.760
TiO_2	-	0.122	-	-	-	-	-	-	-	-
MgO	1.540	1.330	1.825	1.566	1.532	2.529	1.827	1.976	2.082	1.139
MnO	3.790	1.961	3.692	3.996	10.553	5.071	7.823	8.055	1.279	3.121
CaO	1.390	6.462	1.064	1.017	1.310	3.275	0.373	1.066	0.273	1.913
TOTAL	100.356	100.571	99.857	99.521	100.618	100.431	100.901	99.595	100.492	100.101
Formula cations based on 12 oxygens										
Si_{iv}	3.036	3.058	3.026	3.040	3.025	3.045	3.051	3.051	3.011	3.024
Al^{iv}	-	-	-	-	-	-	-	-	-	-
Al^{vi}	1.993	1.960	1.997	2.010	2.061	1.975	1.976	1.993	2.005	2.003
Fe^{3+}	0.007	0.040	0.003	-	-	0.025	0.024	0.007	-	-
Fe^{2+}	2.366	2.044	2.377	2.347	1.844	1.998	2.126	2.018	2.604	2.428
Ti	-	0.007	-	-	-	-	-	-	-	-
Mg	0.185	0.158	0.221	0.190	0.183	0.300	0.219	0.238	0.251	0.138
Mn	0.259	0.132	0.254	0.275	0.716	0.343	0.532	0.552	0.088	0.215
Ca	0.120	0.551	0.093	0.089	0.112	0.280	0.032	0.092	0.024	0.166
TOTAL	7.967	7.954	7.970	7.949	7.940	7.967	7.961	7.952	7.982	7.974
Mol% pyr	6.29	5.36	7.49	6.549	6.41	10.14	7.44	8.18	8.46	4.683
Mol% gros	4.08	18.67	3.15	3.068	3.92	9.47	1.09	3.16	0.80	5.633
Mol% spes	8.81	4.47	8.62	9.479	25.08	11.60	18.07	18.96	2.97	7.267
Mol% alm	80.46	69.50	80.59	80.903	64.59	67.54	72.21	69.34	87.77	82.388
Mol% andr	0.35	2.00	0.15	-	-	1.25	1.20	0.35	-	-

MUSCOVITES (METAPELITES)

ox/ID	516.1-8 coarse-g.	554-22 coarse-g.	136-12 recryst.	302-11 after sill	And-7 after and	336-1 after and	514 after and	STRIEDEN UNIT 478.21 fine-g.	478.5 fine-g.	478.13 coarse
SiO_2	46.001	45.468	45.414	45.038	45.973	44.278	45.704	45.557	46.715	46.178
Al_2O_3	35.788	34.983	36.154	35.282	41.465	36.534	37.919	39.016	37.376	38.031
FeO	1.129	1.221	0.731	1.169	0.207	0.811	1.682	-	0.693	0.262
TiO_2	0.689	0.366	0.536	0.439	-	0.168	0.221	-	0.145	0.262
MgO	0.275	0.467	0.242	-	-	-	0.348	-	0.302	-
Cr	-	-	-	0.003	-	-	-	-	-	-
CaO	-	0.080	-	-	0.843	0.729	0.823	0.850	0.148	0.089
Na_2O	0.386	0.517	0.757	0.894	5.569	0.329	-	4.280	0.557	3.906
K_2O	9.624	9.353	9.062	0.365	2.615	9.561	9.544	3.119	9.690	9.174
TOTAL	93.891	92.455	92.865	92.148	96.672	92.409	96.241	92.823	95.625	95.056
Formula cations based on 22 oxygens										
Si_{iv}	6.164	6.189	6.127	6.159	6.202	6.039	5.996	5.996	6.130	6.077
Al^{iv}	1.836	1.811	1.873	1.844	1.798	1.961	2.004	2.004	1.870	1.923
Al^{vi}	3.817	3.803	3.878	3.841	4.404	3.914	3.561	4.050	3.912	3.977
Fe^{2+}	0.127	0.139	0.082	0.132	0.022	0.092	0.185	-	0.076	0.046
Ti	0.069	0.038	0.054	0.044	-	0.017	0.022	-	0.014	0.026
Mg	0.055	0.095	0.049	-	-	-	0.068	-	0.059	-
Cr	-	-	-	0.013	-	-	-	-	-	-
Ca	-	0.012	-	-	0.115	0.106	0.116	0.120	0.021	0.013
Na	0.100	0.136	0.198	0.132	1.369	0.087	-	0.192	0.142	0.231
K	1.645	1.624	1.560	1.606	0.423	1.664	1.597	0.524	1.622	1.540
TOTAL	13.813	13.847	13.822	13.873	13.963	13.881	13.848	13.785	13.846	13.833
Mg/Mg+Fe	30.231	40.541	37.090	-	-	-	26.934	-	43.733	-
Mol% mus	94.26	91.65	88.74	87.17	22.19	89.58	93.25	30.18	90.90	12.96
Mol% parag	5.74	7.69	11.26	12.83	71.80	5.73	-	62.91	7.93	86.33
Mol% marg	-	0.66	-	-	6.01	4.69	6.75	6.91	1.16	0.71

OTHER MINERALS

ox/ID	SILLIMANITE 169-6 fibrolite	169-21 prismatic	ANDALUSITE CTD And	And	STAUROLITE (sill-in) (sill-out) 136-20 core	136-21 rim	554-18	CHL 554-16	ILM 31.16	AP 336-5
SiO_2	38.014	37.799	36.688	24.127	27.899	27.989	27.500	41.245	1.266	1.509
Al_2O_3	61.593	61.810	63.434	41.753	52.767	53.475	53.354	15.964	0.472	-
FeO	-	-	-	23.186	12.973	13.018	13.732	24.809	42.397	-
Fe_2O_3	0.241	0.439	0.224	-	-	-	-	-	-	-
Cl	-	-	0.110	-	-	-	-	-	-	0.075
TiO_2	-	-	-	-	0.525	0.494	0.389	-	52.888	-
MnO	-	-	-	0.317	0.239	0.257	0.108	-	4.331	-
MgO	-	-	-	2.727	0.903	0.822	0.803	7.190	-	-
CaO	-	-	-	-	-	-	-	-	-	54.533
Na_2O	-	-	-	-	-	-	-	-	-	-
K_2O	-	-	-	-	-	-	-	0.094	-	-
ZnO	-	-	-	-	0.405	0.480	-	-	-	-
P_2O_5	-	-	-	-	-	-	-	-	-	42.668
TOTAL	99.848	100.048	100.456	92.110	95.712	96.535	95.885	89.302	101.355	98.784
Formula cations based on	5 ox	5 ox	5 ox	12 ox	23 ox	23 ox	23 ox	28 ox	3 ox	25 ox
Si	1.456	1.449	1.444	1.986	3.946	3.926	3.887	8.119	0.031	0.249
Al_{2+}	1.389	1.395	1.470	4.051	8.799	8.715	8.891	3.705	0.014	-
Fe^{2+}	-	-	-	1.596	1.535	1.527	1.623	4.084	0.872	-
Fe^{3+}	0.003	0.007	0.003	-	-	-	-	-	-	-
Cl	-	-	0.007	-	-	-	-	-	-	0.021
Ti	-	-	-	-	0.056	0.052	0.041	-	0.978	-
Mn	-	-	-	0.022	0.029	0.081	0.013	-	0.090	-
Mg	-	-	-	0.334	0.190	0.172	0.169	2.109	-	-
Ca	-	-	-	-	-	-	-	-	-	9.626
Na	-	-	-	-	-	-	-	-	-	-
K	-	-	-	-	-	-	-	0.024	-	-
Zn	-	-	-	-	0.042	0.050	-	-	-	-
P	-	-	-	-	-	-	-	-	-	5.951
TOTAL	2.848	2.850	2.924	7.989	14.598	14.600	14.625	18.040	1.984	15.846

BIOTITES (METAPELITES)

ox/ID	554-15	554-21	136-2	136	336-4	514-7	516.2-12	4o8.5-5
	--- and- zone -- bil	bil	---------- sill - in zone--- increasing structural depth ---------> intergrown with sill	in cont. with garnet				
SiO_2	33.910	35.130	37.167	34.461	36.169	37.331	36.948	36.955
Al_2O_3	19.458	19.736	20.900	21.041	19.437	20.412	19.958	16.736
FeO	23.223	22.203	19.173	20.156	19.733	15.457	19.732	15.039
TiO_2	1.614	1.703	1.620	1.575	2.390	1.530	2.981	1.882
MgO	6.487	6.950	8.917	7.234	8.017	10.455	8.480	13.397
MnO	-	-	-	-	0.119	0.130	-	-
CaO	-	-	-	-	-	0.089	-	-
Na_2O	-	-	-	-	-	-	-	-
K_2O	8.542	8.721	9.092	8.811	9.085	7.680	9.084	9.091
TOTAL	93.233	94.443	96.869	93.277	94.949	93.085	97.183	93.099
Formula cations based on 22 oxygens								
Si_{iv}	5.359	5.434	5.493	5.348	5.501	5.599	5.470	5.615
Al^{iv}	2.641	2.566	2.507	2.652	2.499	2.401	2.530	2.385
Al^{vi}	0.985	1.033	1.135	1.198	0.986	1.208	0.953	0.613
Fe^{2+}	3.070	2.872	2.370	2.616	2.510	1.939	2.443	1.991
Ti	0.192	0.198	0.180	0.184	0.273	0.173	0.332	0.215
Mg	1.528	1.602	1.964	1.673	1.817	2.337	1.871	3.034
Mn	-	-	-	-	0.015	0.017	-	-
Ca	-	-	-	-	-	0.014	-	-
Na	-	-	-	-	-	-	-	-
K	1.722	1.721	1.714	1.744	1.763	1.470	1.716	1.762
TOTAL	15.497	15.428	15.363	15.415	15.364	15.185	15.314	15.535
Mg/Mg+Fe	33.234	35.809	45.318	39.008	41.995	54.655	43.369	61.351

References

ALTHAUS, E.: The triple point andalusite – sillimanite – kyanite: An experimental and petrologic study. – Contrib. Min. & Pet., **16**, 19–24, Heidelberg – Berlin (Springer) 1967.

BEHRMANN, J. H. & PLATT, J. P.: Sense of nappe emplacement from quartz c-axis fabrics; an example from the Betic Cordilleras (Spain). – E. P. S. L., **59**, 208–215, Amsterdam 1982.

BEHRMANN, J. H. & RATSCHBACHER, L.: Archimedes revisited: a structural test of eclogite emplacement models in the Austrian Alps. – Terra Nova, **1**, 242–252, Oxford 1989.

BERNOULLI, D. & JENKINS, H. C.: Alpine Mediterranean, and Central Atlantic Mesozoic facies in relation to the early evolution to the Tethys. – In: DOTT, R. H. & SHAVER, R. H. (eds.): Modern and ancient geosyncline sedimentation – Society of Economic Palaeontologists and Mineralogists Special Publication, **19**, 129–160, 1974.

BREWER, M. S.: Excess radiogenic argon in metamorphic micas from the Eastern Alps, Austria. – E. P. S. L., **6**, 321–331, Amsterdam (Elsevier) 1969.

BREWER, M. S.: K-Ar age studies in the Eastern Alps – the Oberostalpindecke of Kärnten. – Unpubl. D. Phil. thesis, Oxford Univ., 206 pp., 1970.

BUTLER, B. C. M.: Compositions of micas in metamorphic rocks. – In: PITCHER, W. S. & FLINN, G. W. (eds.): Controls of metamorphism, Edinburgh (Oliver and Boyd) 1965.

CIPRIANI, C., SASSI, F. P. & SCOLARI, A.: Metamorphic white micas: definition of paragenetic fields. – Schweiz. Min. Petr. Mitt., **51**, 259–302, Zürich 1971.

CLIFF, R. A.: Strontium isotope distribution in a regionally metamorphosed granite from the Zentralgneiss, southeast Tauernfenster Austria. – Contrib. Min. & Pet., **32**, 274–288, Heidelberg – Berlin (Springer) 1971.

CLIFF, R. A., DROOP, G. T. R. & REX, D. C.: Alpine metamorphism in the south east Tauern Window, Austria: rates of heating, cooling and uplift. – J. Met. Geol., **3**, 403–415, Oxford (Blackwell) 1975.

CLIFF, R. A., NORRIS, R. J., OXBURGH, E. R. & WRIGHT, R. C.: Structural, metamorphic and geochronological studies in the Reisseck and southern Ankogel Groups, the Eastern Alps. – Jb. Geol. B.-A., Wien, **114**, 121–272, 1971.

DEER, W. A., HOWIE, R. A. & ZUSSMAN, J.: An introduction to the Rock Forming Minerals. – 528 pp., London (Longman) 1966.

DEER, W. A., HOWIE, R. A. & ZUSSMAN, J.: Rock-forming Minerals, Vol. 2A. Single-Chain Silicates. – London (Longman) 1987.

DEUTSCH, A.: Young Alpine dykes south of the Tauern Window (Austria): A K-Ar and Sr isotope study. – Contrib. Min. & Pet., **85**, 45–57, Heidelberg – Berlin (Springer) 1984.

DEWEY, J. F.: Extensional collapse of orogens. – Tectonics, vol. **7**, no. 6, 1123–1139, Washington D.C. 1988.

DEWEY, J. F., HELMAN, M. L. TURCO, E., HUTTON, D. H. W. & KNOTT, S. D.: Kinematics of the Western Mediterranean. – In: COWARD, M.- P., DIETRICH, D. & PARK, R. G. (eds.), Alpine Tectonics, Geol. Soc. Special Publication No. 45, 269–283, London 1989.

DEWEY, J. F., PITMAN, W. C., RYAN, W. B. F. & BONNIN, J.: Plate tectonics and the evolution of the Alpine system. – Geol. Soc. of Amer. Bull., **84**, 3138–3180, Boulder, Colorado 1973.

DROOP, G. T. R.: Alpine metamorphism in the south-east Tauern Window, Austria – I. Estimation of P-T-conditions. – Journ. Met. Geol., **3**, 371–402, Oxford (Blackwell) 1985.

ENGLAND, P. C.: Some thermal considerations of the Alpine metamorphism – past, present and future. – Tectonophysics, **46**, 21–40, Amsterdam (Elsevier) 1978.

ENGLAND, P. C. & RICHARDSON, S. W.: The influence of erosion upon the mineral facies of rocks from different metamorphic environments. – Jour. Geol. Soc., **134**, 201–213, London 1977.

ERNST, W. G.: Interpretative synthesis of metamorphism in the Alps. – Bull. Geol. Soc. Amer., **84**, 2053–2978, Boulder, Colorado 1973.

ESSENE, E. J.: Geologic thermometry and barometry. – In: FERRY, J. M (ed.): Characterisation of metamorphism through mineral equilibria. – Min. Soc. Amer., Reviews in Mineralogy, **10**, p. 163, Washington D.C. 1982.

ESSENE, E. J. & FYFE, W. S.: Omphacite in Californian metamorphic rocks. – Contrib. Min. & Pet., **15**, 1–23, Heidelberg – Berlin (Springer) 1967.

EUGSTER, H. P., ALBEE, A. L., BENCE, A. E., THOMPSON, J. B. Jr. & WALDBAUM, D. R.: The two phase region and excess mixing properties of paragonite-muscovite crystalline solutions. – Jour. Petrol., **13**, 147–179, Oxford (University Press) 1972.

EXNER, C.: Erläuterungen zur Geologischen Karte der Umgebung von Gastein. – Geol. B.-A., Wien, **1957**, 168 pp., 1957a.

FAUPL, P. & SAUER, R.: Zur Genese roter Pelite in Turbiditen der Flyschgosau in den Ostalpen (Oberkreide–Alttertiär). – Neues Jahrb. Geol. Paläontol. Mh., **1978**, 65–86, Stuttgart 1978.

FERRY, J. M. & SPEAR, F. S.: Experimental calibaration of the partition of Fe and Mg between garnet and biotite. – Contrib. Min and Pet., **66**, 113–117, Heidelberg – Berlin (Springer) 1978.

FRANK, W.: Evolution of the Austroalpine elements in the Cretaceous. – In: FLÜGEL, H. & FAUPL, P.: Geodynamics of the Eastern Alps, 379–406, Vienna (Deuticke) 1987.

FRISCH, W.: Ein Modell zur alpidischen Evolution und Orogenese des Tauernfensters. – Geol. Rundsch., **65**, 375–393, Stuttgart 1976.

FRISCH, W.: A plate tectonic model of the Eastern Alps. – In: CLOSS, H., ROEDER, D. & SCHMID, K. (eds.): Alps, Apennines and Hellenides, Inter-Union Commission on Geodynamics, Scientific Report No. 38, 167–172, 1978.

FRISCH, W.: Tectonic progradation and plate tectonic evolution of the Alps. – Tectonophysics, **60**, 121–139, Amsterdam (Elsevier) 1979.

GANGULY, J.: Garnet and clinopyroxene solid solutions and geothermometry based on Fe-Mg distribution coefficient. – Geochim. Cosmochim Acta, **43**, 1021–1029, Oxford (Pergamon Press) 1979.

HAWKESWORTH, C. J.: Geochemical studies in and around the south-east corner of the Tauern Window. – Unpubl. D. Phil. Thesis, Oxford, 1974.

HAWKESWORTH, C. J.: Rb-Sr geochronology in the Eastern Alps. – Contrib. Min. & Pet., **54**, 225–244, Heidelberg – Berlin (Springer) 1976.

HAWKESWORTH, C. J., WATERS, P. J. & BICKLE, M. J.: Plate tectonics in the Eastern Alps. – E. P. S. L., **24**, 405–413, Amsterdam 1975.

HESS, I. P. C.: Prograde and retrograde equilibria in garnet-cordierite gneisses in south-central Massachusets, 1971.

HEY, M. H.: A new review of the chlorites. – Min. Mag., **30**, 277–292, London 1954.

HOBBS, B., MEANS, W. D. & WILLIAMS, P. F.: An Outline of Structural Geology. – (John Wiley & Sons, Inc.) 1976.

HOINKES, G.: Mineralaktionen und Metamorphosebedingungen in Metapeliten des westlichen Schneebergzuges und des angrenzenden Altkristallins (Ötztaler Alpen). – Tscherm. Min. Pet. Mitt., **28**, 31–54, 1981.

HOINKES, G. & THÖNI, M.: Zur Abgrenzung der kretazischen Amphibolitfazies im südlichen Ötztal-Kristallin. – Jahrb. 1981, Hochschulschwerpunkt S 15, 87–91, Leoben 1982.

HOKE, L.: Geology of part of the Altkristallin (Eastern Alps). – Unpublished Ph. D. thesis, 245 pp., Cambridge 1987.

HOLDAWAY, M. J.: Stabiity of andalusite and the aluminum silicate phase diagram. – Amer. Jour. Sci., **271**, 97–131, New Haven 1971.

HOLLAND, T. J. B. & POWELL, R.: An internally consistent thermodynamic dataset with uncertainties and correlations: 2. Data and results. – Jour Met. Geol., **3**, 343–370, Oxford (Blackwells) 1986.

HOLLAND, T. J. B. & RAY, N. J.: Glaucophane and pyroxene breakdown reactions in the Pennine units of the Eastern Alps. – Jour. Met. Geol., **3**, 417–370 Oxford (Blackwells) 1985.

HOLLISTER, L. S.: Garnet zoning: an interpretation based on the Rayleigh fractionation model. – Science, **154**, 1647–1651, New York 1966.

HOSCHEK, G.: The stability of staurolite and chloritoid and their significance in metamorphism of pelitic rocks. – Contr. Min. & Pet., **22**, 208–232, Heidelberg – Berlin (Springer) 1969.

HUNZIKER, J. C.: Rb-Sr and K-Ar age determination and the Alpine tectonic history of the Western Alps. – Mem. Ist. Geol. Mineral. Univ. Padova, 1–54, 1974.

JENKYNS, H. C.: Tethys: past and present. – Proc. Geol. Assoc., **91**, 107–118, London 1980.

KANAT, L. H.: Aspects of the geology of southwest Oscar II Land, Spitzbergen. – Unpubl. Ph. D. Thesis, 203 pp., Cambridge 1985.

KERR, A.: Zoning in garnet from the mainland Lewisian. – Min. Mag., **44**, 191–194, London 1981.

LAMBERT, R. St. J.: A potassium-argon study of the margin of the Tauernfenster at Döllach, Austria. – Eclogae Geol. Helv., **63**, 197–205, Lausanne 1970.

LISTER, G. S. & WILLIAMS, P. F.: Fabric development in shear zones. – Jour. Struct. Geol., **1**, 283–297, Oxford (Pergamon Press) 1979.

LISTER, G. S. & WILLIAMS, P.: The partitioning of deformation in flowing rock masses. – Tectonophysics, **92**, 1–33, Amsterdam (Elsevier) 1983.

MEHNERT, K. R.: Migmatites and the origin of granitic rocks. – 393 pp., Amsterdam (Elsevier) 1968.

NEWTON, R. C.: Metamorphic temperatures and pressures of Group B and C eclogite. – Geol. Soc. of Amer. Mem., **164**, 17–31, Oxford (Pergamon Press) 1986.

NEWTON, R. C., CHARLU, T. V. & KLEPPA, O. J.: Thermochemistry of the high structural state plagioclases. – Geochim. Cosmochim. Acta, **44**, 933–941, 1980.

NEWTON, R. C. & HASELTON, H. T.: Thermodynamics of the garnet-plagioclase-Al_2SiO_5-quartz geobarometer. – In: NEWTON, R. C., NAVROTSKY, A. & WOOD, B. J. (eds.): Thermodynamics of Minerals and Melts, 131–148, New York (Springer) 1981.

OBERHAUSER, R.: Beiträge zur Kenntnis der Tektonik und der Paläogeographie während der Oberkreide und dem Paläogen im Ostalpenraum. – Jahrb. Geol. B.-A., Wien, **111**, 115–145, 1968.

OBERHAUSER, R. (Red.): Der Geologische Aufbau Österreichs. – 695 pp., Wien (Springer) 1980.

OXBURGH, E. R.: Superimposed fold systems in the Alkristallin rocks on the S. E. margin of the Tauernfenster. – Verh. Geol. B.-A., Wien, 33–46, 1966.

OXBURGH, E. R. & ENGLAND, P. C.: Heat flow and metamorphic evolution of the Eastern Alps. – Eclog. Geol. Helv., **73**, 379–398, Lausanne 1980.

OXBURGH, E. R., LAMBERT, R. St. J., BAARDSGAARD, H. & SIMONS, J. G.: Potassium Argon age studies across the southeast margin of the Tauern Window, the Eastern Alps. – Verh. Geol. B.-A., Wien, 17–33, 1966.

PLATT, J. P.: Dynamics of orogenic wedges and the uplift of high-pressure metamorphic rocks. – Bull Geol. Soc. Am., **97**, 1037–1053, Boulder, Colorado 1986.

PLATT, J. P.: The uplift of high-pressure low-temperature metamorphic rocks. – Phil. Trans. of R. Soc., Lond. **A321**, 87–102, 1987.

PLATT, J. P., BEHRMANN, J. H.: Structures and fabrics in a crustal-scale shear zone. Betic Cordillera, S. E. Spain. – Jour. Struct. Geol., **8**, 15–33, Oxford (Pergamon Press) 1986.

PLATT, J. P., BEHRMANN, J. H., CUNNINGHAM, P. C., DEWEY, J. F., HELMAN, M., PARISH, M., SHEPLEY, M. G., WALLIS, S., & WESTON, P. J.: Kinematics of the Alpine arc and the motion history of Adria. – Nature, **337**, 158–161, London 1989.

PLATT, J. P. & VISSERS, R. L. M.: Extensional structures in anisotropic rocks. – Jour. Struct. Geol., **2**, 397–410, Oxford (Pergamon Press) 1980.

POWELL, R.: Equilibrium thermodynamics in petrology. – 284 pp., London (Harper Row) 1978.

POWELL, R.: Geothermometry and geobarometry: a discussion. – Jour. Geol. Soc., **142**, 29–38, London 1985.

POWELL, R. & HOLLAND, T. J. B.: An internally consistent thermodynamic data set with uncertainties and correlations: 1. Methods and worked example. – Jour Met. Geol., **3**, 327–342, Oxford (Blackwells) 1986.

RAITH, M., RAASE, P., KREUZER, H. & MÜLLER: The age of the Alpidic metamorphism in the Western Tauern Window, Austrian Alps, according to radiometric dating. – In: CLESS, H., ROEDER, D. & SCHMID, K. (eds.): Alps, Appenines and Hellenides, Inter-Union Commission on Geodynamics, Scientific Report No. 38, 140–149, 1978.

RICHARDSON, S. W., GILBERT, M. C. & BELL, P. M.: Experimental determination of the kyanite-andalusite and andalusite-sillimanite equilibria; the alumina silicate triple point. – Amer. Jour. Sci., **267**, 259–272, New Haven 1969.

SALJE, E.: Heat capacities and entropies of andalusite and sillimanite: their influence of fibrolitization on the phase diagram of the Al_2SiO_5-polymorphs. – Amer. Min., **71**, 1366–1371, Lawrence, Kansas (Allen Press) 1986.

SANDER, B.: Einführung in die Gefügekunde der geologischen Körper. 1. Teil: Allgemeine Gefügekunde und Arbeiten im Bereich Handstück bis Profil. – Wien – Innsbruck (Springer) 1948.

SANDER, B.: Einführung in die Gefügekunde der geologischen Körper. 2. Teil: Die Korngefüge. – Wien – Innsbruck (Springer) 1950.

SCHMID, S. M. & CASEY, M.: Complete fabric analysis of some commonly observed quartz c-axis patterns. – A. G. U. Mon. 36 – The Patterson volume (edited by HOBBS, B. E. & HEARD, H. C.) 263–286, 1986.

SELVERSTONE, J.: Petrologic constraints in imbrication metamorphism and uplift in the S. W. Tauern Window, Eastern Alps. – Tectonics, **4**, 687–704, Washington D.C. 1985.

SELVERSTONE, J.: Evidence for east–west crustal extension in the Eastern Alps: implications for the unroofing history of the Tauern Window. – Tectonics, **7**, 87–105, Washington D.C. 1988.

SEDGWICK, A.: Tertiary formations of Austria and Bavaria. – Phil. Mag., London 1830.

SIMPSON, C. & SCHMID, S.: An evaluation of criteria to deduce the sense of movement in sheared rocks. – Bull. Geol. Soc. Am., **94**, 1281–1288, Boulder, Colorado 1983.

STATHAM, P. J.: A comparative study of techniques for quantitative analysis of the X-ray spectra obtained with a Si(Li)detector. – X-ray spectrometry, **5**, 16–28, 1976.

STORRE, B. & KAROTKE, E.: Experimental data on melting reactions of muscovite + quartz in the system K_2O-Al_2O_3-SiO_2-H_2O at 20 kb water pressure (short communication). – Contrib. Min. & Pet, **36**, 343–345, Heidelberg – Berlin (Springer) 1972.

SWEATMAN, R. R. & LONG, J. V. P.: Quantitative electron probe microanalysis of rock forming minerals. – Jour. Pet., **10**, 332–379, Oxford (University Press) 1969.

THOMPSON, J. B.: The graphical analysis of mineral assemblages in pelitic schists. – Amer. Min., **42**, 842–858, Lawrence, Kansas (Allen Press) 1957.

THOMPSON, P. H.: Isograd Patterns and Pressure – Temperature Distribution during Regional Metamorphism. – Contrib. Min. & Pet., **57**, 277–295, 1976.

THÖNI, M.: The thermal climax of the early Alpine Metamorphism in the Austroalpine Thrust Sheet. – Mem. di Science Geologiche, Padova, **36**, 211–238, 1983.

TOLLMANN, A.: Geologie von Österreich, Bd. 1: Die Zentralalpen. – 766 pp., Wien (Deuticke) 1977b.

TRACY, R. J., ROBINSON, P. & THOMPSON, A. B.: Garnet composition and zoning in the determination of temperature and pressure of metamorphism, Central Massachusetts. – Amer. Min., **61**, 762–775, Lawrence, Kansas (Allen Press) 1976.

VOLL, G.: New work on petrofabrics. – Geol. J., **2** (3), 503–597, Great Yarmouth, Norfolk 1976.

WALLIS, S. R.: The structural and kinematic development of the Austroalpine Pennine boundary in the S. E. Tauern, Eastern Alps. – Unpublished Ph. D. Thesis, Oxford 1988.

WATERS, D. J.: Structural, metamorphic and geochronological studies in the South-East Tauern. – Unpubl. D. Phil. Thesis, Oxford, 1976.

WICKHAM, S. M.: The segregation and emplacement of granitic magmas. – Jour. Geol. Soc., **144**, 281–297, London 1987.

Manuskript bei der Schriftleitung eingelangt am 18. Dezember 1989.